Role of the *Arabidopsis thaliana* transcription factor BBX14 in retrograde and stress acclimation signaling pathways

Dissertation
zur Erlangung des Doktorgrades
der Naturwissenschaften
(Dr. rer. nat.)

an der Fakultät für Biologie
der Ludwig-Maximilians-Universität München
vorgelegt von

Vasil Atanasov

München, 2024

Diese Dissertation wurde angefertigt unter der Leitung von PD Dr. Tatjana Kleine im Bereich „Molekulare Pflanzenwissenschaften“ an der Fakultät für Biologie der Ludwig-Maximilians-Universität München

Datum der Abgabe: 04.07.2024
Datum der mündlichen Prüfung: 01.10.2024
Erstgutachter: PD Dr. Tatjana Kleine
Zweitgutachter: Prof. Thomas Nägele

Statutory declaration

Eidesstattliche Erklärung

Ich versichere hiermit an Eides statt, dass die vorgelegte Dissertation von mir selbstständig und ohne unerlaubte Hilfe angefertigt wurde. Des Weiteren erkläre ich, dass ich nicht anderweitig ohne Erfolg versucht habe, eine Dissertation einzureichen oder mich der Doktorprüfung zu unterziehen. Die folgende Dissertation liegt weder ganz noch in wesentlichen Teilen einer anderen Prüfungskommission vor.

Vasil Atanasov
München, den 04.07.2024

Statutory declaration

I declare that I have authored this thesis independently and that I have not used other than the declared (re)sources. As well I declare that I have not submitted a dissertation without success and not passed the oral exam. The present dissertation (neither the entire dissertation nor parts) has not been presented to another examination board.

Vasil Atanasov
München, 04.07.2024

Contents

Abbreviations

BBX	B-box protein
bp	base pairs
CCT	CONSTANS, CO-like and TOC1
Chl	Chlorophyll
Col-0	Arabidopsis ecotype Columbia-0
COP1	Constitutively Photomorphogenic 1
CRY	Cryptochrome
DNA	Deoxyribonucleic acid
F_v/F_m	Maximum quantum yield of PSII
GFP	Green fluorescent protein
GLK	GOLDEN2-LIKE transcription factor
gun	genomes uncoupled mutant
HL	High Light
HY5	Elongated Hypocotyl 5
HYH	HY5 Homolog
LHC	Light-harvesting complex
LHCB	Light-harvesting chlorophyll a/b-binding
LIN	Lincomycin
mRNA	messenger ribonucleic acid
MS	Murashige and Skoog medium
NF	Norflurazon
NGE	Nuclear gene expression
OGE	Organellar gene expression
PAM	Pulse-Amplitude-Modulation
PGE	Plastid gene expression
PhANGs	Photosynthesis-associated nuclear-encoded genes
PHY	Phytochrome
PIF	Phytochrome Interacting Factor
PSII	Photosystem II
ROS	Reactive oxygen species
RS	Retrograde signaling
TF	Transcription factor
WT	Wild-type

Abstract

Light signaling plays an essential role in controlling higher plants' early developmental process termed as photomorphogenesis. The development of seedlings capable of photosynthesis necessitates the orchestration of both light and retrograde biogenic signaling pathways. Transcriptional regulation stands as a pivotal mechanism, orchestrated by a dynamic interplay of transcription factors and regulatory proteins, meticulously modulating gene expression. Despite considerable characterization of transcription factors and regulators within the light-signaling pathway, their intricate interactions largely remain elusive. Notably, a plethora of transcription factors in plants have garnered attention for their pivotal roles in orchestrating light-regulated development. Among these, the B-box (BBX) family of transcription factors, distinguished by the presence of zinc-finger BBX domains in their N-terminal region, holds prominence. BBX proteins emerge as central players in regulatory networks governing various growth and developmental processes, spanning seedling photomorphogenesis, photoperiodic regulation of flowering, shade avoidance, and responses to diverse biotic and abiotic stresses.

In a previous study exploring the response to high light (HL) and biogenic signals, BBX14, alongside GLK1, was identified within a core module. Utilizing inhibitors targeting chloroplast development, in this thesis it was uncovered that *BBX14* is directly targeted by GLK1, as evidenced by chromatin immunoprecipitation-Seq experiments. Furthermore, RNA-Seq analysis hinted at a potential role for BBX14 in regulating the circadian clock. Additionally, BBX14 was found to contribute to chlorophyll biosynthesis upon the early onset of light, promote photomorphogenesis and influence the accumulation of the chlorophyll precursor, Pchlide, in the dark. Conversely, a knockout of *BBX14* resulted in a long hypocotyl phenotype dependent on retrograde signaling, similar to the *glk1* mutant. Notably, the expression of *BBX14* and *BBX15* during biogenic signaling was contingent upon GUN1. Investigating their role in GUN-type biogenic signaling, it was observed that overexpression of BBX14 or BBX15 led to the de-repression of *CA1* mRNA levels under norflurazon conditions, while transcripts levels of the *LHCB1.2* marker remained unaffected. Finally, BBX14 was identified to be crucial for plants to acclimate to HL stress.

In summary, BBX14 emerges as a pivotal component in the integration of biogenic signals and as a nuclear target downstream of the GUN1/GLK1 module. Its established significance in seedling development and its central role in plastid-to-nucleus signaling render BBX14 a promising candidate for further characterization and exploration.

Kurzfassung

Lichtsignale spielen eine wesentliche Rolle bei der Steuerung des frühen Entwicklungsprozesses höherer Pflanzen, der als Photomorphogenese bezeichnet wird. Die Entwicklung von Keimlingen, die Photosynthese betreiben können, erfordert die Integration sowohl von Licht als auch von retrograden biogenen Signalwegen. Die Transkriptionsregulation ist ein zentraler Mechanismus, der durch ein dynamisches Zusammenspiel von Transkriptionsfaktoren und regulatorischen Proteinen gesteuert wird, die die Genexpression akkurat modulieren. Trotz der umfangreichen Charakterisierung von Transkriptionsfaktoren und Regulatoren innerhalb des Lichtsignalwegs sind ihre komplizierten Interaktionen noch weitgehend unbekannt. Mittlerweile hat eine Vielzahl von noch nicht eingehend erforschten pflanzlichen Transkriptionsfaktoren aufgrund ihrer zentralen Rolle bei der Orchestrierung der lichtgesteuerten Entwicklung Aufmerksamkeit erregt. Unter diesen ist die B-Box-Familie (BBX) von Transkriptionsfaktoren, die sich durch das Vorhandensein von Zink-Finger-BBX-Domänen in ihrer N-terminalen Region auszeichnen, besonders hervorzuheben. BBX-Proteine spielen eine zentrale Rolle in regulatorischen Netzwerken, die verschiedene Wachstums- und Entwicklungsprozesse steuern, darunter die Photomorphogenese der Keimlinge, die photoperiodische Regulation der Blüte, die Vermeidung von Schatten und die Reaktion auf verschiedene biotische und abiotische Stressfaktoren.

In einer früheren Studie, in der die Reaktion auf hohe Lichtintensität (HL) und biogene Signale untersucht wurde, wurde BBX14 neben GLK1 in einem Kernmodul identifiziert. Unter Verwendung von Inhibitoren, die die Chloroplastenentwicklung hemmen, wurde in dieser Dissertation aufgedeckt, dass GLK1 den Promotor von *BBX14* direkt bindet, was durch Chromatin-Immunpräzipitations-Sequenzierung belegt wurde. Darüber hinaus deutete eine RNA-Sequenz-Analyse auf eine mögliche Rolle von BBX14 bei der Regulierung der zirkadianen Uhr hin. Weiterhin wurde festgestellt, dass BBX14 bei frühem Lichteinfall zur Chlorophyllbiosynthese beiträgt, die Photomorphogenese fördert und die Akkumulation des Chlorophyllvorläufers Pchlide im Dunkeln beeinflusst. Außerdem führte ein Knockout von *BBX14* zu einem langen Hypokotyl-Phänotyp, der von retrograder Signalübertragung abhängig ist, ähnlich wie bei der *glk1* Mutante. Bemerkenswert war auch, dass die Expression von BBX14 und BBX15 während der biogenen Signalübertragung von GUN1 abhängig war. Bei der Untersuchung der Rolle von BBX14 und BBX15 bei der biogenen Signalübertragung vom GUN-Typ wurde festgestellt, dass die Überexpression von BBX14 oder BBX15 unter

Norflurazon-Bedingungen zu einer De-Reprimierung der *CA1* Expression führte, während die Expression vom *LHCB1.2*-Markergen unbeeinflusst blieb. Schließlich wurde festgestellt, dass BBX14 für die Anpassung der Pflanzen an HL-Stress entscheidend ist.

Zusammenfassend lässt sich sagen, dass sich BBX14 als eine zentrale Komponente in der Integration biogener Signale downstream vom GUN1/GLK1-Moduls etabliert hat. Eine etablierte Bedeutung in der Keimlingsentwicklung und ein aufkeimendes Potenzial in der Plastiden-zu-Kern-Signalübertragung machen BBX14 zu einem vielversprechenden Kandidaten für die weitere Charakterisierung und Erforschung pflanzlicher Transkriptionsfaktoren.

1. Introduction

1.1. General elements of retrograde signaling

In higher plants, the plastid genome contains fewer than 100 open reading frames. The majority of the over 3000 polypeptides found in the photosynthetically active plastids called chloroplast are transcribed from nuclear-localized genes and imported post-translationally into the chloroplast. The nucleus, on the other hand, harbors genes crucial for chloroplast gene expression, such as components of the transcription and translation machinery, proteins constituting the protein import apparatus as well as the photosynthetic machinery (Kleine et al., 2009; Richter et al., 2023). Therefore, effective organelle biogenesis and metabolism require coordinated gene expression across eukaryotic cell compartments (Archibald, 2015). Proper assembly of multiprotein complexes of mixed genetic origin relies on the coordination of organellar gene expression (OGE) and nuclear gene expression (NGE) at multiple levels (Zhang et al., 2023). Given the limited number of chloroplast-encoded proteins, mainly involved in OGE and photosynthesis, precise coordination of gene expression between the plastid and the nucleus is pivotal for the efficient assembly of protein complexes (Gollan et al., 2015). This coordination is a multifaceted two-way process involving both anterograde signaling, in which nuclear genes directly control OGE, and retrograde signaling (RS), where information about the chloroplast's development and metabolic state is transmitted to the nucleus to modulate NGE of chloroplast-localized proteins appropriately (Chi et al., 2013; Terry & Smith, 201).

The control of NGE via retrograde signals plays a pivotal role in establishing the photoautotrophic lifestyle and efficient allocation of resources under conditions of reduced organelle metabolic function (Nott et al., 2006). In later stages of development, RS may adjust NGE in response to changes in chlorophyll biosynthetic flux or modulate expression in response to alterations in photosynthetic flux or damage to chloroplasts caused by high irradiance (Koussevitzky et al., 2007; Martin et al., 2016). Consequently, intracellular communication between organelles is of paramount importance for maintaining the appropriate balance of gene expression in a dynamic environment, particularly in consideration of the effects of abiotic stress factors. (Leister et al., 2014; Leister et al., 2017). The close interplay between plastids and nucleus, and thus the interdependence between chloroplast and NGE, is further highlighted by the fact that expression of several nuclear-encoded photosynthetic genes is significantly reduced in the absence of functional chloroplasts (Nott et al., 2006). Similar effects are observed when inducing carotenoid deficiency with the herbicide norflurazon.

Furthermore, inhibiting chloroplast development by arresting plastid gene expression (PGE) through chloramphenicol treatment in turn inhibits nuclear photosynthetic gene expression (Oemuller et al., 1986). Together, these findings suggest a significant interdependence between chloroplast and nuclear gene expression.

Almost over three decades ago, the idea of a plastid-generated factors triggering retrograde signaling was proposed. Subsequent genetic and biochemical studies in a variety of organisms have established multiple communication pathways between chloroplasts and the nucleus. However, the components of these pathways remain incompletely understood up to date. (Richter et al., 2023). Retrograde signals are thought to originate from four main sources: (i) the tetrapyrrole pathway, (ii) OGE, (iii) reactive oxygen species (ROS), or (iv) the redox state of the organelle (Leister et al., 2014). Indeed, while the conventional understanding of plastid signaling implicated minute amounts of signaling molecules, recent years have seen a shift in this perspective. It's now suggested that alterations in the concentrations of chloroplast metabolites could also influence NGE regulation. Over the past five years, five chloroplast metabolites have emerged as potential retrograde signals: (i) heme; (ii) phosphonucleotide PAP (3′-phosphoadenosine 5′-phosphate); (iii) β-cyclocitral (β-CC), an oxidation byproduct of β-carotene; (iv) methylerythritol cyclodiphosphate (MEcPP), a precursor of carotenoids, and consequently, of β-carotene; and (v) cleavage product(s) of ζ-carotene and/or phytofluene (Kleine & Leister, 2016). Metabolites are strong candidates for RS mediators due to their reflection of organelle metabolic states, although nucleic acids, ROS, and transcription factors have also been implicated (Sun et al., 2011). Thus, alternations in the metabolic profile of the cytosol triggered by the organelles could well be used by the cell to adjust NGE, either by using a metabolite directly as a signaling molecule or by converting an appropriate metabolite into an active signaling molecule in the cytosol (Leister et al., 2012). Two principal modes of RS molecule transfer - passive diffusion and active transport - add complexity to the signaling cascade. While the classical scenario proposes that signaling factors are generated within organelles, exported, traverse the cytosol, and act in the nucleus, recent research challenges this view (Leister, 2012). Although several such putative messenger molecules have been identified, their role and function often intertwine with other pathways outside of RS, making them difficult to study independently of one another (Kleine & Leister, 2013).

Changes in the developmental or metabolic state of chloroplasts or mitochondria can have profound effects on NGE, resulting in significant changes in transcript profiles and cell development. Moreover, it's intriguing that nuclear genes encoding chloroplast proteins generally exhibit a degree of co-regulation, regardless of their specific biochemical functions

(Leister, 2012), such as those encoding photosystem subunits, thereby underscoring the dual role of photosynthesis as both a stimulus and a target of retrograde regulation (Kleine et al., 2021). Furthermore, a comprehensive analysis of transcript profiles in the model organism *Arabidopsis thaliana* (hereafter Arabidopsis) revealed that genes relevant to chloroplasts and mitochondria are coordinated in their activity (Leister et al., 2011). This coordination extends to gene sets involved in organellar energy production or OGE within each organelle and in the nucleus. Additionally, this highlights the presence of dynamic transcriptional networks, both between and within organelles (Leister et al., 2011). These networks dynamically adjust organelle activity in response to changes in cellular energy levels and environmental stresses (Barkan, A., & Goldschmidt-Clermont, M., 2000; Chi et al., 2013).

As mentioned above, retrograde signaling plays a critical role in coordinating chlorophyll biosynthesis with the expression of nuclear-encoded chlorophyll-binding proteins, such as LHCA and LHCB proteins. Moreover, over the years, compiling evidence have suggested that precursors of the chlorophyll biosynthesis, namely Mg-protoporphyrinIX (Mg-protoIX), and Mg-protoporphyrinIX-methylesters (Mg-protoIXme), could act as regulators of NGE (Kleine et al., 2009). Studies on *C. reinhardtii* and higher plants have shown that the accumulation of porphyrin intermediates between protoIX and Mg-protoIXme is crucial for repressing *LHCB* transcripts. In addition, treatments inhibiting protochlorophyllide (Pchlide) synthesis in higher plants lead to the accumulation of Mg-protoIX and Mg-protoIXme, which affects *LHCB* mRNA levels (Nott et al., 2006). It's believed that impaired chloroplast function causes increase in Mg-protoIX accumulation, which may diffuse or be actively transported to the cytoplasm, where it binds to unidentified proteins, initiating regulation of nuclear-encoded photosynthetic genes (Strand et al., 2003). However, further investigation is required to determine the exact integration point between Mg-ProtoIX and PGE signals, as well as the identity of yet unknown cytosolic components involved in this signaling transduction pathway. Contrary to earlier assumptions by Strand et al., (2003), however, Mg-protoIX is no longer believed to function directly as a signaling molecule (Mochizuki et al., 2008; Moulin et al., 2008). Instead, perturbations in the tetrapyrrole synthesis due to mutations in key enzymes are believed to induce localized ROS production or alter plastid redox states, potentially mediating RS (Kleine et al., 2009). Thus, suggesting that reduction in protein synthesis rates or the synthesis of specific plastid proteins during early plastid development generate retrograde signals (Leister et al., 2014). However, OGE-dependent signaling was shown to persist in mature leaf tissues, as observed in mutants with defective components of the OGE machinery, for example the Arabidopsis lines lacking the plastid- and mitochondria-localized prolyl-tRNA

synthetase PRORS1 (Pesaresi et al., 2006; Leister and Kleine et al., 2016). When OGE is perturbed simultaneously in both mitochondria and chloroplasts, there is a more pronounced down-regulation of nuclear photosynthetic genes compared to treatments affecting OGE in only one organelle. For instance, the double mutant *prpl11mrpl11*, characterized by impaired ribosomal function in both plastids and mitochondria, consistently exhibited lower transcript levels than either the single mutants *prpl11* or *mrpl11* (Pesaresi et al., 2006). This indicates that both plastid OGE and mitochondrial OGE play roles in stimulating NGE under the specific growth conditions examined in the study (Leister et al., 2011). In addition to that, the regulation of NGE was found to involve synergistic contributions from both chloroplast and mitochondrial translation rates, as evidenced in studies on the plastid and mitochondrial ribosome deficient mutants *prpl11* and *mrpl11*, respectively (Leister et al., 2014).

1.1.1. GUN-type retrograde signaling

The *genomes uncoupled* (*gun)* mutants, identified through genetic screens involving chemical inhibitors, have played a crucial role in deciphering RS (Susek et a., 1993). Initially five mutants (*gun1–gun5*) were identified by their sustained expression of photosynthesis-associated nuclear genes (*PhANGs*), such as the marker gene *LHCB* coding for light-harvesting chlorophyll a/b-binding proteins of photosystem (PS) II despite impaired plastid development due to stressors such as norflurazon (NF) and lincomycin (LIN), which inhibit carotenoid biosynthesis and protein synthesis in the plastid, respectively (Susek et al., 1993). Over the years other mutants that display such distinctive molecular phenotype have been identified, like for instance the *gun6-1D* mutant overexpressing the plastid ferrochelatase 1 (FC1), however its behavior under LIN requires further investigation (Richter et al., 2023). Among these mutants, however, *gun1* exhibits distinctive *PhANG* expression under both LIN and NF treatment, whereas *gun2–gun5* respond only to NF treatment (Leister & Kleine, 2016). Since *GUN2–GUN6* genes encode for proteins involved in the regulation of tetrapyrrole biosynthesis, it is feasible that disruptions in those pathways could result in the accumulation of intermediates that, when exported out of the chloroplast, alternate the expression of nuclear-encoded genes. The *gun* mutants, thereby reveal the indirect or intermediate role of Mg-protoIX in RS, as mutations in *GUN2*, *GUN3*, *GUN4*, and *GUN5* (all linked to porphyrin biosynthesis), lead to decreased Mg-protoIX accumulation and consequently to impaired plastid control of NGE (Mochizuki et al., 2001; Larkin et al., 2003).

As mentioned above, the *gun1* mutant stands out as a unique case among the classical *gun* mutants due to its LIN-specific phenotype. GUN1's exact molecular function remains enigmatic (S. Honkanen & I. Small, 2022), although its pentatricopeptide repeat (PPR) domain suggests an RNA-binding role (A. Barkan & I. Small, 2014), GUN1 has been associated with potential retrograde signals involving tetrapyrrole biosynthesis, specifically heme, as it seems to directly bind tetrapyrroles (Colombo et al., 2016; Wu et al., 2018; Shimizu et al. 2019). The involvement of heme in GUN1-mediated RS still requiring further experimental proof, as its role in RS currently appears controversial (Richter et al., 2023). What makes it even more interesting is that absence of GUN1 evokes a specific response under LIN treatments, which is not the case in the other initially identified *gun* mutants, and GUN1 itself is not connected to the tetrapyrrole biosynthesis pathways as a PRR protein in any way (Koussevitzky et al., 2007). Instead, its RNA-binding function is thought to manifest itself in RNA editing during chloroplast-to-nucleus signaling as shown in NF-treated *gun1* mutants that exhibit altered efficiency of plastid-RNA editing (Zhao et al., 2019).

GUN1's crucial role in the retrograde signaling cascade is further highlighted by its ability to directly interact with heme and other metal-porphyrins (Shimizu et al., 2019), which affects the tetrapyrrole biosynthesis pathway and enhances FC1 chelatase activity (Woodson et al., 2011). This observation supports the hypothesis that GUN1's signaling role may manifest through changes in tetrapyrrole metabolism (Shimizu et al., 2019), proposing tetrapyrroles as crucial mediators of a singular biogenic chloroplast-to-nucleus signaling pathway (Terry et al., 2013). It has been proposed that a specific heme pool generated by flux through FC1 functions as a positive signal in the *gun1* mutant, with GUN1 acting as a bottleneck for heme signal generation (Shimizu et al., 2019). More recently, the identification of the dominant *gun6* mutant, characterized by increased FC1 activity, suggests a central role for heme synthesized by FC1 as a retrograde signal or its precursor (Woodson et al., 2011).

Although there has been significant progress in this direction, it remains challenging to elucidate the detailed signaling mechanism and confirm the exclusivity of the tetrapyrrole-mediated GUN signaling pathway. The *gun1* mutant has been suggested to operate independently from tetrapyrrole-mediated GUN signaling, which complicates the pathway's comprehensive understanding. Experimental evidence shows that changes in GUN1 levels affect tetrapyrrole metabolism, leading to alterations in NGE, with GUN1 overexpression restricting the flow through both branches of the tetrapyrrole pathway thereby affecting the accumulation of Pchlide and heme (Shimizu et al., 2019).

1.1.2. *gun* mutants and beyond

The GUN1 protein is a unique candidate for examining retrograde signaling in the context of chloroplast development. The name-giving *gun* phenotype that arises when inhibitors of OGE like LIN are applied, however, also holds true for mutants that are not lacking any of the GUN proteins involved in tetrapyrrole biosynthesis (GUN2–GUN5). For instance, the *glk1glk2* (*golden2-like 1 golden2-like 2*) double mutant also displays a subtle *gun* phenotype (Waters et al., 2009). The *GLK1* and *GLK2* genes, which are essential for nuclear photosynthetic gene expression and chloroplast development, encode a pair of partially redundant nuclear-localized transcription factors in land plants. Notably, GLK1 and GLK2 play crucial roles in the expression of nuclear genes encoding proteins involved in photosynthesis (Waters et al., 2009). It has been observed that the *glk1glk2* double mutant accumulates abnormal levels of tetrapyrroles, suggesting a potential link between tetrapyrrole intermediates and the phenotype associated with mutants in the GUN pathway (Waters et al., 2009). Interestingly, among the original five *gun* mutants, *gun1–gun4* are known to exhibit disruptions in tetrapyrrole synthesis, suggesting that changes in the levels of tetrapyrrole intermediates could contribute to the *gun* phenotype. This has been investigated by examining the response of the pale green *glk1glk2* mutant to treatment with NF or LIN, which are known to induce the *gun* phenotype indicating its partial derepression of nucleus-encoded photosynthesis genes in response to NF or LIN treatment (Fitter et al., 2002; Waters et al., 2009). In the *glk1glk2* double mutant, genes encoding proteins associated with light-harvesting and chlorophyll biosynthesis are notably downregulated, resulting in a pale green phenotype (Waters et al., 2009). This also hints at the idea that perturbations in the tetrapyrrole pool may influence the GUN pathway. Interestingly, overexpression of either GLK1 or GLK2 effectively complements this defect, leading to *LHCB* transcript levels approximately 2-fold higher than those observed in wild-type adult plants (Kleine and Leister, 2016).

Moreover, perturbations in OGE, induced either by inhibitors or mutations such as *mterf6-1* or *prors1-2*, have been found to downregulate *GLK1* and *GLK2* transcripts, further emphasizing the intricate regulatory network involving these transcription factors and their role in coordinating organellar gene expression (Kleine & Leister, 2013). This notion is further supported by the finding that overexpression of GLK1 and GLK2 following either NF or LIN treatment evokes a strong *gun* phenotype (Leister & Kleine, 2016). This, together with the finding that disturbances in OGE cause down-regulation of *GLK* transcripts hints that this repression is required for an operational signaling event under disadvantageous conditions. So

far, the overexpression of both GLK1 and GLK2 has been independently shown to result in gun phenotype both under NF and LIN treatment with oeGLK2 displaying a weaker one than oeGLK1 (Leister & Kleine, 2016; Kleine, 2016) . Thereby setting them apart from the other *gun* mutants, which display *gun* phenotypes only under NF conditions and not under LIN conditions, but rather akin to the phenotype of the *gun1* mutant (Leister & Kleine, 2016).

In Arabidopsis lines overexpressing GLK1 or GLK2, transcript levels of genes encoding key enzymes in the tetrapyrrole pathway, such as *GUN4*, *GUN5*, and *PORA-C*, are notably induced, suggesting a potential increase in flux through this pathway. This increased flux is reflected in elevated chlorophyll levels observed in GLK overexpression lines (Waters et al., 2009). Consequently, two distinct scenarios may explain the *gun* phenotype observed in lines overexpressing GLKs: first, alterations in tetrapyrrole pools; and second, chloroplast signals received by GLK transcription factors, that prompt the activation of their down-stream target genes, which include *LHCB* and tetrapyrrole genes. Conversely, in unfavorable conditions where GLKs are downregulated, their target genes are consequently downregulated as well (Martin et al., 2016).

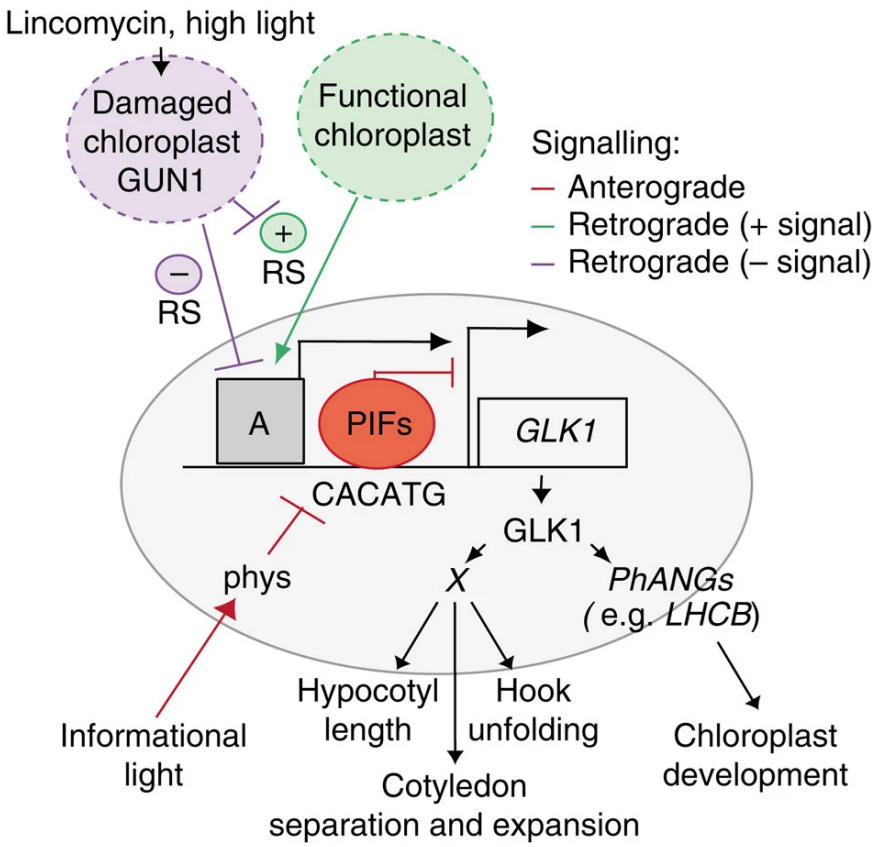

Figure 1. The regulation of photomorphogenesis involves antagonistic interactions between PIF-mediated light signaling and GUN1-mediated retrograde signaling (modified after Martin et al., 2016).

PIFs bind to the GLK1 promoter via a PBE motif (CACATG), leading to direct repression of GLK1 expression in dark conditions. However, there are unidentified transcriptional activators, represented by A, which are poised on the promoter and constitutively activate GLK1 expression. Upon receiving informational light signals, activated phytochromes induce the degradation of PIFs (red lines), thereby derepressing GLK1 expression through the action of A. Subsequently, GLK1 directly promotes the expression of photosynthesis-associated nuclear genes (PhANGs) and potentially other genes (referred to as 'Gene(s) X') involved in seedling development. Disruption of chloroplast integrity by factors like lincomycin or high light triggers the emission of a negative retrograde signal (purple line) from dysfunctional chloroplasts. This negative RS induces GUN1-mediated repression of GLK1 expression by diminishing the effectiveness of A. Conversely, functional chloroplasts may produce a positive retrograde signal (green line) essential for the expression and/or activity of A. However, when chloroplast function is compromised, GUN1 facilitates the disruption of this positive RS.

It is widely speculated that other transcription factors may also play significant roles in plastid signaling pathways, with GLK1 and GLK2 being proposed as strong candidates for such involvement. Notably, GUN-type retrograde signaling influences nuclear transcription factors such as ELONGATED HYPOCOTYL 5 (HY5) and the GLKs, as well by the photoreceptor CRYPTOCHROME 1 (CRY1) impacting the expression of genes involved in seedling and chloroplast development, thereby establishing a link between light signaling and RS as means

to regulate NGE (Li et al., 2022). The most prominently studied is the relationship between GUN1-mediated RS and GLK1, whose expression is inhibited in response to PHYTOCHROME-INTERACTING FACTOR (PIF)-mediated light signals (Martin et al., 2016). Upon exposure to light, the degradation of PIFs - induced by phytochromes - alleviates the repression of GLK1 expression, thereby initiating the transition from skotomorphogenesis to photomorphogenesis, provided that the plastid remains functionally intact. This allows GLK1 to regulate the expression of photosynthetic genes (i.e. *LHCB* gene family) and potentially other down-stream target genes involved in various aspects of photomorphogenesis (i.e. cotyledon unfolding and hypocotyl elongation). However, in instances of plastid damage (i.e. lincomycin and/or high light), RS is activated and counteracts the light-induced de-repression of GLK1. This occurs through a GUN1-facilitated, PIF-independent pathway, effectively dampening normal photomorphogenesis to protect the seedling under unfavorable conditions. Concurrently, the chloroplast acts as a sensor of excessive light levels (when the phytochrome/PIF system becomes saturated), preventing potential irreversible damage (Martin et al., 2016; Leivar et al., 2009). Therefore, the coordination of external light cues together with internal chloroplast integrity is essential for promoting photomorphogenesis. The phytochrome/PIF light signaling system monitors transitions between darkness and light, as well as the quality and periodicity of light, to optimize light-regulated development. This mechanism serves to protect the plant from photo-oxidative damage by minimizing the exposure of tissues to harmful radiation. Specifically, the GUN1/GLK1-mediated RS antagonizes phytochrome/PIF signaling, leading to the inhibition of cotyledon separation and expansion when chloroplast integrity is compromised. This effectively reduces the surface area exposed to potentially harmful irradiance levels. Although the exact mechanism remains unclear, it does not involve the re-accumulation of PIF proteins under these conditions, suggesting the involvement of undefined components (Martin et al., 2016). Overall, the GUN1-mediated RS and the PIF-light signaling system converge together establishing a molecular framework that integrates phytochrome and retrograde signals at a central node to regulate NGE, thus providing new insight into how plants coordinate light responses with the status of the chloroplasts for optimal growth development and photosynthetic capacity (**Figure 1**).

Finally, recent evidence suggests that GUN1 may exert even greater influence on GLK1 protein by regulating its stability through ubiquitin-mediated proteolysis, a mechanism possibly more crucial than transcriptional regulation described above. Recent studies indicate that GLK1 participates in GUN1 signaling following chloroplast damage, together with BBX16, a BBX-type zinc-finger transcription factor, playing a role in this process. Mutations in *BBX16*

significantly alleviate the *gun1* phenotype induced by LIN treatment and suppress the *gun1*-like phenotype observed in GLK1 overexpressing lines (Veciana et al., 2022).

1.2. The BBX transcription factor family

Transcriptional regulation is a crucial mechanism that governs gene expression in plants. Mutations in transcription factors (TFs) often underlie informative phenotypes and many TFs have been identified that act as central regulators of various plant processes. TFs are proteins that initiate gene expression and typically harbor a DNA-binding domain (DBD) for specific DNA sequence recognition. Proteins that lack a DBD but interact with DNA-binding counterparts to form transcriptional complexes, are also categorized as TFs.

The genome of Arabidopsis contains approximately 25.498 protein-coding genes (Arabidopsis Genome Initiative 2000), including a significant number of TFs, with analyses suggesting a count exceeding 2000 that encode TF (Riechmann et al., 2000). Compared to organisms such as *Drosophila melanogaster* and *Caenorhabditis elegans*, which have similar genome sizes to Arabidopsis, the model land plant has a significantly higher number of TF genes, accounting for 5-10% of the total genes. This exceeds the TF ratios in *D. melanogaster* (4.7%) and *C. elegans* (3.6%), although it remains comparable to that of humans (6.0%) (Duvuluri et al., 2003; Guo et al., 2005; Mitsuda & Ohme-Takagi, 2009).

Arabidopsis TFs are also characterized by a greater quantity and diversity of DBDs, hinting at a significant role in plant transcriptional regulation greater than that of other species. Their complexity arises from a diverse range of gene families with varying DNA-binding specificities. Although significant efforts have been made to identify TF functions, many of their roles remain unclear.

Transcription factors in Arabidopsis are abundant and diverse, comprising numerous gene families. For example, zinc-finger TFs make up approximately 20% of all. Many are specific to plants (ca. 45 %) and possess DBDs unique to this group. Plant-specific families include AP2-ERF, NAC, Dof, YABBY, WRKY, GARP, TCP, SBP, ABI3-VP1 (B3), EIL, and LFY. Additionally, Arabidopsis TFs are often organized into gene families with shared DBDs, such as AP2-ERF and NAC, resulting in large loci counts (Riechmann et al., 2000). Evolutionary processes have led to significant diversification in each eukaryotic lineage, resulting in the emergence of new proteins that regulate lineage-specific activities (Riechmann et al., 2000). The plant zinc finger family is a prime example of such diversification. It is a large group of proteins that can be further categorized into distinct subfamilies.

1.2.1. Classification, phylogeny, and structural complexities among BBX proteins

Zinc-finger proteins have finger-like protrusions that can bind metals such as zinc, and they exhibit diversified functionalities. These proteins often have specialized interaction domains and are known for their ability to bind DNA, RNA, or other proteins (Khanna et al., 2009). Additionally, certain Zinc-finger proteins, exemplified by the B-box (BBX) proteins, are presumed to facilitate protein-protein interactions (Borden et al., 1995; Rushton et al., 1995; Yanagisawa, 1995; de Pater et al., 1996; Torok and Etkin, 2001). The BBX family is a subset of zinc-finger proteins that includes one or more B-box domains. These domains are characterized by specific tertiary structures that are stabilized through zinc ion binding (Klug and Schwabe, 1995). Although the precise biochemical functions of BBX proteins are still unknown, on molecular level they are believed to play a role in modulating protein-protein interactions, particularly within transcriptional complexes (Khanna et al., 2009).

The B-box domain is present in over 1500 proteins across multicellular and certain unicellular eukaryotes (Meroni and Diez-Roux, 2005). In plant systems it appears in the N-terminus either as a single B-box or in tandem repeats designated as B-box1 (B1) and B-box2 (B2), respectively (Massiah et al., 2006, 2007; Short and Cox, 2006), and with some having a CCT (CONSTANS, CO-like, and TOC1) domain in the C-terminus (Griffiths et al., 2003; Robson et al., 2001). The classification of BBX proteins into structural groups has shed light on their diversity. A recent phylogenetic analysis in Arabidopsis identified a gene family of 32 members encoding BBX proteins, named from BBX1 to BBX32 (Khanna et al., 2009). This study classified AtBBX proteins into five structural groups (I–V). The AtBBX members of structure group I (BBX1 to BBX6) contain two B-boxes in tandem (B1 and B2) along with a CCT domain. In these proteins, the B1 domain is located N-terminal to the B2 domain and is separated by 5 to 20 residues. Similarly, the AtBBX members of structure group II (BBX7 to BBX13) also contain B1, B2, and CCT domains, with slight differences in the consensus sequences of the B2 domain compared to structure group I (Chang et al., 2008). Structure group III (BBX14–BBX17) consists of AtBBX members with a single B-box domain associated with a CCT domain. On the other hand, structure group IV (BBX18 to BBX25) comprises BBX proteins with B1 and B2 domains but lacking the CCT domain. Lastly, members of structure group V (BBX26–BBX32) carry a single B-box domain without a CCT domain (Khanna et al., 2009). This classification framework aids in understanding the structural nuances and functional implications within the BBX protein family (Riechmann et al., 2000; Klug and Schwabe, 1995). This clustering of BBX proteins into five structural groups was also confirmed by a recent study in rice (Huang et al., 2012). In Arabidopsis, 21 out of the 32 BBX proteins

possess tandem B-boxes (BBX1–13 and BBX18–25), while the remaining 11 (BBX14–BBX17 and BBX26–BBX32) contain a single B-box. Similarly, in rice (*Oryza sativa*), 17 out of the 30 BBX proteins feature tandem B-boxes at their N termini (Crocco & Botto, 2013). This shared structural feature between Arabidopsis and rice underscores the conservation of the B-box domain in plants (Huang et al., 2012).

The structural analysis of BBX proteins revealed notable similarities and differences among the various structure groups. For instance, there is a high sequence similarity between the B1 domains of structure groups I, II, and IV, which have double B-boxes, and the single B-box domains of structure groups III and V. However, the B1 consensus domain of structure group V has one fewer amino acid in the 7th position compared to the other structure groups. Despite this difference, the number of cysteine residues in the B1 consensus domains remains conserved across all structure groups, indicating a retained topology among BBX proteins (Crocco & Botto, 2013; Torok et al., 2001). Similarly, while the topology of the B2 domain is conserved across all structure groups, there is a low percent sequence identity between structure groups I, II, and IV (Tamura et al., 2011). This suggests an early evolutionary origin of the B2 domain compared to the B1 domain, with the B2 domain of structure group I likely arising independently from those of structure groups II and IV likely originating from segmental duplications and internal deletion events in plant genomes. Despite these variations, the conservation of topology between the B1 and B2 consensus sequences underscores the essential role of this domain in molecular function.

Amino acid alterations in the consensus sequences of B1 and B2 domains have been linked to dysfunctional proteins with implications for plant development. This highlights the importance of maintaining the conservation of B-box domains across green plants, suggesting that BBX proteins' functional diversification may be driven by conserved sequences outside of the B-box domain. Additionally, seven novel motifs (M1 to M7) were identified, each shared by BBX members within the same structure group. For instance, the M1 motif found in BBX members of structure group I contains a conserved valine next to a proline (VP pair), known to be critical for BBX protein-protein interaction. Interestingly, this VP pair was also conserved at the C-terminus in a significant proportion of BBX members across other structure groups (Gangappa & Botto, 2014). These findings suggest that while some BBX proteins may have undergone domain loss in recent evolutionary events, they still retain other common characteristics specific to their structure group. Furthermore, phylogenetic analysis revealed that BBX proteins within the same structure group were primarily classified based on amino acid similarity, with secondary classification based on the organization of B-box and CCT domains.

The five BBX structure groups are thought to have evolved constrained by the conservation of amino acid sequences in the two B-boxes but radiating variation into nuclear-localization signal motif (NLS) and the novel motifs (M1–M7) of each structural group, suggesting that these features serve as the functional basis for the BBX protein diversity in green plants (Khanna et al., 2009; Crocco & Botto, 2013).

1.2.2. BBX proteins are involved in both cooperative and antagonistic interactions during various physiological processes

BBX proteins are encoded by highly conserved genes found in multicellular species, including blue-green algae and mosses, implying an ancient origin of approximately one billion years ago, that predates land plant colonization by over 450 million years. The widespread presence of BBX genes across various species, spanning from algae to monocots and dicots, indicates an ancient origin of these genes. While most green algae typically possess a single B-box motif, the identification of two B-box motifs in the unicellular green alga *C. reinhardtii* implies that the duplication event of the B-box likely occurred prior to the colonization of land plants (Kenrick and Crane, 1997; Peers and Niyogi, 2008). The significant expansion of BBX proteins throughout evolution, coupled with their high conservation across the plant kingdom, suggests that BBX proteins may have played essential roles in the adaptation of land plants. This evolutionary trajectory underscores the fundamental importance of BBX proteins in the evolutionary history and diversification of plant species, especially regarding interaction with other TFs to regulate gene transcription.

As mentioned previously BBX-containing protein are hypothesized to play a role in modulating protein-protein interactions, particularly within transcriptional complexes (Brandao et al., 2009). Indeed, BBX proteins play a central role in transcriptional regulation, as evidenced by their physical interactions with the transcription factor ELONGATED HYPOCOTYL 5 (HY5) and HOMOLOG of HY5 (HYH), as the case with BBX22, 24 and 25 (Datta et al., 2008; Gangappa et al., 201; 2015). Site-directed mutations in B-box motifs, disrupt these interactions, emphasizing the significance of the B-box motif in mediating BBX-HY5 interactions. Functional divergence is exemplified by BBX proteins, which act both as transcriptional coactivators (e.g. BBX21 and BBX22) and corepressors (e.g. BBX24 and BBX25) of HY5-mediated transcriptional activity (Chang et al., 2008; Gangappa et al., 2015). Furthermore, epistatic analyses have revealed complex relationships between BBX proteins and another key regulator of seedling development CONSTITUTIVE PHOTOMORPHOGENIC1 (COP1) and

influence its activity (Gangappa & Botto, 2014). Some BBX proteins repress COP1 function, while others enhance it. For examples, BBX4, BBX20, BBX21, and BBX22 repress COP1 function (Yan et al., 2011; Chang et al., 2013), whereas BBX24 and BBX25 are known to enhance its function (Gangappa, Crocco, et al., 2013; Gangappa, Holm, et al., 2013). On the other hand, COP1 interacts with and facilitates the degradation of various BBX proteins, including CO (CONSTANS)/BBX1, BBX22, BBX24, and BBX25 (Datta et al, 2008a; Datta et al., 2008b; Crocco et al., 2010). This intricate regulatory network is contributed to by direct interactions between BBX proteins and COP1, or by the recruitment of BBX proteins by COP1 into nuclear speckles. The critical VP pair located at the C-terminus of BBX proteins is essential for their interaction with COP1. In plants, COP1 functions as an E3 ubiquitin ligase, suppressing light signaling by ubiquitylating and subsequently degrading target photoreceptors and downstream TFs. Since plants lack TRIM/RBCC proteins, which are found in animals and possess E3 ubiquitin ligase activity (Lorick et al., 1999), it has been proposed that the BBX-COP1 protein complex serves as the functional equivalent of E3 ubiquitin ligase activity in green plants (Meroni and Diez-Roux, 2005). Phylogenetic analysis suggests that 45% of the BBX proteins analyzed possess the VP pair, making them potential candidates to participate in BBX-COP1 protein complexes. In addition to the B-box domain, the CCT domain and the VP pair in BBX proteins also have important roles in protein-protein interactions. For instance, BBX1, BBX16, and other BBX proteins containing the CCT domain interact with DNA binding proteins such as NUCLEAR FACTOR-Y (NF-Y) through the CCT domain (Cao et al., 2014). This interaction facilitates nuclear localization, and the CO/NF-Y complex binds to conserved CCAAT *cis*-elements in promoter regions (Vaishak et al., 2019).

The diverse roles of BBX proteins in seedling (de)-etiolation, hypocotyl growth, anthocyanin production, chlorophyll accumulation, lateral root growth, cotyledon unfolding and other developmental processes are underscored by their interplay, which is evidenced by mutual enhancement or inhibition (Gangappa & Botto, 2014). On physiological levels, BBX proteins have diverse functions in regulating the transition from skotomorphogenesis (or etiolation) to photomorphogenesis (or de-etiolation), with the former occurring in the dark and the latter in the light (Sullivan and Deng, 2003). In their natural environment, seeds germinating in soil experience complete darkness or very low light intensity, prompting them to undergo skotomorphogenesis as they emerge through the soil to reach light. Subsequently, exposure to light triggers the transition to photomorphogenic development (Frankhauser and Chory, 1997). Dark-grown seedlings exhibit elongated hypocotyls, unexpanded cotyledons with nonphotosynthetic etioplasts and apical hook that protects the apical meristem from damage

(Han et al., 2020). Conversely, exposure to light initiates photomorphogenic development, characterized by dampening of hypocotyl elongation, hook unfolding, and expansion of green cotyledons containing functional photosynthesis-driving chloroplasts to maximize light absorption. The ability to switch from etiolated/skotomorphogenic to de-etiolated/photomorphogenic state is essential for seedling survival. The process is initiated upon light perception and involves massive transcriptome changes, especially genes involved in photosynthesis, and is under tight temporal regulation (Ma et al., 2001; Shi et al., 2018; Tripathi et al., 2019; Jing & Lin, 2020).

Some members of the BBX protein family oppose each other in the context of skotomorphogenesis and photomorphogenesis, which distinguishes them from other TF families (**Figure 2**). For instance, it has been shown that BBX4, BBX11, BBX20, BBX21, BBX22 and BBX23 promote photomorphogenesis, whereas BBX18, BBX19, BBX24, BBX25, BBX28, BBX29 and BBX30–32 suppress photomorphogenesis (Datta et al., 2008; Chang et al., 2011; Holtan et al., 2011; Yan et al., 2011; Fan et al., 2012; Gangappa, Crocco, et al., 2013; Gangappa, Holm, et al., 2013; Gangappa & Botto, 2014; Wei et al., 2016; Xu et al., 2016; Zhang et al., 2017; Job et al., 2018; Lin et al., 2018 Xu et al., 2018; Heng et al., 2019; Wang et al., 2019; Song et al., 2020; Singh & Datta, 2022). This is supported by studies on mutants lacking BBX proteins resulting in various light-dependent phenotypes reflected in hypocotyl shortening or elongation. For instance, mutant seedlings lacking BBX24, BBX25, or BBX32 exhibit short hypocotyls in response to red, far-red, and blue light, indicating that these proteins suppress photomorphogenesis regardless of the photoreceptor type involved (Gangappa & Botto, 2014). Conversely, overexpression of BBX18 and BBX19 leads to longer hypocotyls compared to wild-type plants under continuous red and far-red light, which is not the case in seedlings devoid of BBX18 and BBX19, suggesting that these proteins may have redundant functions during de-etiolation (Indorf et al., 2007). BBX21 has been found to enhance the functions of both BBX20 and BBX22 while suppressing the function of BBX32. BBX32, on the other hand, physically interacts with BBX21 and diminishes HY5-mediated transcriptional activity (Tripathi et al., 2017). Intriguingly, both BBX21 and BBX22 directly interact with HY5, boosting its activity. Moreover, the epistatic interaction observed between BBX24 and BBX25 indicates that they enhance each other's function but can also independently regulate seedling photomorphogenesis. BBX24 and BBX25 act as transcriptional corepressors of HY5, forming inactive heterodimers with it and consequently reducing its transcriptional activity on target genes like *CHI* and *CHS*, which are involved in

anthocyanin biosynthesis (Gangappa, Crocco, et al., 2013; Gangappa, Holm, et al., 2013; Job et al., 2018; Yadukrishnan et al., 2018).

Light receptor cells are instrumental in perceiving and transmitting light signals to key light regulatory proteins, including HY5, HYH, COP1, and PHYTOCHROME INTERACTING FACTORS (PIFs), which collectively orchestrate the regulation of skoto- and photomorphogenesis (Vaishak et al., 2019). At the core of the light-dependent signal transduction network governing this transition from skoto- to photomorphogenesis lies the E3 ubiquitin ligase COP1. COP1 acts as a central integrator of signals from photoreceptors and orchestrates the activity of various downstream components like HY5 (Podolec & Ulm, 2018; Han et al., 2020), GLK1 and GLK2 (Waters et al., 2009). In general, HY5 and HYH function as positive regulators of photomorphogenesis, while COP1 and PIFs act as negative regulators in this intricate process (Osterlund et al, 2000; Jiao et al., 2007; Kami et al., 2010). Under light conditions, HY5 and HYH operate effectively, but in darkness, the COP1/SUPPRESSOR OF phyA-105 (SPA) complex orchestrates their targeted degradation, concomitant with the cytosolic partitioning of COP1 in light and its nuclear relocation in darkness (Osterlund et al, 2000). PIFs (PIF1, PIF3-8) accumulate predominantly in the dark and undergo light-induced degradation in a phytochrome-dependent manner (Jiao et al., 2007; Kami et al., 2010), exerting either inhibitory or activating effects on the expression of light-induced or light-repressed genes, respectively (Leivar et al., 2009; Zhang et al., 2013). The quadruple mutant *pifq*, lacking PIF1, PIF3, PIF4, and PIF5, exhibits a partially constitutively photomorphogenic phenotype in the dark, suggesting that PIFs promote skotomorphogenesis (Leivar et al., 2008; Shin et al., 2009). Upon exposure to light, active phytochromes induce the inactivation and degradation of PIFs via the 26S proteasome-mediated pathway. This process enables seedlings to initiate light-regulated gene expression and embark on a photomorphogenic developmental program (Leivar et al., 2008, 2009). The functional association of BBX proteins with PIFs in seedling photomorphogenesis is an emerging area of study. For instance, BBX23, regulated by PIF3, participates in the repression of hook unfolding during the dark-to-light transition. PIF1 and PIF3 directly regulate the transcription of BBX23 and HY5 by binding to their promoters (Zhang et al., 2017). BBX19, a negative regulator, facilitates the derepression of PIF4 and PIF5 by recruiting ELF3 to COP1 for degradation, revealing the complex interplay between BBX proteins and PIFs in seedling photomorphogenesis (Xu et al., 2013).

The HY5-COP1 regulatory module is pivotal for the regulation of BBX proteins in photomorphogenesis (Xu, 2020). Almost all BBX genes possess light-regulated *cis*-elements on their promoters, crucial for their light-responsive expression, which directly respond to

photoreceptors, especially phytochromes. Additionally, G-box and its variants, binding sites for HY5 and PIFs, are commonly found on BBX promoters (Lee et al., 2007; Yilmaz et al., 2011). This collective regulation forms a central hub integrating complex signaling networks of light and hormonal pathways, finely tuning early developmental events like seedling photomorphogenesis through modulation of downstream factors (Gray, 2004; de Wit et al., 2016). BBX proteins, like BBX21 and BBX22, interact with HY5, influencing its transcriptional and post-transcriptional regulation and promoting photomorphogenesis. BBX23, acting redundantly with BBX22, cooperates with HY5 to positively regulate photomorphogenesis (**Figure 2**). Conversely, negative regulators such as BBX24, BBX25, and BBX32 rely on HY5 for their function. BBX24 hinders HY5 from binding to its target promoters, while BBX25 inhibits the transcriptional regulation of BBX22 by HY5. BBX28, another negative regulator, interacts with HY5 and impedes its binding on downstream targets, akin to BBX24's mechanism. The intricate relationship between COP1 and BBX proteins, further highlights the involvement of the HY5-COP1 module in BBX regulation (Holm et al., 2001; Holtan et al., 2011; Jiang et al., 2012; Gangappa, Crocco, et al., 2013; Job et al., 2018, Lin et al., 2018).

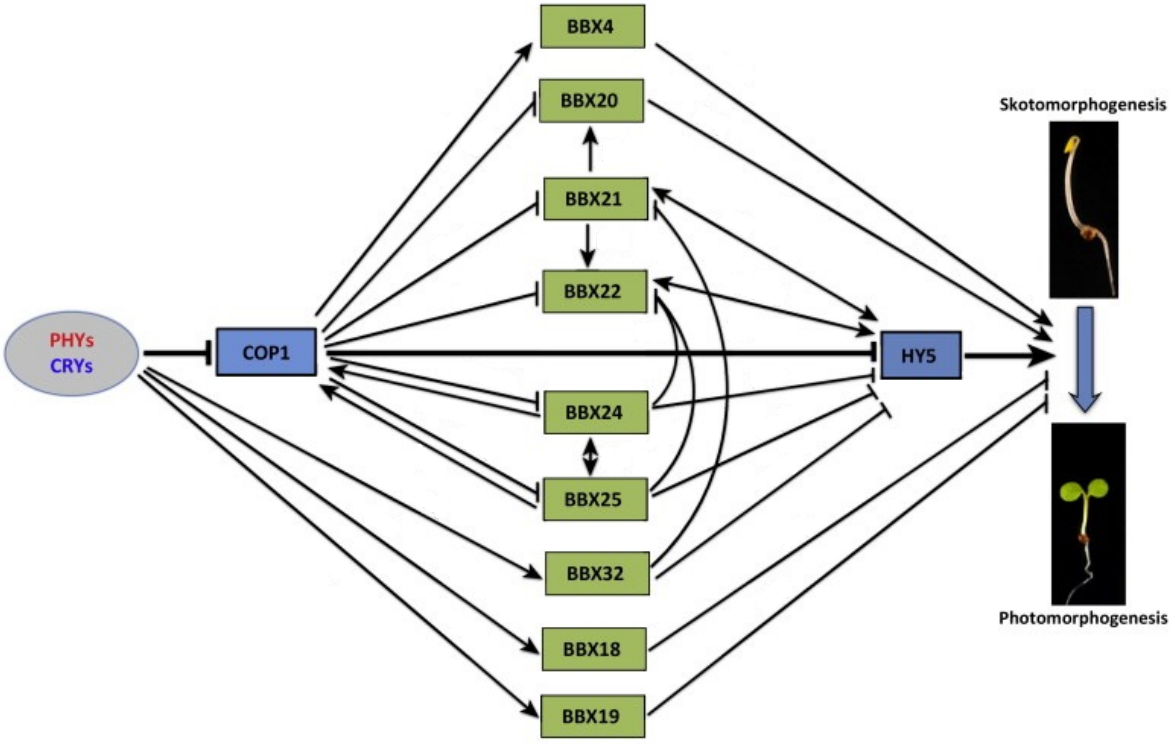

Figure 2. BBX transcription factors on the interface between light perception and photomorphogenesis (adapted after Gangappa & Brotto, 2014).

BBX proteins play crucial roles in seedling photomorphogenesis by integrating light signals perceived by phytochrome (PHYs) and cryptochrome (CRYs) photoreceptors through the COP1 and HY5 signaling pathway. Specifically, BBX4 is involved in integrating red light signals, while BBX20 integrates both red and blue light signals. The remaining BBX proteins integrate signals from red, far-red, and blue light. BBX4, BBX20, BBX21, and BBX22 promote photomorphogenesis by inhibiting COP1 function. BBX4 and BBX20 interact directly with COP1, whereas BBX21 and BBX22 colocalize with COP1. Additionally, BBX21 and BBX22 directly interact with HY5, enhancing its functions, which leads to the inhibition of hypocotyl growth and increased pigment accumulation. Concurrently, HY5 enhances the functions of BBX21 and BBX22. Moreover, BBX21 enhances the functions of both BBX20 and BBX22 to further inhibit hypocotyl growth. In contrast, BBX18, BBX19, BBX24, BBX25, and BBX32 act as inhibitors of seedling photomorphogenesis. BBX24 and BBX25 directly interact with HY5 and COP1, thereby suppressing HY5 function and enhancing COP1 action. Through a negative feedback mechanism, COP1 degrades both BBX24 and BBX25. On the other hand, BBX32 directly interacts with BBX21, forming inactive heterodimers and reducing HY5 transcriptional activity, thus exhibiting antagonistic functions with HY5.

The intersection of BBX proteins with hormonal pathways further complicates the regulatory network governing seedling photomorphogenesis. Hormonal signaling pathways involving BBX proteins are not well understood, with limited evidence supporting their roles in brassinosteroid (BR) and gibberellin (GA) signaling. Members like BBX18 and BBX24 are known to be involved in GA signaling, influencing hypocotyl length, while BBX20 integrates

signals from both BR and light pathways, connecting them with photomorphogenesis. Additionally, BBX21 modulates ABA signaling and gibberellin catabolism, highlighting the intricate crosstalk between hormonal pathways and BBX-mediated photomorphogenic responses (Chen et al., 2008; Sun et al., 2010; Wang et al., 2011; Fan et al., 2012). On the other hand, BBX18 promotes hypocotyl growth by influencing bioactive GA levels, suggesting a role in GA signaling pathways (Chang et al., 2008). Furthermore, BBX proteins play a role in various hormonal signaling pathways, with interactions implicated in responses to abiotic and biotic stresses. Differential expression of several BBX genes (e.g. *BBX14*, *BBX28* and *BBX29*), among other members of group III and IV, are induced by ABA, cADPR, and low temperatures, as they are predicted to contain putative ARABIDOPSIS RESPONSE REGULATOR 10 (ARR10) binding sites on their promoters, indicating their potential involvement in stress signaling (Sanchez et al., 2004; Cutler et al., 2010).

1.3. Abiotic stress regulation

Abiotic stresses, such as extreme temperatures, salinity, and limited water availability, are environmental conditions that can significantly impede plant growth and productivity. These stresses can alter plant morphology and physiology, inhibiting cell division and affecting crucial processes like photosynthesis (Foyer et al., 2016).

Plants have developed rapid response mechanisms to adverse conditions, which involve interconnected molecular networks governed by signal cascades (Fowler et al., 2002). Stress response components include signal perception, transduction, and expression of stress-responsive genes (Hrmova & Lopato, 2014). When stress signals are perceived, plant cells activate receptors or sensors, triggering rapid responses that transmit external signals to intracellular counterparts. Upon exposure to stress, major signal cascades, such as MAPK and CDPK pathways are activated, leading to the upregulation or downregulation of specific genes (Erpen et al., 2018). The response of plants to abiotic stress involves complex physiological and biochemical changes, often associated with modified gene expression patterns (Nuruzzaman et al., 2013). Stress initiation activates initial sensors, which activate cytoplasmic $Ca2^{+}$ and protein signaling pathways, resulting in altered gene expression and physiological adjustments. Abiotic stresses cause significant changes in gene expression and protein turnover, highlighting the importance of transcriptional and post-transcriptional regulation in adapting cellular functions to environmental changes (Pfannschmidt et al., 1999; Leister et al., 2017). Photosynthesis, as a fundamental process, is particularly vulnerable to abiotic stress at various stages, affecting factors such as CO_2 diffusion, PSII efficiency, electron transport, and enzyme activities (Saibo et al., 2009).

As abiotic stresses can affect photosynthesis in both the short and long term, gene expression regulation becomes crucial. Transcription factors are important in stress acclimation as they regulate the expression of stress-responsive genes, influencing essential aspects of plant function such as environmental responses, hormone signaling, and developmental processes (Foyer et al., 2016; Hoang et al., 2017; Inukai et al., 2017). They are modulated by stress signals such as ABA, redox state, and ATP/NADPH content, and play a crucial role in coordinating adaptive responses to abiotic stress (Suzuki et al., 2013). Distinct regulons, such as the CBF/DREB, NAC/ZF-HD, AREB/ABF, and MYC/MYB regulons, are identified in the context of photosynthesis-related responses to stress (Erpen et al., 2018). Under abiotic stress, the MYB TF family, traditionally associated with single MYB repeats, is involved in regulating photosynthesis-related genes (Dubos et al., 201). Additionally, MYB-related TFs, such as

CCA1, GLK1, and GLK2 (Fitter et al., 2002), have been implicated in the stress-induced regulation of photosynthesis-related genes (Baillo et al., 2019).

Other transcription factors, such as HY5, which is known for its involvement in light-mediated CAB gene expression, may also play a role in the response to abiotic stress. HY5, which is a bZIP-type TF, regulates several genes related to photosynthesis, indicating a possible function in stress conditions (Chattopadhyay et al., 1998; Wang et al., 2011; Sornaraj et al.,2016). While there is no direct evidence of HY5's involvement in regulating photosynthesis-related genes under abiotic stress, its upregulation in response to extreme temperatures suggests a possible connection (Li et al., 2021). Additionally, the transcriptional regulation of plastid-encoded photosynthesis genes by environmental stimuli adds complexity to the issue. A comprehensive understanding of chloroplast-encoded gene regulation under abiotic stress is necessary due to the intricate control exerted by nuclear-encoded transcription regulators, such as AtSig5 and AtSig6 (Leister et al., 2017). Moreover, functional studies have shown that NAC genes are induced by various abiotic stresses, resulting in improved drought tolerance when overexpressed. WRKY transcription factors are involved in various processes and control gene expression through positive and negative regulation (Bakshi et al., 2014). Regulatory small RNAs play a crucial role in biotic stress responses by modulating the expression of TFs, guiding the proper progression of biological events. However, the responses of TFs to stress conditions are complex, as a single transcription factor gene may regulate multiple downstream genes, be regulated by different TFs, or respond to various stresses (Baillo et al., 2019).

1.3.1. BBX proteins in the context of abiotic stress

Evidence for the role of BBX proteins in abiotic stress acclimation and signaling pathways is scarce. BBX proteins are involved in abiotic stress responses, such as low temperature, high salinity, drought, heat, and HL. Although abiotic stress tolerance is a polygenic trait, single genes encoding crucial transcriptional regulators can improve plant adaptation to various stresses by regulating gene networks. The significance of BBX proteins in stress tolerance has been revealed by manipulating their genes in transgenic economically essential plants to obtain desirable agronomic characteristics and stress resistance (Shahzad et al., 2021). Some studies propose that BBX proteins, known for their roles in growth and development, also participate in signaling pathways activated by both abiotic and biotic stresses. Many BBX genes show changes in transcript levels under different stress conditions, indicating their involvement in stress responses (Huang et al., 2019). On a broad scale, overexpressing certain BBX genes has been shown to enhance stress tolerance in different plant species, including Arabidopsis,

apples, and rice, improving their resilience to salt and drought stresses, as well as cold tolerance. Their role in stress response is often mediated through their interaction with phytohormones and participation in hormonal signaling pathways that are crucial for the plant's acclimation and adaptation to abiotic stresses.

For instance, it has been revealed that in Arabidopsis BBX18 plays a role in thermotolerance. In experiments, lines with reduced BBX18 expression exhibited enhanced thermotolerance, while overexpression of BBX18 led to reduced thermotolerance. Furthermore, BBX18 was found to negatively regulate the expression of heat-responsive genes like *DGD1*, *Hsp70*, *Hsp101*, and *APX2*, consequently impacting germination and seedling survival after heat treatment (Wang et al., 2013). Another BBX protein, BBX24, has been implicated in salt stress signaling. BBX24 was discovered to confer increased salt tolerance in yeast. Further studies revealed that BBX24 complements the salt-sensitive phenotype of yeast mutants deficient in calcineurin and enhances salt tolerance in wild-type yeast (Lippuner et al., 1996). Overexpression of BBX24 in Arabidopsis also resulted in enhanced salt tolerance compared to wild-type plants, as evidenced by increased root length in transgenic plants exposed to salt stress (Gangappa, Holm et al., 2013). Interestingly, BBX24 does not appear to be directly inducible by salt, suggesting its effects may be mediated through indirect mechanisms (Indorf et al., 2007; Yan et al., 2011). Genome-wide expression analyses indicate potential involvement of BBX proteins in various stress signaling responses. For instance, studies have shown differential expression of BBX genes in response to ABA, cyclic ADP-ribose, and low temperatures. While previous research suggests a role for cADPR in early ABA signaling, direct involvement of BBXs in abiotic stress signaling pathways requires further investigation (Sanchez et al., 2004; Chen et al., 2008).

In the context of HL stress, genes such as *BBX14*, *BBX15*, *BBX16*, and *BBX17* are mentioned as being downregulated in response to HL stress in Arabidopsis. These genes, which were consistently repressed at all time points during the HL stress and are part of clade III in the BBX phylogenetic tree may have a role in the HL response through light signaling pathways (Huang et al., 2019). The downregulation of these BBX genes under HL conditions suggests that they might function in modulating the plant stress response mechanisms, potentially by influencing light-dependent pathways that affect gene expression during HL intensity exposure.

2. Scientific aims of the thesis

The overall aim of this thesis was to provide further insights into the regulatory mechanisms underlying the light-regulated plant development in the context of retrograde signaling. In particular, the molecular role of the Arabidopsis BBX transcription factor, BBX14, in the crosstalk between light and RS during photomorphogenesis was genetically investigated und critically discussed in a comprehensive manner. Furthermore, the study aimed to understand the molecular function of BBX14 in Arabidopsis, particularly focusing on its involvement in the acclimation to HL conditions and its role in seedling establishment. Moreover, the research further aimed to assess the impact of BBX14 on chlorophyll accumulation during early light exposure and to analyze transcriptome changes to identify BBX14 targets and its potential regulatory role in photomorphogenesis.

BBX14, a clade III member of the BBX transcription factor family, was selected for study due to its association with GLK1 and GLK2 in a core module essential for the nuclear retrograde response to changes in organellar gene expression (Leister & Kleine, 2016). This module, identified through database analyses, revealed gene expression alterations similar to those induced by RS-triggering treatments like LIN, NF, or HL in mutants with defective PGE. Additionally, *BBX14* was among the top upregulated genes in transcriptional regulation following GLK1 and GLK2 overexpression, indicating a regulatory link between BBX14 and GLKs (Waters et al., 2009).

Taking all this into account, it was reasoned that BBX14 represents a solid basis for further characterization due to its limited knowledge as important player in seedling development but also as emerging candidate in plastid-to-nucleus signaling.

3. Materials and Methods

3.1. Materials

3.1.1. Chemicals and enzymes

All chemicals utilized in this work were obtained from Invitrogen, Roche Diagnostics, Roth, Sigma-Aldrich, AppliChem, Serva, Merck, Biozym, and GE Healthcare with a purity grade for analysis (p.A.). The enzymes employed in this work were acquired from New England Biolabs and Invitrogen. The work included the use of the following kits: FastGene Gel/PCR Extraction Kit (Nippon Genetics), Direct-zol™ RNA MiniPrep Kit (Zymo Research in Irvine, USA), iScript™ cDNA synthesis kit (Bio-Rad, Munich, Germany) and plasmid DNA extraction kit EasyPure Plasmid MiniPrep Kit (Transgene Biotech, Beijing, China).

3.1.2. Oligonucleotides

All oligonucleotides utilized in this study were synthesized by Metabion (Planegg, Germany) in DST quality (desalt). BioScience Grade water (Roth) was used to prepare a 100 µM stock and a 10 µM working solution which were stored at -20°C. See Table S4. in supplemental information for a list of the oligonucleotides used in this research.

3.1.3. Vectors

Name	Description	Features	Origin/Reference	Use
pAUL1	C-terminal in-frame fusion of protein to HA-tag	3x HA-tag, nosT, Basta^r, 2x p35S CaMV, *ccdB*, *att*R1, *att*R2, Cm^r, Kan^r	Lyska et al., 2013	Overexpression of tag-fused protein
pB7FWG2	C-terminal in-frame fusion of protein to GFP-tag	eGFP-tag, nosT, Basta^r, p35S CaMV, *ccd*B, *att*R1, *att*R2, Cm^r, Sp^r	Karimi et al., 2002	Overexpression of tag-fused protein + subcellular localization
pDONR207	Generation of entry clones for GATEWAY cloning	rrnB T2, rrnB T1, *att*P1, *ccd*B, *att*P2, Kan^r	Invitrogen	Gateway cloning
pHEE401E	Egg cell-specific promoter-controlled expression of 3x FLAG-NLS-zCas9-NLS	3x FLAG-tag, nosT, Cas9, 2x U6-26p U6 promoter, Sm^r, Hyg^r, Kan^r	Addgene #71286; Wang et al., 2015	CRISPR

3.1.4. Antibodies

Name	Use	Dilution	Origin
anti-GFP	primary	1:5000	A6455; Life Technologies
anti-HA	primary	1:1000	G1546; Sigma-Aldrich
anti-BBX14	primary	1:500	BioGenes
anti-mouse	secondary	1:5000	Agrisera
anti-rabbit	secondary	1:10 000	Agrisera

3.1.5. Bacterial strains

Organism	Strain	Features	Origin
E.coli	DH5-alpha	F- 80dlacZ M15 (lacZYA-argF) U169 recA1 endA1hsdR17(rk-, mk+) phoAsupE44 - thi-1 gyrA96 relA1	Woodstock et al., 1989
A. tumefaciens	GV3101	$Gent^r$, Rif^t, pMP90 (pTiC58ΔT-DNA)	Koncz und Schell (1986)

3.1.6. Solutions and media

Purified water of aqua bidest quality (ddH_2O was used to prepare all media, buffers, and solutions via the Milli-Q Plus Water System (Millipore, Bradford, USA). Unless otherwise specified, this is referred to as ddH_2O. Sterilization was accomplished through autoclaving for 20 min at 121°C and 2×10^5 Pa or by employing sterile filters with exclusion limits of 0.22 or 0.45 μm.

Solutions

50x TAE	2 mM 100 mM	Tris-acetate EDTA pH 8.0
TBS-(T)	10 mM 150 mM (0,1 %	Tris pH 8.0 NaCl Tween-20)
1x Running buffer	25 mM 190 mM 0,1 %	Tris base pH 8.3 glycine SDS
Semi-dry transfer buffer	10 % 20 %	1x Running buffer Methanol
De-staining solution	10 % (v/v) 10 % (v/v)	Methanol Acetic acid

Coomassie staining solution	40 % (v/v) 10 % (v/v) 0,1 % (w/v)	Ethanol Acetic acid Coomassie Brilliant Blue R-250
2x Laemli buffer	120 mM 4% SDS 20% glycerol 2.5% 0.01%	Tris pH 6.8 SDS glycerol ß-mercaptoethanol bromophenol blue
DNA extraction buffer	200 mM 25 mM 20 mM 0,5 % (w/v)	Tris base pH 7.5 NaCl EDTA pH 8.0 SDS
Media		
LB (*E.coli* and Agrobacteria)	10 g 5 g 5 g to 1 l with	tryptone NaCl yeast extract H_2O
LB (liquid) (*E.coli* and Agrobacteria)	10 g 5 g 5 g 15 g to 1 l with	tryptone NaCl yeast extract agar H_2O
0.5x MS pH 5.8 (*Arabidopsis thaliana*)	2,2 g 8 g (10 g to 1 l with	Murashige & Skoog medium + vitamins agar sucrose) H_2O

The following antibiotics were used to select bacteria: Ampicillin (Amp^{100}), Kanamycin (Kan^{50}) Spectinomycin ($Spec^{100}$) Gentamycin ($Gent^{30}$), Rifampicin (Rif^{100})

3.1.7. Plant material

All the Arabidopsis lines used in this work were in the Col-0 background unless stated otherwise.

3.1.8. T-DNA lines

Mutant lines *bbx14-1* (SAIL_1221_D02; N878600) and *pifq* (N2107737) were obtained from the North American Arabidopsis Stock Center (https://arabidopsis.info) and Arabidopsis Biological Resource Center (https://abrc.osu.edu/), respectively. Oligonucleotides confirming

the T-DNA insertion in *bbx14-1* line are listed in Table S4. Previous studies have described the *gun1-102* mutant (Tadini et al., 2016), *gun4-2* mutant (Peter and Grimm, 2009), *gun5-1* mutant (Mochizuki et al., 2001), and *glk1* mutant (Waters et al., 2009).

3.1.9. CRISPR lines

The pHEE401-E vector, which provides an egg-cell-specific promoter, was used to generate the CRISPR-Cas lines *bbx14-2* and *bbx14-3* (Wang et al., 2015). The specific guide RNA (gRNA) was designed utilizing the web tool CHOPCHOP (https://chopchop.cbu.uib.no/#). The annealed oligos were inserted into the pHEE401-E vector via a one-step cut and ligate reaction, as detailed by Wang et al. (2015; 2022). Col-0 plants were transformed with the construct via floral dipping using Agrobacterium tumefaciens GV3101 (Clough and Bent, 1998). Positive transformants were selected in the T1 generation on plates supplemented with 50 μg mL−1 hygromycin and 1% (w/v) sucrose in 0.5x MS medium. To identify homozygous *bbx14* mutants, the BBX14 gene was sequenced in the surviving plants with the help of oligonucleotides mentioned in Table S4.

3.1.10. Other transgenic lines

The inducible overexpression line TPT14 (N2101635), TPT15-1 (N2101503) and TPT15-2 (N2101504) expressing the BBX14 transcription factor under the control of a beta-estradiol inducible promote (Coego et al., 2014) was obtained from the Arabidopsis Biological Resource Center (https://abrc.osu.edu/stocks/38). The lines were verified to be homozygous for the transgene and contain a hygromycin resistance marker, used to select positive plants in the first generation.

3.2. Methods

3.2.1. Plant growth conditions

Arabidopsis thaliana plants were cultivated on potting soil (Stender, Schermbeck, Germany) under controlled conditions in a growth-chamber with at approx. 100 μmol photons m^{-2} sec^{-1} with 16h/8h light/dark cycles.

For *in vitro* cultivation Arabidopsis seeds were surface-sterilized in a 10 % bleach solution containing 0.01% Triton-X-100 for 10 min under vigorous shaking. Afterward seeds were plated on sucrose-free agar plates (Sigma-Aldrich/Merck, Darmstadt, Germany) containing 0.5x MS medium (except for experiments performed on plates containing 1 % sucrose) under sterile conditions followed by stratification in dark for 3 days at 4°C before growth at 22°C

under 100 µmol photons m^{-2} sec^{-1} provided by white fluorescent lamps. For experiments involving dark treatment, seeds were exposed to 2 h of white light (100 µmol photons m^{-2} sec^{-1}) following stratification, before allowing to germinate in the dark. For experiments that involved lincomycin (LIN) or norflurazon (NF) treatment, the medium was supplemented with 0.5 mM lincomycin (Sigma-Aldrich) or 5 µM norflurazon (Sigma-Aldrich). Consistent temperature (22°C/20°C during the 16h/8h day/night cycle) and relative humidity (60%) were meticulously maintained under all conditions. For high-light experiments, plants were initially grown for one week in an LED chamber at 80 µmol photons m^{-2} s^{-1} (16-h light/8-h dark cycle) before increasing the irradiance to 1000 µmol photons m^{-2} s^{-1} under precisely controlled temperature conditions.

In experiments conducted using inducible overexpression lines, overexpression was induced by supplementing 0.5x MS medium with 2.5 µM β-estradiol or by spraying 4-days-old seedlings with a solution containing 20 µM β-estradiol (Sigma-Aldrich), 0.01 % Silwet L-77 and 0.2% DMSO. For the experiments illustrated in Figure X, the induction was carried out right after three days of dark treatment. This was then followed by two hours of dark incubation and subsequent growth for at least 16 hours under 100 µmol photons m^{-2} sec^{-1} continuous white light.

3.2.2. Plant phenotypical measurements and data analysis

For hypocotyl and root measurements at least 50 seedlings were recorded using Image J software (http://imagej.en.softonic.com/) and the mean of the 15 longest was calculated unless stated otherwise in the figure description. Experiments were performed twice with consistent results.

Statistically significant differences in relative mRNA expression levels were assessed by applying one-way ANOVA with Tukey's post-hoc HSD test (https://astatsa.com; version August 2021). The significance of differences in chlorophyll accumulation, hypocotyl lengths, F_v/F_m and Y(II) was tested by two-way ANOVA, followed by Tukey's multiple comparison test (as indicated in the Figure legends) using GraphPad Prism version 9.4.1 for Windows (GraphPad Software, www.graphpad.com). All comparisons were made exclusively to the corresponding wild-type (Col-0) sample within the same condition. Only statistically significant differences are presented, as specified in the legends for each figure.

3.2.3. Molecular methods

Standard molecular techniques, as well as media and buffer preparation, were conducted following the protocols described in Sambrook & Russell (2001). Enzymes and kits were utilized in accordance with the manufacturer's instructions, unless stated otherwise.

3.2.3.1. Nucleic acid extraction

Plant tissue was ground into a fine powder using a MM300 Retsch mill (Haan, Germany) for the isolation of genomic DNA (gDNA). To achieve this, freshly harvested plant tissue was shock-frozen in a 2 ml reaction tube containing two steel balls (Ø 5 mm) submerged in liquid nitrogen and grinded for 3 min at 30 Hz/sec. Subsequently, the ground leaf tissue was homogenized with 1 ml of DNA extraction buffer. Following centrifugation, DNA was precipitated from the supernatant with the addition of 700 µl of isopropyl alcohol. After washing the DNA pellet with 1 mL of 70% (v/v) ethanol, it was dissolved in distilled water and stored at 4°C.

To isolate RNA, frozen plant tissue was ground in liquid nitrogen, as described previously, for 30 seconds at 30 Hz/sec. Total RNA from plants was then extracted using Trizol (Invitrogen, Carlsbad, CA) and purified through Direct-zol™ RNA MiniPrep Plus columns (Zymo Research, Irvine, CA) according to the manufacturer's instructions. RNA quality, concentration, and the A260/A280 ratio were evaluated using agarose gel electrophoresis and spectrophotometry, respectively. Subsequently, RNA was isolated and stored at −80°C prior to use.

3.2.3.2. Plasmid DNA isolation

Plasmid DNA was extracted from E. coli cells using plasmid DNA extraction kit EasyPure Plasmid MiniPrep Kit (Transgene Biotech, Beijing, China) from 5 ml overnight liquid cultures that underwent antibiotic selection. The resulting plasmid DNA was then stored at -20°C.

3.2.3.3. Plasmid construction and transformation

To generate stable overexpression lines of BBX14 in the Col-0 background, the coding region of the AT1G68520 gene was amplified from wild-type cDNA using VeriFi ™ polymerase from PCR Biosystems (London, UK) with specific oligonucleotides listed in Table S4. Consecutively the attB-flanked PCR product was then cloned into an entry vector and finally into both the pB7FWG2 and pAUL1 expression vectors using the GATEWAY technology (Invitrogen, Netherlands) in accordance with the manufacturer's protocol. The fusions

generated with the enhanced eGFP- and HA-tag, respectively, were expressed under the control of the Cauliflower Mosaic Virus 35S promoter and transformed into Agrobacterium cells. Both constructs were introduced into Col-0 plants through floral dipping (Clough and Bent, 1998). Restriction analysis and sequencing verified all cloned DNA fragments post plasmid isolation.

3.2.3.4. Standard polymerase chain reaction (PCR)

To amplify specific DNA sections, a standard PCR was conducted utilizing either homemade Taq polymerase or VeriFi ™ polymerase. Plasmid DNA, cDNA, or gDNA was used as template. The reaction sets were formulated as follows:

Taq polymerase reaction	VeriFi polymerase reaction
Template DNA (0.2 µg – 100 ng)	Template DNA (0.2 µg – 100 ng)
Taq reaction buffer (10x)	VeriFi reaction buffer (5x)
Fw-Primer (100 nM)	Fw-Primer (100 nM)
Rev-Primer (100 nM)	Rev-Primer (100 nM)
dNTPs (10 mM per dNTP)	VeriFi polymerase (2 U/µl)
Taq polymerase (0.5 U/µl)	add H_2O to 50 µl
add H_2O to 10-50 µl	

Reactions were performed in a Dyad Thermocycler (Bio-Rad, Munich, Germany) using the program outlined below with 20-35 cycles ranging from step 2 to 4:

1.Initial denaturation	95°C	5 min	1.Initial denaturation	95°C	1 min
2.Denaturation	95°C	30 sec	2.Denaturation	95°C	15 sec
3.Primer annealing	55-60°C	30 sec	3.Primer annealing	60-75°C	15 sec
4.Elongation	72°C	1 min/kb	4.Elongation	72°C	30 sec/kb
5.Final Elongation	72°C	5 min	6.Hold	16°C	∞
6.Hold	16°C	∞			

The annealing temperature was set to 1-4°C below the oligonucleotide's melting temperature, typically between 55°C and 60°C. Elongation time was determined by the size of the DNA

fragment being amplified and set to 1 minute per kilobase (for Taq polymerase) or 30 seconds per kilobase (for VeriFi polymerase). PCR conditions were optimized by varying the annealing temperature, template concentration, and number of cycles used.

PCR reactions were mixed with 0.5 µl of 6x loading dye and separated on a 1% agarose gel supplemented with Midori-Green DNA dye (Nippon Genetics) for 20-30 minutes at 120 V. A FastGene 1 kb plus DNA ladder (Nippon Genetics) served as the size marker.

3.2.3.5 Sequencing

DNA sequencing was performed by the LMU Sequencing Service Unit in Munich, Germany, utilizing the "Cycle, Clean & Run (BigDye v3.1)" protocol. Each reaction consisted of 3.8 µl purified DNA template and 3.2 µl of either the forward or reverse primer.

3.2.4. Gene expression analysis

3.2.4.1 cDNA synthesis and quantitative real-time PCR

First-strand cDNA synthesis was conducted with the iScript™ cDNA synthesis kit (Bio-Rad, Munich, Germany), following the manufacturer's instructions. For reverse transcription, 250 ng total RNA was used as standard, unless otherwise specified. After reverse transcription, the cDNA was diluted at a 1:20 ratio using DNase-/RNase-free water. 2 µl of the diluted cDNA was utilized for quantitative real-time PCR analysis on the CFX Connect Real-Time System. The assay was conducted using Universal SYBR Green Supermix (Bio-Rad, Munich, Germany). The experimental protocol was previously described by Wang et al. (2022), and oligonucleotides are listed in Table S4. Whenever possible, oligonucleotides were designed to flank intron sites as to avoid amplification of gDNA. Gene expression data represents values from three independent biological replicates, each with three technical replicates per measurement. The graphs show the mean expression of the biological replicates, with SEM denoted by error bars. Data evaluation was performed using Bio-Rad's CFX Maestro® software. Gene expression was normalized to the AT4G36800 gene that encodes an RUB1-conjugating enzyme (RCE1).

3.2.4.2. RNA-seq analysis

Total RNA from plants was extracted utilizing Trizol (Invitrogen, Carlsbad, USA) and subsequently purified using Direct-zol™ RNA MiniPrep Plus columns (Zymo Research, Irvine, USA) following the manufacturer's protocol. The quality and integrity of RNA were analyzed using the Agilent 2100 Bioanalyzer (Agilent, Santa Clara, CA). RNA-Seq libraries were generated and sequenced in paired-end mode with 150-bp reads using standard Illumina protocols on either an Illumina HiSeq 2500 (Illumina, San Diego, USA) or Novaseq6000 system by Novogene Biotech (Beijing, China) or Biomarker Technologies GmbH (Münster, Germany), respectively. Every genotype consisted of either three independent biological replicates for Col-0 and *bbx14* seedlings or two independent biological replicates for Col-0, *gun1*, and TPT14 seedlings grown on NF. RNA-Seq reads were analyzed using the Galaxy platform (Afgan et al., 2016) as essentially described before (Xu et al., 2019) However, reads were mapped using the gapped-read mapper RNA STAR (Dobin et al., 2013). In the TPT14 NF experiment, differentially expressed genes were identified using a 2-fold cut-off without adjusting for p-values due to poor read quality in one TPT14 NF replicate. This study aimed to obtain an initial understanding of potential BBX14 targets in RS and was not replicated.

3.2.5. Measurements of physiological and biochemical parameters

3.2.5.1. Chlorophyll and protochlorophyllide content determination

For chlorophyll extraction, approximately 100 mg of leaf tissue from three-week-old plants was ground in liquid nitrogen with 1 ml of ice-cold 80% (v/v) acetone. After removing cell debris by centrifugation chlorophyll absorption was measured spectrophotometrically. Pigment concentrations were calculated following Lichtenthaler's method (1987) and normalized to fresh weight.

To determine protochlorophyllide content in etiolated seedlings, the procedure described by Terry and Kacprzak (2019) was followed. In brief, approximately 100 mg of 4-day-old etiolated seedlings were harvested and stored in liquid nitrogen in under safe green light. The resulting material was homogenized in 400 µl of ice-cold alkaline acetone solution (acetone: 0.1 M NH_4OH; 9:1; (v/v)). Following removal of cell debris by centrifugation for 5 min at full speed and repeated extraction, supernatants were combined, and Pchlide absorption was measured spectrophotometrically after excitation at 440 nm. Pigment concentrations were calculated as relative fluorescence on a per milligram fresh weight basis. All steps were carrier at 4°C, and samples were covered with foil to protect them from light.

3.2.5.2. Chlorophyll fluorescence analysis

In vivo chlorophyll *a* fluorescence of Arabidopsis seedlings was measured using an ImagingPAM chlorophyll fluorometer (Walz GmbH, Effeltrich, Germany) as described previously (Garcia-Molina et al., 2020). In essence, plants were adapted to darkness for at least 30 min before exposure to a to pulsed saturating light flash (8000 µmol photons m^{-2} sec^{-1}) to obtain the maximum PS II quantum yield value ($F_v/F_m = (F_m - F_0)/F_m$). F_0 was measured at a low frequency of pulse-modulated measuring light (4 Hz, intensity 3), while Fm was quantified following saturation pulses of approximately 2700 µmol photons m^{-2} s^{-1} for 0.8 s. The calculations and plotting of the parameters were performed using the ImagingWinGigE software.

3.2.5.3. SDS polyacrylamide gel electrophoresis and immunoblot analysis

The plant tissue was rapidly frozen in liquid nitrogen and ground into a fine powder in a 1.5 mL reaction tube. The ground tissue was mixed with an equal volume of 2x Laemmli sample buffer and incubated for 10 min at 95°C, followed by centrifugation for 5 min. The protein concentration of the resulting supernatant was assessed using the BioRad Protein Assay Dye Reagent Concentrate (BioRad, Munich) according to the Bradford method (1976).

Total proteins were separated based on their molecular weight using 10% (w/v) SDS-polyacrylamide gels in a Mini-PROTEAN Tetra Cell system (BioRad, Munich). Electrophoresis was carried out using 1x Running buffer at 30-50 mM per gel (constant 80 V). Subsequently, a semi-dry western transfer protocol was used to transfer the proteins from the polyacrylamide gel onto a polymeric, protein-binding membrane, allowing for further applications such as immunodetection. To accomplish this, a polyvinylidene fluoride (PVDF) membrane (Millipore in Billerica, Massachusetts) of the same dimensions as the SDS gel was treated with methanol for 30 sec. The SDS gel was subsequently equilibrated in 1x TBS for 5 min. A bubble-free sandwich comprising of three filter paper layers, the membrane, the SDS gel, and another three filter paper layers was constructed on the lower electrode of the Bio-Rad Trans-Blot Turbo electroblot (Munich, Germany), and the device was sealed by placing the second electrode on top. The semi-dry transfer buffer pre-soaked all parts of the sandwich. A constant current of 30 mA per gel (approximately 2 mA/cm^2) was used for transfer. The electrophoresis duration relied on the size of the proteins intended for blotting and ranged from 30 to 50 minutes. Subsequently, the membrane underwent staining for 10 minutes with Coomassie staining solution and was destained with Coomassie destaining solution to certify

protein transfer onto the membrane and elucidate the background. The membrane with the blotted proteins was used immediately for immunodetection.

After western transfer, the membrane was incubated for one hour in a blocking solution consisting of 5% skimmed milk powder in 1x TBS at room temperature while gently shaking. Following this, the membrane was moved to a 2.5 % skimmed milk blocking solution that contained an appropriate concentration of primary antibody (see 3.1.4) and shaken for at least 60 minutes at room temperature or overnight at 4°C. The membrane was washed three times for five minutes in 1x TBST-T before being incubated with the HRP-conjugated secondary antibody in a 2.5 % skimmed milk blocking solution for two hours (see 3.1.4). Following this, the membrane was washed three times again for five minutes with 1x TBST-T. Visualizing the signals was accomplished by using the enhanced chemiluminescence Pierce™ ECL Western-Blotting substrate reagent (ThermoFisher Scientific, Waltham, MA, USA) and an ECL reader system (Fusion FX7, PeqLab). Signals were quantified via ImageJ software (http://rsbweb.nih.gov/ij).

4. Results

4.1. BBX14 is involved in chlorophyll biosynthesis during early stages of light exposure

Seedling development hinges on successful chloroplast biogenesis, which facilitates the transition from heterotrophic to autotrophic growth. Since most seeds germinate underground, seedling development typically commences in darkness, following a skotomorphogenic program known as etiolation. Conversely, light triggers seedling de-etiolation, marked by morphological changes like cotyledon expansion, hypocotyl growth inhibition and greening (Pipitone et al., 2021). On a molecular level, the de-etiolation process is initiated via the PHY-PIF-GLK1 signaling cascade in the nucleus, whereby light exposure via phytochromes triggers the degradation of PIFs, which relieves the repression of *GLK1* expression (Martin et al., 2016). GLK1 then regulates the expression of photosynthetic genes as well as potentially other downstream target genes involved in various aspects of seedling development and chlorophyll accumulation (Waters et al., 2009; Martin et al., 2016). Alongside with this, BBX proteins are well-established factors which play various roles in facilitating seedling development (see 1.2.2). To determine the involvement of BBX14, a member of clade III of the BBX TF family, in seedling development, mutant lines lacking BBX14 were utilized. Specifically, the mutant *bbx14-1* (SAIL_1221_D02) was identified from the SIGnAL database (Alonso et al., 2003) (**Figure 3 A, B**). It was observed that *bbx14-1* expresses *BBX14* transcripts at levels equivalent to 10% of Col-0 levels (**Figure 3 C**). As *bbx14-1* was the only available T-DNA mutant line, two additional CRISPR/Cas9-mediated lines, *bbx14-2,* and *bbx14-3*, were generated. In *bbx14-2*, a premature stop codon was introduced after nucleotide (nt) 924 relative to the start codon due to an insertion, whereas in the *bbx14-3* mutant, a Trp residue was replaced by a Gly residue due to a T-to-G change at nt 925. In *bbx14-2*, *BBX14* transcript levels were reduced to 10%, and in *bbx14-3*, transcript levels were reduced to 25% compared to Col-0 (**Figure 3 C**).

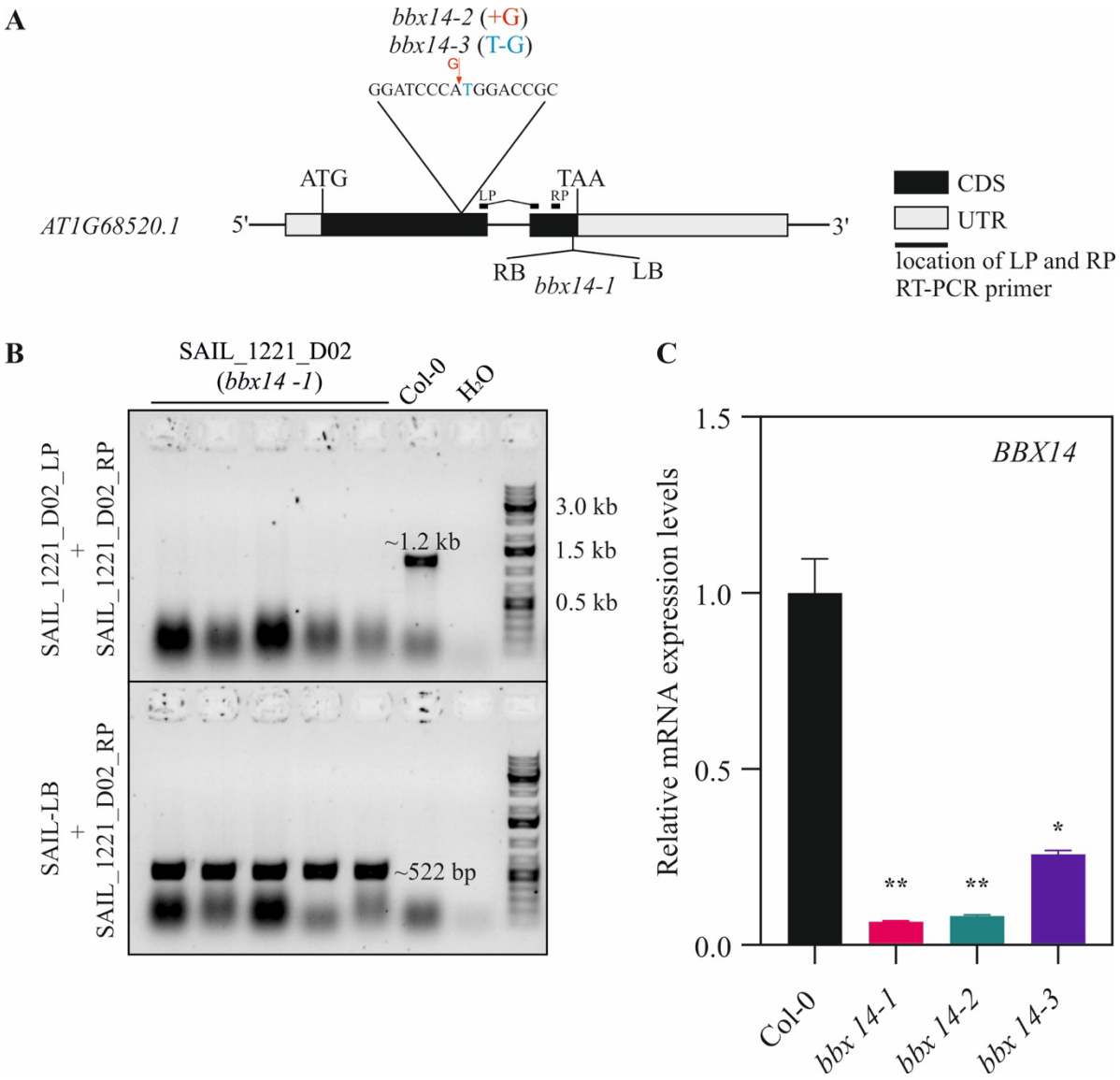

Figure 3. Identification of *bbx14* mutant lines.

(A) Schematic representation of the Arabidopsis *BBX14* coding sequence *(AT1G68520)*. Exons (black boxes), introns (black lines) and the 5' and 3' UTRs (grey boxes) are shown. Locations and orientation of T-DNA insertion (*bbx14-1*) is indicated, as deduced from LB + RP PCR products shown in **(B)**, which were subsequently sequenced. Note that the insertions are not drawn to scale. Furthermore, the locations of the primers used in the RT-qPCR analysis of *BBX14* expression shown **(C)** are indicated as thick black lines. The LP primer is an exon-exon primer spanning intron 1 of *BBX14*, which avoids amplification of genomic DNA. Also indicated is the target sequence of the gRNA used to generate CRSPR-Cas mutant lines. The position of the nucleotide insertion in the *bbx14-2 mutant line* (red arrow), as well as the nucleotide substitution T/G in *bbx14-3* (blue) are shown.

(B) Confirmation and identification of homozygous T-DNA insertions in the different *bbx14* T-DNA line. The gene-specific left and right border primers (LP and RP) were used for amplification of sequences around the T-DNA insertion, and the RP was used together with the T-DNA left border primer (SAIL-LB) for verification of the T-DNA insertion.

(C) RT-qPCR of *BBX14* expression in 7-day-old wild-type Col-0 and *bbx14* mutant seedlings grown under at 16-h light/8-h dark, 100 µmol photons m^{-2} s^{-1}. The results were normalized to AT4G36800, encoding a RUB1-

conjugating enzyme (RCE1). Expression values are reported relative to the corresponding transcript levels in Col-0 which were set to 1. Mean values ± SE were derived from two independent experiments (n=2), each performed with three technical replicates per sample. Statistically significant differences (Tukey's test; $**P < 0.01$, $*P < 0.05$) between Col-0 and mutant samples are indicated by an asterisk.

The role of BBX14 in seedling development was assessed by examining chlorophyll contents in *bbx14* mutant seedlings grown for 3 days in darkness and then transferred into continuous white light for 2, 4, and 8 hours. The seedlings were grown in the absence of exogenous sucrose before exposed to constant white light as to avoid effects of exogenous sucrose on seedling development and variations due to circadian rhythm. GUN4 is known to stimulate chlorophyll biosynthesis (Peter & Grimm, 2009) making the *gun4-2* mutant, which lacks the activator of the GUN5 subunit of the Mg-chelatase required for chlorophyll biosynthesis a suitable control. As depicted in **Figure 4 A**, the *gun4-2* line exhibited reduced chlorophyll levels compared to Col-0 throughout all three time points. In angiosperms, chlorophyll synthesis stops in the absence of light but resumes immediately upon exposure to light (von Wettstein et al., 1995). Chlorophyll levels in the whole seedlings of the tested genotypes increased during the first 4 hours of illumination and continued to increase linearly as the seedlings grew under subsequent illumination for up to 8 hours. Conversely, chlorophyll accumulation in *bbx14* mutant seedlings was significantly reduced when transferred to light for 2 and 4 hours only but remained higher than those of the *gun4-2* mutant throughout the time course experiment. Interestingly, after 8 hours of light chlorophyll levels of the *bbx14* mutants rose back to wild-type levels, thus indicating that BBX14 participates in chlorophyll accumulation during the early onset of light.

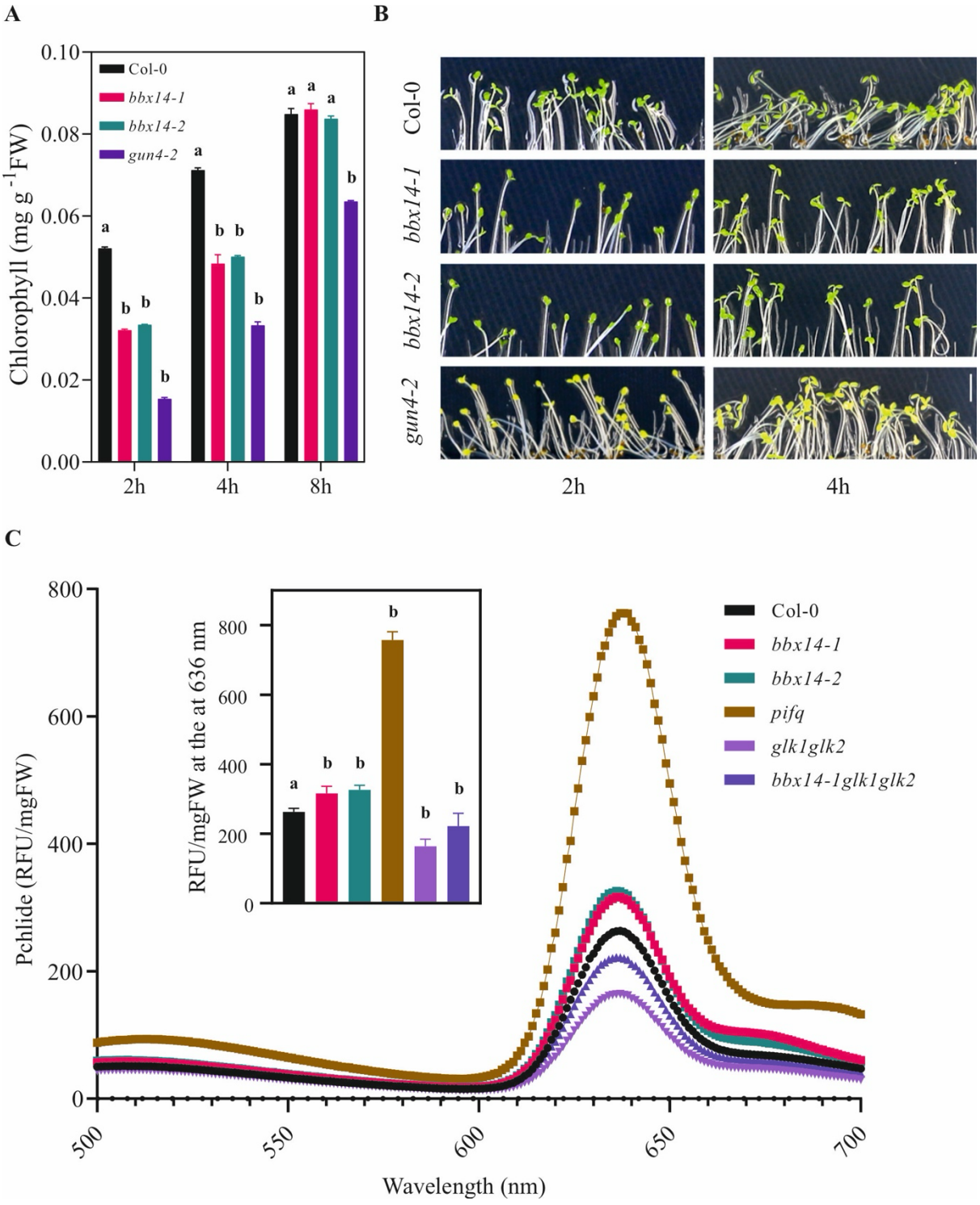

Figure 4. BBX14 is involved in seedling development.

(A) Determination of total chlorophyll (Chl *a* + *b*) content of seedlings grown in darkness for three days and then transferred to at 100 µmol m^{-2} s^{-1} white light for the indicated time. Chlorophyll was acetone-extracted and measured spectrophotometrically, and concentrations were determined as described (see 3.2.5.1). Data are shown as mean values ± SD from 3 different plant pools. Each pool contained more than 100 seedlings. Statistically significant differences between the wild-type and each mutant line at each time point are highlighted by letters above the plots (t-test; a, no significant difference; b, $P < 0.05$).

(B) Phenotypical representation of wild-type (Col-0) and mutant (*bbx14-1*, *bbx14-2,* and *gun4-2*) seedling grown as in **(A)**. Scale bar corresponds to 0,5 cm for all images.
(C) Measurement of protochlorophyllide (Pchlide) by fluorescence spectroscopy in 4-old-old dark-grown wild-type (Col-0) seedlings and mutant lines *bbx14-1*, *bbx14-2*, *pifq*, *glk1glk2* and *bbx14-1×glk1glk2*. Fluorescence spectra were recorded following excitation at 440 nm. The relative fluorescence (RFU) at the 636 nm peak was used as proxy for the quantification of the Pchlide amount and normalized to fresh weight. Data represents mean values of three independent biological replicates ± SD. Statistically significant differences between the wild-type and each mutant line at each time point are highlighted by letters above the plots (t-test; a, no significant difference; b, $P < 0.05$).

Cotyledon expansion and greening are hallmarks for chloroplast biogenesis and initiation of photosynthesis. The delayed chlorophyll accumulation observed in the *bbx14* mutants in the initial 2-4 hours of illumination suggested that photomorphogenesis was impeded when BBX14 is absent (**Figure 4 A**). Indeed, when comparing the same genotypes on a phenotypical level, it was observed that within the first 2 hours of light exposure *bbx14* mutants retained tightly closed cotyledon compared to both WT seedlings and the *gun4-2* line. This phenotype was later abolished by further exposure to light for 2 hours resulting in completely open cotyledons like Col-0 (**Figure 4 B**). This finding, together with the reduced chlorophyll amounts in the *bbx14* mutants, supports the notion that a lack of BBX14 leads to retarded initiation of photomorphogenesis.

Chlorophyll is indispensable for plants due to its essential role in light harvesting and energy transduction in photosynthesis. The Chl biosynthesis pathway in higher plants is complex and is mediated by more than 17 enzymes (Tripathy & Pattanayak, 2012). Plants carrying mutants in this pathway, such as *gun4* and *gun5*, are easily distinguishable by pale green appearance when grown under normal light conditions. This also holds true for the *glk1glk2* double mutant, in which genes required for light-harvesting and chlorophyll biosynthesis are notably downregulated (Waters et al., 2009). While a pale green phenotype was not observed in *bbx14* mutants under normal light conditions, it is not known if BBX14 plays role in chlorophyll in absence of light. Although etiolated seedlings do not synthesize chlorophyll, they prepare for eventual light exposure by accumulating large quantities of Pchlide in developmentally arrested plastids called etioplasts. In higher plants, the strictly light-dependent reduction of Pchlide to chlorophyllide is catalyzed by NADPH:protochlorophyllide oxidoreductase (POR) in the last step of the chlorophyll biosynthesis pathway. The Arabidopsis genome encodes three structurally related but differentially regulated and expressed *POR* genes, *PORA*, *PORB* and *PORC* with *PORA* being expressed primarily early on during etiolation (Paddock et al., 2010).

To establish whether chlorophyll biosynthesis is perturbed in *bbx14* mutants, levels of Pchlide in dark-grown seedling were measured by fluorescence spectroscopy and compared to mutant of higher order namely *pifq*, *glk1glk2* and *bbx14-1×glk1glk2*. The relative fluorescence at 663 nm was used as proxy to determine relative Pchlide levels. As depicted in **Figure 4 C**, levels of Pchlide were slightly elevated in the *bbx14* mutant in comparison to the WT as well as to mutants lacking GLK1 and GLK2. In contrast, the *pifq* mutant, which exhibits a constantly photomorphogenic phenotype even in absence of light, displayed abnormal amount of Pchlide fluorescence. The double *glk1glk2* mutant showed the lowest fluorescence peak, approximately 25 % less than Col-0. Interestingly, in the triple mutant *bbx14-1×glk1glk2* the Pchlide levels increased back close to WT levels, indicating that absence of BBX14 can rescue the compromised flux through the chlorophyll pathway in the *glk1glk2* mutant. Moreover, this suggests that BBX14 exerts a certain degree of influence on Pchlide biosynthesis in the dark and due to its role in promoting photomorphogenesis could represent an additional regulatory node during de-etiolation, that is already initiated in the dark.

Recently, another BBX protein also part of clade III, BBX16, was reported to be involved in the positive regulation of seedling development downstream of the above mentioned PHY-PIF-GLK1 module as direct target of GLK1 (Veciana et al., 2022). Additionally, the finding that all four BBX proteins belonging to clade III (BBX14–BBX17), are significantly enriched (p-value: 2.46 e-05) upon overexpression of GLKs among all 119 genes identified by Waters et al. (2009), implies that BBX14 too could be a direct target of GLK1. To shine light on this notion, a chromatin immunoprecipitation experiment followed by sequencing (ChIP-seq) on 14-day-old seedlings of a plant line expressing *GLK1* from its endogenous promoter in the Col-0 background was carried out (cooperation with HU, Berlin). The ChIP-seq analysis confirmed GLK1 binding to the BBX16 promoter (Veciana et al., 2022) and identified a GLK1-bound genomic region upstream of the BBX14 transcription start site (TSS). Within this region, four GLK1 binding sites were identified (**Figure S1 A**), all matching the CCAATC consensus found in co-expressed photosynthesis-related genes (Kobayashi et al., 2012). Notably, one motif located 70 bp upstream of the TSS closely resembled a GLK1-binding motif identified by protein-binding microarrays (GATTCTGATTGG; Franco-Zorrilla et al., 2014), suggesting strong potential for GLK1 binding. This finding indicated that *BBX14* was indeed a direct target of GLK1, with additional *BBX* genes detected among the top 10 most enriched potential targets (**Figure S1 B**). Furthermore, TIME FOR COFFEE (TIC), a component of the circadian clock, emerged as a top target, suggesting coordinated control of target gene activities. Analysis

revealed enrichment of motifs resembling various TF binding motifs, including bZIP, LOB, C2H2, and GATA (**Figure S1 C**), in GLK1-bound genomic regions, indicating a complex regulatory network involving GLK1. This is further supported by the fact that other TFs such as PIF4, HY5, and PSEUDO-RESPONSE REGULATOR5 (PRR5), involved in light/circadian and cytokinin signaling pathways bind to the BBX14 core promoter in combination with GLK1 (Fu et al., 2022). In addition to that, the GLK1 binding site was submitted to enrichment analysis using the Shiny GO gene set enrichment tool (Ge et al., 2020). A total of 761 and 1365 genes located within 1 kb and 3kb of the GLK1 binding site were analyzed, respectively When classified according to Gene Ontology (GO) terms relating to biological process, cellular compartment, and molecular function, terms related to photosynthesis and light-harvesting appeared to be the most highly represented and significantly enriched terms (**Figure S1 D**). The biological processes that are most enriched, namely photosynthesis, light harvesting, and chlorophyll biosynthesis, suggested that the genes targeted by GLK1 are involved in the expression of nuclear genes related to both LHCB and chlorophyll biosynthesis. This is in accordance with the previous finding suggesting BBX14 to play a role in chlorophyll accumulation during the early stages of light exposure (**Figure 4 A**).

4.2. BBX14 participates in the regulation of genes associated with the circadian clock

During the transition from etiolation to de-etiolation, there is a significant demand for protein synthesis to assemble the abundant photosynthetic complexes within thylakoid membranes. This process, known as the photomorphogenic program, is intricately regulated at multiple levels (Wu, 2014). Transcriptome analyses have demonstrated that upon exposure to light, a substantial portion of Arabidopsis genes undergo differential expression, with approximately three-fifths being upregulated and two-fifths being downregulated (Ma et al., 2001). Emerging from darkness requires a delicate balance, where repressive mechanisms at both the transcriptional and post-transcriptional levels play a crucial role (Hernandez-Verdeja et al., 2022). De-etiolation in Arabidopsis is closely linked to the circadian rhythm, with the circadian clock regulating the timing and extent of light-induced responses during this transition. The clock controls the expression of key genes involved in photomorphogenesis, chloroplast development, and photosynthesis to synchronize these processes with the diurnal cycle. Additionally, the circadian clock influences the sensitivity of plants to light signals, ensuring a coordinated and optimized response to environmental changes (Kato et al., 2007).

To better understand the molecular function of BBX14 during the transition from dark to light, transcriptome analysis was carried out, focusing on targets affected in both light-independent and light-dependent conditions, as well as those common to both. For this purpose, RNAs obtained from 3-day-old etiolated WT and *bbx14-1* seedlings, as well as from 3-day-old etiolated seedlings exposed to 16 hours of light followed by 8 hours of darkness, were subjected to RNA sequencing (RNA-Seq). In dark-grown *bbx14-1* seedlings, the analysis revealed alterations in only a handful of protein-coding transcripts. Specifically, four transcripts were reduced (*ACTIN-RELATED PROTEIN 9* [*ARP9*], *ARABIDOPSIS RESPONSE REGULATOR 7* [*ARR7*], *MEMBRANE-ANCHORED UBIQUITIN-FOLD PROTEIN 5 PRECURSOR* [*MUB5*], and *AT5G26270*), while two were elevated (*QUA-QUINE STARCH* [*QQS*] and *AT3G29633*) compared to the WT control, all showing fold changes greater than two-fold with a statistical significance of $p < 0.05$ (**Figure 5 A, B**; **Table S2**). In contrast to this, *bbx14-1* seedlings exposed to 16 hours of light followed by 8 hours of darkness, 147 protein-coding transcripts showed significant changes compared to WT (>2-fold, $p < 0.5$; **Figure 5 A, B**; Table S3), with 63 being reduced and 84 elevated. Most notably, transcript levels of clade II members *BBX7* and *BBX8* were reduced, alongside lower levels of *PHOTOPERIODIC CONTROL OF HYPOCOTYL 1* (*PCH1*) and higher levels of *XYLOGLUCAN ENDOTRANSGLUCOSYLASE/HYDROLASE 9* (*XTH9*) and *XTH16* transcripts, encoding proteins implicated in cell wall rearrangement. Gene ontology (GO) analysis (DAVID; Sherman et al., 2022) revealed a remarkable 180-fold enrichment of the "rhythmic process" category and almost 50-fold of the "circadian rhythm" among genes with reduced transcript levels (**Figure 5 C**), including genes encoding PSEUDO-RESPONSE REGULATOR5 (PRR5), and the CCT motif-containing response regulator protein TIMING OF CAB EXPRESSION 1 (TOC1), suggestive of potential involvement of BBX14 in circadian regulation, similarly to BBX19 as demonstrated before (Yuan et al., 2021). Moreover, the binding of circadian clock-associated TFs to the BBX14 promoter implies feedback regulatory mechanisms, despite BBX14 not being strongly rhythmically active according to the Arabidopsis eFP Browser (**Figure S8**; Winter et al., 2007) in comparison to other BBX proteins, such as BBX1 and BBX32 (Talar & Kielbowicz-Matuk, 2021). What's more, the anticipated target transcripts of GLKs associated with photosynthetic proteins or chlorophyll biosynthesis (Waters et al., 2009) were not identified in the GO analysis.

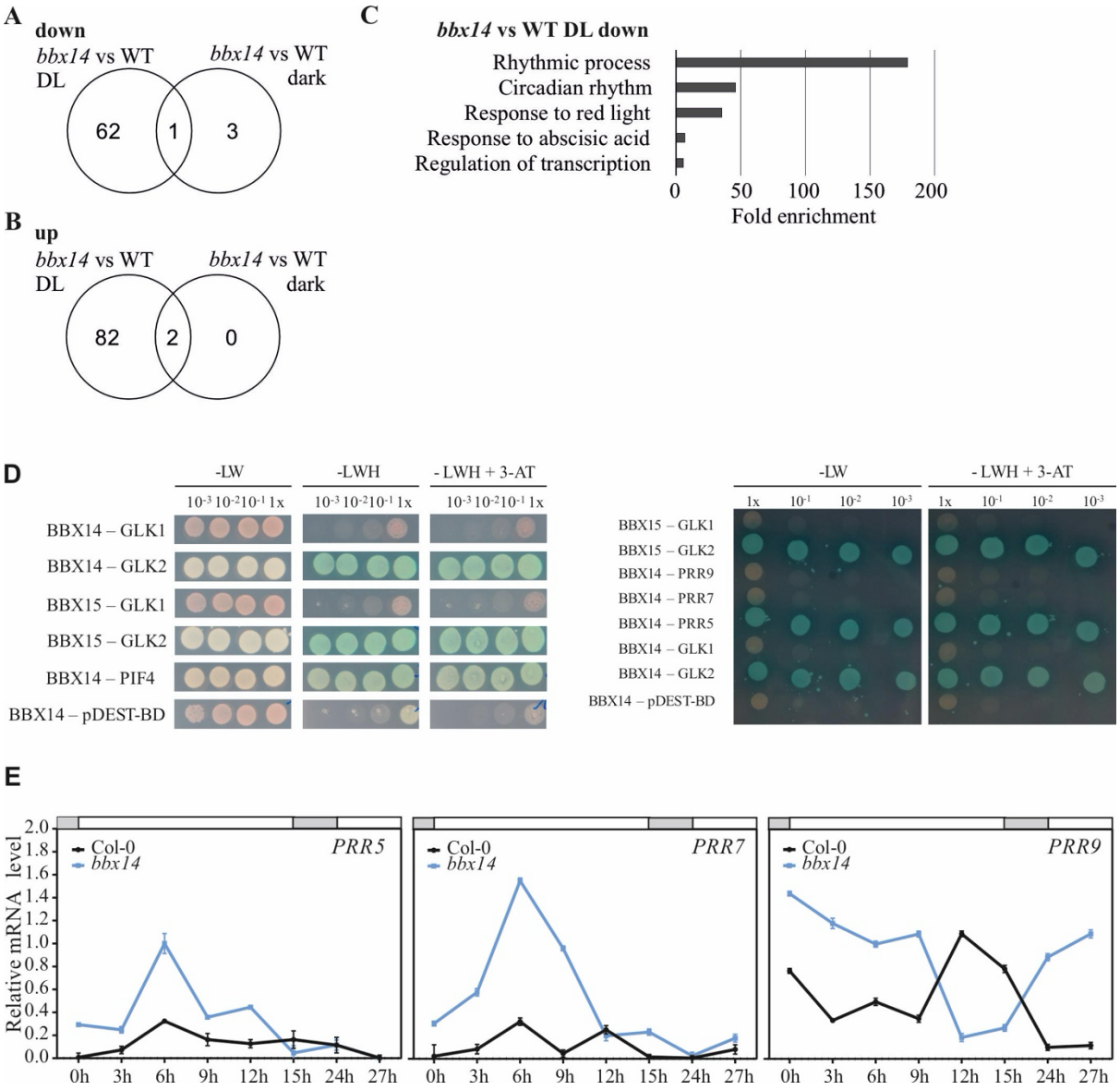

Figure 5. BBX14 is involved in the regulation of circadian clock associated genes.

(A, B) Analysis of transcriptome changes in *bbx14* mutant seedlings. Venn diagrams depicting the degree of overlap between the sets of genes whose expression levels were reduced **(A)** or elevated **(B)** by at least two-fold in *bbx14-1* seedlings that had been exposed to LD (16 h light, 8 h dark) conditions or were grown in darkness compared with the respective WT (Col-0) control.

(C) GO analysis of genes whose expression is down-regulated in light-shifted *bbx14-1* seedlings. GO annotations for the biological process category were extracted from DAVID.

(D) Yeast two-hybrid system to screen for potential interacting partners of BBX14 among known circadian clock proteins. AD, activating domain; BD, binding domain; -LW, synthetic dropout medium without leucine and tryptophan; -LWH, selective medium without leucine, tryptophan, histidine, supplemented with X-alpha-Gal for visualization of interaction and ± 3-AT to avoid background noise from growth at histidine-lacking media. An internal control PP7L with MAIL1 was used as positive control. The empty pGBKT7 plasmid (pDEST-BD) was utilized as a negative control. A representative picture from two independent repetitions with similar results is shown.

(E) RT-qPCR PRR579 time-series mRNA expression patterns in bbx14 vs Col-0. Levels of *PRR5*, *PRR7* and *PRR9* mRNAs in seedlings grown for three days under standard growth conditions at 100 µmol m^{-2} s^{-1} and harvested at the indicated time points. White or gray bars represent subjective day or subjective night, respectively. The results were normalized to *RCE1*. Expression values are reported relative to the corresponding transcript levels in Col-0, which were set to 1. Data are shown as mean values ± SEM from three independent biological replicates, each with three technical replicates.

The participation of BBX proteins as transcriptional regulators in fine-tuning of the circadian clock has been reported on scarcely, with few examples including BBX18 and BBX19, which interact with PRR9, PRR7, and PRR5 in the nucleus from early morning onward to regulate circadian periodicity (Yuan et al., 2021). To test whether BBX14 could also be involved in circadian regulation, a yest-two-hybrid system was utilized to screen for potential interaction partners of BBX14 (**Figure 5 D**). The results demonstrated that BBX14 strongly interacted with PIF4, but not with any PRR member (PRR5, 7, 9) or PIF1-3 tested here. PIFs are known to be involved a wide range of processes, including light signaling, circadian regulation, hormonal signaling, developmental and (a)biotic responses, due to their high diversification (Paik et al., 2017). In the context of BBX proteins, it has been previously shown that PIFs can regulate expression of *BBX* genes (Zhang et al., 2017; Buelbuel et al., 2023), but no reports for interaction on protein levels have emerged.

Strikingly, in addition to complexing with PIF4, BBX14 also interacts with GLK2, whereas it exhibited no interaction with GLK1. This also held true for BBX15, BBX14's closest homolog within clade III (74 % protein homology; Khanna et al., 2009; **Figure S7**), which also displayed strong interaction with GLK2 and none with GLK1. Moreover, interactions were also confirmed to some extend by the prediction aligned error (PAE) plots generated via AlphaFold2, whereby BBX14 was predicted to be an interaction partner of GLK2, not of GLK1, but also surprisingly of PRR5, PPR7 and PRR9, which was not confirmed in the yest-two-hybrid analysis (**Figure S2**).

Although no interaction was observable for BBX14 and the PRRs, the influence of BBX14 on transcript accumulation of PRR5, PRR7 and PRR9 was compared in WT and the *bbx14-1* mutant over a full long-day of normal light condition (**Figure 5 E**). The results showed that absence of BBX14 caused expression of both *PRR5* and *PRR7* to peak 6 hours after onset of light and then to sharply decrease during the day reaching WT levels before night evening, whereas expression in the WT remained steady with almost no fluctuations. On the other hand, expression of *PRR9* in the *bbx14-1* mutant was completely misregulated throughout the whole time period of the measurement, exhibiting opposing expression pattern compared to the WT.

In Arabidopsis, PRRs are essential components of circadian clock that play pivotal roles in coordinating many daily cycling physiological processes by timing the expression of numerous down-stream TFs (Nakamichi et al., 2010). As part of a tightly modulated network with comprising of multiple interconnected regulators, often absence or misregulation of one can cause drastic changes in the expression of other, it is therefore feasible that based on the results here BBX14 is required for the endogenous circadian rhythm by modulating the expression of clock components such as PRRs.

4.3. The elongated hypocotyl of the *bbx14* mutant depends on a retrograde signal

Based on the finding that *BBX14* represents a target of GLK1, their correlation was examined further. Gene expression analysis revealed that mRNA levels of *BBX14* in light-grown *glk1* seedlings (**Figure 6 A**) are dependent on GLK1, which is corroborative with a previous finding by Veciana et al., (2022), suggesting that BBX14 might share function with BBX15 and BBX16. Additionally, *glk1* seedlings were observed to develop longer hypocotyls in the light. Strikingly, hypocotyl lengths of *bbx14* and *glk1* mutants were similarly elongated (**Figure 6 B, C**).

During the early developmental stages of germinating seedlings, chloroplast biogenesis is intricately regulated by environmental cues, with "biogenic control" facilitating signaling from chloroplasts to the nucleus (see 1.1). This process involves a module comprising GLK1 and GUN1 (Leister & Kleine, 2016; Martin et al., 2016). Under conditions of very low white light (1 µmol m^{-2} sec^{-1}), the presence of LIN partially inhibits de-etiolation in WT seedlings, leading to longer hypocotyls (Martin et al., 2016). Since the elongated hypocotyl of the *bbx14* seedlings was observed under 100 µmol m^{-2} sec^{-1}, which is routinely used to screen for *gun* phenotypes, it was further used to compare hypocotyl growth between WT, *bbx14* and *glk1* line in the presence of LIN. When subjected to these conditions, *bbx14* seedlings exhibited extended hypocotyls, akin to *gun* phenotype, suggesting a defect in the regulatory pathway. However, hypocotyl lengths in WT seedlings were further reduced in the presence of LIN (**Figure 6 C**), implying that the etiolation phenotype induced by LIN primarily manifests under extremely low light levels. Concordantly to this, when 2-day-old etiolated seedlings were exposed to white light at levels of 25 µmol m^{-2} sec^{-1}, comparable hypocotyl lengths were observed regardless of the presence of LIN by Martin et al., (2016), indicating that LIN's effect on hypocotyl length is contingent upon light intensity. Notably, the extended hypocotyl phenotype

of *bbx14* and *glk1* seedlings was mitigated when grown on LIN, aligning their hypocotyl lengths with those of the WT (**Figure 6 C**). Moreover, this effect could not be attributed to energy deficiency, as addition of sugar did not alleviate the effects of LIN and did not affect hypocotyl lengths in a significant way (**Figure 6 D**), thus suggesting a dependence on a retrograde signal rather than energy availability. The observed effects of LIN-induced retrograde signal on hypocotyl growth in *bbx14* and *glk1* mutant was also observable when growing seedling in absence of light (**Figure 6 E**) implying that the regulation of hypocotyl growth occurs via a pathway independent of light. It is also noteworthy that hypocotyl growth in mutants deficient of *GLK1* rather mimicked the partial constitutively photomorphogenic dark-grown phenotype the *pifq* mutant with significantly shorter hypocotyls than the WT. This is in stark contrast to the *bbx14* which exhibits significantly elongated hypocotyls in etiolated condition, although not as strong as in presence of light (**Figure 6 C**).

Previous research has demonstrated the antagonistic regulation between RS and phytochrome pathways on the PIF-repressed transcriptional network, with PIF4 and GLK1 binding to the core promoter of *BBX14*. To address this, dark-grown Col-0 and *pifq* seedlings, which lack PIF1, -3, -4, -5, were grown in the presence and absence of LIN and *BBX14* expression was analyzed. In etiolated *pifq* seedlings, mRNA levels of BBX14 were de-repressed compared to WT seedlings, indicating a regulatory role for PIFs in *BBX14* expression, which was abrogated by lincomycin treatment (**Figure 6 F**). Taken together, these results suggested that *BBX14* is a PIF-repressed gene during seedling establishment in the dark and is induced by light in a GLK1-mediated manner.

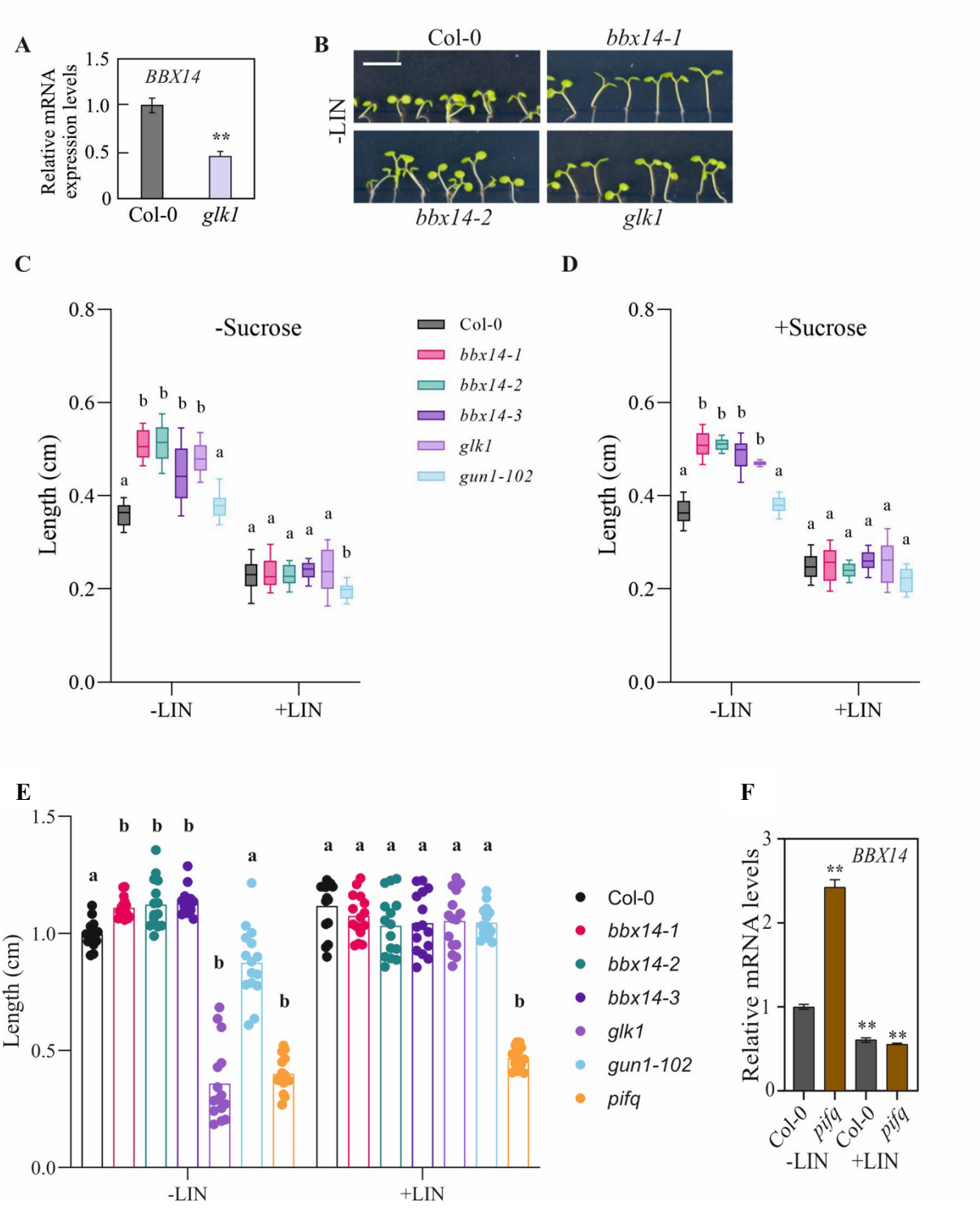

Figure 6. The *bbx14* mutant exhibits a long hypocotyl phenotype that depends on a retrograde signal.

(A) *BBX14* mRNA levels in 3-day-old Col-0 and *glk1* mutant seedlings grown for 3 days under standard growth conditions (16-h light/8-h dark; 100 µmol photons m^{-2} s^{-1}) as determined by RT-qPCR. The results were normalized to *AT4G36800*, which encodes a RUB1-conjugating enzyme (RCE1). Expression levels are reported relative to the corresponding transcript levels in Col-0 which were set to 1. Mean values ± SEM were derived from three independent experiments, each with three technical replicates. Statistically significant differences (Tukey's test; $^{**}P < 0.01$) between wild-type (Col-0) and the *glk1* mutant are indicated.

(B) Phenotypes of Col-0 and mutant (*bbx14-1, bbx14-2, and glk1*) seedlings grown for 6 days under standard growth conditions without lincomycin (-LIN) supplementation. Scale bar = 0.5 cm.
(C) Quantification of hypocotyl lengths of Col-0 and mutant (*bbx14-1, bbx14-2, bbx14-3, glk1 and gun1-102*) seedlings grown for 6 days under standard growth conditions on MS medium without (-LIN), or with inhibitor supplementation (+LIN). The center line of boxplots indicates the median, the box defines the interquartile range, and the whiskers indicate minimum and maximum values from three independent experiments, each containing at least 50 seedlings. Statistically significant differences between the wild-type and each mutant line under every condition are highlighted by letters above the plots (two-way ANOVA; a, no significant difference; b, $P < 0.0002$).
(D) Quantification of hypocotyl lengths of seedlings grown under the same conditions as in **(C)**, but with addition of sucrose (1%) to the growth medium.
(E) Quantification of hypocotyl lengths of dark-grown Col-0 and mutant (*bbx14-1, bbx14-2, bbx14-3, glk1, gun1-102, and pifq*) seedlings grown for 3 days under standard growth conditions on MS medium without (-LIN), or with inhibitor supplementation (+LIN). Data are shown as mean values ± SD of the 15 longest seedlings from three independent experiments. Statistically significant differences between the wild-type and each mutant line under every condition are highlighted by letters above the plots (t-test; a, no significant difference; b, $P < 0.05$).
(F) RT-qPCR of *BBX14* mRNA levels in 3-day-old dark-grown Col-0 and *pifq* seedlings in the absence (-LIN) or presence of lincomycin (+LIN). RT-qPCR was performed and evaluated as described in **(A)**. Expression values are reported relative to the corresponding transcript levels in Col-0 grown without LIN, which were set to 1.

4.4. Repression of *BBX14* expression during biogenic signaling depends on GUN1

BBX14 was identified as part of the OGE core module encompassing other TFs involved in stress and signaling responses that showed differential expression under NF and LIN treatment (Kleine & Leister, 2016). To confirm whether this also applies for other members of the BBX TF family or it's a unique feature of BBX14, data regarding 25 members of the BBX protein family in Arabidopsis was extracted from Genevestigator (https://genevestigator.com) and analyzed. The results indicated that among the *BBX* members evaluated on the Affymetrix ATH1 chip, mRNA levels of *BBX3*, *BBX14*, *BBX16*, and *BBX27* were reduced in seedlings treated with NF, while under LIN conditions, only *BBX14* and *BBX16* mRNAs showed partial repression (**Figure 7 A**). Complementing these findings, re-analysis of previously published RNA-Seq data (Habermann et al., 2020; Richter et al., 2020; Xu et al., 2020) confirmed reduced transcript levels of *BBX14* and *BBX16* under NF and LIN treatments, as indicated by their Transcripts Per Kilobase Million (TPM) values (**Figure 7 B**) and when compared to two controls – *LIGHT HARVESTING CHLOROPHYLL A/B-BINDING PROTEIN 1.2* (*LHCB1.2*) and *BBX8*. *LHCB1.2* expression is known to decrease under NF or LIN treatment, and *BBX8*, representing other BBX members was shown to be unaffected by NF or LIN, behaved as expected, further validating the Genevestigator results (**Figure 7 A**). Additionally, the data

revealed that the decrease in *BBX14* and *BBX16* mRNA levels under NF conditions is mitigated in *gun1* and *gun5* mutants. Since BBX16 has recently been connected to GUN1-mediated RS (Veciana et al., 2022) and similarly affected as BBX14 by NF and LIN treatments based on previously analysis (**Figure 7 B**) it was further tested if this could also be the case for BBX14. The *gun1* mutant is unique as it exhibits de-repression of *PhANGs* (e.g. *LHCB1.2, 1.4* and *2.2*) under LIN conditions. Therefore, to investigate whether LIN-mediated repression of *BBX14* is reliant on GUN1, the expression of *BBX14* mRNA was assessed in 4-day-old Col-0 and *gun1-102* seedlings grown on medium with or without LIN. Under LIN treatment, *BBX14* levels decreased to 17% in Col-0 compared to control conditions (**Figure 7 C**), and this reduction was GUN1-dependent, as *BBX14* expression almost fully recovered in *gun1-102* seedlings treated with LIN. Combined with ChIP-Seq data (**Figure S1**) and the nuclear localization of BBX14 (**Figure 7 D**), these findings suggest that BBX14 may serve as a mediator for GUN1/GLK1-dependent retrograde signals in the nucleus. GUN1-mediated retrograde signaling regulates a multitude of crucial TFs linked to many processes and consequently their down-stream targets (Hernandez-Verdeja et al., 2022). In order to elucidate weather this regulation occurs not only on mRNA levels, but also post-transcriptionally, the steady state expression levels of BBX14 in two *gun* mutants - *gun1-102* and oeGLK1 were compared to the *bbx14* and WT in 7-days-old seedlings in the presence and absence of LIN (**Figure 7 E**). The results revealed that BBX14 accumulation in mutants with lacking GUN1 or overexpression GLK1 is independent of retrograde signaling as addition of LIN to the media did not significantly alter BBX14 protein synthesis, suggesting that the GUN1-mediatited response to RS (i.e. LIN treatment) does not contribute to the protein accumulation but rather negatively impacts the *BBX14* gene expression.

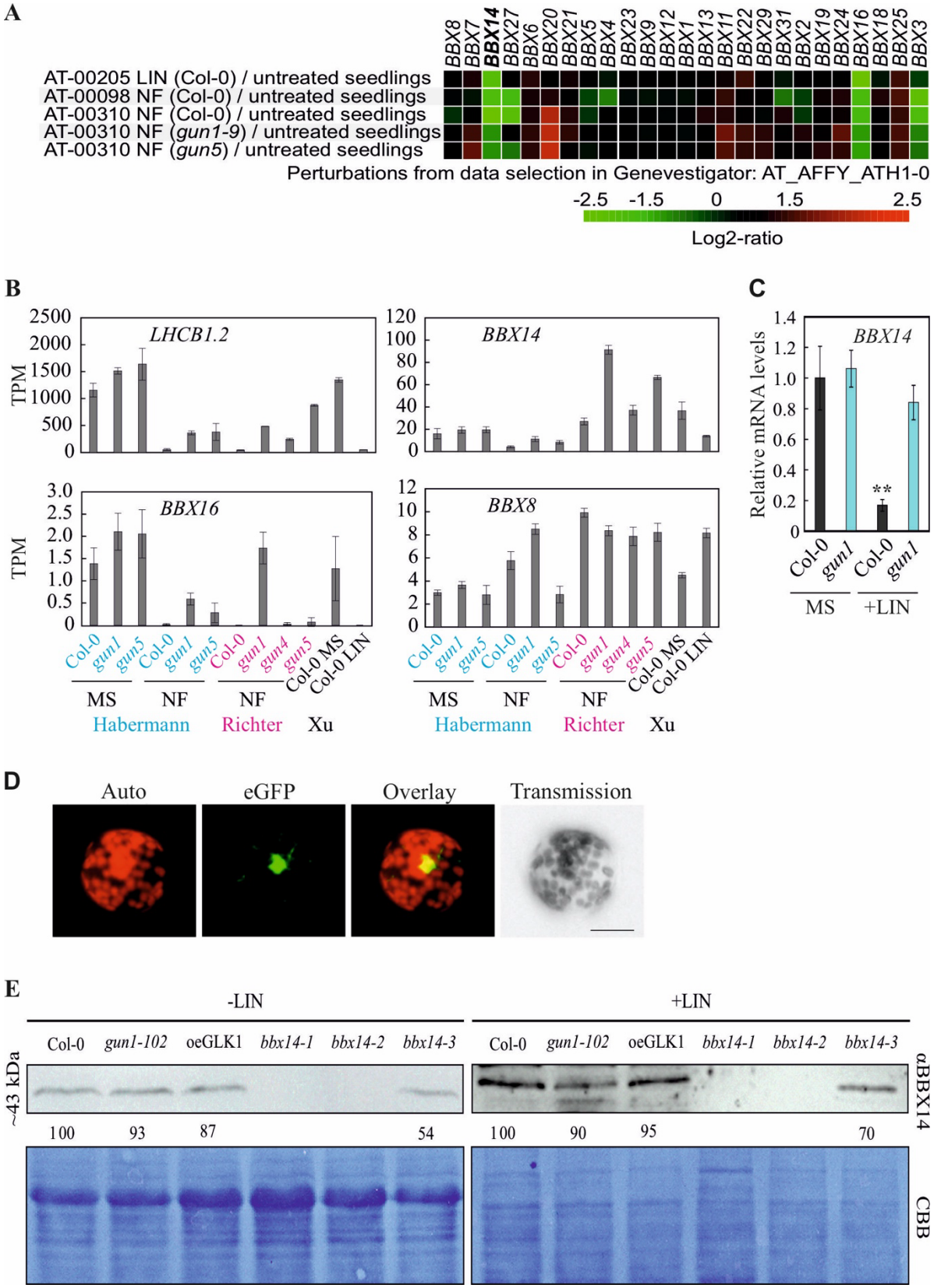

Figure 7. *BBX14* mRNA expression depends on GUN1-mediated RS.

(A) The reduction of *BBX14* mRNA levels during biogenic signaling depends on GUN1. Global profiling of *BBX* mRNA levels in response to perturbations were determined with Genevestigator, and studies involving lincomycin

(LIN) and norflurazon (NF) treatments are shown. Note that seven out of the 32 *BBX* genes were not assessed due to their absence from the Affymetrix ATH1 genome array.

(B) TPM (Transcripts Per Kilobase Million) values of re-analyzed RNA-Seq data published by (Habermann et al., 2020), (Richter et al., 2020) and (Xu et al., 2020).

(C) RT-qPCR of *BBX14* mRNA levels in Col-0 and *gun1* seedlings grown for 4 days in continuous light (100 µmol photons m^{-2} s^{-1}) in the absence (MS) or presence of lincomycin (+LIN). Expression values are reported relative to the corresponding transcript levels in Col-0 grown on MS, which were set to 1. Mean values ± SEM were derived from three independent experiments, each with three technical replicates. Statistically significant differences (Tukey's test; $^{**}P < 0.01$) between wild-type and mutant are indicated.

(D) BBX14 is localized to the nucleus. Fluorescence microscopy of tobacco protoplasts transiently expressing BBX14 fused to eGFP. The eGFP fluorescence (green) and chloroplast autofluorescence (red) are shown together in the overlay picture. BBX14-GFP fusion protein was observed in freshly prepared protoplast two days after Agrobacteria-mediated transfection using a fluorescence microscope Scale bar = 10 µm.

(E) Steady state expression levels of BBX14 in *gun* mutants (*gun1-102* and oeGLK1) compared to *bbx14* mutant lines and wild-type (Col-0). Aliquots of total proteins were isolated from 7-days-old whole seedlings grown on ½ MS medium in absence (-LIN) or presence or 220 mM lincomycin (+LIN) at 100 µmol photons m^{-2} s^{-1} continuous white light. Proteins were fractionated on polyacrylamide gels (10 %) under reducing conditions and subjected to immunoblotting using monoclonal antibody raised against BBX14. PVDF membranes were stained with Coomassie brilliant blue (CBB) to visualize protein loadings after western blot transfer. Band intensity was quantified using ImageJ software.

4.5. Overexpression of BBX14 potentially affects seedling growth

To further evaluate the biological role of BBX14 in seedling establishment and retrograde signaling, mutant lines overexpressing BBX14 were generated and characterized. Based on previous knowledge it was posited that overexpression of BBX14 might induce a *gun* phenotype, or conversely, a deficiency in BBX14 could trigger a *LHCB1.2* hypersensitive phenotype, akin to oeGLK lines (Leister & Kleine, 2016; Martin et al., 2016). To generate plants overexpressing BBX14 (oeBBX14), Col-0 plants were transformed with a DNA fragment comprising the 35S Cauliflower Mosaic Virus promoter and the coding sequence of *BBX14*, fused upstream of either the enhanced green fluorescence protein (eGFP) or a hemagglutinin (HA) tag. Following selection for the resistance marker, 10 lines for each construct were identified, but fusion proteins were detected in only three of the oeBBX14-eGPF lines and two oeBBX14-HA lines (**Figure 8 A**). Only one of these lines exhibited elevated levels (2.2-fold) of the BBX14 transcript compared to Col-0 plants, while the others contained slightly less than the WT control (**Figure 8 B**). As such, the remaining seeds from Col-0 plants bearing the overexpression constructs underwent another round of selection, and all resistant seedlings were transferred to medium without herbicide. Through this process, the

selection process based on a paler and smaller phenotype compared to Col-0 seedlings (**Figure 8 C**). Western blot analysis suggested that the severity of the seedling phenotype might correlate with the degree of BBX14 overexpression (**Figure 8 D**). However, this phenotype was absent in the T2 generation (**Figure 8 E**) as well when seedlings were further grown for up to 3 weeks and longer (**Figure S6**). To elucidate this phenomenon, an inducible BBX14 line (designated TPT14; only one line available) from the TRANSPLANTA collection was utilized (Coego et al., 2014). After 4 days of induction with ß-estradiol, TPT14 seedlings exhibited clear perturbations (**Figure 8 E**) and shorter hypocotyls (**Figure 8 F**), much like lines overexpressing BBX16 (Veciana et al., 20220), whereas they displayed a WT-like hypocotyl length when not induced. As previously shown here, deficiency in BBX14 resulted in longer hypocotyls (**Figure 5**), thus, the hypocotyl phenotype appears to be linked to the degree of BBX14 overexpression. In the T2 generation, the oeBBX14-tag lines only exhibited a 2-fold increase in *BBX14* transcript abundance compared to Col-0 plants, a level of BBX14 overexpression similar to that observed in previously published BBX14 overexpressors (Buelbuel et al., 2023). Conversely, *BBX14* mRNA levels were elevated 5-fold in the induced TPT14 plants (**Figure 8 G**).

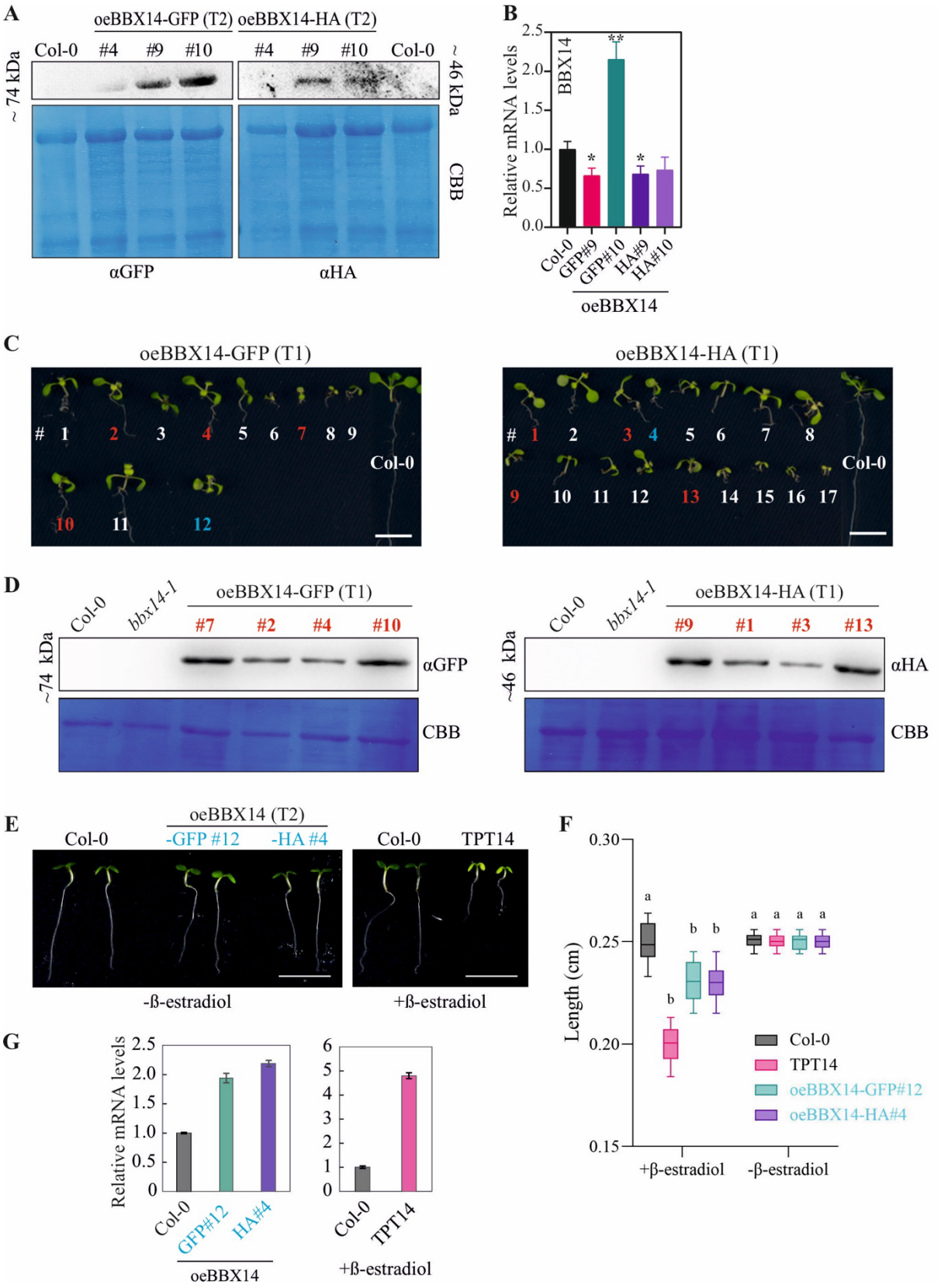

Figure 8. Overexpression of *BBX14* may have detrimental effects on seedling phenotype

(A) Total leaf proteins were isolated from 2-week-old Col-0 and Col-0 plants transformed with constructs containing *BBX14-eGFP* or *BBX14-HA* fusions, which were placed under the control of the *35S* promoter. Aliquots were fractionated by 10% SDS-PAGE gels under reducing conditions and subjected to immunoblotting

using antibodies raised against the GFP- or HA-tag, respectively. PVDF membranes were stained with Coomassie brilliant blue (CBB) to control for protein loading. Representative blots from two experiments are presented. Relative sizes of the BBX14-GFP and BBX14-HA fusion proteins are indicated.

(B) RT-qPCR of *BBX14* mRNA expression in 7-day-old wild-type (Col-0), and in Col-0 plants "overexpressing" BBX14 (oeBBX14). RT-qPCR was performed as described in the legend to Figure 5 **(A)**.

(C) Phenotypes of 10-day-old wild-type (Col-0) seedlings, and Col-0 seedlings transformed with constructs containing the coding region of *BBX14* fused to either the GFP- (left panel) or the HA-tag (right panel), which were placed under the control of the *35S* promoter. Seedlings labeled in red provided the protein extracts from T1 plants that were subjected to SDS-PAGE in panel **(D)**. The T2 generation of seedlings marked in turquoise was utilized to create images and data in panels **(E)** and **(F)**, respectively. Scale bar = 0.5 cm.

(D) Aliquots of total leaf proteins were isolated from plants as indicated in **(C)**, fractionated on SDS-PAGE gels (10%) under reducing conditions, and subjected to immunoblotting using antibodies raised against the GFP- or HA-tag, respectively. PVDF membranes were stained with Coomassie brilliant blue (CBB) to show protein loading.

(E) Phenotypes of 4-day-old Col-0 seedlings and the inducible BBX14 (TPT14) overexpression line grown under standard conditions (16-h light/8-h dark and 100 µmol photons m^{-2} s^{-1}) in the absence (- ß-estradiol) or presence of β-estradiol. Scale bars = 0.5 cm.

(F) Quantification of hypocotyl lengths of seedling grown as in **(E)**. The center line of boxplots indicates the median, the box defines the interquartile range, and the whiskers indicate minimum and maximum values from three independent experiments, each containing at least 50 seedlings. Statistically significant differences between the wild-type and each mutant line under every condition are highlighted by letters above the plots (two-way ANOVA; a, no significant difference; b, $P < 0.0002$).

(G) RT-qPCR of *BBX14* mRNA expression in seedlings shown in panel **(E)**. RT-qPCR was performed and evaluated as described in the legend to Figure 5 **(A)**.

4.6. Role of BBX14 and BBX15 in GUN1-mediated retrograde signaling

Building on the notion that BBX14 is involved in *gun*-type singling via the GUN1/GLK1-module, it was hypothesized that BBX14 could participate in the downregulation of *PhANGs* expression in response to retrograde signals. Therefore, the expression of known RS-regulated *PhANGs* (i.e. *LHCB1.2*, *LCHB1.4*, *LHCB.2.2* and *CA1* (Waters et al., 2009)) was examined. To this end, Col-0, *gun1-102* (as a control), the *bbx14* mutant, and the strongest "overexpression" seedlings obtained (oeBBX14-GFP#10; **Figure 8 B**) were cultured in the presence or absence of LIN for 4 days under continuous light (100 µmol m^{-2} sec^{-1}). Following LIN treatment, *gun1-10*2 exhibited the expected upregulation of *LHCB1.2* mRNA compared to WT seedlings, while *LHCB1.2* levels remained unchanged in both *bbx14* mutants and the "oeBBX14" line (**Figure S3 A**). Additionally, the expression of *LHCB2.1* and *LHCB2.4* was unchanged in lines with altered BBX14 levels (**Figure S3 B**). However, slightly higher *CA1* expression levels were observed in the "oeBBX14" line in comparison to WT (**Figure S3 B**).

Given that a 2.2-fold induction of BBX14 (**Figure 5 B**) might not be sufficient to induce a true *gun* phenotype, instead the *gun* phenotype in the TPT14 line was sought to be examined. To mitigate potential secondary effects (**Figure 8 E**), a different experimental approach to assess *gun* phenotypes was implemented. Seedlings were initially grown for 3 days in darkness in the absence or presence of inhibitors (NF or LIN), then treated with the inducer, returned to darkness for 2 hours, transferred to light for 16 hours (100 µmol m^{-2} sec^{-1}), and subsequently harvested for quantitative real-time PCR (qRT-PCR). Intriguingly, *BBX14* induction was higher in seedlings treated with NF compared to those treated with LIN or grown without inhibitors (**Figure 9 A**). In the absence of inhibitors, *RBCS1A* expression levels resembled those observed in Col-0 across all lines tested, whereas *LHCB1.2* and *CA1* levels were slightly elevated in the *gun1* control and the inducible TPT14 line (**Figure 9 B**). Furthermore, the eligibility of this approach in evaluating *gun* phenotypes was validated by the de-repression of the RS marker genes *LHCB1.2*, *CARBONIC ANHYDRASE 1* (*CA1*), and *RIBULOSE BISPHOSPHATE CARBOXYLASE SMALL CHAIN 1A* (*RBCS1A*) in *gun1* seedlings (**Figure 9 B**). In the TPT14 line, the accumulation of *LHCB1.2* mRNA exhibited considerable variability across experiments and was only upregulated 2-fold (**Figure 9 B**), as indicated by the expression ratio of *LHCB1.2* between NF and MS samples. On the other hand, under NF treatment, the mRNA levels of *CA1* and *RBCS1A* within the TPT14 line were closely resembled those observed in the *gun1* mutant, implying that BBX14 might be required for the de-repression of genes outside of the *LHCB* cluster during biogenic signaling.

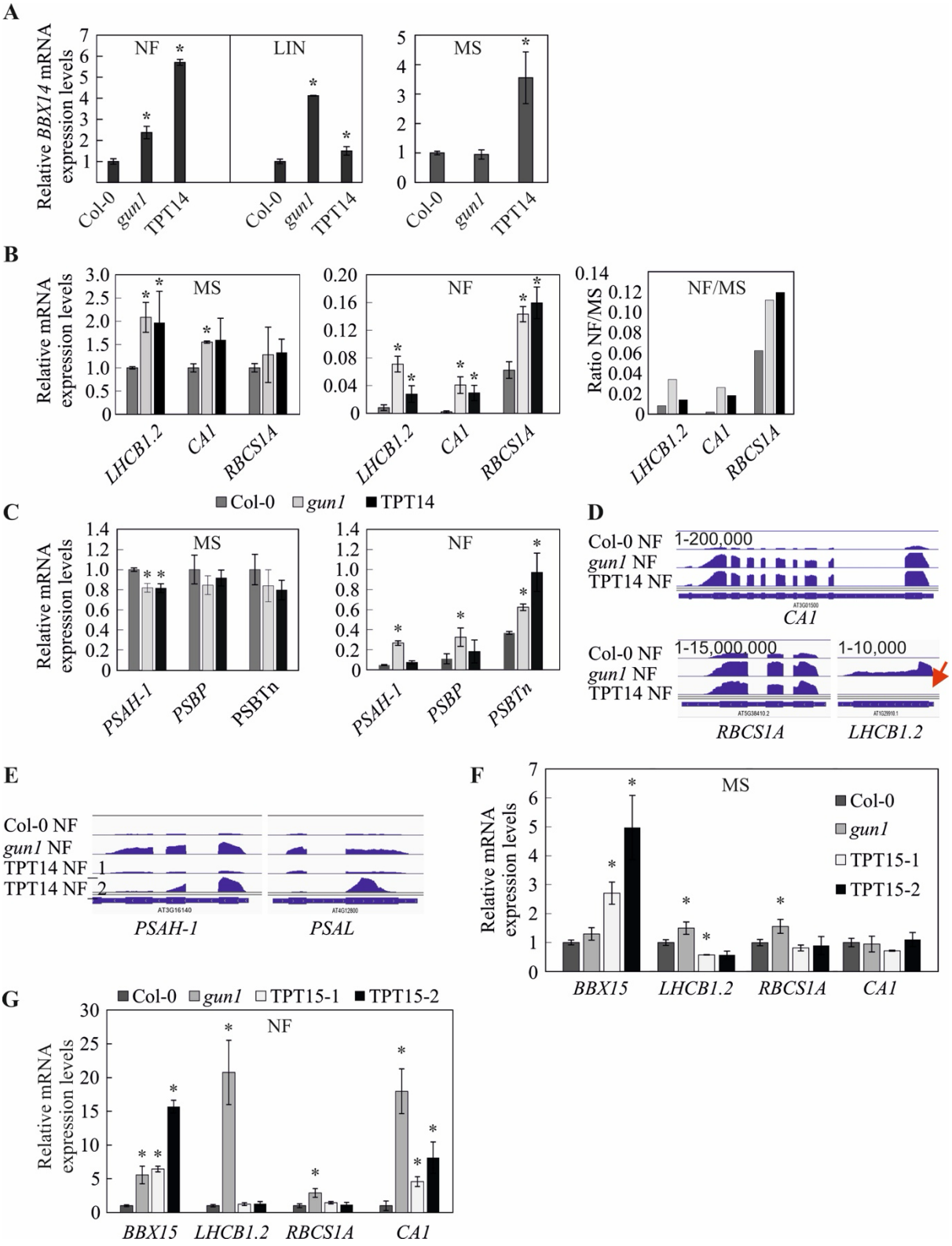

Figure 9. Overexpression of BBX14 or BBX15 does not result in clear *gun* phenotypes.

(A) Levels of *BBX14* mRNAs in seedlings grown for three days in the dark in the presence of NF, LIN, or no supplementation, sprayed with inducer, put back for 2 h in the dark, placed for 16 hours into light (100 µmol m^{-2} s^{-1}) and then harvested for qRT-PCR. The results were normalized to *RCE1*. Expression values are reported relative to the corresponding transcript levels in Col-0, which were set to 1. Mean values were derived from four

independent experiments, each with three technical replicates. Bars indicate standard deviations. Statistically significant differences (Tukey's test; $P < 0.05$) between Col-0 and mutant samples are indicated by an asterisk.
(B, C) Transcript levels of the retrograde marker genes *LHCB1.2*, *CA1*, and *RBCS1A* **(B)**, and *PHOTOSYSTEM I* (*PSI*) *SUBUNIT H-1* (*PSAH-1*), and *PSII SUBUNIT P* (*PSBP*) and -*Tn* (*PSBTn*) **(C)** in seedlings treated as in **(A)**. Statistics were done as described in **(A)**. To account for expression differences in the different genotypes observed in the absence of NF, the ratio of the expression ratio in seedlings grown in the presence of inhibitor to that in seedlings grown in the absence of inhibitor was calculated (NF/MS). The results were normalized to *RCE1*. Mean values were derived from four independent experiments, each with three technical replicates. Bars indicate standard deviations.
(D) Snapshots of RNA-Seq data. The read depths were visualized with the Integrative Genomics Viewer (IGV). The red arrow points out *LHCB1.2* expression, which is not increased in TPT14.
(E) Snapshots demonstrating the accumulation of the photosynthesis genes *PSAH-1* and *PSAL*.
(F, G) Transcript levels of *BBX15* and retrograde marker genes in Col-0, *gun1* and TPT15-1 and -2 seedlings treated as in (**A**) and grown on MS plates without inhibitor **(F)** or supplemented with NF **(G)**. Statistics were done as described in **(A)**.

To gain a comprehensive understanding of potential targets regulated by BBX14 during initial steps of retrograde signaling, RNAs extracted from Col-0, *gun1*, and TPT14 seedlings grown on NF, induced as described above, and subjected to RNA-Seq analysis. In the *gun1* mutant, 901 genes exhibited mRNA levels reduced by more than 2-fold (no adjusted p-value; see 3.2.4.2.) relative to WT, while 1080 genes showed elevated expression, with transcripts encoding LHCB proteins among the most strongly up-regulated (**Figure S4 A**). The number of differentially regulated transcripts in TPT14 was comparatively lower, with 252 genes identified to have elevated expression in both *gun1* and TPT14, whereas 148 exhibited down-regulation in both lines (**Figure S4 A**). These included *RBCS1A* and *CA1*, validating qRT-PCR findings shown previously in **Figure 9 A, B**. Notably, GO analysis of these 252 up-regulated genes revealed "Photosynthesis" and "Cellular nitrogen compound biosynthesis" as significantly enriched categories (**Figure S4 B**). In order to solidify the findings from the RNA-Seq analysis (**Figure S4**) due to the lack of adjusted *P*-value cutoff, three of the identified targets involved in photosynthesis underwent further investigation through RT-qPCR. Under inhibitor-free conditions, mRNA accumulation of *PHOTOSYSTEM I (PSI) SUBUNIT H-1* (*PSAH-1*), *PSII SUBUNIT P* (*PSBP*), and -*Tn* (*PSBTn*) remained comparable across the two genotypes. Upon NF treatment, however, mRNA levels of all examined transcripts were elevated in the *gun1* mutant, with only *PSBT* showing a significant increase in the TPT14 line (**Figure 9 C**). It is noteworthy that *LHCB1.2* did not exhibit higher expression in TPT14 post-NF treatment. This finding is in accordance with the RNA-Seq data visualization whereby read

depths were plotted over *LHCB1.2*, *CA1*, and *RBCS1A* genes (**Figure 9 D**). Furthermore, visualization of photosynthesis transcript accumulation, as identified by the enrichment analysis (**Figure S4**), yielded an inconclusive result (**Figure 9 E**).

Knowledge of the exact molecular function of clade III of AtBBX proteins BBX14–BBX17 is relatively limited. Previous research on BBX16 has provided fundamental data in this regard. In particular, the impact of BBX16 overexpression on *gun* signaling has been highlighted (Veciana et al., 2022). In addition to BBX16 and BBX14 being identified as direct target of GLK1 (**Figure S1**), the promoter of BBX15 was also among the identified targets of GLK1 (**Table S1**) and this finding is further reinforced by the high homology between BBX14 and BBX15 (**Figure S7**). Together, this prompted the evaluation of inducible BBX15 lines, TPT15-1 and -2. Successful induction of BBX15 expression in the TPT15 lines was observed (**Figure 6 F**), with no alterations in the mRNA levels of retrograde marker genes under control conditions (**Figure 9 F**). Upon NF treatment, both TPT15 lines exhibited elevated expression of *CA1*, while *RBCS1A* and *LHCB1.2* levels remained comparable to those in the WT (**Figure 9 G**). These findings indicate that, similar to BBX16 (Veciana et al., 2022), both BBX14 and BBX15 do not directly regulate *LCHB1.2* expression during RS. However, they appear to rather influence the expression of certain *PhANGs*, such as *CA1* and *RBCS1A* (in the case of BBX14) or CA1 (in the case of BBX15). This divergence hints at potential branching in signaling pathways downstream of GLK1, whereby GLK1-mediated regulation of some *PhANGs* could be indirect through the transcriptional control of BBX14 and BXX15, and potentially other factors. This is further supported by the finding that while *LCHB1.4* and *LHCB.2.2* are identified as primary targets of GLK1, *CA1* and *RBCS1A* do not meet the criteria to be classified within this group (Waters et al., 2009).

4.7. BBX14 is required for high light stress acclimation

The reduction in *BBX14* transcript levels under high light conditions has been consistently observed in various studies (Garcia-Molina et al., 2020; Huang et al., 2019; Kleine et al., 2007; Leister & Kleine, 2016). Moreover, *BBX* members, including *BBX14*, have been shown to exhibit significant changes in transcript levels during both short and long term (de)acclimation to HL and when shifted from normal growth light conditions to conditions with increased irradiance, thereby underscoring the role of BBX14 in light stress acclimation. This is further corroborated by data from the Genevestigator perturbations tool (https://genevestigator.com; **Figure 10 A**). Notably, among all the *BBX* members analyzed on the Affymetrix ATH1 chip,

this decrease in expression levels after HL treatment was particularly pronounced for *BBX14*. Furthermore, Huang et al. (2019) identified several *BBX* members as one of the most severely repressed under HL treatment and proposed *BBX14* as one of the top three hub genes in an HL co-expression network, suggesting its pivotal role as a core regulator in the HL response. It is therefore reasonable to assume that overexpression of BBX14 could enhance plant tolerance to HL, with even a 2-fold increase in BBX14 levels potentially offering significant support. To explore the potential role of BBX14 in the response to HL, 1-week-old plants of Col-0, *bbx14-1*, *bbx14-2*, and "oeBBX14" were subjected to increased light intensity (1000 µmol photons m^{-2} sec^{-1}) from their standard growth conditions (80 µmol photons m^{-2} sec^{-1}), a condition known to drastically reduce *BBX14* mRNA levels, as seen by the inhibition of *BBX14* expression for up to 48 hours of HL exposure (**Figure 10 B**). Notably, LED chambers were employed to ensure precise temperature control and eliminate heat contribution. Maximum quantum yield of PSII (F_v/F_m) was monitored under control temperature and humidity conditions, after 3, 8, and 12 hours of HL exposure, and following 12 and 36 hours of de-acclimation under normal growth light conditions. The time series analysis revealed that under control light conditions (0h), *bbx14* and "oeBBX14" seedlings closely resembled the WT (**Figure 10 C**; **Figure S5**), whereas upon HL treatment, the "oeBBX14" line exhibited behavior similar to the WT (**Figure S5**). In contrast, *bbx14* mutant plants exhibited a noticeable reduction in F_v/F_m compared to WT as early as 3 hours into HL exposure (**Figure 10 C, D**), with this reduction persisting in a staggering manner throughout the duration of HL treatment (3h–12h). However, the F_v/F_m values of seedlings lacking BBX14 recovered after de-acclimation in standard growth conditions (**Figure 10 C, D**). Additionally, while the chlorophyll content of *bbx14* mutant seedlings was comparable to that of the WT under normal conditions (0h), it decreased slightly but significantly at all time points of the HL treatment (3h–12h; **Figure 10 E**). Importantly, the observed HL phenotype in *bbx14* mutant was not attributed to reduced chlorophyll accumulation, as evidenced by comparisons with the *gun4-2* mutant, which exhibited reduced chlorophyll levels (**Figure S5 C)** but significantly higher Fv/Fm values (**Figure S5 B)** relative to WT during HL exposure. These findings collectively suggest a beneficial role for BBX14 in maintaining plant growth under the tested HL conditions, reinforcing the notion that HL damage partially inhibits BBX14 induction, in agreement with recent transcriptomic data obtained under HL stress (Huang et al., 2019).

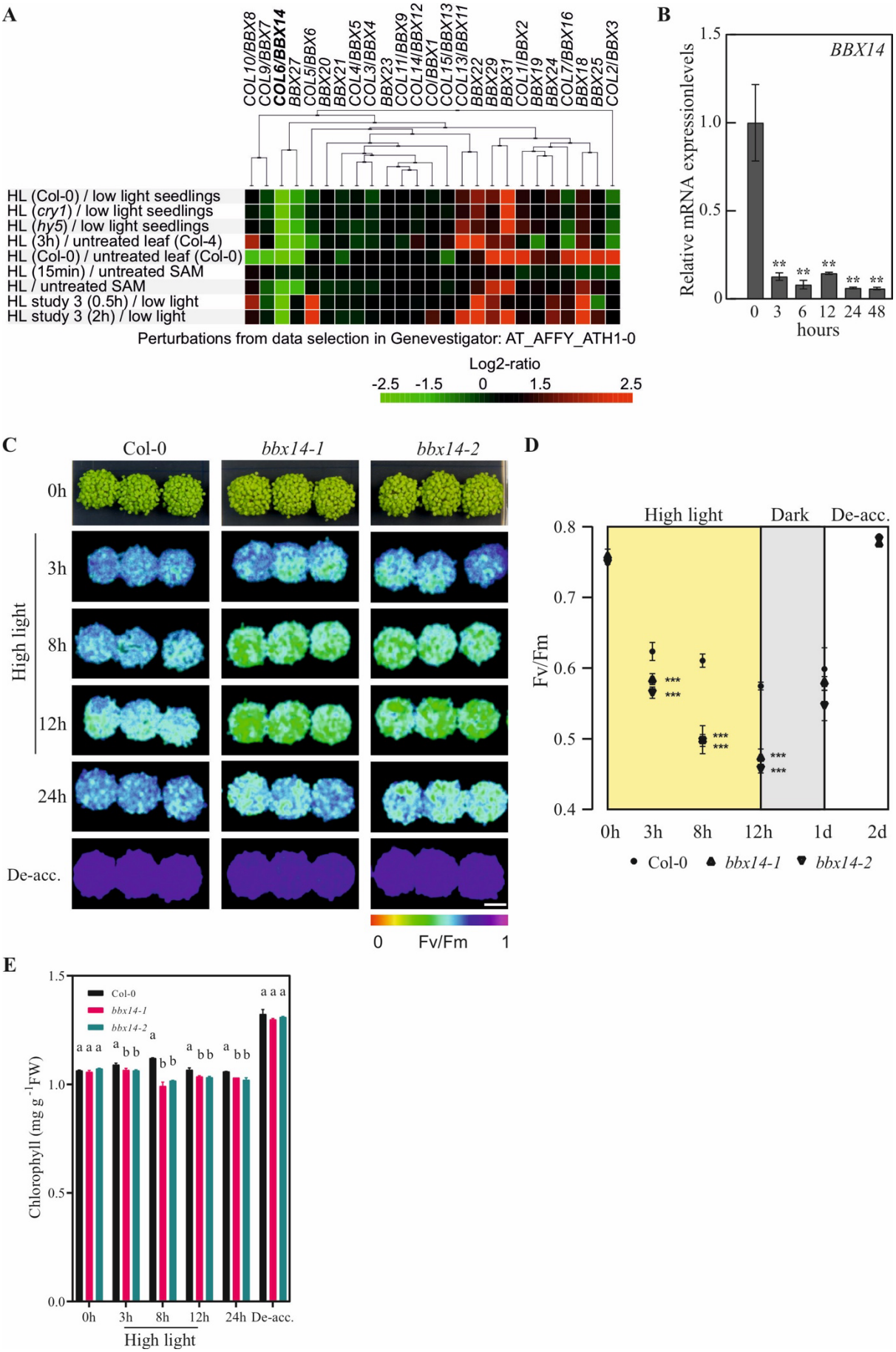
A
COL10/BBX8
COL9/BBX7
COL6/BBX14
BBX27
COL5/BBX6
BBX20
BBX21
COL4/BBX5
COL3/BBX4
BBX23
COL11/BBX9
COL14/BBX12
CO/BBX1
COL15/BBX13
COL13/BBX11
BBX22
BBX29
BBX31
COL1/BBX2
BBX19
BBX24
COL7/BBX16
BBX18
BBX25
COL2/BBX3
HL (Col-0) / low light seedlings
HL (cry1) / low light seedlings
HL (hy5) / low light seedlings
HL (3h) / untreated leaf (Col-4)
HL (Col-0) / untreated leaf (Col-0)
HL (15min) / untreated SAM
HL / untreated SAM
HL study 3 (0.5h) / low light
HL study 3 (2h) / low light
Perturbations from data selection in Genevestigator: AT_AFFY_ATH1-0
Log2-ratio
-2.5 -1.5 0 1.5 2.5
B
BBX14
Relative mRNA expressionlevels
1.5
1.0
0.5
0
0 3 6 12 24 48
hours
C
Col-0
bbx14-1
bbx14-2
0h
3h
8h
12h
24h
De-acc.
High light
0
Fv/Fm
1
D
High light
Dark
De-acc.
Fv/Fm
0.8
0.7
0.6
0.5
0.4
0h 3h 8h 12h 1d 2d
Col-0
bbx14-1
bbx14-2
E
Col-0
bbx14-1
bbx14-2
Chlorophyll (mg g-1FW)
1.5
1.0
0.5
0.0
0h 3h 8h 12h 24h De-acc.
High light

Figure 10. BBX14 is involved in high light (HL) acclimation.

(A) Global profiling of *BBX* mRNA levels in response to perturbations was carried out with Genevestigator, and studies involving HL treatments are shown. The cladogram at the top summarizes the degree of relatedness between the expression profiles of the different *BBX* genes. SAM, shoot apical meristem.

(B) RT-qPCR of *BBX14* expression in 7-day-old Col-0 plants grown under control conditions and then shifted to light level for up to two days. The results were normalized to *AT4G36800*, which encodes a RUB1-conjugating enzyme (RCE1). Expression values are reported relative to the corresponding transcript levels in Col-0, which were set to 1. Mean values ± SE were derived from two independent experiments, each performed with three technical replicates per sample. Statistically significant differences (Tukey's test; $^{**}P < 0.01$) between control and each HL time point are indicated.

(C) Phenotypes and Imaging PAM pictures of Col-0 and mutant (*bbx14-1, bbx14-2*) plants grown for 1 week under control conditions (16-h light/8-h dark, 80 µmol photons m^{-2} s^{-1}; left panel), shifted to high light (HL) conditions (16-h light/8-h dark, 1000 µmol photons m^{-2} s^{-1}), and then de-acclimated (de-acc.) in control conditions. Scale bar = 1 cm.

(D) Photosystem II maximum quantum yield (Fv/Fm) of wild-type (Col-0) and mutant (*bbx14-1 and bbx14-2*) seedlings grown as described in **(C)**.

(E) Determination of total chlorophyll (Chl *a* + *b*) contents of seedlings grown as in **(C)**. Data are shown as mean values ± SD from 3 different plant pools. Each pool contained more than 100 seedlings. Statistically significant differences between the wild-type and each mutant line at each time point are highlighted by letters above the plots (t-test; a, no significant difference; b, $P < 0.05$).

5. Discussion

In Arabidopsis, BBX proteins constitute a diverse family with various members playing distinct roles in plant physiology and development. While BBX14, BBX15, BBX16, and BBX17 have garnered significant attention, other BBX proteins also contribute to various aspects of plant biology. For example, BBX18 has been implicated in the regulation of flowering time through its interaction with CONSTANS (Suarez-Lopez et al., 2001). Similarly, BBX19, another member of the family, has been identified as a regulator of the circadian clock, modulating the expression of genes involved in photoperiodic responses (Yuan et al., 2021). Furthermore, BBX24 has been linked to photomorphogenesis and regulation of hypocotyl elongation in response to light stimuli (Gangappa et al., 2013). Additionally, BBX32 has been associated with the regulation of chloroplast development and photosynthesis-related gene expression (Kang et al., 2019). These studies collectively highlight the diverse functions of BBX proteins in Arabidopsis, spanning from the control of flowering time and circadian rhythms to modulation of light signaling pathways and chloroplast biogenesis. Further exploration of the roles and regulatory mechanisms of other BBX proteins will contribute to a comprehensive understanding of their involvement in plant growth, development, and adaptation to changing environmental conditions. BBX proteins are pivotal regulators of light-responsive genes, integrating diverse light signals from photoreceptors to modulate plant development. Their interactions with signaling pathways, regulation of developmental processes, evolutionary conservation, and potential for crop improvement make them compelling subject for research in the context of photomorphogenesis. Moreover, the multifaceted roles of BBX proteins in light signaling and photomorphogenesis make them intriguing targets for research aimed at understanding how plants perceive and respond to light cues to optimize their growth and development extending beyond developmental processes to encompass responses to environmental cues and stressors.

BBX proteins play crucial roles in plant development and have emerged as significant contributors to the plant's ability to adapt to adverse environmental conditions, as evidenced by studies such as those by Alvarez-Fernandez et al. (2021) and Talar & Kielbowicz-Matuk (2021). Among these proteins, BBX14, along with BBX15–BBX17, is classified within clade III of the B-box proteins, as outlined by the fundamental classification of Arabidopsis BBX transcription factors from Khanna et al. (2009). Despite well-established classification framework and phylogenetic studies within the BBX TF family, not limited to Arabidopsis, but extending across other plant species, such as rice, barley, and maize, the precise biochemical

functions of many members remain largely unknown or poorly understood (Griffiths et al., 2003; Vaishak et al., 2019 Talar & Kielbowicz-Matuk, 2021). The conservation of BBX proteins is observed across various plant species, including cryptogams and entire angiosperms, as evidenced by a similar number of BBX genes present in these species. This conservation is not limited to structural features but may extend to functional aspects as well, as indicated by the evolutionary pattern observed in BBX genes across different plant species. However, despite the continuous discovery of various roles of BBX proteins in Arabidopsis, the extent of their functions in other species is still limited. Even in the well-established model crop plant *Oryza sativa* (rice), only a handful of these proteins have undergone functional characterization with *Hd1*, *OsCO3*, *OsCOL4*, *OsBBX14*, *OsCOL9*, and *OsCOL16* identified to regulate flowering under different light regimes (Huang et al., 2012). Similar to Arabidopsis, rice BBX proteins are also classified into five subfamilies. However, in rice the *OsBBX14* encodes a BBX protein with two B-boxes classified into subfamily IV and lacks a CCT domain (Bai et al., 2016).

Within clade III of BBX proteins in Arabidopsis, BBX16, initially characterized a decade ago, was identified as a phytochrome-B-dependent regulator involved in modulating branching and the shade avoidance response (Wang et al., 2013; Zhang et al, 2014). Over time, further insights into the functionalities of members within this clade have emerged. For instance, recent research has proposed that BBX17 interacts with CONSTANS to exert negative regulation over flowering time (Xu et al., 2022). Moreover, recent investigations by Buelbuel et al. (2023) have revealed BBX14's role in negatively modulating senescence induced by nitrogen starvation and darkness. Additionally, studies have identified BBX14, BBX15, and BBX16 as constituents of a GLK-BBX module implicated in the inhibition of precocious flowering, as demonstrated by Susila et al. (2023). Functional redundancy among BBX proteins complicates their study, as demonstrated by the shorter hypocotyls observed in the *bbx28bbx29bbx30bbx31* quadruple mutant compared to double and single mutants, indicating additive repression of seedling photomorphogenesis by clade V members BBX28-31 (Song et al., 2022). Feedback regulation adds another layer of complexity to the study of BBX proteins. For instance, while *BBX30* and *BBX31* are repressed by HY5 (Heng et al., 2019), BBX28 and BBX29 cooperate to prevent HY5 from binding to *BBX30* and *BBX31* promoters, leading to their expression. Moreover, BBX30 and BBX31 interact with *BBX28* and *BBX29* promoters, enhancing their expression, and BBX29 undergoes COP1-mediated degradation in darkness (Heng et al., 2019; Song et al., 2020), thereby indicating the intricate network that BBX proteins constitute in the regulation of COP1/SPA-HY5-mediated seedling establishment.

Within clade III, BBX15 shows the closest relationship to BBX14, followed by BBX16 and BBX17 (Khanna et al., 2009) While loss of BBX14 resulted in a distinct seedling phenotype (**Figure 6 B, C**), its involvement in flowering time regulation was only evident upon simultaneous knockdown of BBX14, BBX15, and BBX16 (Susila et al., 2023). Conversely, overexpression of BBX16 more clearly revealed cotyledon phenotypes compared to *bbx16* mutant lines (Veciana et al., 2022). Additionally, BBX16 has been recognized as a facilitator of seedling photomorphogenesis and a component acting downstream of the GUN1/GLK1 module in retrograde signaling (Veciana et al., 2022). Similarly, BBX14 captured attention when identified within a core-response module for HL and retrograde signaling, highlighting its involvement at the intersection of seedling development, retrograde signaling, and acclimation pathways (Leister & Kleine et al., 2016). Although *BBX14-16* are all GLK1 targets, future investigations are likely to unveil more intricate modes of action for these proteins, shedding light on whether BBX15 influences seedling development and whether a *bbx14bbx15bbx16* triple mutant exhibits a more pronounced impact on plant development than any of the single or double mutant combinations.

5.1. BBX14 is part of the GLK1/GUN1-dependent retrograde signaling mechanism regulating seedling development

Interactions between cellular compartments play a crucial role in coordinating developmental processes, optimizing metabolic pathways, and orchestrating responses to environmental stimuli and stresses (Xiao et al., 2012). The coordinated regulation of gene expression in both nuclear and plastid genomes through anterograde and retrograde signaling pathways is particularly vital during plastid biogenesis and transition to photomorphogenic program under conditions where chloroplast integrity and function are susceptible to environmental damage. RS pathways, which transmit information from plastids to the nucleus, serve two main functions: optimizing cellular responses to environmental cues (operational control) and regulating chloroplast development, especially plastid biogenesis (biogenic control), by modulating the expression of nuclear genes associated with photosynthesis (Woodson et al., 2013; Hernandez-Verdeja et al., 2022). While the concept of anterograde communication has long been established, the recognition of retrograde control, emerged much later as a widespread phenomenon in eukaryotes. Across all non-photosynthetic eukaryotes, ranging from unicellular fungi to humans, RS pathways play crucial roles in adjusting nuclear gene expression to mitochondrial physiology (Butow and Avadhani, 2004; Battersby and Richter,

2013). Similarly, in photosynthetic eukaryotes, spanning from unicellular algae to seed plants, additional retrograde pathways have been implemented to finely tune nuclear gene expression not only to mitochondrial but also to plastid demands (Woodson and Chory, 2008; Kleine et al., 2009; Van Aken and Whelan, 2012; De Clercq et al., 2013).

The establishment of young seedlings during de-etiolation is a delicate process influenced by various factors, with light playing a pivotal role (Gommers & Monte, 2018). Light triggers transcriptional alterations in numerous genes involved in de-etiolation (Ma et al., 2001), with many directly controlled by the phytochrome/PIF system, including GLK1 (Leivar et al., 2009; Pfeiffer et al., 2014). However, excessive light can be detrimental to chloroplast function, potentially hindering seedling establishment, leading to the initiation of RS and inhibition of de-etiolation (Martín et al., 2016). Chloroplast-derived retrograde signals play crucial roles in regulating photomorphogenesis through the modulation of transcriptional networks involving CRY1 and PIF-GLK1 (Waters et al., 2009; Martín et al., 2016). Additionally, these signals finely tune plant responses to environmental stresses such as drought and high light (Lee et al., 2007; Estavillo et al., 2011; Jung et al., 2013). Among the classical *gun* mutants, affecting enzymes or coenzymes in tetrapyrrole biosynthetic pathways (Mochizuki et al., 2001; Larkin et al., 2003; Strand et al., 2003; Woodson et al., 2011), the identification of the sixth GUN gene, GUN1, has led to the hypothesis that it serves as a central integrator where multiple RS pathways converge (Koussevitzky et al., 2007). GUN1, an enigmatic nuclear-encoded chloroplast-localized PRR protein, plays a crucial role in this process, particularly during the early stages of chloroplast biogenesis and under RS conditions (Wu et al., 2018). Although the precise mechanism remains unclear, GUN1 likely interacts physically with numerous proteins involved in plastid translation machinery, tetrapyrrole biosynthesis and RNA editing (Tadini et al., 2016; Marino et al., 2019; Shimizu et al., 2019; Zhao et al., 2019), suggesting a multifaceted role as a central hub that facilitates a plethora of crucial processes in the cell (Colombo et al., 2016). While GUN1 has predominantly been associated with RS processes as a central regulator of plastid-to-nucleus signaling (Koussevitzky et al., 2007) much about its exact mode of action in plastid protein homeostasis, expression, and accumulation in relation to the activity of RS, precise targets and affected down-stream processes has remained largely unknown. In recent studies GUN1 has been highlighted as key component in the RS-mediated regulation of seedling morphology (Martin et al., 2016, Veciana et al., 2022). Together with other nuclear-localized TFs (i.e. PIFs and GLK1), GUN1 orchestrates the expression of *PhANGs* to modulate chloroplast development (Waters et al., 2009) and seedling development during de-etiolation (Martin et al., 2016). During GUN1-dependent signaling, the GLK1/2

proteins function as key regulators of *PhANG*s transcript accumulation within the nucleus (Leister & Kleine, 2016; Martin et al., 2016; Waters et al., 2009). Recent studies have highlighted the convergence of light-dependent and chloroplast signaling pathways, with BBX16 identified as a component bridging these pathways (Veciana et al., 2022; Leister et al., 2014; Ruckle et al., 2007). BBX16, shown to be a direct target of GLK1, mediates the expression of a subset of GLK1-regulated *PhANGs* under specific conditions, indicating its role in integrating signals from these pathways (Veciana et al., 2022; Susila et al., 2023).

Arabidopsis BBX proteins clustered within the same clade are often found to be involved in the regulation of similar processes (Gangappa & Botto, 2014). As one of the few AtBBX protein that required further study, BBX14 gained prominence upon its discovery within a core-response module implicated in HL and RS, underscoring its role at the crossroads of seedling development, retrograde signaling, and stress acclimation pathways (Leister & Kleine et al., 2016). In this work, the role of BBX14 as an integrator of biogenic signals and nuclear target of retrograde signals downstream of the GUN1/GLK1 module in the context of seedling development under abiotic stress is argued, establishing it as the second BBX protein in Arabidopsis, after BBX16, involved in RS. In particular, *BBX14* displayed light-induced expression in a GLK1-dependent manner as well as is PIF-dependent repression in the dark. Furthermore, BBX14 is revealed to be required for the chlorophyll accumulation during early light exposure, hypocotyl shortening and acclimation to HL stress. The results presented here collectively provide evidence for the GUN1/GLK1-dependnet role of BBX14 in enchanting seedling development during de-etiolation and in biogenic signaling. Additionally, the identification of *BBX14* as direct target of GLK1 sheds light on a novel safeguarding mechanism in modulation of *PhANGs* expression and seedling development during RS activation against unfavorable light conditions.

To expand our understanding of GLK1-mediated regulation, a genome-wide ChIP-Seq approach was employed and identified *BBX14*, *BBX15*, *BBX2*, *BBX4*, and *BBX5* as direct targets of GLK1 (**Figure S1; Table S1**), meeting the first criterion for involvement in the GUN1/GLK-dependent biogenic signaling pathway. The second and third criteria, indicative of transcript reduction in the presence of both NF and LIN and dependence on GUN1, respectively, were evaluated. Among the BBX members satisfying criteria 2 and 3 (**Figure S5**), only BBX14, BBX15, and BBX16 also fulfilled criterion 1. Notably, overexpression of BBX14 resulted in a "*gun*" phenotype akin to oeBBX16 lines (**Figure 9**), indicating that *LHCB1.2* transcript levels remained unrepressed, similar to observations in BBX16 overexpressors (Vaciana et al., 2022). Strikingly, in lines overexpressing BBX15 only one target (*CA1*) was

identified to be de-repressed. Together, these finding are indicative of a diversification of BBX members clade III in their role of regulating *PhANGs*, despite commonality in their up-stream regulation via GLK1. It is, however, crucial to underline the original definition of a *gun* mutant at this point, which hinges on the de-repression of *LHCB1.2* transcript levels despite seedlings being cultivated on NF (or LIN) as postulated initially in several studies (Susek et al., 1993; Ruckle et al., 2007). While the relative gene expression data might suggest higher *LHCB1.2* expression in TPT14 compared to Col-0 when grown on NF (**Figure 9 B**), several points need to be considered: (i) *LHCB1.2* transcript levels exhibited variability from experiment to experiment, (ii) they were already slightly increased on MS without inhibitor (**Figure 9 B**), (iii) they remained lower those observed in the *gun1* mutant, and (iv) notably, they did not show an increase in TPT14 when RNA-Seq data were plotted over the *LHCB1.2* gene (**Figure 9 D**). It is important to interpret these findings cautiously, particularly considering that the stable "overexpression" line, while displaying elevated *CA1* expression levels, it exhibited a 2.2-fold increase in *BBX14* transcript levels compared to Col-0. The reliance solely on RT-qPCR results, especially when dealing with only a 2-fold variation, may not provide entirely reliable insights. Additionally, as discussed by Veciana et al. (2022), the possibility of branching in the signaling pathway downstream of GLK1 might enable BBX14, BBX15, and BBX16 to regulate a subset of target genes, rather than collectively exerting control over all *PhANGs*, with potential additive functions not being excluded. This notion is further supported by the finding that BBX14 and BBX15 appear to influence the expression of certain *PhANGs*, as seen from results presented in **Figure 7**. Hence, classification of BBX14 and BBX15 overexpressors as *gun* mutants based on certain *PhANGs* expression should be further elucidated and critically evaluated as there might yet unknown factors that play a role. Moreover, the observation that reduced GLK1 protein levels in damaged plastids are partially restored by MG132, a proteasome inhibitor, suggests the involvement of the ubiquitin-proteasome system in the degradation of GLK1 in response to plastid signals, further adding to the complexity of the regulatory network (Tokumaru et al., 2017). It therefore stands to reason, whether emerging "*gun"* mutants should be categorized based on subtle *PhANGs* phenotype alone. For instance, among the recently identified new "*gun*" mutants in the GUN1 branch are the overexpressors of MORF2 (Zhao et al., 2019). In this study, RT-qPCR was employed to detect *LHCB1.2* transcript levels that were 3-fold and 2-fold higher in two MORF2 overexpressors, akin to those observed in TPT14. However, it remains unclear whether *LHCB1.2* levels were already elevated in MORF2 lines prior to overexpression when grown in absence of inhibitors. Finally, constitutive expression often confounds primary and secondary effects, that lead to

discrepancies or sometimes pleiotropic effects. Moreover, expression in a wild-type background could hide certain effects or lead to reduced sensitivity to treatments. Hence, the employment of inducible expression approach to overcome this could leads to more reliable and conclusive results, as demonstrated in this work.

In elucidating the regulatory framework downstream of GLK1, it becomes evident that GLK1 directs its influence toward BBX proteins from clade III to intricately modulate seedling development and potentially exert indirect control over specific *PhANGs*, as demonstrated here for BBX14 and BBX15. Concurrently, GLK1 directly regulates other *PhANGs*, as shown by Waters et al., (2009) marking a crucial juncture in the intricate orchestration of seedling morphology downstream of the GUN1/GLK1 module. This unveils a nuanced signaling landscape where the relayed signal from GLK1 diversifies, finely tuning diverse processes pivotal to seedling de-etiolation. Notably, the phenomenon of signal network branching, ubiquitous across organisms, plays a pivotal role in sculpting intricate responses to distinct stimuli (Purvis et al., 2008). It's noteworthy that previous studies have delineated signal branching downstream of the PIFs, orchestrating distinct pathways specific to different organs during seedling de-etiolation. For instance, BBX23 was implicated in primarily regulating hook unfolding in this context (Zhang et al., 2017). The current findings suggest that while the direct targeting of certain *PhANG*s genes by GLK1 facilitates swift adjustments in chloroplast protection in response to light fluctuations, the divergence of the signal to suppress BBX14 and its downstream effectors could entail a more gradual response, particularly in sustained HL conditions, although this hypothesis warrants further exploration, as discussed later.

5.2. Involvement of BBX14 in circadian rhythm dynamics

Another interesting aspect that emerged when analyzing the role of BBX14 during seedling de-etiolation was the potential involvement of BBX14 in the circadian rhythm. Transcriptome analysis of seedling lacking *BBX14* revealed a significant enrichment of down-regulated genes associated with the circadian rhythm when transferred from dark to light, including genes such as *PRR5* and *TOC1* (**Figure 5 C**). Additionally, the misregulated expression of early day *PRR* genes in the *bbx14* mutant supports the notion that BBX14 is likely linked to the circadian cloak (**Figure 5 E**). While it has already been shown that light and the circadian clock can tightly regulate the expression of several BBX members like *BBX2*, *BBX3*, *BBX22*, *BBX24*, and *BBX25* (Ledger et al., 2001, Gangappa & Botto, 2014), evidence of the direct influence of BBX transcription factors on the circadian cloak is rather limited, with the exception of BBX18

and BBX19, which only recently have been reported to interact with PRRs in circadian clock regulation (Yuan et al., 2021). Although similar interaction for BBX14 could not be shown here, another possible mechanism, evidenced here by the interaction with PIF4 (**Figure 5 D**) as means to achieve circadian regulation should not be excluded. PIFs have long been establish as key components of the circadian clock by not only regulating the expression of other clock gene such as *CCA1* and *LHY*, but also by directly interacting with them in protein-protein complexes thereby recruiting other transcription factors to bind promoters of core clock genes. The interaction between PIFs and other TFs allows the coordination of gene expression in response to both light and circadian cues, thereby optimizing plant growth and development in response to environmental conditions. In the context of BBX proteins, interactions with members of the PIF family have only begun to become evident. A study by Bai et al. (2012) demonstrated that PIF1 interacts with BBX18 to regulate light-mediated hypocotyl elongation, whereas Gangappa et al. (2013) showed that PIF3 interacts with BBX32 to regulate photomorphogenesis and flowering time. Moreover, a recent study by Zhang et al. (2021) identified an interaction between PIF7 and BBX24, which regulates shade-induced hypocotyl elongation in Arabidopsis. Finally, BBX23 has been linked to a PIF1/PIF3-HY5 TF cascade regulating photomorphogenesis (Zhang et al., 2017). These studies collectively suggest that there is indeed a link between PIFs and AtBBX proteins, particularly in the regulation of light signaling pathways and circadian clock control. The interactions between PIFs and BBX TFs contribute to the fine-tuning of gene expression and the coordination of seedling growth and development in response to light cues. The identification of BBX14 as an interacting partner of PIF4 in this work sheds new light on the intricate regulatory network governing light-mediated responses in plants. Considering that other BBX protein have been identified to interact with a specific PIF, points towards a trend where PIF-BBX protein complexes functionally cooperate in regulating gene expression and signaling pathways. The specific interaction between PIF4 and BBX14 hints at a tailored regulatory mechanism that may modulate gene expression and signaling pathways in response to environmental cues, particularly light stimuli. This finding underscores the specificity and selectivity of protein-protein interactions in orchestrating complex physiological responses in plants. Moreover, it highlights the functional diversity within the BBX TF family and emphasizes the potential for combinatorial interactions with PIFs to fine-tune gene expression dynamics. Further investigation into the molecular mechanisms underlying the PIF4-BBX14 interaction is, however, required in order to precisely elucidate the regulatory mechanism and whether other TFs are involved in this process, like in case of BBX23 (Zhang et al., 2017).

5.3. BBX14 promotes chlorophyll accumulation and seedling establishment

Upon de-etiolation, the establishment of photosynthetic capacity depends on successful chloroplast biogenesis, a process expected to be intricately coordinated with the metabolism and development of other organelles. In angiosperms, chlorophyll synthesis halts in the absence of light but promptly resumes upon seedling exposure to irradiation (Von Wettstein et al., 1995). Given that all *LHCB* genes and chlorophyll biosynthesis genes are nuclear-encoded, it stands to reason that these genes might be co-regulated to facilitate efficient photosynthetic development. Nonetheless, despite this expectation, few examples of TFs governing chloroplast biogenesis have been identified to directly coordinate photosystem assembly, with prime examples being the homologous pair GLK1 and GLK2 as demonstrated by Waters et al., (2009). The chloroplast, a highly dynamic organelle, undergoes metabolic and functional shifts to adapt to changing environmental conditions. During daylight, it must finely balance light interception and carbon fixation rates, while at night, photosynthesis ceases, and starch reserves are mobilized within the chloroplast. Although many of these adjustments are mediated through rapid post-translational mechanisms, the circadian regulation of numerous photosynthesis-related transcripts suggests that transcriptional control in the nucleus plays a significant role. Findings in this work indicate that BBX14 play a crucial role in orchestrating adequate development of seedlings both during light exposure and darkness (**Figure 4**). This, together with the finding that *BBX14* is bound by GLK1 (**Figure S1**) implies that BBX14 is required for the synchronous transcription of genes essential for de-etiolations processes, which encompass the coordinated transcription of photosynthesis-related genes alongside other aspects. Moreover, the putative interaction between BBX14 and GLK2 further supports this notion (**Figure 5 D**) and highlights a potential functional evolution of GLKs to adjust early seedling establishment in different levels and via different pathways. Moreover, BBX14 is responsive to retrograde signals originating from the chloroplast. Thus, *BBX14* emerges as pivotal nuclear regulator governing photosynthetic capacity (**Figure 7 A, B**).

While several TFs have been implicated in the co-regulation of genes involved in photosynthesis, GLKs stand out as key regulators primarily dedicated to modulating such targets. For instance, the bZIP protein HY5 operates downstream of photoreceptors that oversees photomorphogenesis (Oyama et al., 1997). Despite the prevalence of photosynthesis-related genes among HY5 targets compared to the genome at large, the majority of HY5 targets consist of other TFs, reflecting HY5's broader role as a master regulator of photomorphogenesis (Lee et al., 2007). This is underscored by the identification of BBX proteins as rate-limiting

cofactors of HY5 (Bursch et al., 2020), as well as by their close interplay in facilitating photomorphogenesis (Gangappa, Crocco, et al., 2013; Gangappa, Holm, et al., 2013; Li et al., 2021; Zhang et al., 2017). Intriguingly, HY5 binding sites, primarily G-box elements, are abundant in the promoters of various TFs, including GLK2, yet conspicuously absent in BBX14 and GLK1 promoters (Lee et al., 2007). During the regulation of seedling photomorphogenesis, certain BBX proteins are intricately linked to the COP1/SPA-HY5 regulatory network, as evidenced by studies (Gangappa & Botto, 2014; Song et al., 2020). Many of these BBX proteins interact with COP1 and are modulated in a COP1-dependent manner, and/or exert influence on HY5 transcription, stability, or activity (see 1.2.2). However, whether BBX14 is subject to regulation by the COP/SPA system, and the involvement of HY5 or other interacting proteins in BBX14-mediated seedling development, remain open questions necessitating further investigation.

Another group of TFs known to regulate the expression of photosynthetic genes are the PIF family members (Castillon et al., 2007). PIF3 and PIF4, for instance, exert control over numerous genes involved in photomorphogenesis, including *CHLH* and *CAO*, which encode key enzymes in the chlorophyll biosynthesis pathway (Monte et al., 2004). Although the extent of interaction between BBX14 and other TFs remains to be fully elucidated, given that BBX14 can interact with GLK2 and PIF4, provides an interesting point that links BBX14 to chlorophyll accumulation. Moreover, a study of the chloroplast biogenesis during de-etiolation by Pipitone et al. (2021) showed that the initial time post light exposure is crucial for structure for chloroplast establishment, corroborating with the finding that seedlings lacking *BBX14* displayed a hampered photomorphogenesis during early onset of light (**Figure 4 A, B**). Moreover, the authors showed that while no tremendous changes occurred on proteomic level, including proteins constituting the photosynthetic machinery, the massive reorganization of the transcriptome during photomorphogenesis is the main event that governs the promotion of photomorphogenesis.

5.4. The role of BBX14 in acclimation to light stress

The regulation of gene expression stands as a critical facet of the response and adaptation to high light stress. Extensive evidence indicates that HL induces the transcriptional suppression of genes encoding antenna proteins while simultaneously activating genes responsible for scavenging ROS. What's more, HL can detrimentally damage chloroplast integrity by inducing the overproduction of ROS, disrupting energy metabolism, and impairing antioxidant defense

mechanisms. This damage can have profound effects on photosynthesis, chloroplast function, and overall plant growth and development (Rossel et al., 2002; Kleine et al., 2007; Jung et al., 2013). Hence, the Arabidopsis transcriptional response to HL must be rapidly initiated within seconds or minutes to prevent excessive damage. (Suzuki et al., 2015; Crisp et al., 2017). Furthermore, transcriptional regulatory networks play a pivotal role in mediating light signaling by orchestrating the coordinated activation and repression of specific downstream genes (Jiao et al., 2007). The intricate transcriptomic response to HL stress in plants remains inadequately characterized, partly due to the confounding effects of heat in previous studies. A study by Huang et al. (2019), circumventing heat-induced artifacts, provided valuable insights by elucidating the specific and dynamic transcriptome associated with HL stress in plants. Their study identified *BBX14* and two other uncharacterized genes as core HL-responsive hub genes among a total of 250 HL-responsive genes and revealed the dynamic regulation of key biological processes including hormones, anthocyanin biosynthesis, photosynthesis-related genes, photoreceptors, and genes encoding PIF TFs. Importantly, the indispensable role of PIFs in mediating the plant's response to HL stress was highlighted and specifically showed that PIF4 plays a prominent role in HL stress response. Even though no further evidence was provided that directly links *BBX14* and *PIF4* within the same HL-driven transcriptional network, the above discussed BBX14-PIF4 interaction underscores a potential interplay between the TFs that may be a part of a regulatory mechanism during HL stress and that further research should be attributed to elucidate this relationship.

In this work, it was noteworthy that BBX14 transcript accumulation was significantly hampered in seedling exposed to HL (**Figure 10 A, B**). One plausible hypothesis regarding the function of BBX14 in HL acclimation suggests that overexpression of BBX14 might enhance the plant's ability to tolerate HL conditions. Conversely, it was anticipated that *bbx14* mutant lines would exhibit behavior similar to the wild-type under HL stress, as BBX14 levels are naturally downregulated in these mutants. However, contrary to expectations, the "oeBBX14" plants behaved comparably to the WT under HL conditions (**Figure S5**), while the *bbx14* mutant plants displayed increased susceptibility to HL stress. This observation indicates that BBX14 plays a beneficial role in promoting plant growth and tolerance under HL conditions. This finding aligns with the concept of accelerated HL acclimation, as proposed by Alvarez-Fernandez et al. (2021), which involves a significant enhancement of the operating efficiency of photosystem II (PSII; Y(II)). Given that *BBX14* is co-regulated with *PhANGs* transcripts under HL conditions (Huang et al., 2019; Garcia-Molina et al., 2020), it is plausible that higher BBX14 levels may contribute to increased transcription of *PhANG*s under HL stress, thereby

facilitating enhanced HL acclimation. Conversely, the absence of *BBX14* appears to result in reduced HL tolerance in plants, as evidenced by the observed phenotype in the *bbx14* mutant lines (**Figure 10**). In addition to BBX14, it has been observed that transcriptional levels of all other clade III members, as well as of BBX27, decrease under HL conditions, whereas transcripts of other BBX members, including those from clade V such as BBX29-BBX32, show elevated expression (Garcia-Molina et al., 2020; Huang et al., 2019). Notably, a *bbx32* mutant exhibited slightly higher photosystem II operating efficiency (Y(II)) after 5 days of HL treatment, whereas plants overexpressing BBX32 demonstrated impaired acclimation to HL stress. This pattern parallels the correlation observed between *BBX32* transcript levels and HL phenotype, akin to what has been observed for *BBX14*. However, it is worth mentioning that overexpression of BBX32 was already slightly detrimental under growth conditions with reduced levels of several *PhANGs* transcripts (Alvarez-Fernandez et al., 2021). Interestingly, HL reduces the expression of class III BBX TF genes and *GLK1* (Martin et al., 2016; Huang et al., 2019). This is achieved via HL-mediated antagonization of *GLK1* expression, at least in part through GUN1-mediated retrograde signaling. Furthermore, HL intensities prevent the informational low-light induction of GLK1-induced genes, such as *BBX14* and *BBX16*, or the genes whose light-induction is inhibited by RS. *GLK1* expression under HL is repressed in a PIF-independent fashion by a GUN1-facilitated pathway, to antagonize the light induction of the photomorphogenic program (Martin et al., 2016). Together, with the finding that *BBX14-BBX17* are direct downstream targets of GLK, imply that BBX members of clade III might play a specialized role in the RS-mediated response to chloroplast damage and solidifies them as part of a regulatory stress-induced signaling pathway. Indeed, this function has already been attributed to other members of the BBX TF family in Arabidopsis, such as BBX18 and BBX23 in heat stress responses (Ding et al., 2018), BB24 in salt-induced stress (Gangappa & Botto, 2014) and BBX7 and BBX8 in cold (Li et al., 2021). Moreover, Lyu et al., (2020) conducted a bioinformatics analysis covering all members of BBX TF family and identified that the promoter region of *BBX14* contains *cis* elements related to ABA, light, drought, auxin, and stress responsiveness. This suggests a potential role for BBX14 in the crosstalk between different stress pathways and could be translated to other members of clade III, as some of the *cis* elements are shared across all four members.

In terms of stress acclimation, BBX TF factors are just now emerging as key players and mediators. While no evidence suggests that BBX proteins of clade III are functionally equivalent, the notion that they may be differentially regulated at the transcriptional level should be considered. Given the common occurrence of functional redundancy among

members of the same clade within other TF families (Pfeiffer et al., 2014; Leivar et al., 2020; Martín et al., 2020), it is plausible to speculate that BBX14-BBX16 might share some functional aspects. This redundancy within the clade suggests that the *bbx14* mutant likely retains some functionality, explaining the more prominent hypocotyl phenotypes observed in the *bbx14* mutant compared to lines overexpressing BBX14. Future genetic characterization of higher-order mutant combinations of *bbx14*, *bbx15*, and *bbx16* will shed more light on potential functional redundancy and clarify whether BBX14-BBX16 synergistically contribute to the RS-mediated regulatory response. This would also aid the understanding of the multifaceted role of BBX proteins in other processes and whether absence of several can result in additive phenotype effects. For instance, in case of the *bbx15bbx14* double mutant the maximum PS II quantum yield in young plants was significantly lower already under standard growth conditions (own observations, data not published). Moreover, it will be of interest to explore whether the BBX family of TFs has functionally evolved and diverged to specialize exclusively in glade III clade in RS regulation, or if BBX factors from other clades might also participate in these processes.

In summary, the complexity of BBX proteins' roles in plant development and stress responses, including their impact on chloroplast development, is becoming increasingly apparent. Yet, our comprehension of their specific functions remains incomplete. Challenges such as functional redundancies and feedback loops add layers of complexity to their analysis, necessitating further investigation to unravel the intricate regulatory networks and molecular mechanisms governing signaling and coordinated responses in nuclear gene regulation.

To summarize, this work provides evidence supporting a model wherein *BBX14* is a direct target of GLK1, driving hypocotyl photomorphogenesis under favorable light conditions conducive to seedling de-etiolation, as well as chlorophyll accumulation and HL acclimation. Conversely, activation of GUN1-mediated retrograde signaling inhibits *GLK1*, *BBX14*, and certain *PhANG*s expression, limiting chloroplast development to mitigate light damage and enhance photoprotection. Such a mechanism would safeguard an etiolated seedling, particularly vulnerable upon emergence into excessive light. This transient response likely enables the seedling to avert damage, awaiting a reduction in light intensity due to shading or the natural movement of the sun.

6. References

Afgan, E., Baker, D., van den Beek, M., Blankenberg, D., Bouvier, D., Cech, M., Chilton, J., Clements, D., Coraor, N., Eberhard, C., Gruning, B., Guerler, A., Hillman-Jackson, J., Von Kuster, G., Rasche, E., Soranzo, N., Turaga, N., Taylor, J., Nekrutenko, A. and Goecks, J. (2016). The Galaxy platform for accessible, reproducible and collaborative biomedical analyses: 2016 update. *Nucleic Acids Res*, 44, W3-W10.

Alonso, J. M., Stepanova, A. N., Leisse, T. J., Kim, C. J., Chen, H., Shinn, P., Stevenson, D. K., Zimmerman, J., Barajas, P., Cheuk, R., Gadrinab, C., Heller, C., Jeske, A., Koesema, E., Meyers, C. C., Parker, H., Prednis, L., Ansari, Y., Choy, N., Deen, H., … Ecker, J. R. (2003). Genome-wide insertional mutagenesis of Arabidopsis thaliana. *Science (New York, N.Y.)*, *301*(5633), 653–657.

Alvarez-Fernandez, R., Penfold, C.A., Galvez-Valdivieso, G., Exposito- Rodriguez, M., Stallard, E.J., Bowden, L. (2021). Time-series transcriptomics reveals a BBX32-directed control of acclimation to high light in mature Arabidopsis leaves. *The Plant Journal*, 107, 1363–1386.

Archibald, J. M. (2015). Endosymbiosis and Eukaryotic Cell Evolution. *Current biology : CB*, *25*(19), R911–R921

Bai, B., Zhao, J., Li, Y., Zhang, F., Zhou, J., Chen, F., & Xie, X. (2016). OsBBX14 delays heading date by repressing florigen gene expression under long and short-day conditions in rice. *Plant Sci*, *247*, 25-34.

Baillo, E. H., Kimotho, R. N., Zhang, Z., & Xu, P. (2019). Transcription Factors Associated with Abiotic and Biotic Stress Tolerance and Their Potential for Crops Improvement. *Genes (Basel)*, *10*(10).

Bakshi, M.; Oelmüller, R. (2014). WRKY transcription factors, Plant Signalling and Behavior. *J. Plant Signal. Behav. 9*, e27700.

Barkan, A., and Goldschmidt-Clermont, M. (2000). Participation of nuclear genes in chloroplast gene expression. *Biochimie* 82, 559–572.

Barkan, A., and Small, I. (2014). Pentatricopeptide repeat proteins in plants. *Annu. Rev. Plant Biol.* 65, 415–442.

Battersby, B.J., Richter, U. (2013). Why translation counts for mitochondria: retrograde signalling links mitochondrial protein synthesis to mitochondrial biogenesis and cell proliferation. *J Cell Sci* 126: 4331–4338

Bolger, A.M., Lohse, M. and Usadel, B. (2014). Trimmomatic: a flexible trimmer for Illumina sequence data. *Bioinformatics*, 30, 2114-2120.

Borden, K.L., Lally, J.M., Martin, S.R., O'Reilly, N.J., Etkin, L.D., and Freemont, P.S. (1995). Novel topology of a zinc-binding domain from a protein involved in regulating early Xenopus development. *EMBO J*. 14: 5947–5956.

Brandão, M. M., Dantas, L. L., & Silva-Filho, M. C. (2009). AtPIN: Arabidopsis thaliana protein interaction network. *BMC bioinformatics*, *10*, 454.

Buelbuel, S., Sakuraba, Y., Sedaghatmehr, M., Watanabe, M., Hoefgen, R., Balazadeh, S., & Mueller-Roeber, B. (2023). Arabidopsis BBX14 negatively regulates nitrogen starvation- and dark-induced leaf senescence. *The Plant journal : for cell and molecular biology*, *116*(1), 251–268.

Bursch, K., Toledo-Ortiz, G., Pireyre, M., Lohr, M., Braatz, C., & Johansson, H. (2020). Identification of BBX proteins as rate-limiting cofactors of HY5. *Nat Plants*, *6*(8), 921-928.

Butow, R.A., Avadhani, N.G. (2004) Mitochondrial signaling: the retrograde response. *Mol Cell* 14: 1–15

Cao, S., Kumimoto, R. W., Gnesutta, N., Calogero, A. M., Mantovani, R., & Holt, B. F., 3rd (2014). A distal CCAAT/NUCLEAR FACTOR Y complex promotes chromatin looping at the FLOWERING LOCUS T promoter and regulates the timing of flowering in Arabidopsis. *The Plant cell*, *26*(3), 1009–1017.

Castillon, A., Shen, H., and Huq, E. (2007). Phytochrome interacting factors: Central players in phytochrome-mediated light signaling networks. *Trends Plant Sci*. 12: 514–521.

Chang, C. S., Li, Y. H., Chen, L. T., Chen, W. C., Hsieh, W. P., Shin, J., Jane, W. N., Chou, S. J., Choi, G., Hu, J. M., Somerville, S., & Wu, S. H. (2008). LZF1, a HY5-regulated transcriptional factor, functions in Arabidopsis de-etiolation. *The Plant journal: for cell and molecular biology*, 54(2), 205–219

Chang, C. S., Maloof, J. N., & Wu, S. H. (2011). COP1-mediated degradation of BBX22/LZF1 optimizes seedling development in Arabidopsis. *Plant physiology*, *156*(1), 228–239.

Chattopadhyay, S., Ang, L.H., Puente, P., Deng, X.W., Wie, N. (1998). Arabidopsis bZIP protein HY5 directly interacts with light-responsive promoters in mediating light control of gene expression. *The Plant Cell* 10: 673–683.

Chen, H., Zhang, J., Neff, M. M., Hong, S. W., Zhang, H., Deng, X. W., & Xiong, L. (2008). Integration of light and abscisic acid signaling during seed germination and early seedling development. *Proceedings of the National Academy of Sciences of the United States of America*, *105*(11), 4495–4500.

Chi, W., Sun, X., and Zhang, L. (2013). Intracellular signaling from plastid to nucleus. *Annu. Rev. Plant Biol.* 64, 559–582.

Chi, W., Sun, X., Zhang, L. (2013). Intracellular signaling from plastid to nucleus. Annu Rev *Plant Biol* 64: 559–582

Coego, A., Brizuela, E., Castillejo, P., Ruíz, S., Koncz, C., del Pozo, J. C., Piñeiro, M., Jarillo, J. A., Paz-Ares, J., León, J., & TRANSPLANTA Consortium (2014). The TRANSPLANTA collection of Arabidopsis lines: a resource for functional analysis of transcription factors based on their conditional overexpression. *The Plant journal : for cell and molecular biology*, *77*(6), 944–953.

Cohen, S.P.; Leach, J.E. (2019). Abiotic and biotic stresses induce a core transcriptome response in rice. *Sci. Rep.* 1–11.

Colombo, M., Tadini, L., Peracchio, C., Ferrari, R., and Pesaresi, P. (2016). GUN1, a jack-of-all-trades in chloroplast protein homeostasis and signaling. *Front. Plant Sci.* 7:1427.

Crisp, P.A., Ganguly, D.R., Smith, A.B., Murray, K.D., Estavillo, G.M., Searle, I., Ford, E., Bogdanović, O., Lister, R., Borevitz, J.O. (2017). Rapid recovery gene downregulation during excess-light stress and recovery in Arabidopsis. *Plant Cell* 29, 1836–1863.

Crocco, C. D., Holm, M., Yanovsky, M. J., & Botto, J. F. (2010). AtBBX21 and COP1 genetically interact in the regulation of shade avoidance. *The Plant journal: for cell and molecular biology*, *64*(4), 551–562.

Crocco, C. D., & Botto, J. F. (2013). BBX proteins in green plants: insights into their evolution, structure, feature and functional diversification. *Gene*, *531*(1), 44-52.

Cutler, S. R., Rodriguez, P. L., Finkelstein, R. R., & Abrams, S. R. (2010). Abscisic acid: emergence of a core signaling network. *Annual review of plant biology*, *61*, 651–679.

Datta, S., Hettiarachchi, C., Johansson, H., & Holm, M. (2007). SALT TOLERANCE HOMOLOG2, a B-box protein in Arabidopsis that activates transcription and positively regulates light-mediated development. *The Plant cell*, *19*(10), 3242–3255.

Datta, S., Johansson, H., Hettiarachchi, C., Irigoyen, M. L., Desai, M., Rubio, V., & Holm, M. (2008). LZF1/SALT TOLERANCE HOMOLOG3, an Arabidopsis B-box protein involved in light-dependent development and gene expression, undergoes COP1-mediated ubiquitination. *The Plant cell*, *20*(9), 2324–2338.

Davuluri, R.V., Sun, H., Palaniswamy, S.K., Matthews, N., Molina, C., Kurtz, M. (2003). AGRIS: Arabidopsis gene regulatory information server, an information resource of Arabidopsis cis- regulatory elements and transcription factors. *BMC Bioinformatics* 4: 25.

De Clercq, I., Vermeirssen, V., Van Aken, O., Vandepoele, K., Murcha, M.W., Law, S.R., Inzé, A., Ng, S., Ivanova, A., Rombaut, D. (2013). The membrane-bound NAC transcription factor ANAC013 functions in mi- tochondrial retrograde regulation of the oxidative stress response in Arabidopsis. *Plant Cell* 25: 3472–3490

de Pater, S., Greco, V., Pham, K., Memelink, J., and Kijne, J. (1996). Characterization of a zinc-dependent transcriptional activator from Arabidopsis. *Nucleic Acids Res*. 24: 4624–4631.

de Wit, M., Galvão, V. C., & Fankhauser, C. (2016). Light-Mediated Hormonal Regulation of Plant Growth and Development. *Annual review of plant biology*, *67*, 513–537.

Ding L, Wang S, Song Z-T, Jiang Y, Han J-J, Lu S-J, Li L, Liu J-X. (2018). Two B-box domain proteins, BBX18 and BBX23, interact with ELF3 and regulate thermomorphogenesis in Arabidopsis. *Cell Reports* 25: 1718–1728.e4.

Dobin, A., Davis, C. A., Schlesinger, F., Drenkow, J., Zaleski, C., Jha, S., Batut, P., Chaisson, M., & Gingeras, T. R. (2013). STAR: ultrafast universal RNA-seq aligner. *Bioinformatics*, *29*(1), 15-21.

Dubos, C.; Stracke, R.; Grotewold, E.; Weisshaar, B.; Martin, C.; Lepiniec, L. (2010). MYB transcription factors in Arabidopsis. *Trends Plant Sci. 15*, 573–581.

Erpen, L.; Devi, H.S.; Grosser, J.W.; Dutt, M. (2018). Potential use of the DREB/ERF, MYB, NAC and WRKY transcription factors to improve abiotic and biotic stress in transgenic plants. *Plant Cell Tissue Organ Cult. 132*, 1–25.

Estavillo, G.M., Crisp, P.A., Pornsiriwong, W., Wirtz, M., Collinge, D., Carrie, C., Giraud, E., Whelan, J., David, P., Javot, H. (2011). Evidence for a SAL1- PAP chloroplast retrograde pathway that functions in drought and high light signaling in Arabidopsis. *Plant Cell* 23: 3992–4012

Fan, X. Y., Sun, Y., Cao, D. M., Bai, M. Y., Luo, X. M., Yang, H. J., Wei, C. Q., Zhu, S. W., Sun, Y., Chong, K., & Wang, Z. Y. (2012). BZS1, a B-box protein, promotes photomorphogenesis downstream of both brassinosteroid and light signaling pathways. *Molecular plant*, *5*(3), 591–600.

Fankhauser, C., and Chory, J. (1997). Light control of plant development. *Annu. Rev. Cell Dev. Biol*. 13: 203-229.

Fitter, D.W., Martin, D.J., Copley, M.J., Scotland, R.W., and Langdale, J.A. (2002). GLK gene pairs regulate chloroplast develop- ment in diverse plant species. *Plant J*. 31: 713–727.

Fitter, D.W., Martin, D.J., Copley, M.J., Scotland, R.W., Langdale, J.A. (2002). GLK gene pairs regulate chloroplast development in diverse plant species. *The Plant Journal* 31: 713–727.

Fowler, S., Thomashow, M.F. (2002). Arabidopsis transcriptome profiling indi- cates that multiple regulatory pathways are activated during cold acclimation in addition to the CBF cold response pathway. *The Plant Cell* 14: 1675 – 1690.

Foyer, C.H.; Rasool, B.; Davey, J.W.; Hancock, R.D. (2016). Cross-tolerance to biotic and abiotic stresses in plants: A focus on resistance to aphid infestation. *J. Exp. Bot. 67*, 2025–2037.

Franco-Zorrilla, J.M., Lopez-Vidriero, I., Carrasco, J.L., Godoy, M., Vera, P. & Solano, R. (2014). DNA-binding specificities of plant transcription factors and their potential

to define target genes. *Proceedings of the National Academy of Sciences of the USA*, 111, 2367–2372.

Fu, L. Y., Zhu, T., Zhou, X., Yu, R., He, Z., Zhang, P., Wu, Z., Chen, M., Kaufmann, K., & Chen, D. (2022). ChIP-Hub provides an integrative platform for exploring plant regulome. *Nature communications*, *13*(1), 3413.

Gangappa, S. N., & Botto, J. F. (2014). The BBX family of plant transcription factors. *Trends Plant Sci*, *19*(7), 460-470.

Gangappa, S. N., Crocco, C. D., Johansson, H., Datta, S., Hettiarachchi, C., Holm, M., & Botto, J. F. (2013). The Arabidopsis B-BOX protein BBX25 interacts with HY5, negatively regulating BBX22 expression to suppress seedling photomorphogenesis. *Plant Cell*, *25*(4), 1243-1257.

Gangappa, S. N., Holm, M., & Botto, J. F. (2013). Molecular interactions of BBX24 and BBX25 with HYH, HY5 HOMOLOG, to modulate Arabidopsis seedling development. *Plant Signal Behav*, *8*(8).

Garcia-Molina, A., Kleine, T., Schneider, K., Muhlhaus, T., Lehmann, M. and Leister, D. (2020). Translational Components Contribute to Acclimation Responses to High Light, Heat, and Cold in Arabidopsis. *iScience*, 23, 101331

Garcia-Molina, A., Kleine, T., Schneider, K., Muhlhaus, T., Lehmann, M. & Leister, D. (2020). Translational components contribute to acclimation responses to high light, heat, and cold in Arabidopsis. *iScience*, 23, 101331.

Ge, S.X., Jung, D., Yao, R. (2020). ShinyGO: a graphical gene-set enrichment tool for animals and plants. *Bioinformatics*. 36(8):2628-2629.

Gollan, P. J., Tikkanen, M., and Aro, E. M. (2015). Photosynthetic light reactions: integral to chloroplast retrograde signalling. *Curr. Opin. Plant Biol.* 27, 180–191.

Gommers, C.M.M., Monte, E. (2018). Seedling establishment: a dimmer switch-regulated process between dark and light signaling. *Plant Physiology* 176: 1061–1074.

Gray, W. M. (2004). Hormonal regulation of plant growth and development. *PLoS biology*, *2*(9), E311.

Griffiths, S., Dunford, R.P., Coupland, G., Laurie, D.A. (2003). The evolution of CONSTANS-like gene families in barley, rice, and Arabidopsis. *Plant Physiol*. 131, 1855–1867

Guo, A., He K., Liu, D., Bai, S., Gu X., Wei, L. (2005). DATF: a database of Arabidopsis transcription factors. *Bioinformatics* 21: 2568–2569.

Habermann, K., Tiwari, B., Krantz, M., Adler, S.O., Klipp, E., Arif, M.A. (2020). Identification of small non-coding RNAs responsive to GUN1 and GUN5 related retrograde signals in Arabidopsis thaliana. *The Plant Journal*, 104, 138–155.

Han, X., Huang, X. & Deng, X.W. (2020). The photomorphogenic central repressor COP1: conservation and functional diversification during evolution. *Plant Communications*, 1, 100044.

Heng, Y., Lin, F., Jiang, Y., Ding, M., Yan, T., Lan, H. (2019). B-box containing proteins BBX30 and BBX31, acting downstream of HY5, negatively regulate photomorphogenesis in Arabidopsis. *Plant Physiology*, 180, 497–508.

Heng, Y., Lin, F., Jiang, Y., Ding, M., Yan, T., Lan, H., Zhou, H., Zhao, X., Xu, D., Deng, X.W. (2019). B-box containing proteins BBX30 and BBX31, acting downstream of HY5, negatively regulate photomorphogenesis in Arabidopsis. *Plant Physiology* 180: 497–508.

Hernandez-Verdeja, T., Vuorijoki, L., Jin, X., Vergara, A., Dubreuil, C., & Strand, A. (2022). GENOMES UNCOUPLED1 plays a key role during the de-etiolation process in Arabidopsis. *New Phytol*, *235*(1), 188-203.

Hoang, X.L.T.; Nhi, D.N.H.; Thu, N.B.A.; Thao, N.P.; Tran, L.-S.P. (2017). Transcription Factors and Their Roles in Signal Transduction in Plants under Abiotic Stresses. *Curr. Genomics. 18*, 483–497.

Holm, M., Hardtke, C. S., Gaudet, R., & Deng, X. W. (2001). Identification of a structural motif that confers specific interaction with the WD40 repeat domain of Arabidopsis COP1. *The EMBO journal*, *20*(1-2), 118–127.

Holtan, H. E., Bandong, S., Marion, C. M., Adam, L., Tiwari, S., Shen, Y., Maloof, J. N., Maszle, D. R., Ohto, M. A., Preuss, S., Meister, R., Petracek, M., Repetti, P. P., Reuber, T. L., Ratcliffe, O. J., & Khanna, R. (2011). BBX32, an Arabidopsis B-Box protein, functions in light signaling by suppressing HY5-regulated gene expression and interacting with STH2/BBX21. *Plant physiology*, *156*(4), 2109–2123.

Honkanen, S., & Small, I. (2022). The GENOMES UNCOUPLED1 protein has an ancient, highly conserved role but not in retrograde signalling. *The New phytologist*, 236(1), 99–113.

Hrmova, M., & Lopato, S. (2014). Enhancing Abiotic Stress Tolerance in Plants by Modulating Properties of Stress Responsive Transcription Factors. In *Genomics of Plant Genetic Resources* (pp. 291-316).

Huang, J., Zhao, X., & Chory, J. (2019). The Arabidopsis Transcriptome Responds Specifically and Dynamically to High Light Stress. *Cell Rep*, *29*(12), 4186-4199 e4183.

Huang, J., Zhao, X., Weng, X., Wang, L., & Xie, W. (2012). The rice B-box zinc finger gene family: genomic identification, characterization, expression profiling and diurnal analysis. *PLoS One*, *7*(10), e48242.

Indorf, M., Cordero, J., Neuhaus, G., & Rodríguez-Franco, M. (2007). Salt tolerance (STO), a stress-related protein, has a major role in light signalling. *The Plant journal : for cell and molecular biology*, *51*(4), 563–574.

Inukai, S.; Kock, K.H.; Bulyk, M.L. (2017). Transcription factor-DNA binding: Beyond binding site motifs. *Curr. Opin. Genet. 34*, 110–119.

Jiang, L., Wang, Y., Li, Q. F., Björn, L. O., He, J. X., & Li, S. S. (2012). Arabidopsis STO/BBX24 negatively regulates UV-B signaling by interacting with COP1 and repressing HY5 transcriptional activity. *Cell research*, *22*(6), 1046–1057.

Jiao, Y., Lau, O. S., & Deng, X. W. (2007). Light-regulated transcriptional networks in higher plants. *Nature reviews. Genetics*, *8*(3), 217–230. Kami, C., Lorrain, S., Hornitschek, P., & Fankhauser, C. (2010). Light-regulated plant growth and development. *Current topics in developmental biology*, *91*, 29–66.

Jiao, Y., Lau, O.S., and Deng, X.W. (2007). Light-regulated transcriptional networks in higher plants. *Nat. Rev. Genet* 8, 217–230.

Jing, Y., Lin, R. (2020). Transcriptional regulatory network of the light signaling pathways. *New Phytologist* 227: 683–697.

Job, N., Yadukrishnan, P., Bursch, K., Datta, S., & Johansson, H. (2018). Two B-Box Proteins Regulate Photomorphogenesis by Oppositely Modulating HY5 through their Diverse C-Terminal Domains. *Plant Physiol*, *176*(4), 2963-2976.

Jung, H-S., Crisp, P.A., Estavillo, G.M., Cole, B., Hong, F., Mockler, T.C., Pogson, B.J., and Chory, J. (2013). Subset of heat-shock transcription factors required for the early response of Arabidopsis to excess light. *Proc. Natl. Acad. Sci. USA* 110, 14474–14479.

Jung, H.S., Crisp, P.A., Estavillo, G.M., Cole, B., Hong, F., Mockler, T.C., Pogson, B.J., Chory, J. (2013). Subset of heat-shock transcription factors required for the early response of Arabidopsis to excess light. *Proc Natl Acad Sci USA* 110: 14474–14479

Karimi, M., Inzé, D., Depicker, A. (2002) GATEWAY vectors for Agrobacterium mediated plant transformation. *Trends Plant Sci*. 7(5):193-5.

Kato, T., Murakami, M., Nakamura, Y., Ito, S., Nakamichi, N., Yamashino, T., & Mizuno, T. (2007). Mutants of circadian-associated PRR genes display a novel and visible phenotype as to light responses during de-etiolation of Arabidopsis thaliana seedlings. *Biosci Biotechnol Biochem*, *71*(3), 834-839.

Kaufmann, K., Muino, J.M., Osteras, M., Farinelli, L., Krajewski, P. and Angenent, G.C. (2010). Chromatin immunoprecipitation (ChIP) of plant transcription factors followed by sequencing (ChIP-SEQ) or hybridization to whole genome arrays (ChIP-CHIP). *Nat Protoc*, 5, 457-472.

Kenrick, P., Crane, P.R. (1997). The origin and early evolution of plants on land. *Nature*, 389 , pp. 33-39

Khanna, R., Shen, Y., Toledo-Ortiz, G., Kikis, E. A., Johannesson, H., Hwang, Y. S., & Quail, P. H. (2006). Functional profiling reveals that only a small number of phytochrome-regulated early-response genes in Arabidopsis are necessary for optimal deetiolation. *The Plant cell*, *18*(9), 2157–2171.

Khanna, R., Kronmiller, B., Maszle, D. R., Coupland, G., Holm, M., Mizuno, T., & Wu, S. H. (2009). The Arabidopsis B-box zinc finger family. *Plant Cell*, *21*(11), 3416-3420.

Kiełbowicz-Matuk A. (2012). Involvement of plant C(2)H(2)-type zinc finger transcription factors in stress responses. *Plant science : an international journal of experimental plant biology*, *185-186*, 78–85.

Kleine, T., Kindgren, P., Benedict, C., Hendrickson, L., and Strand, A. (2007). Genome-wide gene expression analysis reveals a critical role for CRYPTOCHROME1 in the response of Arabidopsis to high irradiance. *Plant Physiol*. 144, 1391–1406.

Kleine, T., Maier, U. G., & Leister, D. (2009). DNA transfer from organelles to the nucleus: the idiosyncratic genetics of endosymbiosis. *Annual review of plant biology*, *60*, 115–138.

Kleine, T., Voigt, C., & Leister, D. (2009). Plastid signalling to the nucleus: messengers still lost in the mists? *Trends Genet*, *25*(4), 185-192.

Kleine, T., & Leister, D. (2013). Retrograde signals galore. *Front Plant Sci*, *4*, 45.

Kleine, T., & Leister, D. (2016). Retrograde signaling: Organelles go networking. *Biochim Biophys Acta*, *1857*(8), 1313-1325.

Kleine, T., Nagele, T., Neuhaus, H. E., Schmitz-Linneweber, C., Fernie, A. R., Geigenberger, P., Grimm, B., Kaufmann, K., Klipp, E., Meurer, J., Mohlmann, T., Muhlhaus, T., Naranjo, B., Nickelsen, J., Richter, A., Ruwe, H., Schroda, M., Schwenkert, S., Trentmann, O., Leister, D. (2021). Acclimation in plants - the Green Hub consortium. *Plant J*, *106*(1), 23-40.

Klug, A., and Schwabe, J.W.R. (1995). Zinc fingers. FASEB J. 9: 597–604.

Kobayashi, K., Obayashi, T. & Masuda, T. (2012) Role of the G-box element in regulation of chlorophyll biosynthesis in Arabidopsis roots. *Plant Signaling & Behavior*, 7, 922–926.

Koussevitzky, S., Nott, A., Mockler, T.C., Hong, F., Sachetto-Martins, G., Surpin, M., Lim, J., Mittler, R., Chory, J. (2007). Signals from chloroplasts converge to regulate nuclear gene expression. *Science* 316: 715–719

Koussevitzky, S., Nott, A., Mockler, T.C., Hong, F., Sachetto-Martins, G., Surpin, M., Lim, J., Mittler, R., Chory, J. (2007). Signals from chloroplasts converge to regulate nuclear gene expression. *Science* 316: 715–719

Kumagai, T., Ito, S., Nakamichi, N., Niwa, Y., Murakami, M., Yamashino, T., and Mizuno, T. (2008). The common function of a novel subfamily of B-Box zinc finger proteins with reference to circadian-associated events in *Arabidopsis thaliana*. *Biosci. Biotechnol. Bio- chem*. 72: 1539–1549.

Langmead, B. and Salzberg, S.L. (2012). Fast gapped-read alignment with Bowtie 2. *Nat Methods*, 9, 357-359

Larkin, R. M., Alonso, J. M., Ecker, J. R., and Chory, J. (2003). GUN4, a regulator of chlorophyll synthesis and intracellular signaling. *Science* 299, 902–906.

Ledger, S., Strayer, C., Ashton, F., Kay, S.A., Putterill, J. (2001). Analysis of the function of two circadian-regulated CONSTANS-LIKE genes. *Plant J* 26: 15–22

Lee, J., He, K., Stolc, V., Lee, H., Figueroa, P., Gao, Y., Tongprasit, W., Zhao, H., Lee, I., & Deng, X. W. (2007). Analysis of transcription factor HY5 genomic binding sites revealed its hierarchical role in light regulation of development. *The Plant cell*, *19*(3), 731–749.

Lee, J., He, K., Stolc, V., Lee, H., Figueroa, P., Gao, Y., Tongprasit, W., Zhao, H., Lee, I., and Deng, X.W. (2007). Analysis of transcription factor HY5 genomic binding sites revealed its hierarchical role in light regulation of development. *Plant Cell* 19: 731–749.

Lee, K.P., Kim, C., Landgraf, F., Apel, K. (2007). EXECUTER1- and EXECUTER2-dependent transfer of stress-related signals from the plastid to the nu- cleus of Arabidopsis thaliana. *Proc Natl Acad Sci USA* 104: 10270–10275

Leister, D. (2012). Retrograde signaling in plants: from simple to complex scenarios. *Front Plant Sci*, *3*, 135.

Leister, D., & Kleine, T. (2016). Definition of a core module for the nuclear retrograde response to altered organellar gene expression identifies GLK overexpressors as gun mutants. *Physiol Plant*, *157*(3), 297-309.

Leister, D., Romani, I., Mittermayr, L., Paieri, F., Fenino, E., & Kleine, T. (2014). Identification of target genes and transcription factors implicated in translation-dependent retrograde signaling in Arabidopsis. *Mol Plant*, *7*(7), 1228-1247.

Leister, D., Wang, L., & Kleine, T. (2017). Organellar Gene Expression and Acclimation of Plants to Environmental Stress. *Front Plant Sci*, *8*, 387.

Leister, D., Wang, X., Haberer, G., Mayer, K. F., & Kleine, T. (2011). Intracompartmental and intercompartmental transcriptional networks coordinate the expression of genes for organellar functions. *Plant Physiol*, *157*(1), 386-404.

Leivar, P., Martın, G., Soy, J., Dalton-Roesler, J., Quail, P.H., Monte, E. (2020). Phytochrome-imposed inhibition of PIF7 activity shapes photoperiodic growth in Arabidopsis together with PIF1, 3, 4 and 5. *Physiologia Plantarum* 169: 452–466.

Leivar, P., Monte, E., Oka, Y., Liu, T., Carle, C., Castillon, A., Huq, E., Quail, P.H. (2008). Multiple phytochrome-interacting bHLH transcription factors repress premature seedling photomorphogenesis in darkness. *Current Biology* 18: 1815–1823.

Leivar, P., Tepperman, J.M., Monte, E., Calderon, R.H., Liu, T.L., Quail, P.H. (2009). Definition of early transcriptional circuitry involved in light-induced reversal of PIF-imposed repression of photomorphogenesis in young Arabidopsis seedlings. *Plant Cell.*; 21(11):3535-53.

Li, M., Lee, K. P., Liu, T., Dogra, V., Duan, J., Li, M., Xing, W., & Kim, C. (2022). Antagonistic modules regulate photosynthesis-associated nuclear genes via GOLDEN2-LIKE transcription factors. *Plant Physiol*, *188*(4), 2308-2324.

Li, Y., Shi, Y., Li, M., Fu, D., Wu, S., Li, J., Gong, Z., Liu, H., & Yang, S. (2021). The CRY2-COP1-HY5-BBX7/8 module regulates blue light-dependent cold acclimation in Arabidopsis. *Plant Cell*, *33*(11), 3555-3573.

Liao, Y., Smyth, G.K. and Shi, W. (2014). featureCounts: an efficient general purpose program for assigning sequence reads to genomic features. *Bioinformatics*, 30, 923-930

Lin, F., Jiang, Y., Li, J., Yan, T., Fan, L., Liang, J., Chen, Z. J., Xu, D., & Deng, X. W. (2018). B-BOX DOMAIN PROTEIN28 Negatively Regulates Photomorphogenesis by Repressing the Activity of Transcription Factor HY5 and Undergoes COP1-Mediated Degradation. *The Plant cell*, *30*(9), 2006–2019.

Lippuner, V., Cyert, M. S., & Gasser, C. S. (1996). Two classes of plant cDNA clones differentially complement yeast calcineurin mutants and increase salt tolerance of wild-type yeast. *The Journal of biological chemistry*, *271*(22), 12859–12866.

Lorick, K. L., Jensen, J. P., Fang, S., Ong, A. M., Hatakeyama, S., & Weissman, A. M. (1999). RING fingers mediate ubiquitin-conjugating enzyme (E2)-dependent ubiquitination. *Proceedings of the National Academy of Sciences of the USA*, *96*(20), 11364–11369.

Love, M.I., Huber, W. and Anders, S. (2014). Moderated estimation of fold change and dispersion for RNA-seq data with DESeq2. *Genome Biol*, 15, 550.

Lyska, D., Engelmann, K., Meierhoff, K., Westhoff, P. (2013). pAUL: a gateway-based vector system for adaptive expression and flexible tagging of proteins in Arabidopsis. *PLoS One*. 8(1)

Lyu, G., Li, D., Li, S. (2020). Bioinformatics analysis of BBX family genes and its response to UV-B in Arabidopsis thaliana. *Plant Signaling & Behavior* 15: 1782647.

Ma, L., Li, J., Qu, L., Hager, J., Chen, Z., Zhao, H., Den,g X.W. (2001). Light control of Arabidopsis development entails coordinated regulation of genome expression and cellular pathways. *The Plant Cell* 13:2589–2607.

Marino, G., Naranjo, B., Wang, J., Penzler, J-F., Kleine, T., Leister, D. (2019). Relationship of GUN1 to FUG1 in chloroplast protein homeostasis. *The Plant Journal* 99: 521–535.

Martin, G., Leivar, P., Ludevid, D., Tepperman, J. M., Quail, P. H., & Monte, E. (2016). Phytochrome and retrograde signalling pathways converge to antagonistically regulate a light-induced transcriptional network. *Nat Commun*, *7*, 11431.

Martın, G., Veciana, N., Boix, M., Rovira, A., Henriques, R., Monte, E. (2020). The photoperiodic response of hypocotyl elongation involves regulation of CDF1 and CDF5 activity. *Physiologia Plantarum* 169: 480–490.

Massiah, M.A. (2007). Solution structure of the MID1 B-box2 CHC(D/C)C(2)H(2) zinc-binding domain: insights into an evolutionarily conserved RING fold. *J. Mol. Biol*. 369, 1–10.

Massiah, M.A., Simmons, B.N., Short, K.M., Cox, T.C. (2006). Solution structure of the RBCC/TRIM B-box1 domain of human MID1: B-box with a RING. *J. Mol. Biol*. 358, 532–545.

Meroni, G., Diez-Roux, G. (2005). TRIM/RBCC, a novel class of 'single protein RING finger' E3 ubiquitin ligases. *Bioessays* 27, 1147–1157.

Mitsuda, N., & Ohme-Takagi, M. (2009). Functional analysis of transcription factors in Arabidopsis. *Plant Cell Physiol*, *50*(7), 1232-1248.

Mochizuki, N., Brusslan, J. A., Larkin, R., Nagatani, A., and Chory, J. (2001). *Arabidopsis* genomes uncoupled 5 (GUN5) mutant reveals the involvement of Mg-chelatase H subunit in plastid-to-nucleus signal transduction. *Proc. Natl. Acad. Sci. U.S.A.* 98, 2053–2058.

Mochizuki, N., Tanaka, R., Tanaka, A., Masuda, T., & Nagatani, A. (2008). The steady-state level of Mg-protoporphyrin IX is not a determinant of plastid-to-nucleus signaling in Arabidopsis. *Proceedings of the National Academy of Sciences of the United States of America*, *105*(39), 15184–15189.

Monte, E., Tepperman, J.M., Al-Sady, B., Kaczorowski, K.A., Alonso, J.M., Ecker, J.R., Li, X., Zhang, Y., and Quail, P.H. (2004). The phytochrome-interacting transcription factor, PIF3, acts early, selectively, and positively in light-induced chloroplast development. *Proc. Natl. Acad. Sci. USA* 101: 16091–16098.

Moulin, M., McCormac, A. C., Terry, M. J., & Smith, A. G. (2008). Tetrapyrrole profiling in Arabidopsis seedlings reveals that retrograde plastid nuclear signaling is not due to Mg-protoporphyrin IX accumulation. *Proceedings of the National Academy of Sciences of the USA*, *105*(39), 15178–15183.

Nakamichi, N., Kiba, T., Henriques, R., Mizuno, T., Chua, N. H., & Sakakibara, H. (2010). PSEUDO-RESPONSE REGULATORS 9, 7, and 5 are transcriptional repressors in the Arabidopsis circadian clock. *Plant Cell*, *22*(3), 594-605.

Nott, A., Jung, H. S., Koussevitzky, S., & Chory, J. (2006). Plastid-to-nucleus retrograde signaling. *Annu Rev Plant Biol*, *57*, 739-759.

Nuruzzaman, M., Sharoni, A. M., & Kikuchi, S. (2013). Roles of NAC transcription factors in the regulation of biotic and abiotic stress responses in plants. *Front Microbiol*, *4*, 248.

Oelmüller, R., Levitan, I., Bergfeld, R., Rajasekhar, V. K., & Mohr, H. (1986). Expression of nuclear genes as affected by treatments acting on the plastids. *Planta*, 168(4), 482–492.

Osterlund, M. T., Hardtke, C. S., Wei, N., & Deng, X. W. (2000). Targeted destabilization of HY5 during light-regulated development of Arabidopsis. *Nature*, *405*(6785), 462–466.

Oyama, T., Shimura, Y., and Okada, K. (1997). The Arabidopsis HY5 gene encodes a bZIP protein that regulates stimulus-induced devel- opment of root and hypocotyl. *Genes Dev*. 11: 2983–2995.

Paddock, T.N., Mason, M.E., Lima, D.F., Armstrong, G.A. (2010) Arabidopsis protochlorophyllide oxidoreductase A (PORA) restores bulk chlorophyll synthesis and normal development to a porB porC double mutant. *Plant Mol Biol*. 72(4-5):445-57.

Peers, G., & Niyogi, K. K. (2008). Pond scum genomics: the genomes of Chlamydomonas and Ostreococcus. *The Plant cell*, *20*(3), 502–507.

Paik, I., Kathare, P. K., Kim, J. I., & Huq, E. (2017). Expanding Roles of PIFs in Signal Integration from Multiple Processes. *Mol Plant*, *10*(8), 1035-1046.

Pesaresi, P., Masiero, S., Eubel, H., Braun, H.P., Bhushan, S., Glaser, E., Salamini, F., and Leister, D. (2006). Nuclear photosynthetic gene expression is synergistically modulated by rates of protein syn- thesis in chloroplasts and mitochondria. *Plant Cell*. 18, 970–991.

Pfannschmidt, T., Nilsson, A., Allen, J.F. (1999). Photosynthetic control of chloroplast gene expression. *Nature* 397: 625–628.

Pfeiffe,r A., Shi, H., Tepperman, J.M., Zhang, Y., Quail, P.H. (2014). Combinatorial complexity in a transcriptionally centered signaling hub in Arabidopsis. *Molecular Plant* 7: 1598–1618.

Pipitone, R., Eicke, S., Pfister, B., Glauser, G., Falconet, D., Uwizeye, C., Pralon, T., Zeeman, S.C., Kessler, F., Demarsy, E. (2021). A multifaceted analysis reveals two distinct phases of chloroplast biogenesis during de-etiolation in *Arabidopsis*. *Elife*. 25;10:e62709.

Podolec, R. & Ulm, R. (2018). Photoreceptor-mediated regulation of the COP1/-SPA E3 ubiquitin ligase. *Current Opinion in Plant Biology*, 45, 18–25.

Purvis, J., Ilango, V., Radhakrishnan, R. (2008). Role of network branching in eliciting differential short-term signaling responses in the hypersensitive epidermal growth factor receptor mutants implicated in lung cancer. *Biotechnology Process* 24: 540–553.

Quinlan, A.R. and Hall, I.M. (2010). BEDTools: a flexible suite of utilities for comparing genomic features. *Bioinformatics*, 26, 841-842.

Richter, A.S., Tohge, T., Fernie, A.R. & Grimm, B. (2020). The genomes uncoupled-dependent signalling pathway coordinates plastid biogenesis with the synthesis of anthocyanins. *Philosophical Transactions of the Royal Society of London. Series B, Biological Sciences*, 375, 20190403.

Richter, A. S., Nagele, T., Grimm, B., Kaufmann, K., Schroda, M., Leister, D., & Kleine, T. (2023). Retrograde signaling in plants: A critical review focusing on the GUN pathway and beyond. *Plant Commun*, *4*(1), 100511.

Riechmann, J.L., Heard, J., Martin, G., Reuber, L., Jiang, C., Keddie, J. (2000). Arabidopsis transcription factors: genome-wide comparative analysis among eukaryotes. *Science* 290: 2105–2110.

Robson, F., Costa, M. M., Hepworth, S. R., Vizir, I., Piñeiro, M., Reeves, P. H., Putterill, J., & Coupland, G. (2001). Functional importance of conserved domains in the flowering-time gene CONSTANS demonstrated by analysis of mutant alleles and transgenic plants. *The Plant journal: for cell and molecular biology*, 28(6), 619–631.

Rossel, J.B., Wilson, I.W., and Pogson, B.J. (2002). Global changes in gene expression in response to high light in Arabidopsis. *Plant Physiol*. 130, 1109–1120.

Ruckle, M.E., DeMarco, S.M. & Larkin, R.M. (2007). Plastid signals remodel light signaling networks and are essential for efficient chloroplast bio- genesis in Arabidopsis. *Plant Cell*, 19, 3944–3960.

Rushton, P.J., Macdonald, H., Huttly, A.K., Lazarus, C.M., and Hooley, R. (1995). Members of a new family of DNA-binding proteins bind to a conserved cis-element in the pro- moters of alpha-Amy2 genes. *Plant Mol. Biol*. 29: 691–702.

Saibo, N. J., Lourenco, T., & Oliveira, M. M. (2009). Transcription factors and regulation of photosynthetic and related metabolism under environmental stresses. *Ann Bot*, *103*(4), 609-623.

Sambrook, J. & Russell, D.W. (2001). Molecular Cloning A Laboratory Manual, 3rd edition. New York: Cold Spring Harbor Laboratory Press.

Sánchez, J. P., Duque, P., & Chua, N. H. (2004). ABA activates ADPR cyclase and cADPR induces a subset of ABA-responsive genes in Arabidopsis. *The Plant journal: for cell and molecular biology*, *38*(3), 381–395.

Shahzad, R., Jamil, S., Ahmad, S., Nisar, A., Amina, Z., Saleem, S., Zaffar Iqbal, M., Muhammad Atif, R., & Wang, X. (2021). Harnessing the potential of plant transcription factors in developing climate resilient crops to improve global food security: Current and future perspectives. *Saudi J Biol Sci*, *28*(4), 2323-2341.

Sherman, B.T., Hao, M., Qiu, J., Jiao, X., Baseler, M.W., Lane, H.C. (2022). DAVID: a web server for functional enrichment analysis and func- tional annotation of gene lists (2021 update). *Nucleic Acids Research*, 50, W216–W221.

Shi, H., Lyu, M., Luo, Y., Liu, S., Li, Y., He, H., Wie, N., Deng, X.W., Zhong, S. (2018). Genome-wide regulation of light-controlled seedling morphogenesis by three families of transcription factors. *Proceedings of the National Academy of Sciences, USA* 115: 6482–6487.

Shimizu, T., Kacprzak, S. M., Mochizuki, N., Nagatani, A., Watanabe, S., Shimada, T., Tanaka, K., Hayashi, Y., Arai, M., Leister, D., Okamoto, H., Terry, M. J., & Masuda, T. (2019). The retrograde signaling protein GUN1 regulates tetrapyrrole biosynthesis. *Proc Natl Acad Sci U S A*, *116*(49), 24900-24906.

Shimizu, T., Kacprzak, S. M., Mochizuki, N., Nagatani, A., Watanabe, S., Shimada, T., Tanaka, K., Hayashi, Y., Arai, M., Leister, D., Okamoto, H., Terry, M. J., & Masuda, T. (2019). The retrograde signaling protein GUN1 regulates tetrapyrrole biosynthesis. *Proc. Natl. Acad. Sci. USA*, 116(49), 24900–24906.

Shin, J., Kim, K., Kang, H., Zulfugarov, I.S., Bae, G., Lee, C-H., Lee, D., Choi, G. (2009). Phytochromes promote seedling light responses by inhibiting four negatively- acting phytochrome-interacting factors. *Proceedings of the National Academy of Sciences, USA* 106: 7660–7665.

Short, K.M., Cox, T.C. (2006). Sub-classification of the RBCC/TRIM superfamily reveals a novel motif necessary for microtubule binding. *J. Biol. Chem*. 281, 8970–8980.

Singh, D., Datta, S. (2023). BBX30/miP1b and BBX31/miP1a form a positive feedback loop with ABI5 to regulate ABA-mediated postgermination seedling growth arrest. *New Phytol.* 238(5):1908-1923.

Song, Z., Yan, T., Liu, J., Bian, Y., Heng, Y., Lin, F. (2020). BBX28/BBX29, HY5 and BBX30/31 form a feedback loop to fine-tune photomorphogenic development. *The Plant Journal*, 104, 377–390.

Song, Z., Yan, T., Liu, J., Bian, Y., Heng, Y., Lin, F., Jiang, Y., Deng, XW., Xu, D. (2020). BBX28/BBX29, HY5 and BBX30/31 form a feedback loop to fine-tune photomorphogenic development. *The Plant Journal* 104: 377–390.

Sornaraj, P., Luang,S., Lopato, S., Hrmova, M. (2016). Basic leucine zipper (bZIP) transcription factors involved in abiotic stresses: A molecular model of a wheat bZIP factor and implications of its structure in function. *Biochim. Biophys. Acta 1860*, 46–56.

Strand, A., Asami, T., Alonso, J., Ecker, J.R., Chory, J. (2003). Chloroplast to nucleus communication triggered by accumulation of Mg-protoporphyrin IX. *Nature* 421: 79–83

Strand, A., Asami, T., Alonso, J., Ecker, J.R., Chory, J. (2003). Chloroplast to nucleus communication triggered by accumulation of Mg-protoporphyrinIX. *Nature* 421:79–83

Sullivan, J.A., and Deng X.W. (2003). From seed to seed: The role of photoreceptors in *Arabidopsis* development. *Dev. Biol*. 260: 289–297.

Sun, Y., Fan, X. Y., Cao, D. M., Tang, W., He, K., Zhu, J. Y., He, J. X., Bai, M. Y., Zhu, S., Oh, E., Patil, S., Kim, T. W., Ji, H., Wong, W. H., Rhee, S. Y., & Wang, Z. Y. (2010). Integration of brassinosteroid signal transduction with the transcription network for plant growth regulation in Arabidopsis. *Developmental cell*, *19*(5), 765–777.

Sun, X., Feng, P., Xu, X., Guo, H., Ma, J., Chi, W., Lin, R., Lu, C., & Zhang, L. (2011). A chloroplast envelope-bound PHD transcription factor mediates chloroplast signals to the nucleus. *Nat Commun*, *2*, 477.

Susek, R. E., Ausubel, F. M., and Chory, J. (1993). Signal transduction mutants of arabidopsis uncouple nuclear *CAB* and *RBCS* gene expression from chloroplast development. *Cell* 74, 787–799.

Susila, H., Nasim, Z., Gawarecka, K., Jung, J. Y., Jin, S., Youn, G., & Ahn, J. H. (2023). Chloroplasts prevent precocious flowering through a GOLDEN2-LIKE-B-BOX DOMAIN PROTEIN module. *Plant Commun*, *4*(3), 100515.

Suzuki, N., Devireddy, A.R., Inupakutika, M.A., Baxter, A., Miller, G., Song, L., Shulaev, E., Azad, R.K., Shulaev, V., and Mittler, R. (2015). Ultra-fast alterations in mRNA levels uncover multiple players in light stress acclimation in plants. *Plant J*. 84, 760–772.

Suzuki, N., Miller, G., Salazar, C., Mondal, H. A., Shulaev, E., Cortes, D. F. (2013). Temporal-spatial interaction between reactive oxygen species and abscisic acid regulates rapid systemic acclimation in plants. *Plant Cell* 25, 3553–3569.

Suzuki, N., Miller, G., Salazar, C., Mondal, H. A., Shulaev, E., Cortes, D. F., Shuman, J. L., Luo, X., Shah, J., Schlauch, K., Shulaev, V., & Mittler, R. (2013). Temporal-spatial interaction between reactive oxygen species and abscisic acid regulates rapid systemic acclimation in plants. *The Plant cell*, *25*(9), 3553–3569.

Tadini, L., Pesaresi, P., Kleine, T., Rossi, F., Guljamow, A., Sommer, F., Muehlhaus, T., Schroda, M., Masiero, S., Pribil, M. (2016). GUN1 controls accumulation of the plastid ribosomal protein s1 at the protein level and interacts with proteins involved in plastid protein homeostasis. *Plant Physiology* 170: 1817–1830.

Talar, U., & Kielbowicz-Matuk, A. (2021). Beyond Arabidopsis: BBX Regulators in Crop Plants. *Int J Mol Sci*, *22*(6).

Tamura, K., Peterson, D., Peterson, N., Stecher, G., Nei, M., Kumar, S. (2011). MEGA5: molecular evolutionary genetics analysis using maximum likelihood, evolutionary distance, and maximum parsimony methods. *Mol. Biol. Evol*. 28, 2731–2739.

Terry, M. J., and Smith, A. G. (2013). A model for tetrapyrrole synthesis as the primary mechanism for plastid-to-nucleus signaling during chloroplast biogenesis. *Front. Plant Sci.* 4:14.

Terry, M.J., Kacprzak, S.M. (2019). A Simple Method for Quantification of Protochlorophyllide in Etiolated Arabidopsis Seedlings. *Methods Mol Biol*. 2026:169-177.

Terry, M.J., Smith, A.G. (2013). A model for tetrapyrrole synthesis as the primary mechanism for plastid-to-nucleus signaling during chloroplast biogenesis. *Front Plant Sci* 4: 14

Tokumaru, M., Adachi, F., Toda, M., Ito-Inaba, Y., Yazu, F., Hirosawa, Y. (2017). Ubiquitin-proteasome dependent regulation of the GOLDEN2-LIKE 1 transcription factor in response to plastid signals. *Plant Physiology*, 173, 524–535.

Torok, M., and Etkin, L.D. (2001). Two B or not two B? Overview of the rapidly expanding B-box family of proteins. *Differentiation* 67: 63–71.

Tripathi, P., Carvallo, M., Hamilton, E. E., Preuss, S., & Kay, S. A. (2017). Arabidopsis B-BOX32 interacts with CONSTANS-LIKE3 to regulate flowering. *Proc Natl Acad Sci U S A*, *114*(1), 172-177.

Tripathi, S., Hoang, Q.T.N., Han, Y.J., Kim, J.I. (2019). Regulation of Photomorphogenic Development by Plant Phytochromes. *Int J Mol Sci*. 20(24):6165.

Tripathy, B. C., & Pattanayak, G. K. (2012). Chlorophyll biosynthesis in higher plants. *Photosynthesis: plastid biology, energy conversion and carbon assimilation*, 63-94.

Vaishak, K. P., Yadukrishnan, P., Bakshi, S., Kushwaha, A. K., Ramachandran, H., Job, N., Babu, D., & Datta, S. (2019). The B-box bridge between light and hormones in plants. *J Photochem Photobiol B*, *191*, 164-174.

Van Aken, O., Whelan, J. (2012). Comparison of transcriptional changes to chloroplast and mitochondrial perturbations reveals common and specific responses in Arabidopsis. *Front Plant Sci* 3: 281

Veciana, N., Martin, G., Leivar, P., & Monte, E. (2022). BBX16 mediates the repression of seedling photomorphogenesis downstream of the GUN1/GLK1 module during retrograde signalling. *New Phytol*, *234*(1), 93-106.

Von Wettstein, D., Gough, S., Kannangara, C.G. (1995). Chlorophyll biosynthesis. *The Plant Cell* 7:1039–1057.

Wang, C. Q., Sarmast, M. K., Jiang, J., & Dehesh, K. (2015). The Transcriptional Regulator BBX19 Promotes Hypocotyl Growth by Facilitating COP1-Mediated EARLY FLOWERING3 Degradation in Arabidopsis. *The Plant cell*, *27*(4), 1128–1139.

Wang, H., Zhang, Z., Li, H., Zhao, X., Liu, X., Ortiz, M. (2013). CONSTANS-LIKE 7 regulates branching and shade avoidance response in Arabidopsis. *Journal of Experimental Botany*, 64, 1017–1024.

Wang, J.; Zhou, J.; Zhang, B.; Vanitha, J.; Ramachandran, S.; Jiang, S.Y. (2011). Genome-wide Expansion and Expression Divergence of the Basic Leucine Zipper Transcription Factors in Higher Plants with an Emphasis on Sorghum. *J. Integr. Plant Biol. 53*, 212–231.

Wang, L., Xu, D., Scharf, K., Frank, W., Leister, D. and Kleine, T. (2022). The RNA-binding protein RBP45D of Arabidopsis promotes transgene silencing and flowering time. *Plant J*, 109, 1397-1415.

Wang, Q., Tu, X., Zhang, J., Chen, X., & Rao, L. (2013). Heat stress-induced BBX18 negatively regulates the thermotolerance in Arabidopsis. *Molecular biology reports*, *40*(3), 2679–2688.

Wang, Q., Zeng, J., Deng, K., Tu, X., Zhao, X., Tang, D., & Liu, X. (2011). DBB1a, involved in gibberellin homeostasis, functions as a negative regulator of blue light-mediated hypocotyl elongation in Arabidopsis. *Planta*, *233*(1), 13–23.

Wang, Z.P., Xing, H.L., Dong, L., Zhang, H.Y., Han, C.Y., Wang, X.C. and Chen, Q.J. (2015). Egg cell-specific promoter-controlled CRISPR/Cas9 efficiently generates homozygous mutants for multiple target genes in Arabidopsis in a single generation. *Genome Biol*, 16, 144.

Waters, M.T., Moylan, E.C., and Langdale, J.A. (2008). GLK transcription factors regulate chloroplast development in a cell- autonomous manner. Plant J. 56: 432–444.

Waters, M. T., Wang, P., Korkaric, M., Capper, R. G., Saunders, N. J., & Langdale, J. A. (2009). GLK transcription factors coordinate expression of the photosynthetic apparatus in Arabidopsis. *Plant Cell*, *21*(4), 1109-1128.

Wei, C. Q., Chien, C. W., Ai, L. F., Zhao, J., Zhang, Z., Li, K. H., Burlingame, A. L., Sun, Y., & Wang, Z. Y. (2016). The Arabidopsis B-box protein BZS1/BBX20 interacts with HY5 and mediates strigolactone regulation of photomorphogenesis. *Journal of genetics and genomics*, *43*(9), 555–563.

Winter, D., Vinegar, B., Nahal, H., Ammar, R., Wilson, G.V. & Provart, N.J. (2007). An "Electronic Fluorescent Pictograph" browser for exploring and analyzing large-scale biological data sets. *PLoS One*, 2, e718.

Woodson, J. D., Perez-Ruiz, J. M., & Chory, J. (2011). Heme synthesis by plastid ferrochelatase I regulates nuclear gene expression in plants. *Current biology : CB*, 21(10), 897–903.

Woodson, J.D., Chory, J. (2008). Coordination of gene expression between organellar and nuclear genomes. *Nat Rev Genet* 9: 383–395

Woodson, J.D., Perez-Ruiz, J.M., Schmitz, R.J., Ecker, J.R., Chory, J. (2013) Sigma factor-mediated plastid retrograde signals control nuclear gene expression. *Plant J* 73: 1–13

Wu, G. Z., Chalvin, C., Hoelscher, M., Meyer, E. H., Wu, X. N., & Bock, R. (2018). Control of Retrograde Signaling by Rapid Turnover of GENOMES UNCOUPLED1. *Plant physiology*, 176(3), 2472–2495.

Wu, S.H. (2014). Gene expression regulation in photomorphogenesis from the perspective of the central dogma. *Annual Review of Plant Biology* 65:311–333.

Xiao, Y., Savchenko, T., Baidoo, E.E.K., Chehab, W.E., Hayden, D.M., Tolstikov, V., Corwin, J.A., Kliebenstein, D.J., Keasling, J.D., Dehesh, K. (2012). Retrograde

signaling by the plastidial metabolite MEcPP regulates expression of nuclear stress-response genes. *Cell* 149: 1525–1535

Xu, D. (2020). COP1 and BBXs-HY5-mediated light signal transduction in plants. *The New Phytologist*, 228, 1748–1753.

Xu, D., Jiang, Y., Li, J., Holm, M., & Deng, X. W. (2018). The B-Box Domain Protein BBX21 Promotes Photomorphogenesis. *Plant physiology*, *176*(3), 2365–2375.

Xu, D., Jiang, Y., Li, J., Lin, F., Holm, M., & Deng, X. W. (2016). BBX21, an Arabidopsis B-box protein, directly activates HY5 and is targeted by COP1 for 26S proteasome-mediated degradation. *Proceedings of the National Academy of Sciences of the United States of America*, *113*(27), 7655–7660.

Xu, D., Marino, G., Klingl, A., Enderle, B., Monte, E., Kurth, J., Hiltbrunner, A., Leister, D. and Kleine, T. (2019). Extrachloroplastic PP7L Functions in Chloroplast Development and Abiotic Stress Tolerance. *Plant Physiol*, 180, 323-341.

Yadukrishnan, P., Job, N., Johansson, H., & Datta, S. (2018). Opposite roles of group IV BBX proteins: Exploring missing links between structural and functional diversity. *Plant Signal Behav*, *13*(8), e1462641.

Yan, H., Marquardt, K., Indorf, M., Jutt, D., Kircher, S., Neuhaus, G., & Rodríguez-Franco, M. (2011). Nuclear localization and interaction with COP1 are required for STO/BBX24 function during photomorphogenesis. *Plant physiology*, *156*(4), 1772–1782.

Yan, W., Chen, D., Smaczniak, C., Engelhorn, J., Liu, H., Yang, W., Graf, A., Carles, C.C., Zhou, D.X. and Kaufmann, K. (2018). Dynamic and spatial restriction of Polycomb activity by plant histone demethylases. *Nat Plants*, 4, 681-689.

Yanagisawa, S. (1995). A novel DNA-binding domain that may form a single zinc finger motif. *Nucleic Acids Res*. 23: 3403– 3410.

Yilmaz, A., Mejia-Guerra, M. K., Kurz, K., Liang, X., Welch, L., & Grotewold, E. (2011). AGRIS: the Arabidopsis Gene Regulatory Information Server, an update. *Nucleic acids research*, *39*(Database issue), D1118–D1122.

Yuan, L., Yu, Y., Liu, M., Song, Y., Li, H., Sun, J., Wang, Q., Xie, Q., Wang, L., & Xu, X. (2021). BBX19 fine-tunes the circadian rhythm by interacting with PSEUDO-RESPONSE REGULATOR proteins to facilitate their repressive effect on morning-phased clock genes. *Plant Cell*, *33*(8), 2602-2617.

Zhang, X., Huai, J., Shang, F., Xu, G., Tang, W., Jing, Y., & Lin, R. (2017). A PIF1/PIF3-HY5-BBX23 Transcription Factor Cascade Affects Photomorphogenesis. *Plant Physiol*, *174*(4), 2487-2500.

Zhang, Y., Liu, T., Meyer, C.A., Eeckhoute, J., Johnson, D.S., Bernstein, B.E., Nusbaum, C., Myers, R.M., Brown, M., Li, W. and Liu, X.S. (2008). Model-based analysis of ChIP-Seq (MACS). *Genome Biol*, 9, R137.

Zhang, Y., Mayba, O., Pfeiffer, A., Shi, H., Tepperman, J.M., Speed, T.P., Quail, P.H. (2013). A quartet of PIF bHLH factors provides a transcriptionally centered signaling hub that regulates seedling morphogenesis through differential expression-patterning of shared target genes in Arabidopsis. *PLoS Genetics* 9: e1003244.

Zhang, Y., Tian, L., & Lu, C. (2023). Chloroplast gene expression: Recent advances and perspectives. *Plant communications*, *4*(5), 100611.

Zhang, Z., Ji, R., Li, H., Zhao, T., Liu, J., Lin, C. (2014). CONSTANS-LIKE 7 (COL7) is involved in phytochrome B (phyB)-mediated light-quality regulation of auxin homeostasis. *Molecular Plant*, 7, 1429–1440.

Zhao, X., Huang, J., and Chory, J. (2019). GUN1 interacts with MORF2 to regulate plastid RNA editing during retrograde signaling. *Proc. Natl. Acad. Sci. USA* 116:10162–10167.

Zhao, X., Huang, J., Chory, J. (2019). GUN1 interacts with MORF2 to regulate plastid RNA editing during retrograde signaling. *Proceedings of the National Academy of Sciences, USA* 116: 10162–10167.

7. Supplemental information

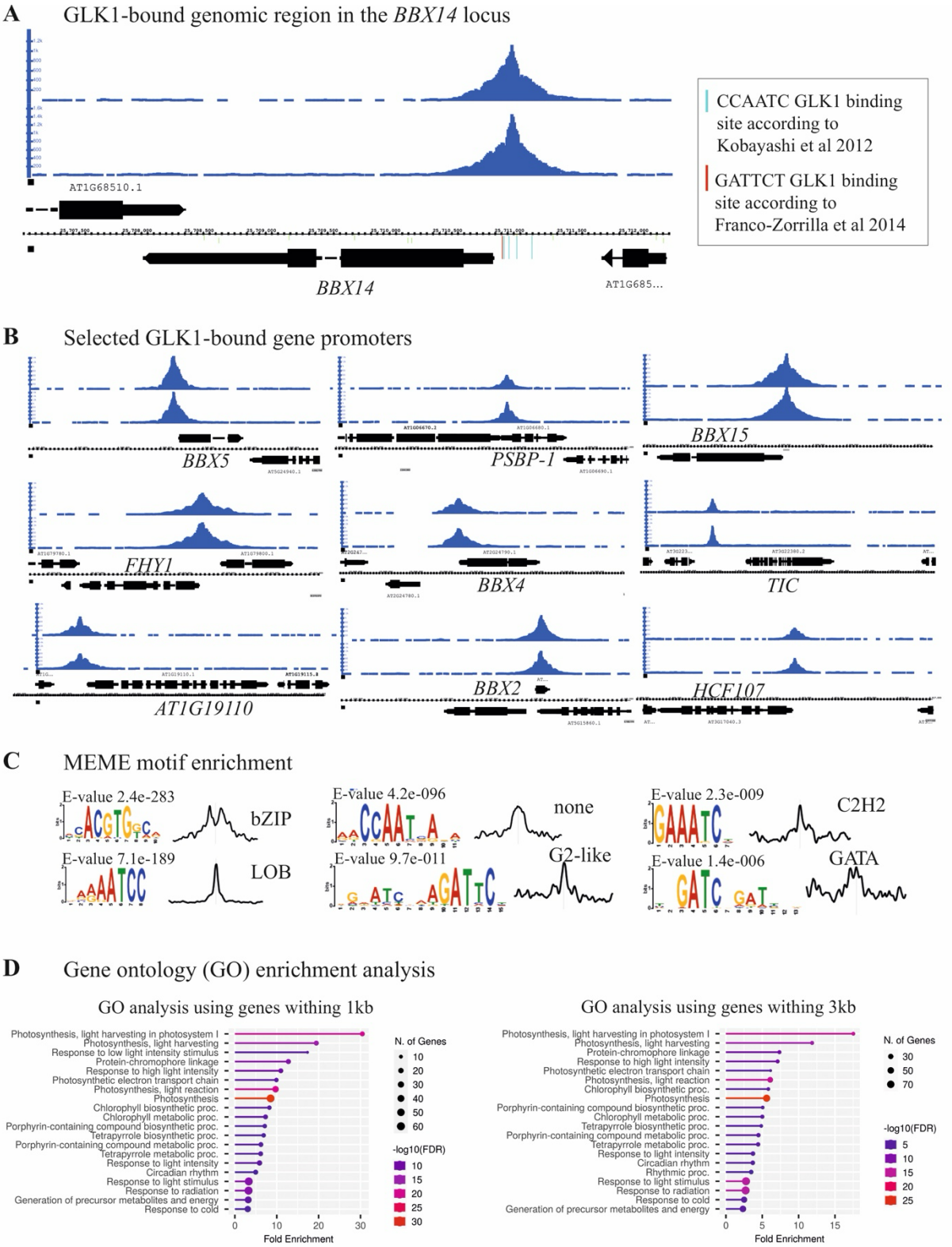

Figure S1. *BBX14* is a target of GLK1.

(A) Chromatin-immunoprecipitation followed by sequencing (ChIP-seq) was performed with 14-day-old seedlings of a plant line that expresses GLK1 from its endogenous promoter in the Col-0 background (*pGLK1*:*GLK1-GFP*), and a snapshot of the *BBX14* gene region is shown.

(B) Snapshots of selected genes targeted by GLK1.

(C) Additional motifs bound by GLK1 identified by the MEME Suite (Bailey *et al.*, 2015).

(D) Top 20 ranked GO terms according to fold enrichment within 1 kb (left side) and 3 kb (right side) of GLK1 binding site. A total of 761 and 1365 genes withing 1 kb and 3 kb of the GLK1 binding site were analyzed, respectively. GO terms are presented in biological pathways on the y-axis and ranked from highest to lowest fold enrichment. Circle sizes indicate the gene count in a GO term. A cut-off of 5-fold enrichment compared to the expected frequency in the Arabidopsis genome was applied. The gradual color represents the FDR (Benjamini-Hochberg). Results were visualized at $P < 0.05$ using ShinyGO v0.7 (http://bioinformatics.sdstate.edu/go75/).

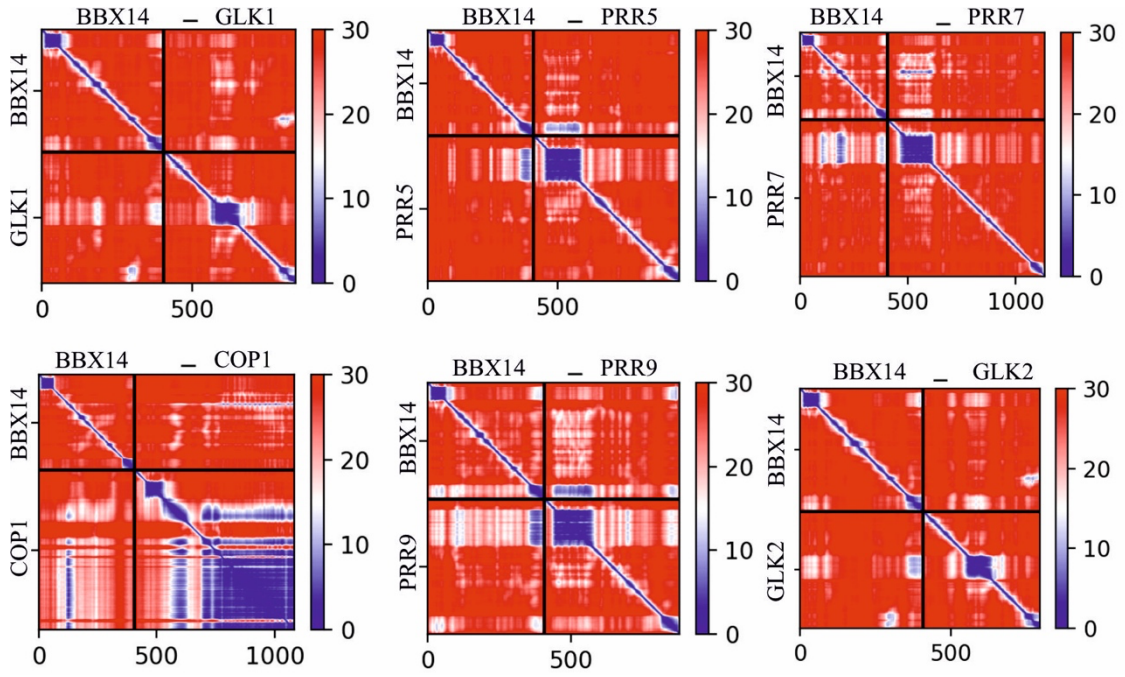

Figure S2. Prediction aligned error (PAE) plot for potential interacting partners of BBX14.

The score displays the calculated error of the predicted distance for every pair of residues. Both axes indicate the position of the individual amino acids. The uncertainty in the predicted distance of two amino acids is color coded from 0 Å (blue) to 30 Å (red). The color of the intersection of a horizontal line drawn from the position of an amino acid on the y-axis and a vertical line from the position of another amino acid on the x-axis indicates the error in the predicted distance between these two residues. The upper left quadrant in all plots corresponds to errors in the distances of residues within BBX14, the lower right quadrant to errors within the respective potential interacting partner, the upper right and lower left quadrant to errors between BBX14 and potential interacting partner. Plots were generated via AlphaFold2 (https://alphafold.ebi.ac.uk).

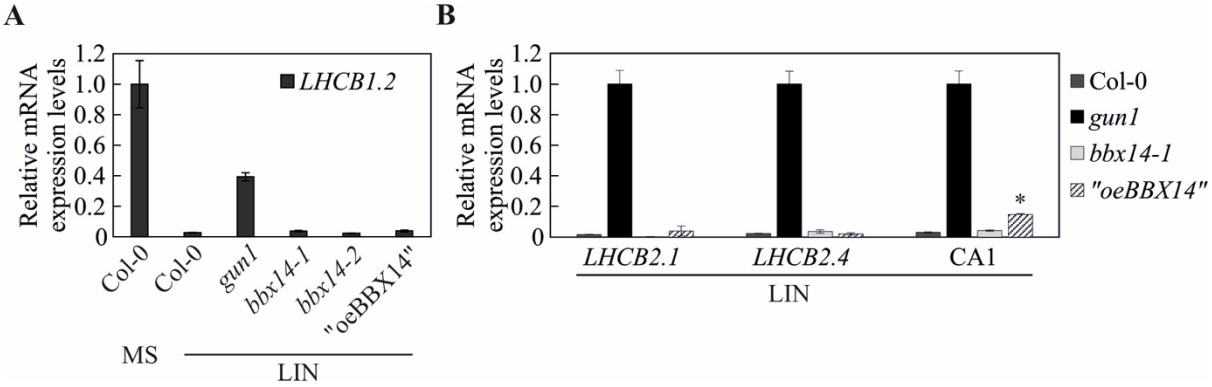

Figure S3. Investigation of putative *gun* phenotypes of seedlings containing altered levels of *BBX14*.

RT-qPCR of retrograde marker genes *LHCB1.2* **(A)**, and *LHCB2.1*, *LHCB2.4* and *CA1* **(B)** in Col-0, *gun1* and *bbx14-1* mutants, and the *35S*:*BBX14* line with strongest overexpression (2.5-fold) of *BBX14* ("oeBBX14"). Seedlings were grown for 4 days in continuous light (100 µmol photons m^{-2} s^{-1}) in the absence (MS) or presence of lincomycin (LIN). RT-qPCR was performed as described in the legend to **Figure 3 (C)**.

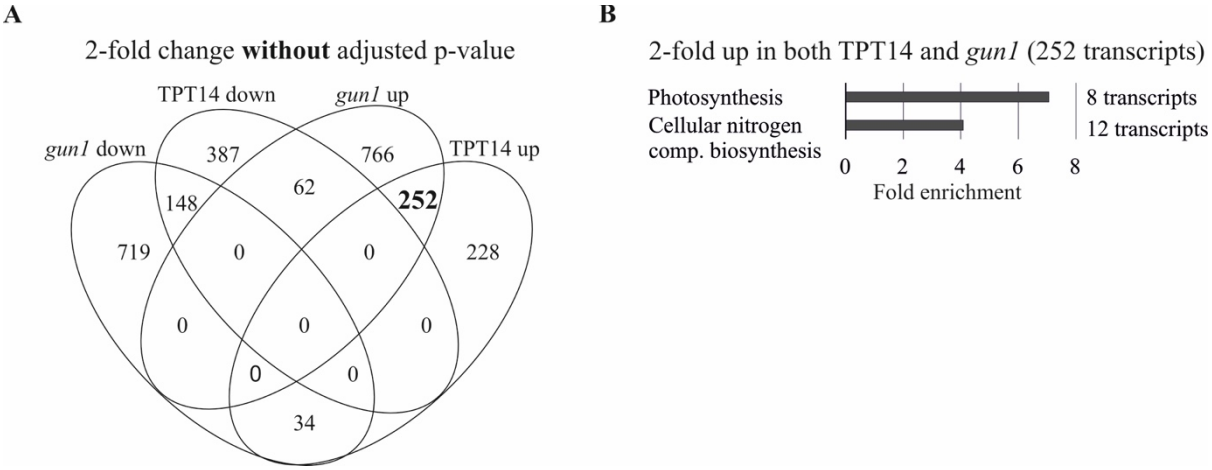

Figure S4. RNA-Seq of Col-0, TPT14 and gun1 seedlings.

(A) Analysis of transcriptome changes in *gun1* and TPT14 seedlings. Venn diagrams depicting the degree of overlap between the sets of genes whose expression levels were reduced or elevated by at least 2-fold in seedlings that had been treated like in **Figure 9 (A)** compared with the WT (Col-0) control. Note that gene sets were selected based on two-fold change without adjusted p-value

(B) GO analysis of genes whose expression is upregulated in both *gun1* and TPT14 seedlings. The bar lengths represent the frequency of assignment (expressed as fold change compared with the whole genome) to the respective GO categories. GO annotations were determined with agriGO (Du et al., 2010).

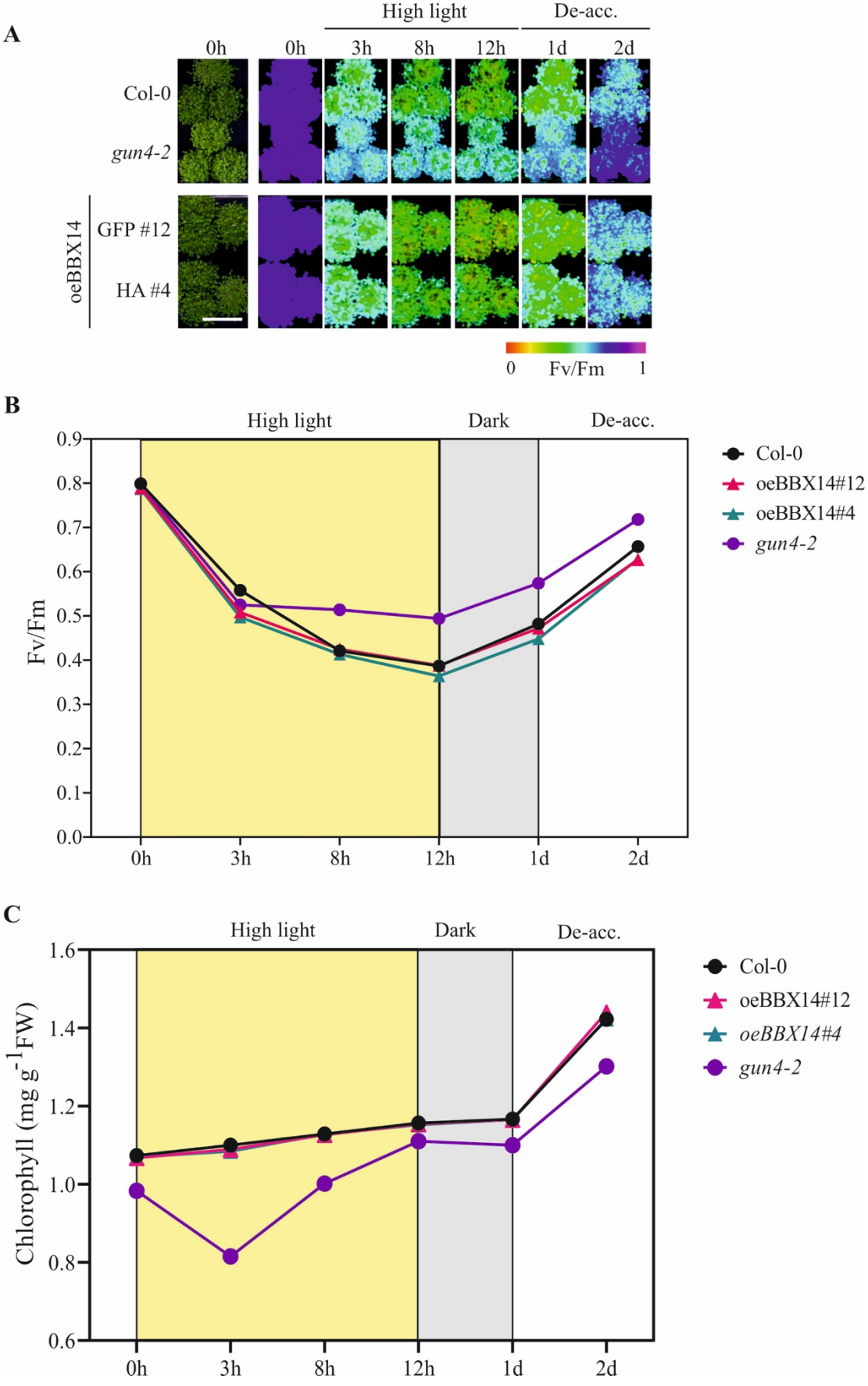
A
High light
De-acc.
0h
0h
3h
8h
12h
1d
2d
Col-0
gun4-2
oeBBX14
GFP #12
HA #4
0
Fv/Fm
1
B
High light
Dark
De-acc.
Fv/Fm
0.9
0.8
0.7
0.6
0.5
0.4
0.3
0.2
0.1
0.0
0h
3h
8h
12h
1d
2d
Col-0
oeBBX14#12
oeBBX14#4
gun4-2
C
High light
Dark
De-acc.
Chlorophyll (mg g-1FW)
1.6
1.4
1.2
1.0
0.8
0.6
0h
3h
8h
12h
1d
2d
Col-0
oeBBX14#12
oeBBX14#4
gun4-2

Figure S5. Hight light acclimation of *gun4-2* and "oeBBX14" plants.

(A) Phenotypes and ImagingPAM pictures of wild-type (Col-0) and mutant (*gun4-2*, oeBBX14-GFP#12 and oeBBX14-HA#4) seedling grown for 1 week under control conditions (16-h light/8-h dark, 80 µmol photons m^{-2} s^{-1}; left panel), shifted to HL conditions (16-h light/8-h dark, 1000 µmol photons m^{-2} s^{-1}), and then de-acclimated (de-acc.) in control conditions for the indicated time. A representative image from three independent plates is shown. Scale bar = 1 cm.

(B) Photosystem II maximum quantum yield (Fv/Fm) of wild-type (Col-0) and mutant (*gun4-2*, oeBBX14-GFP#12 and oeBBX14-HA#4) seedlings grown as described in **(A)**. Data is shown as mean values ± SEM of three measuring points from three different plant pools. Each pool contained more than 50 seedlings.

(C) Determination of total chlorophyll (Chl *a* + *b*) contents of seedlings grown as in **(A)**. Data are shown as mean values ± SD from three different plant pools. Each pool contained more than 50 seedlings.

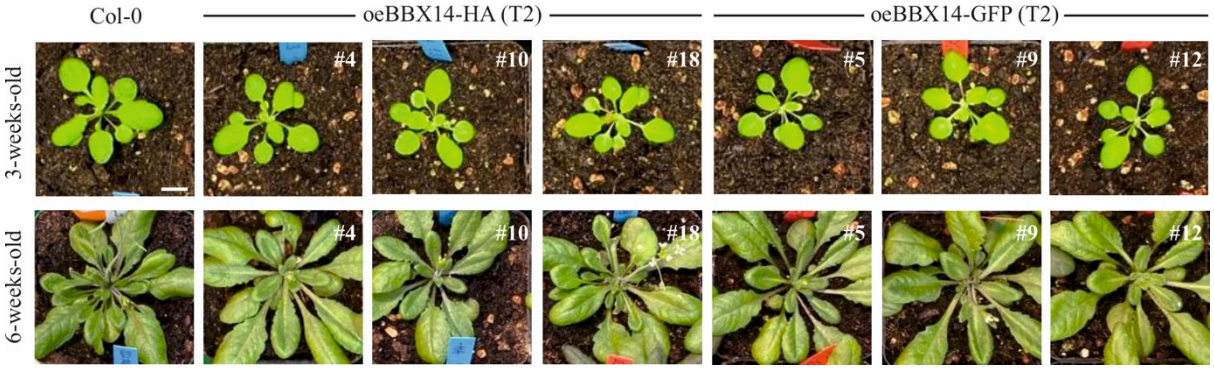

Figure S6. Plants overexpressing BBX14 are indistinguishable from Col-0 plant at later developmental stages. Growth phenotypes of 3-weeks-old (upper panel) and 6-weeks-old (lower panel) wild-type (Col-0) and Col-0 plants carrying constructs overexpressing BBX14 under the *35S* promoter (oeBBX14-HA and oeBBX14-GFP). Seedlings were first selected on plates containing 7,6 µg/ml BASTA and surviving seedlings were transferred to soil following growth at 100 µmol m^{-2} s^{-1} for two weeks. Scale bar = 1 cm.

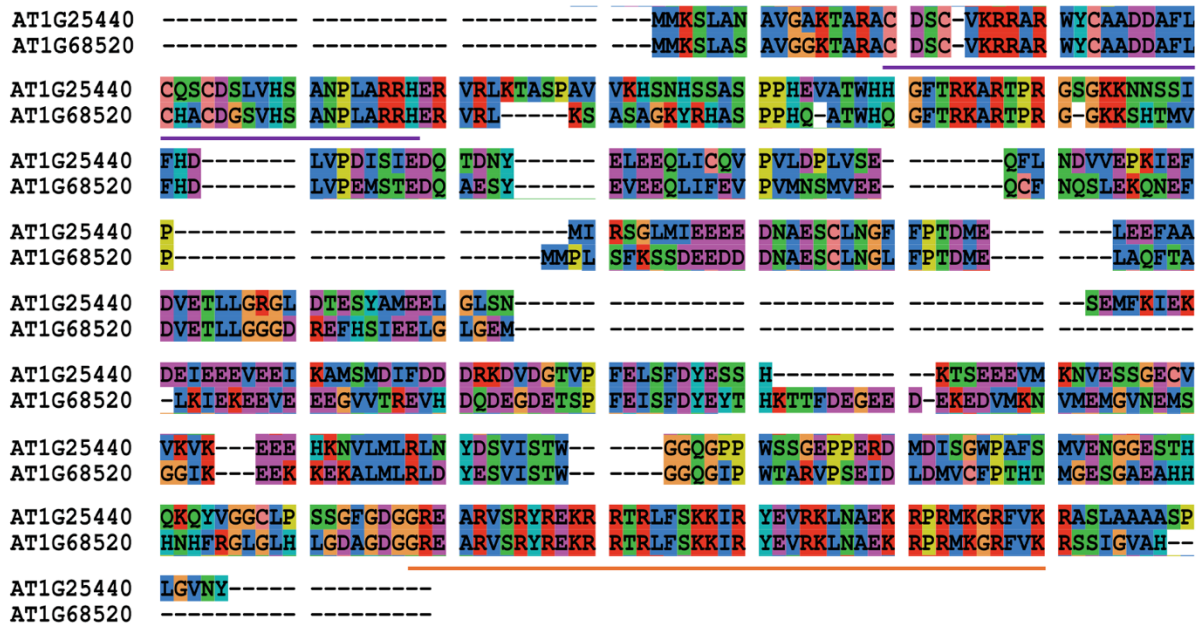

Figure S7. FASTA format sequence alignment of Arabidopsis *BBX14* (AT1G68520) and *BBX15* (AT1G25440) proteins with MUSCLE. The conserved amino acids are color-labelled to indicate identical and similar amino acids purple and orange lines indicate the B-box B1 and CCT domains, respectively.

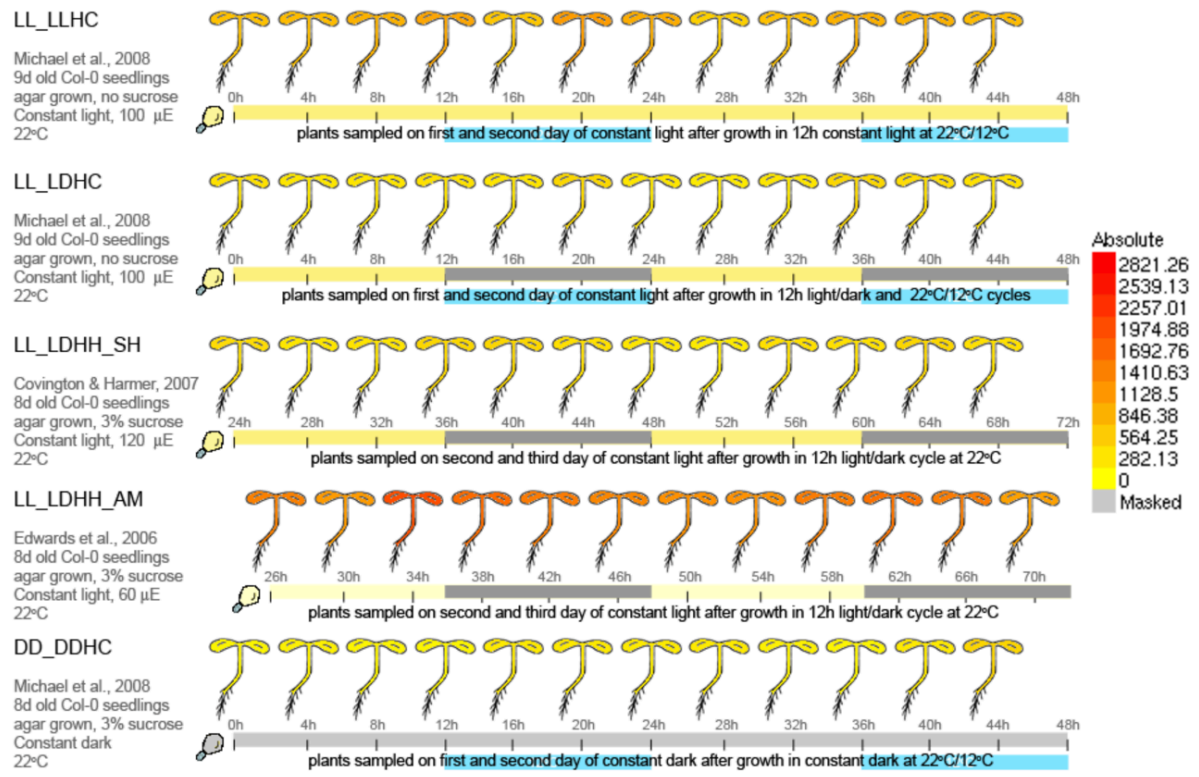

Figure S8. Circadian series expression of Arabidopsis *BBX14* (AT1G68520) according to the eFP browser. Light eFP Browser imagine of circadian expression for *BBX14* (http://bar.utoronto.ca/; Winter et al., 2007) from Arabidopsis seedlings grown under different conditions as indicated on left. Data from AtGenExpress Consortium and other labs, as indicated. Data normalized by the GCOS method with TGT value of 100. The AtGenExpress data were generated from triplicates and the average is shown. For the eFP Browser "relative" view the values are

displayed relative to the first sample in the series, or to the dark control, in the case of the AtGenExpress. Yellow and grey bars indicate lighting regimes prior to constant light or dark. Blue bars indicate the entrainment temperature dipped to 12°C from 22°C.

Table S1. GLK1 ChIP-seq data analysis. Peaks with adjusted P-values < 0.05 are shown. Analysis was performed by DESeq 2 of both ChIP-seq samples versus input DNA.

Postion	baseMean	log2(FC)	lfcSE	p-value	p-adj	gene 1 kb upstream to 1 kb downstream	gene 3 kb upstream to 3 kb downstream
Chr1-8935495	2409,93413	5,47880403	0,28030011	2,22E-85	8,53E-82	AT1G25440	AT1G25440 AT1G25450
Chr5-8589274.5	2353,81906	5,24178963	0,27734361	5,70E-80	1,10E-76	AT5G24930	AT5G24930 AT5G24940
Chr1-25711091	1832,54032	4,64310229	0,25651423	1,57E-73	2,01E-70	AT1G68520 AT1G68526	AT1G68510 AT1G68520 AT1G68526 AT1G68530
Chr1-30018343	1688,68773	4,70446474	0,2603393	2,72E-73	2,61E-70	AT1G79790 AT1G79800	AT1G79770 AT1G79780 AT1G79790 AT1G79800 AT1G79810 AT1G09917
Chr5-5178146	1772,31986	4,67088078	0,26987461	2,06E-67	1,58E-64	AT5G15845 AT5G15850 AT5G15853 AT5G15860	AT5G15845 AT5G15850 AT5G15853 AT5G15860
Chr2-10567022.5	1107,71032	4,70111504	0,28363292	5,31E-62	3,40E-59	AT2G24780 AT2G24790	AT2G24765 AT2G24780 AT2G24790
Chr3-7910129	1229,30575	4,61857993	0,2894482	1,28E-57	7,04E-55		AT3G22370 AT3G22380
Chr3-5812881.5	916,404219	4,60941725	0,28982539	2,97E-57	1,42E-54	AT3G17040	AT3G17040
Chr1-6601966	1259,01107	4,18520159	0,2694263	1,03E-54	4,37E-52	AT1G19100 AT1G19110	AT1G19100 AT1G19110
Chr1-2047811	1107,81187	4,30391715	0,29316483	4,27E-49	1,64E-46	AT1G06670 AT1G06680	AT1G06670 AT1G06680 AT1G06690
Chr2-6947106	955,027933	3,79535098	0,26699538	3,70E-46	1,29E-43	AT2G15950 AT2G15960	AT2G15950 AT2G15960 AT2G15970
Chr3-5469893	914,62533	3,82009504	0,27614518	7,99E-44	2,56E-41	AT3G16130 AT3G16140	AT3G16130 AT3G16140 AT3G16150
Chr1-29735975	767,521719	3,86730836	0,28536224	3,84E-42	1,13E-39	AT1G79040 AT1G79050	AT1G79030 AT1G79040 AT1G79050
Chr3-17494708.5	1066,66378	3,64683189	0,27157796	2,06E-41	5,66E-39	AT3G47470 AT3G07765	AT3G47460 AT3G47470 AT3G07765 AT3G47480
Chr4-7521478	909,165409	3,73601401	0,28442695	1,03E-39	2,65E-37	AT4G12800	AT4G12790 AT4G12800 AT4G12810
Chr1-27778671.5	988,16484	3,79191187	0,28963629	1,83E-39	4,39E-37	AT1G73870	AT1G73860 AT1G73870 AT1G73875
Chr1-22444513	793,390027	3,69267589	0,28247872	2,37E-39	5,35E-37	AT1G60950 AT1G60960	AT1G60940 AT1G60950 AT1G60960
Chr1-20803511	678,001962	3,81587188	0,29509678	1,51E-38	3,21E-36	AT1G55670 AT1G55673 AT1G55675	AT1G55660 AT1G55670 AT1G55673 AT1G55675 AT1G55680
Chr5-6739797.5	1110,48377	3,72400869	0,29040316	6,05E-38	1,22E-35	AT5G19930 AT5G19940 AT5G19950	AT5G19920 AT5G19930 AT5G19940 AT5G19950
Chr1-3530286.5	718,645702	3,5985147	0,28115831	8,32E-38	1,60E-35	AT1G04813 AT1G10657	AT1G04813 AT1G10657 AT1G10660
Chr5-22038305	594,090954	3,78106019	0,29846923	4,44E-37	8,11E-35	AT5G54260 AT5G54270	AT5G54260 AT5G54270 AT5G54280
Chr1-10477613	632,207279	4,07630856	0,33407579	1,52E-34	2,66E-32	AT1G29930	AT1G29920 AT1G29930 AT1G29940
Chr2-8736699.5	490,237818	3,61972123	0,30071888	1,14E-33	1,90E-31	AT2G20250 AT2G20260	AT2G20250 AT2G20260 AT2G20270
Chr1-16851322	421,703564	3,80938568	0,32739505	1,36E-31	2,18E-29	AT1G44446	AT1G44414 AT1G44446 AT1G44478
Chr4-2673061	602,265691	3,68597858	0,32180058	1,12E-30	1,72E-28	AT4G05180	AT4G05180 AT4G05190
Chr4-493529	658,480066	3,6412469	0,32132658	4,56E-30	6,73E-28	AT4G01150	AT4G01140 AT4G01150 AT4G01160
Chr2-13007314	835,414879	3,22182484	0,285632	8,27E-30	1,18E-27	AT2G08395 AT2G08400	AT2G30520 AT2G08395 AT2G08400 AT2G30530
Chr5-26568578	506,076031	3,47225364	0,30793945	8,64E-30	1,19E-27	AT5G66564 AT5G66567 AT5G66568 AT5G66570	AT5G66558 AT5G66560 AT5G66562 AT5G66564 AT5G66567 AT5G66568 AT5G66570
Chr5-579290	459,815645	3,25792496	0,29979385	8,26E-28	1,09E-25	AT5G02580	AT5G02560 AT5G02570 AT5G02580
Chr2-14524078.5	578,815087	3,12587692	0,28975061	1,96E-27	2,51E-25	AT2G08665 AT2G34420 AT2G34430	AT2G34410 AT2G08665 AT2G34420 AT2G34430 AT2G34450 AT2G34440
Chr4-14204041.5	496,993318	3,36292155	0,31194044	2,12E-27	2,63E-25	AT4G28750 AT4G28755	AT4G28740 AT4G28750 AT4G28755
Chr2-16501629	439,177224	3,26886425	0,30478827	3,88E-27	4,66E-25	AT2G39540 AT2G39550	AT2G39530 AT2G39540 AT2G39550
Chr3-8381301	433,63109	3,28759826	0,31237178	3,33E-26	3,87E-24		AT3G23400 AT3G23410
Chr3-23301766.5	661,607602	3,03730266	0,28907096	4,01E-26	4,52E-24	AT3G63060 AT3G63070	AT3G63052 AT3G09885 AT3G63060 AT3G63070
Chr3-21242398.5	375,7608	3,22241626	0,30950238	1,10E-25	1,20E-23	AT3G08925 AT3G57410	AT3G57400 AT3G08915 AT3G08925 AT3G57410
Chr2-14849448	398,002668	3,21257648	0,31137489	2,94E-25	3,14E-23	AT2G35250 AT2G35260	AT2G35250 AT2G35260
Chr1-21092763.5	403,070738	3,32608114	0,32253416	3,10E-25	3,22E-23	AT1G56340 AT1G56345	AT1G56340 AT1G56345 AT1G56350
Chr4-14135369	375,750488	3,23311524	0,31620181	7,67E-25	7,75E-23	AT4G28610 AT4G28620	AT4G28600 AT4G28610 AT4G28620 AT4G28630
Chr1-10722416.5	750,980338	2,85954782	0,28032713	9,84E-25	9,69E-23	AT1G30380	AT1G30370 AT1G30380
Chr2-1824422	364,572406	3,63593831	0,36395058	8,41E-24	8,08E-22	AT2G05100	AT2G05100
Chr1-7140368.5	524,320548	3,14977162	0,32029362	4,02E-23	3,76E-21		AT1G20610 AT1G20620
Chr5-4634111.5	517,177939	2,74258464	0,27941881	4,84E-23	4,42E-21	AT5G14370	AT5G14360 AT5G14370 AT5G14380
Chr1-754289	388,254512	2,89819197	0,29929914	1,78E-22	1,59E-20	AT1G03130 AT1G03140	AT1G03110 AT1G03120 AT1G03130 AT1G03140 AT1G03150
Chr4-13908325.5	287,121021	3,19483847	0,33120496	2,55E-22	2,23E-20	AT4G27940 AT4G07925	AT4G27940 AT4G07925 AT4G27950
Chr2-19446724	328,892628	3,26191251	0,33923185	3,44E-22	2,93E-20	AT2G47390 AT2G47400	AT2G47390 AT2G09895 AT2G47400 AT2G47410
Chr3-20476601.5	394,959985	3,23193089	0,34138576	1,44E-21	1,20E-19	AT3G08455 AT3G08460 AT3G08465	AT3G55240 AT3G08455 AT3G08460 AT3G08465 AT3G55250
Chr4-2351860.5	261,232522	3,2382759	0,34243124	1,59E-21	1,30E-19	AT4G04640	AT4G04915 AT4G04640 AT4G04650
Chr4-5723447	377,292288	2,94084354	0,31288829	2,75E-21	2,20E-19	AT4G08920	AT4G08920
Chr5-309136.5	398,206726	2,82904951	0,30271672	4,57E-21	3,58E-19	AT5G01800 AT5G01810	AT5G01800 AT5G01810
Chr4-8883873.5	267,506709	3,30724974	0,35694453	9,71E-21	7,46E-19	AT4G15560	AT4G15560
Chr1-28750747	245,729714	3,3464456	0,36314381	1,55E-20	1,17E-18	AT1G76610	AT1G76600 AT1G76610
Chr4-11334308.5	346,47426	2,8152397	0,30596438	1,77E-20	1,31E-18	AT4G21270 AT4G21280	AT4G21270 AT4G21280 AT4G21300
Chr4-13725519.5	435,055305	2,79478152	0,30444817	2,16E-20	1,56E-18	AT4G27435 AT4G27440	AT4G27430 AT4G27435 AT4G27440 AT4G27450
Chr2-19473022	420,479216	2,81221466	0,30650188	2,25E-20	1,60E-18	AT2G47450	AT2G47440 AT2G47450
Chr5-7270482.5	234,767599	3,2635319	0,35717346	3,21E-20	2,24E-18	AT5G00440 AT5G03325 AT5G03335	AT5G00440 AT5G03325 AT5G03335 AT5G21990
Chr3-2441263.5	340,765347	2,80284898	0,30705722	3,49E-20	2,39E-18	AT3G07650	AT3G07640 AT3G07650
Chr2-1800587	390,03103	3,21602512	0,35326999	4,37E-20	2,94E-18	AT2G05070	AT2G05060 AT2G05070
Chr5-4392371	435,629441	2,85628879	0,31464799	5,54E-20	3,67E-18	AT5G13630 AT5G13640	AT5G13630 AT5G13640
Chr1-5447414	602,368854	2,58548736	0,28805949	1,41E-19	9,18E-18	AT1G15810 AT1G15820 AT1G05207 AT1G15830 AT	AT1G15810 AT1G05203 AT1G15820 AT1G05207 AT1G15830 AT1G15825
Chr5-5664235	282,230832	2,92882259	0,33103038	4,47E-19	2,86E-17		AT5G17230 AT5G17240
Chr1-21626255.5	421,154911	3,50815071	0,3969021	4,84E-19	3,04E-17	AT1G58290	AT1G58290 AT1G58300
Chr5-23786837.5	344,36647	2,84526035	0,32441202	8,89E-19	5,51E-17		AT5G58900 AT5G58910
Chr1-2952980	347,541182	3,04032769	0,34688724	9,37E-19	5,71E-17	AT1G09157 AT1G09160	AT1G09155 AT1G09157 AT1G09160
Chr5-1337036.5	295,264508	2,83880858	0,32822605	2,60E-18	1,56E-16	AT5G04670 AT5G04660	AT5G04670 AT5G04660
Chr1-25174963.5	245,672032	2,89139299	0,33828075	6,30E-18	3,72E-16	AT1G08917 AT1G08923 AT1G67265	AT1G08917 AT1G08923 AT1G67265
Chr5-2679239.5	345,999827	2,62540198	0,31583891	4,69E-17	2,73E-15	AT5G08320	AT5G08315 AT5G08320 AT5G08330 AT5G08335
Chr5-8372853	348,022819	2,49838311	0,30118232	5,42E-17	3,11E-15	AT5G24520	AT5G24510 AT5G24520
Chr3-2717593.5	401,370896	2,62900953	0,31763681	6,33E-17	3,57E-15	AT3G08930 AT3G08940	AT3G08930 AT3G08940 AT3G08943
Chr3-629891.5	401,31445	3,27339536	0,39610419	7,04E-17	3,92E-15	AT3G02870 AT3G01195	AT3G02860 AT3G02870 AT3G01195 AT3G02875
Chr5-23692349	407,237787	2,36851772	0,28804856	9,95E-17	5,46E-15	AT5G58610 AT5G58620	AT5G58610 AT5G58620 AT5G08870
Chr4-5779468.5	291,18108	2,82113809	0,34513467	1,49E-16	8,07E-15	AT4G09010 AT4G05690 AT4G09012	AT4G09000 AT4G05685 AT4G09010 AT4G05690 AT4G09012
Chr2-13020189.5	337,089763	2,45500664	0,30252337	2,43E-16	1,29E-14	AT2G30570 AT2G30575	AT2G30550 AT2G30560 AT2G30570 AT2G30575
Chr1-3019459.5	326,762468	2,76642957	0,34180503	2,90E-16	1,52E-14	AT1G09340 AT1G09350	AT1G09340 AT1G09350 AT1G09360
Chr1-26621856.5	253,497217	2,68946998	0,33892342	1,05E-15	5,45E-14	AT1G70600 AT1G70610	AT1G70590 AT1G70600 AT1G70610
Chr3-19807381.5	257,57505	2,66117989	0,33685209	1,39E-15	7,13E-14		AT3G53420 AT3G53430
Chr2-6523848.5	186,469398	3,09792973	0,39290931	1,58E-15	7,97E-14	AT2G00600	AT2G15050 AT2G00600
Chr4-10414577	264,942887	2,64418291	0,33980801	3,59E-15	1,79E-13	AT4G19010 AT4G19020	AT4G19010 AT4G19020
Chr1-19052672	279,477021	2,56673899	0,33560419	1,02E-14	5,02E-13	AT1G51390 AT1G07733 AT1G51400 AT1G07737 AT	AT1G51380 AT1G51390 AT1G07733 AT1G51400 AT1G07737 AT1G51402 AT1G07743
Chr4-6408085	365,523408	2,7429888	0,36179287	1,71E-14	8,29E-13	AT4G10330 AT4G10340	AT4G10330 AT4G10340
Chr5-19648336	340,125873	2,95536549	0,39214295	2,41E-14	1,16E-12	AT5G48480	AT5G48480 AT5G48485 AT5G48490
Chr1-22422153	168,574981	2,95402121	0,4018479	9,83E-14	4,66E-12		AT1G60900
Chr5-25071345.5	291,058912	2,45895647	0,3355498	1,17E-13	5,46E-12	AT5G62430 AT5G62440	AT5G62430 AT5G62440

Postion	baseMean	log2(FC)	lfcSE	p-value	p-adj	gene 1 kb upstream to 1 kb downstream	gene 3 kb upstream to 3 kb downstream
Chr1-29429351.5	232,838336	2,51691092	0,34398791	1,27E-13	5,87E-12	AT1G09793 AT1G09797 AT1G78230	AT1G78220 AT1G09793 AT1G09797 AT1G78230
Chr5-25192020	282,495617	2,4527708	0,33572427	1,38E-13	6,29E-12	AT5G62720	AT5G62710 AT5G62720
Chr1-29359559	307,341144	2,21017088	0,30267142	1,42E-13	6,39E-12	AT1G78070	AT1G78070 AT1G09965
Chr5-14913749	352,57226	2,22165993	0,30589478	1,90E-13	8,46E-12	AT5G37540	AT5G37540
Chr5-3163830.5	288,881667	2,47731774	0,34126855	1,95E-13	8,60E-12	AT5G01655	AT5G10100 AT5G01655 AT5G10110
Chr5-3000587	332,730129	2,39264584	0,32992232	2,05E-13	8,95E-12	AT5G09680 AT5G09690	AT5G09670 AT5G09680 AT5G09690
Chr4-13194596	287,680476	2,23049248	0,30787873	2,17E-13	9,35E-12	AT4G25990	AT4G25990 AT4G26000
Chr1-24097897.5	251,440879	2,36996217	0,32746775	2,29E-13	9,76E-12	AT1G64850 AT1G64860	AT1G64840 AT1G64850 AT1G64860
Chr3-15092591	273,274712	2,49088199	0,34423885	2,31E-13	9,76E-12	AT3G43110	AT3G43110 AT3G43120
Chr1-2641910.5	252,629369	2,50415883	0,34863687	3,42E-13	1,43E-11	AT1G08380 AT1G08390	AT1G08370 AT1G08380 AT1G08390 AT1G08400
Chr3-17551253.5	380,700712	2,1003592	0,29402767	4,55E-13	1,88E-11	AT3G47610	AT3G47610
Chr5-23165996	237,324756	2,58409966	0,36355015	5,89E-13	2,41E-11		AT5G57170 AT5G57180
Chr1-18176415.5	247,027667	2,43361732	0,34479602	8,44E-13	3,41E-11	AT1G49130 AT1G49140	AT1G49120 AT1G49130 AT1G49140 AT1G49150 AT1G49160
Chr4-455753.5	258,879762	2,26164933	0,32157174	1,01E-12	4,04E-11	AT4G01040 AT4G01050	AT4G01037 AT4G01040 AT4G01050
Chr1-6445314	192,412376	2,59927465	0,3698751	1,05E-12	4,16E-11		AT1G18700
Chr3-7377267.5	229,493095	2,31297184	0,32940376	1,10E-12	4,29E-11	AT3G21055 AT3G21060	AT3G21055 AT3G21060 AT3G21070
Chr3-5358786	232,266918	2,29892257	0,327738	1,15E-12	4,48E-11	AT3G15840 AT3G15850	AT3G15830 AT3G15840 AT3G15850 AT3G15860
Chr2-19643996.5	308,541278	2,19027011	0,31531946	1,88E-12	7,21E-11	AT2G48010 AT2G48020	AT2G48000 AT2G48010 AT2G48020
Chr1-22700027.5	249,920188	2,2889345	0,32992443	1,99E-12	7,57E-11	AT1G61520	AT1G61520 AT1G61540
Chr5-426313	248,709806	2,3531707	0,34112132	2,63E-12	9,90E-11	AT5G02150 AT5G02160	AT5G02140 AT5G00815 AT5G02150 AT5G00820 AT5G02160 AT5G02170
Chr4-12876944	236,09355	2,24446301	0,32816187	3,97E-12	1,48E-10	AT4G25070 AT4G25080	AT4G25070 AT4G25080 AT4G25090
Chr5-21763594	188,356799	2,45798329	0,36061529	4,68E-12	1,73E-10	AT5G53570	AT5G53570 AT5G53580
Chr3-20772072	293,637642	2,86793519	0,4253847	7,81E-12	2,86E-10		AT3G55970
Chr1-5018113.5	214,507682	2,28318798	0,3402062	9,65E-12	3,50E-10		AT1G14620 AT1G14630
Chr3-18819454	204,250679	2,33677691	0,34843768	9,97E-12	3,58E-10		AT3G50660
Chr3-17758246.5	237,454194	2,26298626	0,33753391	1,01E-11	3,59E-10	AT3G48090 AT3G48100	AT3G48090 AT3G48100
Chr3-9045332.5	203,923784	2,28885327	0,34244036	1,16E-11	4,10E-10	AT3G24770	AT3G24770 AT3G00440
Chr2-19227539	210,680848	2,58421856	0,38744326	1,28E-11	4,42E-10		AT2G46780
Chr1-3951164	215,320427	2,3334748	0,3498783	1,28E-11	4,42E-10	AT1G11710 AT1G11720 AT1G04873	AT1G11710 AT1G11720 AT1G04873
Chr4-13279675.5	257,504273	2,26013832	0,33890761	1,29E-11	4,42E-10		AT4G26200 AT4G26210
Chr2-7934727.5	208,852675	2,31888642	0,35012551	1,76E-11	5,98E-10	AT2G18230 AT2G18240	AT2G18220 AT2G18230 AT2G18240 AT2G18245
Chr4-18233421.5	179,778927	2,43129872	0,36957379	2,37E-11	8,00E-10	AT4G39150	AT4G39140 AT4G39150 AT4G39160
Chr3-22745644	243,948469	2,3126954	0,35388158	3,18E-11	1,06E-09	AT3G61470	AT3G61460 AT3G61470
Chr3-21831371	414,344428	1,90079268	0,29250277	4,06E-11	1,34E-09	AT3G59060 AT3G09185 AT3G59068 AT3G59070	AT3G59060 AT3G09185 AT3G59068 AT3G59070
Chr5-208869	337,514266	2,43836244	0,37925706	6,41E-11	2,10E-09	AT5G01520 AT5G01530	AT5G01520 AT5G01530 AT5G01540 AT5G01542
Chr4-1176213.5	203,221963	2,21384926	0,34484604	6,82E-11	2,22E-09	AT4G02670	AT4G02660 AT4G02670 AT4G04235
Chr3-17228690	183,521248	2,35502311	0,36764345	7,48E-11	2,41E-09	AT3G46780	AT3G46780 AT3G46790
Chr3-21949644.5	265,419256	2,07720927	0,32584128	9,15E-11	2,92E-09	AT3G59400 AT3G59410	AT3G59390 AT3G59400 AT3G59410
Chr3-21076386.5	240,968889	2,07607209	0,32570551	9,20E-11	2,92E-09	AT3G56930 AT3G56940 AT3G08795	AT3G56930 AT3G56940 AT3G08795 AT3G56950 AT3G08805
Chr3-4462010.5	196,310512	2,21242221	0,34915911	1,18E-10	3,70E-09	AT3G13640 AT3G13650	AT3G13640 AT3G13650 AT3G13660
Chr1-20814667.5	249,116056	2,20050251	0,34948685	1,52E-10	4,76E-09		AT1G55690
Chr2-12666964.5	207,075061	2,83248926	0,45106162	1,70E-10	5,26E-09	AT2G29620 AT2G29628 AT2G29630	AT2G29620 AT2G29628 AT2G29630
Chr3-20340740.5	404,945354	2,17805329	0,34750312	1,83E-10	5,63E-09	AT3G54880 AT3G54890 AT3G54900	AT3G54880 AT3G54890 AT3G54900 AT3G54910
Chr4-297330.5	196,60045	2,15334717	0,34386802	1,90E-10	5,79E-09	AT4G00720	AT4G00720 AT4G00730
Chr1-25047903.5	228,475179	2,18623661	0,34941685	1,96E-10	5,94E-09	AT1G67080 AT1G67090	AT1G67080 AT1G67090
Chr2-14593861.5	201,257046	2,15410187	0,34540928	2,24E-10	6,72E-09		AT2G34650 AT2G34655
Chr3-4541862.5	193,580899	2,21964699	0,35612934	2,29E-10	6,82E-09	AT3G13800	AT3G13800 AT3G13810
Chr3-3684763	209,259599	2,15080087	0,34654729	2,71E-10	7,97E-09	AT3G11670	AT3G11670 AT3G11680
Chr3-1817795	201,749035	2,18965825	0,35283067	2,72E-10	7,97E-09	AT3G06030	AT3G06030
Chr1-11216013.5	252,1341	2,10475821	0,34041141	3,15E-10	9,15E-09	AT1G31330 AT1G31335	AT1G31320 AT1G31330 AT1G31335 AT1G31340
Chr3-9700699	175,584516	2,31207654	0,37463973	3,38E-10	9,77E-09		AT3G26490
Chr2-7125935	183,28369	2,21285904	0,36117447	4,48E-10	1,28E-08	AT2G06635 AT2G16440	AT2G16430 AT2G06625 AT2G06635 AT2G16440
Chr5-2758765	165,503153	2,20774744	0,36384261	6,48E-10	1,84E-08	AT5G08520 AT5G08530	AT5G08520 AT5G08530
Chr3-20167516	173,053858	2,25421087	0,37217624	6,94E-10	1,96E-08	AT3G54460 AT3G54470	AT3G54460 AT3G54470
Chr1-19454671	155,148945	2,30979745	0,38235919	7,66E-10	2,15E-08	AT1G52220 AT1G52230 AT1G52240	AT1G52220 AT1G52230 AT1G52240
Chr3-22078296	177,052333	2,15148796	0,35840178	9,68E-10	2,68E-08	AT3G59765 AT3G59770	AT3G59760 AT3G59765 AT3G59770
Chr3-22962508.5	240,499839	1,93504918	0,32236122	9,70E-10	2,68E-08		AT3G62000 AT3G62010
Chr1-26477793	224,169833	2,30387814	0,38571796	1,16E-09	3,18E-08	AT1G70300	AT1G70290 AT1G70300
Chr3-5433969	165,68428	2,15464141	0,36074486	1,17E-09	3,18E-08	AT3G16000 AT3G16010	AT3G16000 AT3G16010
Chr1-10476025.5	111,477865	2,5550036	0,4302906	1,44E-09	3,90E-08	AT1G29920	AT1G29910 AT1G29920 AT1G29930 AT1G29940
Chr1-28892328.5	217,742577	2,61569641	0,44107627	1,51E-09	4,06E-08	AT1G76920	AT1G09915 AT1G09687 AT1G09693 AT1G76920 AT1G76930
Chr2-9914300.5	152,414304	2,21205869	0,37357352	1,60E-09	4,23E-08	AT2G23300	AT2G23300
Chr1-1236308	216,565027	1,94101764	0,32780634	1,60E-09	4,23E-08	AT1G04530 AT1G04540	AT1G04520 AT1G04530 AT1G04540
Chr5-7738511	206,451549	1,98140201	0,33517232	1,69E-09	4,46E-08	AT5G23060 AT5G00450	AT5G23050 AT5G23060 AT5G00450 AT5G23065
Chr4-9906031.5	156,969071	2,20278526	0,37285636	1,73E-09	4,53E-08	AT4G17810	AT4G17810
Chr1-28643800.5	179,501993	2,15732223	0,36631256	1,94E-09	5,03E-08	AT1G76350 AT1G76360	AT1G76350 AT1G76360 AT1G09623
Chr1-2300371.5	228,870033	2,07192913	0,35322166	2,23E-09	5,76E-08	AT1G07480	AT1G07480 AT1G04587 AT1G07485 AT1G07490
Chr3-2712484.5	351,785917	1,950822	0,33352857	2,47E-09	6,33E-08	AT3G08910 AT3G08920 AT3G08930	AT3G08900 AT3G02085 AT3G08910 AT3G08920 AT3G08930
Chr1-692651.5	138,844933	2,3240226	0,39777054	2,57E-09	6,53E-08	AT1G03000 AT1G03010	AT1G03000 AT1G03010
Chr3-21036229.5	142,201011	2,27319225	0,39369069	3,87E-09	9,78E-08	AT3G56800 AT3G56810	AT3G56780 AT3G56790 AT3G56800 AT3G56810
Chr4-17312455.5	213,197721	2,35878527	0,40904148	4,04E-09	1,01E-07	AT4G36730 AT4G09375	AT4G36720 AT4G36730 AT4G09375 AT4G36740
Chr1-4708485.5	145,647965	2,31773229	0,40305547	4,45E-09	1,11E-07		AT1G13720 AT1G13730
Chr1-23553336	135,108681	2,38799715	0,41861133	5,83E-09	1,44E-07	AT1G63490	AT1G63490 AT1G63500
Chr5-16203585.5	202,299882	1,91305395	0,33602829	6,24E-09	1,54E-07	AT5G40460	AT5G06065 AT5G40460 AT5G06075
Chr5-24642010.5	204,346636	2,01970354	0,35571228	6,82E-09	1,67E-07		AT5G61270 AT5G61280
Chr5-21337252.5	222,891974	2,04366248	0,3602376	7,01E-09	1,70E-07	AT5G52570 AT5G52580	AT5G52560 AT5G52570 AT5G52580
Chr2-18961155	164,576971	2,09117671	0,3686667	7,05E-09	1,70E-07	AT2G46140 AT2G46150	AT2G46140 AT2G46150 AT2G46160
Chr5-22650042.5	165,43068	2,06628112	0,36434463	7,09E-09	1,70E-07	AT5G55920	AT5G55920 AT5G55930
Chr2-15066267	200,588248	1,87991742	0,33342705	8,59E-09	2,05E-07	AT2G35880 AT2G08775 AT2G35890	AT2G35880 AT2G08775 AT2G35890
Chr3-5620703	233,412145	1,80738702	0,32099889	8,98E-09	2,13E-07	AT3G16520	AT3G16510 AT3G16520 AT3G16525
Chr3-1175324	134,247524	2,28859627	0,40712351	9,47E-09	2,23E-07	AT3G04420 AT3G04430	AT3G04420 AT3G04430
Chr3-8686006.5	313,702518	1,78329437	0,31743804	9,67E-09	2,26E-07	AT3G24050	AT3G24040 AT3G24050
Chr1-28549872	307,567709	2,17098923	0,39001132	1,30E-08	3,02E-07	AT1G76080 AT1G76090	AT1G76070 AT1G76080 AT1G76090
Chr3-3879005.5	236,558228	1,81696537	0,32665475	1,33E-08	3,07E-07	AT3G12150 AT3G12160	AT3G12145 AT3G12150 AT3G12160 AT3G12170
Chr1-10473476.5	123,278421	2,41439919	0,43408587	1,33E-08	3,07E-07	AT1G29910	AT1G29900 AT1G29910 AT1G29920
Chr1-11463920	208,250081	1,94497639	0,3520082	1,64E-08	3,76E-07	AT1G31910 AT1G31920	AT1G31910 AT1G31920 AT1G31930
Chr5-23167782	153,965159	2,16390314	0,39417035	2,01E-08	4,57E-07	AT5G57180	AT5G57180
Chr1-24048625	125,184196	2,33370531	0,42535811	2,05E-08	4,63E-07	AT1G64720	AT1G64710 AT1G64720 AT1G64740
Chr4-13022572.5	526,693456	1,65170461	0,30125837	2,09E-08	4,70E-07	AT4G25490	AT4G07395 AT4G03125 AT4G25490 AT4G25500
Chr1-1624782.5	123,804927	2,18520139	0,39998702	2,34E-08	5,22E-07	AT1G05500	AT1G05490 AT1G05500
Chr3-16038314	121,731982	2,19114223	0,40128003	2,38E-08	5,27E-07	AT3G06795	AT3G44380 AT3G06795
Chr1-8542014.5	169,070141	1,91207179	0,35186944	2,75E-08	6,08E-07	AT1G24145 AT1G24147	AT1G05857 AT1G24145 AT1G24147 AT1G24148

Postion	baseMean	log2(FC)	lfcSE	p-value	p-adj	gene 1 kb upstream to 1 kb downstream	gene 3 kb upstream to 3 kb downstream
Chr4-13827912	187,010817	2,19978086	0,40539694	2,88E-08	6,31E-07	AT4G27700 AT4G27710	AT4G27690 AT4G27700 AT4G27710 AT4G27720
Chr5-22597714.5	199,386945	1,91719808	0,35587402	3,58E-08	7,80E-07	AT5G55830 AT5G55835 AT5G55840	AT5G55830 AT5G55835 AT5G55840
Chr1-4771564.5	144,591869	2,04192923	0,38253918	4,70E-08	1,02E-06		AT1G05037 AT1G13950
Chr5-15421278	204,896547	1,96199514	0,36839556	5,03E-08	1,08E-06	AT5G38510 AT5G38520	AT5G38510 AT5G38520 AT5G38530
Chr2-18107214	106,29394	2,3653855	0,44503427	5,33E-08	1,14E-06	AT2G43680	AT2G43660 AT2G43670 AT2G43680
Chr3-20474906	145,324515	2,00894918	0,37808064	5,38E-08	1,15E-06	AT3G55240	AT3G55230 AT3G55240 AT3G08455 AT3G08460 AT3G08465
Chr2-878063	140,811246	2,05318998	0,38727806	5,74E-08	1,22E-06	AT2G03000	AT2G03000 AT2G03010
Chr1-9329042	255,209846	1,88769563	0,35651347	5,95E-08	1,26E-06	AT1G26920	AT1G26920 AT1G26921
Chr3-5020480.5	230,091509	1,99652208	0,3787088	6,75E-08	1,42E-06	AT3G14920 AT3G14930	AT3G14910 AT3G14920 AT3G14930
Chr4-17735222.5	251,096746	1,68260542	0,3200033	7,28E-08	1,52E-06		AT4G09655
Chr2-19232287	198,813895	1,74675257	0,33240669	7,41E-08	1,54E-06	AT2G46780 AT2G46790	AT2G46780 AT2G46790
Chr1-7570798	178,411832	1,80730837	0,34431028	7,64E-08	1,58E-06	AT1G21590 AT1G21600	AT1G21590 AT1G21600
Chr4-16647344	184,558987	1,99004651	0,38018191	8,27E-08	1,70E-06		AT4G34950 AT4G34960
Chr1-7932484.5	147,442485	1,99396469	0,38359882	1,01E-07	2,06E-06	AT1G05747 AT1G22470	AT1G22460 AT1G05747 AT1G22470 AT1G22480
Chr3-19791826.5	215,312794	1,71825805	0,33085094	1,03E-07	2,10E-06	AT3G53380 AT3G53390	AT3G53370 AT3G53380 AT3G53390
Chr2-383548.5	207,973093	2,26459549	0,43671614	1,08E-07	2,18E-06		AT2G01850
Chr1-30267367	141,821356	1,93503644	0,37397832	1,14E-07	2,30E-06	AT1G80490	AT1G80490
Chr3-3758337.5	154,423541	2,04820719	0,39778132	1,31E-07	2,62E-06	AT3G11890 AT3G11900	AT3G11890 AT3G11900 AT3G11910
Chr1-7043399	239,684198	1,61829817	0,31508587	1,40E-07	2,79E-06	AT1G20340 AT1G20350	AT1G20340 AT1G20350 AT1G05537
Chr5-23981880.5	206,94217	1,8108018	0,35298843	1,45E-07	2,87E-06	AT5G59470 AT5G59480	AT5G59470 AT5G59480 AT5G59490
Chr1-4994561	155,027491	2,21593481	0,43627517	1,90E-07	3,73E-06	AT1G05097	AT1G14580 AT1G05097 AT1G05103 AT1G05107
Chr1-26811996.5	180,977962	1,7635617	0,34734546	1,91E-07	3,75E-06	AT1G71080 AT1G71090	AT1G71070 AT1G71080 AT1G71090 AT1G71100
Chr2-7821547	160,420536	1,83093721	0,3619638	2,11E-07	4,12E-06	AT2G17970 AT2G17972 AT2G07015 AT2G17975	AT2G17970 AT2G17972 AT2G07015 AT2G17975 AT2G17980
Chr1-5885072	155,929884	1,86332486	0,36886341	2,19E-07	4,23E-06	AT1G17210 AT1G17220	AT1G17210 AT1G17220
Chr3-10289458	168,847274	2,09525361	0,41479366	2,19E-07	4,23E-06	AT3G27785	AT3G27770 AT3G27785
Chr1-21167323.5	117,82445	2,17073361	0,42982834	2,21E-07	4,24E-06	AT1G56500 AT1G56510	AT1G56500 AT1G56510
Chr1-25395007	180,745267	1,95663777	0,38908537	2,47E-07	4,71E-06	AT1G67740	AT1G67730 AT1G67740
Chr5-3771790	215,144009	1,67284146	0,33339778	2,62E-07	4,97E-06	AT5G11700 AT5G11710	AT5G11700 AT5G11710
Chr3-23153679	189,888688	1,84960787	0,36927525	2,74E-07	5,18E-06	AT3G62600 AT3G62610	AT3G62600 AT3G62610 AT3G62615
Chr3-20872534	137,050267	1,88835622	0,3777346	2,88E-07	5,42E-06	AT3G56270	AT3G56270
Chr1-29313671.5	387,19942	3,42820314	0,68758856	3,08E-07	5,78E-06	AT1G77960	AT1G77950 AT1G77960 AT1G77980
Chr5-23966211.5	248,326975	1,66312082	0,33533064	3,53E-07	6,58E-06		AT5G59420 AT5G59430
Chr4-6100669	142,037094	1,8866928	0,38134813	3,76E-07	6,98E-06	AT4G09649 AT4G09650	AT4G09647 AT4G09649 AT4G09650
Chr1-30419585.5	152,275721	1,96066879	0,39717972	3,98E-07	7,34E-06	AT1G80960 AT1G09997 AT1G80970	AT1G80960 AT1G09997 AT1G80970 AT1G80980
Chr2-8059275.5	176,026991	1,7642152	0,35886304	4,41E-07	8,11E-06	AT2G18560	AT2G18560
Chr1-7038187.5	224,669171	1,62828316	0,33161989	4,55E-07	8,32E-06	AT1G20330	AT1G20330
Chr1-27302337.5	113,890572	2,00274858	0,40807045	4,60E-07	8,38E-06	AT1G72510	AT1G72510
Chr2-6018383	172,897805	1,90619311	0,38911294	4,82E-07	8,73E-06	AT2G14210	AT2G14210
Chr2-14577090	185,189026	1,92498735	0,3934445	4,97E-07	8,94E-06	AT2G34610 AT2G34620	AT2G34610 AT2G34620 AT2G34630
Chr5-4156624	205,184883	1,74067142	0,35580218	4,98E-07	8,94E-06	AT5G13100	AT5G13090 AT5G13100 AT5G13110
Chr5-1578925.5	225,008929	1,73442352	0,35480994	5,09E-07	9,08E-06	AT5G05330 AT5G05340	AT5G05320 AT5G05330 AT5G05340
Chr3-20477921	174,899046	1,7009229	0,34840748	5,25E-07	9,34E-06	AT3G08455 AT3G08460 AT3G08465	AT3G55240 AT3G08455 AT3G08460 AT3G08465 AT3G55250 AT3G55252
Chr4-18580356.5	112,636881	1,98762466	0,40746152	5,36E-07	9,48E-06	AT4G40085 AT4G40080 AT4G40090	AT4G40070 AT4G40085 AT4G40080 AT4G40090 AT4G09995 AT4G40100
Chr1-907630.5	169,27582	1,81934741	0,37321205	5,44E-07	9,59E-06	AT1G03620 AT1G03630	AT1G03620 AT1G03630 AT1G03640 AT1G03650
Chr5-24482466	162,994275	2,06353376	0,42349521	5,51E-07	9,65E-06	AT5G60850 AT5G08975	AT5G60850 AT5G08975 AT5G60860 AT5G08980
Chr4-17996551.5	175,876032	1,67491379	0,34493214	6,00E-07	1,05E-05	AT4G38460	AT4G38440 AT4G38460 AT4G09705 AT4G38470
Chr5-5678801.5	247,501227	1,59107266	0,32936787	6,80E-07	1,18E-05	AT5G17260 AT5G02685	AT5G17260 AT5G02685 AT5G17270
Chr1-6352268.5	164,088473	1,68924997	0,3511812	7,54E-07	1,30E-05	AT1G18450 AT1G18460	AT1G18450 AT1G18460
Chr3-22906511	164,003743	1,75035845	0,3639211	7,56E-07	1,30E-05	AT3G61880	AT3G61870 AT3G61880
Chr4-16195644.5	123,928263	2,19206059	0,45651167	7,86E-07	1,35E-05	AT4G33770	AT4G33760 AT4G33770
Chr5-19563948.5	170,36043	1,96069499	0,40840952	7,90E-07	1,35E-05	AT5G48250 AT5G48270	AT5G48240 AT5G48250 AT5G48270
Chr2-19154056.5	201,034005	1,63843027	0,34350993	9,23E-07	1,57E-05	AT2G46660	AT2G46640 AT2G46650 AT2G46660
Chr3-4035593.5	138,15622	1,84429319	0,38720125	9,53E-07	1,61E-05		AT3G12690 AT3G12700
Chr2-18007523.5	126,709879	1,97661193	0,41579616	9,98E-07	1,68E-05	AT2G43340 AT2G43350	AT2G09445 AT2G09450 AT2G43340 AT2G43350 AT2G09455
Chr1-12239468	95,8323806	2,05572743	0,43401647	1,09E-06	1,82E-05	AT1G33760	AT1G33750 AT1G33760 AT1G33770
Chr2-12233091.5	109,215776	1,93844591	0,40935322	1,09E-06	1,83E-05		AT2G28560
Chr5-24887208.5	107,511669	2,07960592	0,44041658	1,17E-06	1,94E-05		AT5G61960 AT5G61970
Chr1-4458778	250,37033	1,88911264	0,40043504	1,19E-06	1,97E-05	AT1G13080	AT1G04987 AT1G13080 AT1G13090
Chr1-19432928.5	121,374509	1,98048017	0,42132973	1,30E-06	2,14E-05		AT1G52185 AT1G07793 AT1G52190
Chr4-13911246.5	205,613188	1,59449139	0,34181667	1,54E-06	2,53E-05	AT4G27950	AT4G07925 AT4G27950 AT4G07955
Chr2-8880515	87,8456146	2,2121003	0,47429506	1,55E-06	2,53E-05	AT2G20610	AT2G20610
Chr3-4723918.5	153,357511	1,80017867	0,38708318	1,65E-06	2,69E-05	AT3G02895	AT3G14205 AT3G02895
Chr3-5123667.5	613,304354	1,40956349	0,30421113	1,80E-06	2,91E-05	AT3G00330	AT3G15210 AT3G00330 AT3G03035 AT3G03045 AT3G15220
Chr4-7192105.5	84,594542	2,35187857	0,51293608	2,27E-06	3,66E-05	AT4G12000	AT4G11990 AT4G12000
Chr5-22115827.5	183,365079	1,62806228	0,35553957	2,33E-06	3,75E-05	AT5G54470	AT5G54470 AT5G54480
Chr3-20556713	214,433242	1,47763491	0,32275265	2,34E-06	3,75E-05	AT3G55440 AT3G55450	AT3G55440 AT3G55450
Chr2-18790412	160,520522	1,61670888	0,35352229	2,40E-06	3,83E-05	AT2G45600 AT2G45610	AT2G45590 AT2G45600 AT2G45610 AT2G45620
Chr2-15043612	164,574551	1,78758211	0,39118758	2,44E-06	3,88E-05	AT2G35795 AT2G35800	AT2G35790 AT2G35795 AT2G35800
Chr3-11798805	110,308378	1,9081091	0,41819582	2,52E-06	3,99E-05	AT3G30165	AT3G30165
Chr4-446974	150,930645	1,65065571	0,36201076	2,56E-06	4,03E-05	AT4G01023 AT4G01026 AT4G03845 AT4G01030	AT4G01020 AT4G01023 AT4G01026 AT4G03845 AT4G01030
Chr1-26695279	282,602217	1,42107014	0,31339826	2,89E-06	4,53E-05	AT1G70780	AT1G70780 AT1G09197
Chr4-10255749.5	123,727964	1,98253074	0,43757537	2,94E-06	4,59E-05	AT4G18620	AT4G18610 AT4G18620 AT4G18630
Chr1-1531339	130,593942	1,8999304	0,42021779	3,07E-06	4,76E-05	AT1G05260 AT1G05270	AT1G05260 AT1G05270
Chr1-8060832	134,748307	1,734338	0,38364409	3,08E-06	4,76E-05	AT1G22770	AT1G22760 AT1G22770
Chr2-15520180	140,470378	1,72370738	0,38132238	3,09E-06	4,76E-05		AT2G08845 AT2G36960
Chr1-1830064	97,1381371	1,92922453	0,42758808	3,21E-06	4,93E-05	AT1G06040 AT1G06045 AT1G06050	AT1G06030 AT1G06040 AT1G06045 AT1G06050 AT1G06060
Chr3-6182490.5	254,98048	1,38365212	0,30752665	3,41E-06	5,22E-05	AT3G18050	AT3G18050 AT3G18060
Chr1-24127077.5	108,761822	1,96144773	0,43604886	3,43E-06	5,22E-05	AT1G64950	AT1G64940 AT1G64950 AT1G64960
Chr3-10524098.5	105,728833	1,87430237	0,41729336	3,54E-06	5,37E-05	AT3G28216 AT3G28220	AT3G28210 AT3G28216 AT3G28220
Chr5-14123427.5	151,485662	1,650776	0,36763741	3,56E-06	5,38E-05	AT5G35970	AT5G35970
Chr3-607816	142,836708	1,89469341	0,42263994	3,68E-06	5,54E-05	AT3G02800 AT3G02810	AT3G02780 AT3G02790 AT3G02800 AT3G02810
Chr4-13675207.5	291,987224	1,3632445	0,3048914	3,89E-06	5,83E-05	AT4G27310	AT4G27300 AT4G27310
Chr3-22170089	168,140707	1,80324676	0,40376655	3,98E-06	5,93E-05	AT3G60030 AT3G09315	AT3G60030 AT3G09315
Chr1-8996142.5	97,0829799	1,93191513	0,43258552	3,99E-06	5,93E-05	AT1G25570 AT1G25580	AT1G25570 AT1G25580
Chr4-1440072.5	131,517581	1,78711251	0,40064999	4,09E-06	6,06E-05	AT4G03280 AT4G03285	AT4G03280 AT4G03285 AT4G03290
Chr3-16412811	97,0253523	1,97904748	0,44629254	4,62E-06	6,82E-05	AT3G44940	AT3G44940
Chr5-20728195	134,543429	1,66591736	0,37579846	4,65E-06	6,84E-05		AT5G50940 AT5G50950
Chr3-22376047	178,725869	1,74288446	0,39355498	4,74E-06	6,95E-05	AT3G60540	AT3G60530 AT3G60540 AT3G09465
Chr1-8598692	124,880567	1,72991842	0,39112652	4,87E-06	7,11E-05	AT1G05863	AT1G24260 AT1G05863 AT1G24265
Chr1-19825500	148,970998	1,62102361	0,36680581	4,95E-06	7,20E-05		
Chr2-17582818	155,259544	2,15806847	0,48845218	4,98E-06	7,21E-05	AT2G42180 AT2G42190	AT2G42170 AT2G42180 AT2G42190
Chr5-24461117.5	163,565942	1,58901424	0,36047481	5,21E-06	7,53E-05	AT5G60800	AT5G60800 AT5G00690

Postion	baseMean	log2(FC)	lfcSE	p-value	p-adj	gene 1 kb upstream to 1 kb downstream	gene 3 kb upstream to 3 kb downstream
Chr1-26241709.5	154,696169	1,79578006	0,40807899	5,40E-06	7,76E-05	AT1G69760	AT1G69760
Chr1-11204881	100,040988	2,22722886	0,50649439	5,48E-06	7,85E-05		
Chr3-5763405.5	168,18748	1,57409927	0,35832028	5,59E-06	7,98E-05	AT3G16870	AT3G16860 AT3G03385 AT3G16870
Chr5-1279938.5	176,139329	1,58606631	0,36126014	5,66E-06	8,05E-05	AT5G04490	AT5G04480 AT5G04490
Chr4-7589888	134,477132	1,92183721	0,4395153	6,14E-06	8,70E-05	AT4G12980	AT4G12970 AT4G12980 AT4G05995
Chr2-14426272	127,8422	1,70443382	0,39191524	6,84E-06	9,65E-05	AT2G34160	AT2G34150 AT2G34160 AT2G34170
Chr1-20976239.5	103,91568	1,81126468	0,4167417	6,92E-06	9,74E-05	AT1G56080 AT1G56085	AT1G56080 AT1G56085 AT1G56090
Chr3-17760894	124,987606	1,85212498	0,42657733	7,07E-06	9,90E-05	AT3G48100 AT3G07865	AT3G48090 AT3G48100 AT3G07865 AT3G48110
Chr4-1292644	139,988638	1,75815031	0,40708165	7,84E-06	0,00010947	AT4G02920	AT4G02920 AT4G02930
Chr5-370381	121,922124	1,66973591	0,38728374	8,11E-06	0,00011285	AT5G01950 AT5G01960	AT5G01950 AT5G01960 AT5G01970
Chr1-27627870	187,484079	1,55405052	0,36231734	8,97E-06	0,00012429	AT1G73470 AT1G73480	AT1G73460 AT1G73470 AT1G73480
Chr1-23516796	135,043722	1,79799004	0,41931921	9,02E-06	0,00012458	AT1G63420	AT1G08613 AT1G63420
Chr1-7732541	110,420156	1,76663907	0,41464378	1,02E-05	0,00013982		AT1G21970 AT1G21980
Chr3-17560937.5	157,002161	1,55426953	0,36480314	1,02E-05	0,00013982	AT3G47620	AT3G47620 AT3G47630
Chr5-25629552.5	194,046123	1,48820474	0,3494097	1,03E-05	0,00014018	AT5G64030 AT5G64040 AT5G64050	AT5G64030 AT5G64040 AT5G64050
Chr4-10321850.5	184,320211	1,4661444	0,34546475	1,10E-05	0,00014951	AT4G18800 AT4G18810	AT4G18790 AT4G18800 AT4G18810
Chr4-17986348	163,326006	1,50539028	0,35520097	1,13E-05	0,00015291	AT4G38420 AT4G38430	AT4G38420 AT4G38430 AT4G38440
Chr5-5363238	132,203587	1,7149018	0,40579133	1,19E-05	0,00016077	AT5G16390 AT5G16400	AT5G16380 AT5G16390 AT5G16400 AT5G16410
Chr2-17057369.5	154,149423	1,49931422	0,3558683	1,26E-05	0,00016884	AT2G40860 AT2G40880 AT2G40890	AT2G40860 AT2G40880 AT2G40890 AT2G09205
Chr5-21571860	102,501701	1,87634098	0,44537078	1,26E-05	0,00016884	AT5G53180 AT5G53190	AT5G53180 AT5G53190
Chr2-14331382	115,948036	1,95340922	0,46369924	1,26E-05	0,00016884		AT2G33860
Chr1-24959316	156,683204	1,60962801	0,38584566	1,51E-05	0,00020157	AT1G66900	AT1G66890 AT1G66900 AT1G66910
Chr5-25065719.5	136,689563	1,54957199	0,37181171	1,54E-05	0,00020448	AT5G62420 AT5G09065 AT5G09070	AT5G62420 AT5G09065 AT5G09070
Chr1-4996046	127,482581	1,75550303	0,42260059	1,63E-05	0,00021626	AT1G05103 AT1G05107	AT1G05097 AT1G05103 AT1G05107 AT1G14590
Chr4-15291113.5	438,264048	1,1715656	0,28238694	1,67E-05	0,00022052	AT4G31550	AT4G08515 AT4G31550
Chr3-5242421	116,911652	1,62527812	0,39198434	1,69E-05	0,00022219		AT3G03115 AT3G15510
Chr1-22200279	129,608379	1,58023172	0,38171629	1,74E-05	0,00022778	AT1G60190 AT1G60200	AT1G60190 AT1G60200
Chr5-3509736	123,205039	1,7519379	0,42391082	1,79E-05	0,00023404	AT5G11060	AT5G11060
Chr4-1495483.5	148,699456	1,51885515	0,3681613	1,85E-05	0,00024075	AT4G03390 AT4G04625	AT4G03390 AT4G04625 AT4G03400
Chr5-22665507	144,656555	1,66981812	0,40561726	1,92E-05	0,00024926	AT5G55960	AT5G55960 AT5G55970
Chr4-11786361	243,742407	1,26860284	0,30925511	2,05E-05	0,00026465	AT4G22290 AT4G22300	AT4G22290 AT4G22300 AT4G22305
Chr2-2588374	149,102527	1,60397231	0,39129535	2,07E-05	0,00026719	AT2G06510 AT2G06520 AT2G06530	AT2G06510 AT2G06520 AT2G06530
Chr3-3988706	71,8552366	2,0528084	0,50172517	2,14E-05	0,00027522	AT3G12570	AT3G12570 AT3G12580
Chr1-7703349.5	93,7401018	1,8043958	0,4413293	2,17E-05	0,00027781	AT1G21920	AT1G21920
Chr2-9265912	270,284424	1,2487188	0,30589864	2,23E-05	0,00028465	AT2G21660 AT2G21670	AT2G21655 AT2G21660 AT2G21670 AT2G21680
Chr1-7340760.5	146,441401	1,47497563	0,36178779	2,28E-05	0,00029015		AT1G21000
Chr1-19580793	91,6509765	1,80757332	0,44443282	2,38E-05	0,00030158	AT1G52565	AT1G52565 AT1G52570
Chr1-9959999	148,555717	1,47403084	0,36293044	2,44E-05	0,00030799		AT1G28375
Chr1-2374813.5	122,487169	1,58569062	0,39063879	2,46E-05	0,00030994	AT1G07670	AT1G07670 AT1G07680
Chr1-25622646	152,900711	1,59711872	0,3941075	2,53E-05	0,00031794	AT1G68360	AT1G68360
Chr1-4577838.5	176,123394	1,47339024	0,36364361	2,54E-05	0,00031794	AT1G13360	AT1G13350 AT1G13360 AT1G05007
Chr1-28689456.5	148,394457	1,51265191	0,37435276	2,66E-05	0,00033219	AT1G76460 AT1G76465 AT1G76470	AT1G76460 AT1G76465 AT1G76470 AT1G76480
Chr1-11923980.5	159,242504	1,52639789	0,37875231	2,79E-05	0,00034647	AT1G32900	AT1G32900 AT1G32910
Chr4-10101988	414,803813	3,30917229	0,82130366	2,80E-05	0,00034668	AT4G18270	AT4G18270 AT4G18280
Chr1-11605826.5	86,0321133	1,78596582	0,44334829	2,81E-05	0,00034676	AT1G32200 AT1G32210	AT1G32200 AT1G32210 AT1G32220
Chr3-10287764.5	97,7603372	1,69437993	0,42197111	2,97E-05	0,00036521	AT3G27770 AT3G27785	AT3G05285 AT3G27750 AT3G27770 AT3G27785
Chr1-3444357	195,905324	1,33270182	0,33212016	3,00E-05	0,00036821	AT1G10470	AT1G10470
Chr1-1745451	211,505611	1,32921353	0,33264103	3,22E-05	0,00039402	AT1G05805	AT1G05800 AT1G05805 AT1G05810
Chr4-14564707.5	131,890552	1,61385249	0,40497031	3,37E-05	0,00041111	AT4G29735	AT4G29730 AT4G29735 AT4G29740
Chr2-17695942.5	117,692462	1,57026798	0,39411456	3,38E-05	0,00041123	AT2G42490	AT2G42490 AT2G42500
Chr4-13983961.5	118,693402	1,54968681	0,39044208	3,61E-05	0,00043704	AT4G28180 AT4G08015 AT4G28190	AT4G28162 AT4G28160 AT4G28170 AT4G08005 AT4G28180 AT4G08015 AT4G28190
Chr1-11532009	172,463986	1,35090584	0,34116542	3,75E-05	0,00045313	AT1G32050 AT1G32060	AT1G32050 AT1G32060 AT1G32070
Chr1-2197340.5	199,332301	1,40639384	0,3562985	3,95E-05	0,00047584	AT1G07160	AT1G07150 AT1G07160 AT1G07170
Chr5-13689693.5	80,4108496	1,85977866	0,47198079	4,07E-05	0,00048814	AT5G35480 AT5G35490	AT5G35475 AT5G35480 AT5G35490 AT5G00525
Chr4-17755103	95,3445786	1,97212953	0,50311867	4,43E-05	0,00053006	AT4G37770	AT4G37770
Chr4-8203327	131,255526	1,51131829	0,38611367	4,54E-05	0,00053862	AT4G14230	AT4G14230 AT4G14240
Chr4-10352265.5	99,4382286	1,73759877	0,44395478	4,54E-05	0,00053862	AT4G18890	AT4G18880 AT4G18890
Chr4-11907942	111,137759	1,55594496	0,39756368	4,54E-05	0,00053862	AT4G22620 AT4G22630	AT4G22620 AT4G22630 AT4G22635
Chr3-22328241	153,463936	1,49505146	0,38229949	4,60E-05	0,00054372	AT3G60400	AT3G09365 AT3G60400
Chr2-9140407.5	138,313648	1,48129889	0,37980535	4,81E-05	0,00056618	AT2G21370	AT2G21360 AT2G21370 AT2G21380
Chr1-4928637	105,114937	1,63156515	0,41845742	4,83E-05	0,00056648	AT1G14400 AT1G14410	AT1G14390 AT1G14400 AT1G14410 AT1G14420
Chr3-6855666	114,304203	1,61277826	0,41368739	4,84E-05	0,00056648	AT3G19720 AT3G19740	AT3G19720 AT3G19740
Chr5-4600963	135,727451	1,5394851	0,39517121	4,89E-05	0,00057132	AT5G14250 AT5G14260	AT5G14250 AT5G14260
Chr2-13172144	81,9990938	1,88895705	0,4857168	5,03E-05	0,00058563	AT2G30942 AT2G30945	AT2G30940 AT2G30942 AT2G30945 AT2G30950
Chr5-18575327.5	105,934348	1,64045372	0,42209128	5,09E-05	0,00058994	AT5G45800	AT5G45790 AT5G45800
Chr5-4653042.5	110,551669	1,65932658	0,42709179	5,11E-05	0,00059064	AT5G14430	AT5G14420 AT5G14430 AT5G14440
Chr3-4124149.5	145,147085	1,44218127	0,37124275	5,12E-05	0,00059064	AT3G12920 AT3G02605	AT3G12920 AT3G02605 AT3G02615
Chr1-7339786	94,9764683	1,67976166	0,43297473	5,23E-05	0,0006015	AT1G21000	AT1G05613 AT1G21000
Chr1-1197864	132,391593	1,47849805	0,38247787	5,54E-05	0,00063518	AT1G04425 AT1G04430	AT1G04425 AT1G08835 AT1G04430
Chr3-2015774.5	175,413513	1,33431891	0,34579879	5,70E-05	0,0006515	AT3G06500 AT3G06510	AT3G06500 AT3G06510
Chr1-268291	157,785976	1,35837216	0,3525452	5,83E-05	0,00066464	AT1G01715 AT1G04043 AT1G01720	AT1G01710 AT1G01715 AT1G04043 AT1G01720 AT1G01725 AT1G04047 AT1G01730
Chr5-251599.5	115,475391	1,5530977	0,4036568	5,96E-05	0,00067765	AT5G01670	AT5G01660 AT5G01670 AT5G01680
Chr3-17478840.5	105,996229	1,58922268	0,41384265	6,15E-05	0,00069637		AT3G47430
Chr5-23952254	118,18318	1,7564001	0,45749072	6,17E-05	0,00069704	AT5G59370 AT5G59380	AT5G59370 AT5G59380 AT5G59385 AT5G59390
Chr5-3473604.5	123,580526	1,51321536	0,39428803	6,21E-05	0,0006978	AT5G10980	AT5G10965 AT5G10980
Chr1-2013675.5	125,104689	1,49524353	0,38964037	6,21E-05	0,0006978	AT1G06570 AT1G06580	AT1G06560 AT1G04483 AT1G06570 AT1G06580 AT1G06590
Chr1-7088544.5	398,577635	1,21765954	0,31760062	6,31E-05	0,00070592	AT1G20450	AT1G20440 AT1G20450 AT1G20460
Chr2-17591939	144,5407	1,73087436	0,4518605	6,39E-05	0,00071362	AT2G42210 AT2G42220	AT2G42200 AT2G09340 AT2G42210 AT2G42220 AT2G42230
Chr5-3284051	98,6383519	1,76515224	0,46090934	6,41E-05	0,00071397	AT5G10450	AT5G10440 AT5G10450
Chr2-8912879.5	235,522828	1,28089602	0,33494165	6,56E-05	0,00072792	AT2G20670	AT2G20670
Chr5-17172015.5	142,902245	1,46856418	0,38614615	7,14E-05	0,00079057	AT5G42820 AT5G06395 AT5G42825	AT5G42810 AT5G42820 AT5G06395 AT5G42825
Chr5-388897	145,026856	1,5494306	0,40789526	7,28E-05	0,00080285	AT5G02020 AT5G02025	AT5G02010 AT5G02020 AT5G02025
Chr1-10288066	101,351217	1,60065336	0,42151534	7,31E-05	0,0008045	AT1G29390 AT1G29395	AT1G29380 AT1G29390 AT1G29395 AT1G29400
Chr2-19065547	98,0784585	1,58001091	0,41665998	7,47E-05	0,00081949	AT2G46440 AT2G46450	AT2G46440 AT2G46450
Chr4-15067010.5	100,417837	1,60301444	0,42341282	7,66E-05	0,00083764	AT4G30960	AT4G08385 AT4G30960 AT4G30970
Chr3-5603626	109,015712	1,5146509	0,40044237	7,76E-05	0,00084707	AT3G16480 AT3G16490	AT3G16480 AT3G16490
Chr1-29765805.5	307,386185	1,0956938	0,29245825	8,97E-05	0,00097336	AT1G79120	AT1G79120
Chr2-11566569	180,487007	1,27992824	0,34165151	8,97E-05	0,00097336	AT2G27080 AT2G27090	AT2G27080 AT2G27090
Chr4-16997044	126,714286	1,42484747	0,38071805	9,11E-05	0,00098531	AT4G35890	AT4G35880 AT4G35890
Chr2-380206.5	76,7041112	1,76834316	0,4741232	9,58E-05	0,00103315		
Chr5-5090895.5	109,969759	1,49381987	0,40057555	9,61E-05	0,00103315	AT5G15640	AT5G15640 AT5G15650
Chr1-26123095	152,321544	1,38937877	0,3731104	9,81E-05	0,0010526	AT1G69490 AT1G69500	AT1G69490 AT1G69500

Postion	baseMean	log2(FC)	lfcSE	p-value	p-adj	gene 1 kb upstream to 1 kb downstream	gene 3 kb upstream to 3 kb downstream
Chr1-5981799	105,659512	1,5183815	0,40875808	0,00010175	0,0010884	AT1G17420 AT1G17430	AT1G17420 AT1G17430 AT1G17440
Chr4-6406579	84,6296713	1,63232659	0,44138593	0,00010857	0,00115812	AT4G10330	AT4G10320 AT4G10330 AT4G10340
Chr1-3759195	179,007654	1,36609111	0,37363907	0,000128	0,00136157	AT1G11220	AT1G11210 AT1G11220
Chr3-18839694.5	163,56745	1,39086069	0,38085421	0,00013013	0,00137731	AT3G50700	AT3G50690 AT3G50700
Chr1-9408243.5	233,100502	1,2323645	0,33746663	0,0001302	0,00137731	AT1G27100	AT1G27090 AT1G27100
Chr2-15916991.5	121,143897	1,38366641	0,38214094	0,00014683	0,00154899	AT2G38025 AT2G38030 AT2G38040	AT2G38020 AT2G38025 AT2G38030 AT2G38040
Chr4-13015729.5	198,027671	1,43675224	0,39730986	0,00014948	0,0015726	AT4G25470	AT4G25450 AT4G25470 AT4G07385 AT4G25480
Chr3-22732494	180,919993	1,36879323	0,37947556	0,00015484	0,00162455	AT3G61420 AT3G61430	AT3G61420 AT3G61430
Chr2-8118317.5	178,12345	1,2437964	0,34596354	0,00016209	0,00169601	AT2G18730	AT2G18720 AT2G18721 AT2G18730
Chr3-3534960.5	93,3996573	1,56123141	0,43527758	0,00016741	0,00174692	AT3G11280 AT3G11285 AT3G11290	AT3G11280 AT3G11285 AT3G11290
Chr1-10375352	120,497508	1,36907637	0,38382028	0,00018056	0,00187905	AT1G29670	AT1G29660 AT1G29670 AT1G29680
Chr3-10434064.5	94,5478311	1,57790352	0,44366605	0,00018791	0,00195016	AT3G28040	AT3G28030 AT3G28040
Chr5-1518130.5	89,359259	1,52394642	0,42997681	0,00019686	0,00203762		AT5G05130 AT5G05140
Chr3-143704.5	127,425884	1,38154148	0,39006497	0,00019869	0,00205094	AT3G01370 AT3G01380	AT3G01370 AT3G01380
Chr3-2011925	150,364717	1,2830149	0,36283283	0,00020304	0,00209025	AT3G06500	AT3G06500
Chr1-5532132.5	93,9493481	1,51123635	0,42789371	0,00020637	0,00211886	AT1G16150	AT1G16150
Chr5-23670190.5	125,093087	1,37315541	0,38890739	0,00020715	0,00212122	AT5G58560	AT5G58550 AT5G58560 AT5G58570 AT5G08840
Chr1-4230515.5	221,55022	1,14331832	0,32390991	0,00020798	0,00212408		AT1G12420
Chr1-20763829.5	156,90407	1,2563826	0,35601525	0,00020856	0,00212428	AT1G55580	AT1G55580
Chr3-489343.5	187,842555	1,18107561	0,33497135	0,00021102	0,00214372	AT3G02380 AT3G02390 AT3G02400 AT3G02410	AT3G02370 AT3G02380 AT3G02390 AT3G02400 AT3G02410
Chr5-24478709.5	125,979346	1,33126278	0,37807452	0,00021483	0,00217662		AT5G60850
Chr1-27160466	175,850061	1,21243412	0,344708	0,000218	0,00220293	AT1G72175	AT1G72170 AT1G72175 AT1G72180
Chr2-13785035.5	124,978126	1,67774706	0,47746512	0,00022082	0,00222559	AT2G32460	AT2G32460 AT2G32470 AT2G08520
Chr1-10065537	104,306457	1,54476928	0,43981001	0,00022208	0,00223239		AT1G28630 AT1G28640
Chr1-27714031.5	142,648692	1,28440674	0,36620578	0,00022631	0,00225983	AT1G73687 AT1G73690	AT1G09865 AT1G73687 AT1G73690
Chr3-17182735.5	141,800535	1,3695357	0,39050364	0,00022651	0,00225983	AT3G46630 AT3G46640	AT3G46620 AT3G46630 AT3G46640 AT3G46650
Chr5-23673432	132,404194	1,43623515	0,40956189	0,0002268	0,00225983	AT5G58560 AT5G58570 AT5G08840 AT5G58575	AT5G58560 AT5G58570 AT5G08840 AT5G58575
Chr3-2757171	85,01878	1,60216318	0,45693355	0,00022716	0,00225983	AT3G09030 AT3G09032	AT3G09020 AT3G09030 AT3G09032 AT3G09035
Chr1-27048282.5	101,405217	1,62937391	0,46494622	0,00022879	0,00227015		
Chr5-18697573	128,890261	1,3953564	0,39849316	0,00023125	0,00228868	AT5G46110	AT5G46100 AT5G46110 AT5G46105
Chr3-6639515.5	89,7959072	1,49705815	0,42819726	0,00023598	0,00232945	AT3G19184 AT3G19190	AT3G19180 AT3G19184 AT3G19190
Chr4-1229573	216,800691	1,11493865	0,31902035	0,00023714	0,00233487	AT4G02760 AT4G02770	AT4G02760 AT4G02770
Chr3-3621006.5	104,4508	1,85397847	0,53080114	0,000239	0,0023472	AT3G11490 AT3G02425 AT3G11500	AT3G11490 AT3G02425 AT3G11500 AT3G11505 AT3G11510
Chr4-13250086.5	126,141002	1,3859068	0,39723811	0,00024255	0,00237596	AT4G07535	AT4G26140 AT4G07535 AT4G07545 AT4G26150
Chr3-1730261.5	150,778245	1,24914572	0,35877488	0,00024912	0,00243418	AT3G01765 AT3G01775 AT3G05810	AT3G05800 AT3G01765 AT3G01775 AT3G05810 AT3G05820
Chr5-9793539.5	132,014376	1,3259824	0,3813807	0,00025372	0,00247283	AT5G27670 AT5G27680	AT5G27660 AT5G27670 AT5G27680
Chr1-9393487	136,374211	1,30118173	0,37450657	0,00025601	0,00248879	AT1G27045 AT1G27050	AT1G27045 AT1G27050 AT1G27060
Chr2-16473935.5	73,8563931	1,62195972	0,46855696	0,00026848	0,00260345	AT2G39450 AT2G39460	AT2G39445 AT2G39450 AT2G39460 AT2G39470
Chr4-12758002	100,252612	1,44638674	0,41873218	0,00027596	0,00266922	AT4G24740 AT4G24750	AT4G24740 AT4G24750
Chr5-162212	79,8572344	1,55463425	0,45028602	0,00027766	0,00267892	AT5G01390 AT5G01400	AT5G01390 AT5G01400
Chr5-690239	152,454148	1,43438125	0,41633185	0,00028523	0,00274507	AT5G02940 AT5G02950	AT5G02940 AT5G02950 AT5G02960
Chr4-15312891	103,970124	1,39213022	0,40521571	0,0002957	0,00283871	AT4G31590	AT4G31590 AT4G31600
Chr1-19225906	94,3220961	1,48487432	0,43316159	0,00030403	0,00291143	AT1G51805	AT1G51805 AT1G51810
Chr1-26331876.5	160,075667	1,26283758	0,36900834	0,00031053	0,00296625	AT1G69910	AT1G69910 AT1G69920
Chr3-5119782.5	111,132762	1,41186862	0,41361045	0,00032064	0,00305527	AT3G15200	AT3G15190 AT3G03025 AT3G15200 AT3G15210
Chr5-14888449	125,350939	1,29367048	0,37930073	0,00032401	0,00307386	AT5G37490 AT5G37500	AT5G37480 AT5G37485 AT5G37490 AT5G37500
Chr3-23334375.5	122,19693	1,32410774	0,38824227	0,0003242	0,00307386	AT3G63160 AT3G63170	AT3G63150 AT3G63160 AT3G63170 AT3G63180
Chr1-27790809.5	76,6251354	1,56267219	0,458649	0,00032826	0,00310474	AT1G73910 AT1G73920	AT1G73890 AT1G73900 AT1G73910 AT1G73920
Chr3-9073650.5	90,0165943	1,51374243	0,44466688	0,00033177	0,00313022	AT3G24860 AT3G04825	AT3G24840 AT3G24850 AT3G24860 AT3G04825 AT3G24870 AT3G04835
Chr4-17115069.5	109,8012	1,62035195	0,47615189	0,00033323	0,00313631	AT4G36160 AT4G36170	AT4G36160 AT4G36170
Chr5-5172942	99,2209241	1,46819469	0,43171681	0,00033591	0,00314652	AT5G15840 AT5G15843 AT5G15845	AT5G15833 AT5G15840 AT5G15843 AT5G15845
Chr1-29521104	63,1397944	1,83838441	0,54057555	0,00033596	0,00314652	AT1G09813 AT1G78470	AT1G78460 AT1G09813 AT1G78470 AT1G78476
Chr4-16102359	116,66394	1,31695117	0,38767481	0,00034058	0,00318207	AT4G33465 AT4G33467 AT4G33470	AT4G33460 AT4G33465 AT4G33467 AT4G33470
Chr1-28554395.5	413,218668	0,957335	0,28201362	0,00034359	0,00320242	AT1G76100 AT1G76110	AT1G76090 AT1G76100 AT1G76110
Chr1-26476352.5	105,335235	1,46230708	0,43110907	0,00034697	0,00322603		AT1G70290 AT1G70300
Chr2-9386505	83,1075378	1,4915242	0,44040282	0,00035366	0,00328031	AT2G22070 AT2G22080	AT2G22070 AT2G22080 AT2G22090 AT2G22088
Chr2-12893957.5	104,200498	1,41240353	0,41763052	0,00035987	0,00332991		AT2G30220
Chr1-3296373	113,506629	1,42139411	0,42318478	0,0003914	0,00361297	AT1G10090 AT1G10095	AT1G10090 AT1G10095
Chr1-28170933	109,942646	1,37886039	0,41083818	0,00039509	0,00363823	AT1G75010 AT1G75020	AT1G75010 AT1G75020
Chr5-2665679.5	105,857959	1,34692318	0,40190437	0,00040209	0,00368533	AT5G08280 AT5G01545 AT5G08290	AT5G08270 AT5G08280 AT5G01545 AT5G08290 AT5G08300
Chr1-1705128	86,4303976	1,50307899	0,44850235	0,00040212	0,00368533	AT1G05680	AT1G05675 AT1G05680 AT1G05690
Chr4-16167091	89,4489117	1,43546006	0,42876696	0,00040716	0,00372263	AT4G33650 AT4G33660	AT4G33650 AT4G33660 AT4G33666 AT4G08815 AT4G33670 AT4G08825
Chr4-744233	97,3943074	1,37982991	0,41251091	0,00041148	0,00375318	AT4G01720	AT4G01720
Chr5-4735220	132,591262	1,2956612	0,38756631	0,00041429	0,0037698	AT5G14690	AT5G14680 AT5G14690
Chr5-4426705.5	146,544133	1,3328443	0,39886702	0,00041652	0,00378119	AT5G13710	AT5G13710 AT5G13720 AT5G13730
Chr1-16709686	76,582418	1,58491252	0,47509028	0,00042493	0,00384842	AT1G44000	AT1G44000
Chr1-899570	347,347972	0,97068109	0,29125741	0,00043	0,00388516	AT1G03600	AT1G03590 AT1G03600 AT1G03610
Chr1-9492825	100,354362	1,40777659	0,42328457	0,00044076	0,00396671	AT1G27320 AT1G27330	AT1G27320 AT1G27330 AT1G27340
Chr3-10949840.5	121,257133	1,28149933	0,38533992	0,00044109	0,00396671		AT3G05605
Chr1-30376423.5	106,147848	1,38186281	0,41571042	0,00044352	0,00397372	AT1G80830	AT1G80830
Chr3-1984150.5	122,473745	1,34674804	0,4051827	0,00044399	0,00397372	AT3G06460 AT3G06470	AT3G06455 AT3G06460 AT3G06470 AT3G06480
Chr1-10046585.5	109,92643	1,35147806	0,40668118	0,00044497	0,00397372	AT1G28580 AT1G28590	AT1G28570 AT1G28580 AT1G28590
Chr5-2921220	91,8686645	1,51830338	0,45781297	0,00045588	0,00406168	AT5G09400 AT5G09410	AT5G09400 AT5G09410
Chr4-16505664	89,0807957	1,45784325	0,44009384	0,00046221	0,00410852	AT4G34555	AT4G34550 AT4G34555 AT4G34560
Chr1-30239224.5	171,263394	1,13478108	0,3427549	0,00046521	0,00412561	AT1G80420 AT1G09967 AT1G09973	AT1G80420 AT1G80430 AT1G09967 AT1G09973 AT1G80440
Chr3-22934635	141,86372	1,23156474	0,37211155	0,00046704	0,00413232	AT3G61930	AT3G61920 AT3G61930 AT3G61940
Chr1-8321491.5	76,6414265	1,52096786	0,46190003	0,00049589	0,00437747	AT1G23440	AT1G23420 AT1G05817 AT1G23440
Chr3-20606171	193,021001	1,29614425	0,39370404	0,00049707	0,00437787	AT3G55560	AT3G55560 AT3G55566
Chr4-9255928.5	112,44249	1,28323041	0,39005468	0,00050116	0,00440381	AT4G16380	AT4G16380 AT4G16390
Chr4-14391943	174,807366	1,27052039	0,38682515	0,00051085	0,00447868	AT4G29180	AT4G29180 AT4G29190
Chr5-25920468	128,55747	1,29494858	0,39698763	0,00055327	0,00483953	AT5G64840 AT5G64850	AT5G64840 AT5G64850
Chr1-27383324.5	83,2085259	1,59498474	0,48917197	0,00055592	0,00484872	AT1G72740 AT1G72750 AT1G72755	AT1G72740 AT1G72750 AT1G72755 AT1G72760
Chr1-27990942	131,612532	1,23743025	0,37956704	0,00055685	0,00484872	AT1G74470	AT1G74460 AT1G74470 AT1G74480
Chr1-25781732.5	261,512184	1,21297214	0,37285292	0,00057053	0,00495662	AT1G68670	AT1G68660 AT1G68670
Chr1-21553287	111,11096	1,29719852	0,39930209	0,00057974	0,00502529	AT1G58200 AT1G58210	AT1G58200 AT1G58210 AT1G58215
Chr5-1640836.5	83,3838037	1,48318901	0,45676339	0,00058279	0,00504035	AT5G05550 AT5G05560	AT5G05540 AT5G05550 AT5G05560
Chr1-29644120	92,3524795	1,38292289	0,42664712	0,00059477	0,00513244	AT1G78850	AT1G78850 AT1G78860
Chr1-28319071	109,775131	1,31754074	0,40665773	0,0005978	0,00514702	AT1G75450 AT1G09557	AT1G75450 AT1G09557
Chr1-26164660	93,3394353	1,39545387	0,43095713	0,00060178	0,00516967	AT1G69570	AT1G69570 AT1G69572
Chr4-17709261.5	111,186175	1,30562274	0,40378566	0,00061151	0,00524154	AT4G37690 AT4G37700	AT4G09575 AT4G09605 AT4G37690 AT4G37700
Chr5-26453147.5	144,591114	1,45285048	0,44952261	0,00061467	0,00525684	AT5G66190 AT5G66200	AT5G66180 AT5G66190 AT5G66200 AT5G66210
Chr5-16635504	201,461101	1,09839072	0,34038084	0,00062559	0,00533841	AT5G41600	AT5G41590 AT5G41600 AT5G41605 AT5G41610 AT5G41612

Postion	baseMean	log2(FC)	lfcSE	p-value	p-adj	gene 1 kb upstream to 1 kb downstream	gene 3 kb upstream to 3 kb downstream
Chr4-485100	185,698774	1,08942122	0,33783013	0,00063039	0,00535213	AT4G01120 AT4G01130	AT4G01120 AT4G01130
Chr3-21303489	118,129445	1,23544946	0,38324783	0,00063288	0,00535213	AT3G57540	AT3G57540
Chr4-17290088.5	118,580475	1,29276868	0,40103967	0,00063308	0,00535213	AT4G36670	AT4G36660 AT4G36670 AT4G36680
Chr5-7266230	110,466964	1,27470115	0,39548928	0,00063406	0,00535213	AT5G21280	AT5G21970 AT5G21280
Chr1-24898519.5	145,060458	1,42872747	0,44328458	0,00063417	0,00535213		AT1G66750
Chr2-14267974.5	117,921231	1,23376796	0,38289108	0,00063596	0,00535543	AT2G33730 AT2G33735	AT2G33720 AT2G33730 AT2G33735 AT2G33740
Chr1-1953941	139,530937	1,2592033	0,3912955	0,00064536	0,00542269	AT1G04453 AT1G06410	AT1G06400 AT1G04453 AT1G06410
Chr3-23186010	174,379809	1,22250888	0,3801618	0,0006505	0,00545397	AT3G62690 AT3G62695	AT3G62680 AT3G62690 AT3G62695
Chr4-10578477.5	86,3183073	1,41063535	0,43881167	0,00065297	0,00546275	AT4G19395 AT4G06880	AT4G19390 AT4G19395 AT4G06880 AT4G19400 AT4G19410
Chr1-18322102.5	131,885622	1,21807883	0,37951887	0,00066475	0,00554922	AT1G49500	AT1G49490 AT1G49500
Chr4-12869937	97,8636506	1,3439055	0,41886194	0,00066722	0,00555774	AT4G25040 AT4G25050	AT4G25040 AT4G25050 AT4G25070
Chr2-10105276.5	82,5606185	1,4927216	0,46643019	0,0006864	0,00570512		AT2G23740 AT2G23755 AT2G23760
Chr5-24574299	65,934137	1,69894716	0,53172697	0,00069879	0,0057956	AT5G61070 AT5G61090	AT5G61070 AT5G61090
Chr5-6791874.5	125,494667	1,20865268	0,37848238	0,00070299	0,00581789	AT5G20110	AT5G20100 AT5G20110
Chr1-2866722	128,09038	1,23514496	0,3869327	0,0007061	0,00583105	AT1G04683 AT1G08920	AT1G04677 AT1G04683 AT1G08920
Chr1-7975296.5	87,67162	1,40271887	0,43967168	0,00071043	0,00585422		AT1G22570
Chr5-21407140	115,609187	1,30165736	0,40891729	0,00072834	0,00598888		AT5G52820
Chr4-9250420	137,40136	1,18697182	0,37307607	0,00073237	0,00600917	AT4G16370	AT4G16370 AT4G06390
Chr1-13126661.5	102,582029	1,36400473	0,42891959	0,00073614	0,00602721		AT1G35580
Chr1-6822854.5	145,863261	1,26991613	0,39985542	0,00074676	0,00608911	AT1G19720 AT1G19730	AT1G19720 AT1G19730 AT1G19740
Chr3-508807	188,218509	1,06401999	0,33505738	0,00074754	0,00608911	AT3G02460 AT3G02470	AT3G02460 AT3G02470
Chr2-10836000	140,721971	1,21618791	0,38304204	0,00074898	0,00608911	AT2G25460	AT2G25460 AT2G25470
Chr5-6046190	69,400501	1,49960484	0,47236582	0,00075004	0,00608911		
Chr3-5081632.5	102,344283	1,35802997	0,42957412	0,00078522	0,00636131	AT3G15095	AT3G15090 AT3G15095 AT3G15110
Chr4-11638924	82,4678387	1,41323112	0,44780555	0,00080001	0,00646272	AT4G21926 AT4G21930	AT4G21920 AT4G21926 AT4G21930 AT4G21940
Chr3-1423778.5	91,3356994	1,3457878	0,42648916	0,00080111	0,00646272	AT3G05090 AT3G05100	AT3G05090 AT3G05100 AT3G05110
Chr4-9254347.5	113,675711	1,28498562	0,40796975	0,00081717	0,00657846	AT4G16380	AT4G06390 AT4G16380
Chr1-30187158	127,354801	1,21779268	0,38685683	0,0008222	0,00660509	AT1G80280 AT1G80290	AT1G80280 AT1G80290
Chr5-8732099.5	102,132535	1,27702139	0,40608114	0,00083116	0,00666316		
Chr4-17998832	112,853357	1,25173049	0,39819746	0,00083473	0,00666407	AT4G09705 AT4G38470	AT4G38460 AT4G09705 AT4G38470
Chr1-18307215.5	80,924562	1,58742451	0,50498869	0,00083474	0,00666407	AT1G49450	AT1G49450 AT1G49460
Chr4-10604843	63,634104	1,72419797	0,54923224	0,0008468	0,00674626	AT4G19440 AT4G06895	AT4G19440 AT4G06895 AT4G19450
Chr3-7503769.5	120,075828	1,2506818	0,39850315	0,00084922	0,00675158		AT3G21320
Chr5-16894529.5	78,9724765	1,60245196	0,51226787	0,00087954	0,00697821	AT5G42250	AT5G42242 AT5G42250
Chr4-5189697	51,6652688	1,74830714	0,55893301	0,00088019	NA	AT4G08230	AT4G08230
Chr1-1922186	101,72328	1,26536579	0,40468135	0,00088354	0,00699545	AT1G06290	AT1G06270 AT1G06280 AT1G06290
Chr2-12205797.5	76,0056577	1,44069527	0,46085388	0,00088558	0,00699714		
Chr1-29890343.5	97,2564529	1,37125139	0,43908883	0,00089525	0,00705904	AT1G79450 AT1G79460	AT1G79440 AT1G79450 AT1G79460
Chr1-25775687	90,4074697	1,4190296	0,45542954	0,00091722	0,00721428	AT1G68650	AT1G68650 AT1G68660
Chr5-2578247.5	127,164346	1,17969593	0,37867439	0,00091869	0,00721428	AT5G08040 AT5G08050	AT5G08030 AT5G08040 AT5G08050 AT5G08055 AT5G08060
Chr3-20330670	92,6966056	1,31019444	0,42141512	0,0009385	0,00735475	AT3G54860 AT3G54870	AT3G54860 AT3G54870
Chr1-20448885.5	123,144628	1,42486142	0,45889643	0,00095148	0,0074413	AT1G54820	AT1G54820 AT1G54830
Chr4-2718003.5	99,0658057	1,39380484	0,45007968	0,00097812	0,00763413	AT4G05320	AT4G05310 AT4G05320 AT4G05330
Chr5-19241587	146,620629	1,12372963	0,36296798	0,00098093	0,00764049	AT5G47430 AT5G47435	AT5G47430 AT5G47435 AT5G47440
Chr5-24973059.5	102,055628	1,26775369	0,41032579	0,00100204	0,00778914	AT5G62170	AT5G62170
Chr1-20772	122,074644	1,1819392	0,38314321	0,00101828	0,00789935		AT1G01040 AT1G03993
Chr2-6639585.5	66,2721278	1,56922783	0,50918505	0,00102862	0,00796351	AT2G15270 AT2G15280	AT2G15270 AT2G15280 AT2G15290
Chr5-7986578	79,5175746	1,42471301	0,46337894	0,00105386	0,00814036	AT5G23680 AT5G03635 AT5G23690	AT5G23670 AT5G23680 AT5G03635 AT5G23690
Chr2-11810432	135,995521	1,23657016	0,40225473	0,0010557	0,00814036	AT2G27690	AT2G27690 AT2G00840
Chr2-11978139.5	90,8487669	1,29704836	0,4221827	0,00106228	0,00817465	AT2G28105 AT2G28110	AT2G28100 AT2G28105 AT2G28110
Chr5-18589312	203,617402	1,09630659	0,35696251	0,00106597	0,00818664	AT5G45820 AT5G45830	AT5G45810 AT5G45820 AT5G45830
Chr1-17892583	81,7731386	1,36376854	0,444266	0,00107133	0,00821137	AT1G48410	AT1G48410
Chr3-18629310	100,711203	1,2888453	0,41996727	0,00107418	0,00821681	AT3G50240 AT3G50250	AT3G50240 AT3G50250
Chr5-25876630.5	91,5401217	1,45934296	0,47564642	0,00107703	0,00821745		AT5G64730 AT5G64735
Chr3-22634186.5	121,539875	1,20337421	0,39227155	0,00107854	0,00821745	AT3G61150	AT3G61150 AT3G61160
Chr2-8550096.5	93,3250124	1,36089766	0,44450646	0,00110081	0,0083685	AT2G19810	AT2G19810
Chr1-813061.5	109,59195	1,2621959	0,41233767	0,00110272	0,0083685	AT1G03290 AT1G03300 AT1G03310	AT1G03290 AT1G03300 AT1G03310
Chr5-25423172	268,961624	0,92244081	0,30152817	0,00110957	0,0084031	AT5G63490 AT5G09165 AT5G63500 AT5G63510	AT5G63490 AT5G09160 AT5G09165 AT5G63500 AT5G63510 AT5G63520
Chr3-18873143.5	69,2431836	1,60245519	0,5239082	0,00111166	0,0084031	AT3G50770	AT3G50770 AT3G50780
Chr4-6879944.5	59,9538142	1,61329808	0,52841533	0,0011325	0,00854382		AT4G05865 AT4G05870
Chr5-4535335.5	87,2941779	1,33075787	0,43636728	0,00114562	0,00862148	AT5G14050 AT5G14060	AT5G14040 AT5G14050 AT5G14060
Chr1-6512951	120,963363	1,15469442	0,37868855	0,00114729	0,00862148		AT1G18860 AT1G18870
Chr3-1617500	96,477703	1,42076296	0,46676575	0,00116787	0,00875906	AT3G05570 AT3G05580	AT3G05560 AT3G05570 AT3G05580
Chr5-24906776	156,774966	1,21431389	0,39911543	0,00117306	0,00878079	AT5G09035	AT5G09035 AT5G61997 AT5G09040 AT5G09045
Chr2-17489888.5	103,687231	1,21879338	0,40100568	0,00118548	0,00885649	AT2G41900	AT2G41900
Chr5-4542713.5	101,572498	1,2946526	0,4262625	0,00119386	0,00890179	AT5G14070 AT5G14080	AT5G02145 AT5G14070 AT5G14080
Chr3-5297744	108,930168	1,23190809	0,40588478	0,00120221	0,00894667	AT3G15620 AT3G15630 AT3G15635	AT3G15620 AT3G15630 AT3G15635 AT3G15640
Chr5-25704503	241,519002	1,09702072	0,36161919	0,00120813	0,00897336	AT5G64260	AT5G64260 AT5G64270
Chr1-10806609	132,340864	1,26867604	0,41837687	0,00121318	0,00899348	AT1G30500 AT1G30510	AT1G06343 AT1G30500 AT1G30510 AT1G30515
Chr2-14665654.5	119,189136	1,16783121	0,38710434	0,00127713	0,00944929	AT2G34770	AT2G34750 AT2G34770 AT2G08680 AT2G34780
Chr1-26663164.5	86,9239677	1,3649262	0,45267562	0,00128387	0,00948092	AT1G70710	AT1G70710
Chr1-29117557	111,817729	1,28634573	0,42687274	0,00129162	0,00951979	AT1G77480 AT1G77490	AT1G77480 AT1G77490
Chr1-4394489	83,0001545	1,31841155	0,4381462	0,00131025	0,0096267	AT1G12900 AT1G12910	AT1G04983 AT1G12890 AT1G12900 AT1G12910 AT1G12920
Chr5-24417434.5	69,185605	1,47866773	0,49143736	0,00131114	0,0096267	AT5G08970 AT5G60720	AT5G60710 AT5G08970 AT5G60720
Chr1-2152403	112,506815	1,16160831	0,38780239	0,0013706	0,01004409	AT1G07000 AT1G07010	AT1G06990 AT1G07000 AT1G07010 AT1G04537 AT1G07020
Chr3-15952317	207,463579	1,15550199	0,38616104	0,00138451	0,01012671	AT3G44260	AT3G44250 AT3G44260 AT3G44261 AT3G44265
Chr2-14253274.5	111,728887	1,185921	0,3979492	0,00144086	0,01051882	AT2G33685 AT2G33690 AT2G33700	AT2G33680 AT2G33685 AT2G33690 AT2G33700 AT2G33705
Chr3-23276671	141,22359	1,10539015	0,37134116	0,0014566	0,01061358	AT3G62980	AT3G62980
Chr1-8010829	86,7591319	1,40389793	0,47341717	0,00151117	0,01099034		AT1G22650
Chr5-26933195	86,0247174	1,27969979	0,43272327	0,00155165	0,01126336	AT5G67480 AT5G67488 AT5G67490	AT5G67470 AT5G67480 AT5G67488 AT5G67490 AT5G67500
Chr5-24829728.5	125,240316	1,31216126	0,44477638	0,00158805	0,01150587	AT5G61790 AT5G61800	AT5G61780 AT5G61790 AT5G61800 AT5G61810
Chr3-3545591	89,9766199	1,37902363	0,46753648	0,00159117	0,01150676	AT3G11320	AT3G11310 AT3G11320
Chr1-1028662	161,538103	1,04043794	0,35318102	0,00161005	0,01162144	AT1G04000	AT1G03990 AT1G04000 AT1G04010
Chr3-1634793	139,845051	1,09189472	0,37083494	0,00161779	0,01165537	AT3G05625 AT3G05630	AT3G05620 AT3G05625 AT3G05630
Chr2-15099824	185,45948	1,08343047	0,36810263	0,00162375	0,01167643		
Chr3-23289575.5	158,754426	1,0519903	0,35755222	0,00162944	0,01169545	AT3G63010	AT3G63010
Chr4-14442959	165,044007	1,04652046	0,35686335	0,00168094	0,01204256		AT4G29330
Chr4-17522740.5	91,2117184	1,33353843	0,45656648	0,00174568	0,01248308		AT4G37235 AT4G37240
Chr2-14782607	91,6496196	1,37320819	0,4705928	0,0017612	0,01257065	AT2G35070	AT2G35070
Chr2-10684178.5	84,5628397	1,31955805	0,45309309	0,0017937	0,01277886	AT2G25110	AT2G25100 AT2G25110
Chr5-1711462	97,924392	1,23769918	0,42538049	0,00180929	0,01286608		AT5G05700
Chr5-20943211.5	119,89364	1,11115206	0,38241976	0,00183285	0,01298951		AT5G51550 AT5G51560

Postion	baseMean	log2(FC)	lfcSE	p-value	p-adj	gene 1 kb upstream to 1 kb downstream	gene 3 kb upstream to 3 kb downstream
Chr3-3443074.5	213,358586	0,93891806	0,32315351	0,00183342	0,01298951	AT3G10985	AT3G10980 AT3G10985 AT3G10986
Chr5-1308470.5	97,4157367	1,23783406	0,42698184	0,00187158	0,0132355	AT5G04560	AT5G04550 AT5G04560
Chr5-14594472.5	105,261929	1,33523737	0,46146494	0,00190502	0,01344721	AT5G36940 AT5G36950	AT5G36940 AT5G36950
Chr5-973934.5	146,299509	1,02589815	0,35468341	0,00191135	0,01346713	AT5G03720 AT5G03730	AT5G03710 AT5G03720 AT5G03730
Chr3-2529015.5	63,4095334	1,4361833	0,49679514	0,00192072	0,01350838	AT3G07930 AT3G07940	AT3G07920 AT3G07930 AT3G07940 AT3G07950
Chr3-4976129	81,2246219	1,28016554	0,44326094	0,00193811	0,01360575	AT3G03005	AT3G14810 AT3G03005 AT3G14820
Chr2-18859522.5	101,969996	1,17547503	0,40751486	0,0019602	0,01373573	AT2G45800 AT2G09665 AT2G45810	AT2G45790 AT2G45800 AT2G09665 AT2G45810
Chr2-17472899.5	153,375864	1,05103718	0,36464508	0,00197356	0,01380416	AT2G41870	AT2G41860 AT2G41870 AT2G41880
Chr4-4073685	65,9159435	1,4697849	0,51053671	0,00199531	0,01393092	AT4G06746	AT4G06744 AT4G06746
Chr1-28315829	108,58827	1,14033531	0,39627181	0,00200319	0,01395751	AT1G75440 AT1G75450	AT1G75440 AT1G09553 AT1G75450 AT1G09557
Chr2-14931557.5	90,5620105	1,30906132	0,45502274	0,00200792	0,01395751	AT2G35550 AT2G35555	AT2G35540 AT2G35550 AT2G35555 AT2G35580
Chr4-8695965.5	144,777246	1,12164707	0,38992329	0,00201003	0,01395751	AT4G02945 AT4G15236	AT4G15233 AT4G02945 AT4G15236
Chr2-13826365	144,443922	1,04007151	0,3625938	0,00206263	0,01429696	AT2G32560	AT2G00860 AT2G32560 AT2G32580 AT2G32590
Chr4-17386278	207,168019	0,95657647	0,33428695	0,00210792	0,01458454		AT4G09395 AT4G36900
Chr2-12603804	96,055756	1,28137639	0,44841119	0,00213434	0,01474078	AT2G29360	AT2G29350 AT2G29360 AT2G29370
Chr1-30194868	110,727123	1,18917712	0,41652706	0,00215197	0,01483289	AT1G80300 AT1G80325 AT1G80310 AT1G80315	AT1G80300 AT1G80325 AT1G80310 AT1G80315 AT1G80320
Chr1-19513039	102,411133	1,32697188	0,46487431	0,0021554	0,01483289	AT1G52390	AT1G52380 AT1G52390 AT1G52400
Chr1-30380458.5	85,5005613	1,33199732	0,46678088	0,00216147	0,01484803		
Chr2-10267273.5	142,472362	1,16537219	0,40851276	0,00216735	0,0148618	AT2G24150	AT2G24150
Chr3-10256204.5	208,445312	1,15021401	0,40328175	0,00217133	0,0148626	AT3G27680 AT3G27690 AT3G27700	AT3G27670 AT3G27680 AT3G27690 AT3G27700
Chr2-6400395	102,539255	1,16634214	0,40965594	0,00220579	0,01507162	AT2G14890	AT2G14890
Chr1-24915648.5	84,4818941	1,37388454	0,48319719	0,00223231	0,01522568		AT1G08847 AT1G66783
Chr1-2437239.5	123,496728	1,10294359	0,38810155	0,00224232	0,01526685	AT1G07885 AT1G07890	AT1G07880 AT1G07885 AT1G07890
Chr1-25752603.5	103,813545	1,17036535	0,41207071	0,00225423	0,01532076	AT1G08997 AT1G68580	AT1G68570 AT1G08997 AT1G68580
Chr3-9756104.5	79,0500374	1,27746286	0,4499112	0,00226016	0,01533394	AT3G26570	AT3G26560 AT3G26570 AT3G26580
Chr4-14990318.5	76,0404543	1,33246152	0,47059149	0,00231679	0,01566517	AT4G30780	AT4G30780 AT4G30790
Chr1-6687189.5	100,871343	1,14527997	0,40449056	0,00231714	0,01566517	AT1G19340	AT1G19330 AT1G19350
Chr1-8337154	217,649036	0,89139861	0,31568345	0,00237356	0,01601843	AT1G23480 AT1G23490	AT1G23480 AT1G23490 AT1G23500
Chr5-8707835	72,5845959	1,32263345	0,46869648	0,0023867	0,01605877	AT5G25190	AT5G25190
Chr2-18866944	122,218664	1,11063282	0,39359317	0,00238791	0,01605877	AT2G45830	AT2G45820 AT2G45830 AT2G45840
Chr1-23126385	84,8762181	1,24088741	0,44007599	0,00240334	0,01613432		AT1G62480
Chr5-1073512.5	103,78882	1,29239457	0,45857517	0,00241406	0,01617801	AT5G03970 AT5G03980	AT5G03970 AT5G03980 AT5G03990
Chr5-13902705.5	136,665016	1,35625026	0,48139066	0,00242102	0,01619637	AT5G35735	AT5G35735
Chr1-9202407	33,7476191	1,93465418	0,68785136	0,0024571	NA		AT1G26620
Chr5-22400932.5	69,7651401	1,38733806	0,49451243	0,00251219	0,01677706	AT5G55220 AT5G55230	AT5G55220 AT5G55230
Chr1-29365779.5	342,510743	0,83934318	0,29946345	0,00253287	0,0168858	AT1G78080	AT1G78080
Chr3-3919379.5	126,87434	1,07007645	0,38207979	0,00254989	0,01696982	AT3G12280 AT3G12290	AT3G12280 AT3G12290 AT3G12300
Chr3-4184673	68,1390702	1,44164226	0,51767369	0,00267765	0,0177892	AT3G13060 AT3G13061 AT3G13062	AT3G13060 AT3G13061 AT3G13062 AT3G13065
Chr1-8987883	73,3931889	1,44508667	0,51902929	0,00268291	0,01779341		
Chr1-1504877	50,2792645	1,52896668	0,54940178	0,00269322	NA	AT1G05200	AT1G05180 AT1G05190 AT1G05200
Chr3-2348777	129,16123	1,04244686	0,37485076	0,00270988	0,01794126	AT3G07350	AT3G00240 AT3G01965 AT3G07350 AT3G01975 AT3G01985
Chr1-7884610.5	97,1941898	1,17797877	0,42381776	0,00272258	0,0179791	AT1G22310 AT1G22320	AT1G22310 AT1G22320 AT1G22330
Chr3-22337715.5	95,897748	1,17297227	0,42205953	0,00272496	0,0179791	AT3G60420 AT3G60440	AT3G60415 AT3G60420 AT3G60440 AT3G09395
Chr5-21053620.5	68,9557967	1,44118151	0,51920341	0,00275368	0,01813747		AT5G51800 AT5G51810
Chr2-1094711.5	70,3661349	1,33778608	0,48325143	0,00281746	0,01852575	AT2G03580 AT2G03590	AT2G03580 AT2G03590 AT2G03600
Chr5-8777541.5	81,5912442	1,21193102	0,43792103	0,00282471	0,01854167	AT5G25280 AT5G03955	AT5G25280 AT5G03955 AT5G25290 AT5G25300
Chr3-22910808	91,5054737	1,20078049	0,43430992	0,00284788	0,01866186		AT3G61880
Chr1-28052401.5	83,9157806	1,26915739	0,46109108	0,00295703	0,01933759	AT1G74670	AT1G74670 AT1G74675
Chr4-7284434.5	56,9602815	1,46381682	0,53189826	0,00296107	0,01933759	AT4G12220 AT4G12230	AT4G12210 AT4G12220 AT4G12230
Chr1-12059689	74,6650217	1,29404747	0,47068564	0,0029863	0,01946926	AT1G33250	AT1G33250
Chr3-3863504.5	114,514143	1,12583858	0,41020872	0,00302969	0,01971866	AT3G12120 AT3G12130	AT3G12120 AT3G12130
Chr5-828942.5	105,170485	1,11167545	0,40613217	0,00309799	0,02012906		AT5G03370
Chr5-21095469	159,973866	0,99956095	0,36542349	0,0031157	0,02020997	AT5G51910 AT5G51915	AT5G51900 AT5G51910 AT5G51915 AT5G51920
Chr2-621094.5	107,044604	1,09542526	0,4007874	0,00313627	0,0203091	AT2G02360 AT2G02370	AT2G02350 AT2G02360 AT2G02370
Chr4-12556201.5	89,0354913	1,20271796	0,44037224	0,00315579	0,02040106	AT4G24190 AT4G24200	AT4G24190 AT4G24200
Chr3-6958801	139,415185	0,97962319	0,35882762	0,00316608	0,02043319	AT3G19970	AT3G19960 AT3G19970 AT3G19980
Chr1-564515.5	89,3364562	1,1768411	0,43239495	0,00324754	0,02092375	AT1G02640	AT1G02630 AT1G02640
Chr5-25087192	86,8694615	1,2648596	0,46485119	0,00325425	0,02093185		AT5G62480 AT5G62490
Chr4-12760886	80,5019698	1,20776197	0,44400747	0,00326273	0,02095128	AT4G24750 AT4G24760	AT4G24750 AT4G24760
Chr1-4535188.5	76,2615024	1,47540217	0,54318077	0,00330153	0,02114203		AT1G05003
Chr1-26513014	180,820309	0,94164652	0,34669891	0,00330344	0,02114203	AT1G70370	AT1G70370
Chr3-11384153	81,657082	1,2276413	0,45250645	0,00333405	0,0212699	AT3G29575	AT3G29575
Chr5-21619776.5	109,806673	1,1824727	0,43586459	0,0033345	0,0212699	AT5G53290	AT5G53290
Chr4-14884634.5	96,7633041	1,11260199	0,41056974	0,0033652	0,02143012		AT4G30440 AT4G30450
Chr3-19449061.5	73,0207983	1,28409173	0,47488045	0,00342519	0,02177604		AT3G52460 AT3G52470 AT3G52480
Chr3-18499065.5	44,2328405	1,54166096	0,5703384	0,00343518	NA	AT3G49880 AT3G49890	AT3G49880 AT3G49890 AT3G49900
Chr5-26507795.5	98,5696636	1,19513621	0,44302801	0,0034915	0,02216093	AT5G66350 AT5G09605 AT5G09615	AT5G66350 AT5G09605 AT5G09615 AT5G66360
Chr3-21760306.5	80,976231	1,29165184	0,48031661	0,00358152	0,0226948	AT3G58850	AT3G58840 AT3G58850
Chr2-8900135.5	73,1080182	1,54891166	0,57820724	0,00369413	0,0233698	AT2G20630 AT2G20635	AT2G20625 AT2G20630 AT2G20635
Chr4-9453371.5	106,799808	1,11654838	0,4181458	0,00378989	0,02393612	AT4G16790	AT4G16780 AT4G16790 AT4G16800
Chr4-15486478	187,536277	0,89851091	0,33666821	0,00380578	0,02399701		AT4G32010 AT4G32020
Chr5-26229483	249,382229	0,85308598	0,3197689	0,00381725	0,02402992	AT5G65630 AT5G09405	AT5G65630 AT5G09405
Chr5-26499000	114,042645	1,07758036	0,40470191	0,00387638	0,02436217	AT5G66320 AT5G00725	AT5G66320 AT5G00725 AT5G66330 AT5G66335
Chr1-2165354	69,3449489	1,36769028	0,5140328	0,00389885	0,02446336	AT1G07050 AT1G07051 AT1G07060	AT1G07040 AT1G07050 AT1G07051 AT1G07060 AT1G04557
Chr3-16465186	64,9200642	1,37620926	0,51767829	0,00392533	0,02458936	AT3G45010	AT3G45010
Chr2-17886142	115,089401	1,22946486	0,46284904	0,00395019	0,02470478	AT2G43010	AT2G09410 AT2G43010
Chr1-7267564	107,2668	1,04213507	0,39312846	0,00401416	0,025064	AT1G20890	AT1G20880 AT1G20890
Chr3-17532593.5	49,445329	1,44814427	0,54683837	0,00404593	NA	AT3G47580 AT3G07785	AT3G47570 AT3G47580 AT3G07785
Chr3-3923560	92,508894	1,11739332	0,42298778	0,00412494	0,02571393	AT3G12300 AT3G12320	AT3G12290 AT3G12300 AT3G12320 AT3G12340
Chr2-19622436	154,018208	0,94063518	0,35661061	0,0041734	0,02597385	AT2G47940	AT2G47940 AT2G01000 AT2G47950
Chr3-9719865	56,124553	1,3964537	0,53081481	0,00425954	0,02646702	AT3G05045 AT3G05055	AT3G05045 AT3G05055 AT3G26520
Chr2-15616265	106,903771	1,03710056	0,39443273	0,00427745	0,02653539		AT2G37170 AT2G37180 AT2G37190
Chr2-18822410.5	192,811444	0,85281131	0,32444086	0,0042874	0,02654103	AT2G45680 AT2G45685 AT2G45690	AT2G45680 AT2G45685 AT2G45690
Chr1-10400472.5	67,6059191	1,27966972	0,4869038	0,00429218	0,02654103	AT1G29720 AT1G29730	AT1G29720 AT1G29730
Chr1-26118156	109,19406	1,18356056	0,45061905	0,00431313	0,02662768	AT1G69480 AT1G69485	AT1G69480 AT1G69485
Chr5-26185785	68,4809333	1,2991611	0,4955041	0,00437208	0,02694831	AT5G65510	AT5G65500 AT5G65510
Chr5-1931115.5	162,371647	0,94443191	0,36130922	0,00447555	0,02754016	AT5G06310 AT5G06320 AT5G01255	AT5G06310 AT5G06320 AT5G01255 AT5G06330
Chr1-28147973.5	57,009911	1,32917473	0,50860177	0,00448245	0,02754016	AT1G74930 AT1G74940	AT1G74930 AT1G74940 AT1G74950
Chr2-18912851	232,021921	0,81397109	0,31180372	0,00452018	0,02772763	AT2G45960 AT2G45970	AT2G45960 AT2G45970
Chr5-206248.5	94,1970615	1,11407344	0,4277645	0,00460165	0,02818236	AT5G01510 AT5G01520	AT5G01510 AT5G01520 AT5G01530
Chr4-7926356	43,7594973	1,54281076	0,59247093	0,00460676	NA	AT4G13615	AT4G13615
Chr5-1879866.5	66,4262864	1,30333298	0,50059803	0,00461316	0,02820788	AT5G06210 AT5G06220	AT5G06200 AT5G06210 AT5G06220

Postion	baseMean	log2(FC)	lfcSE	p-value	p-adj	gene 1 kb upstream to 1 kb downstream	gene 3 kb upstream to 3 kb downstream
Chr4-6044593.5	91,2436892	1,0909905	0,41917922	0,00462488	0,02823454	AT4G09560	AT4G09560
Chr5-26635084.5	96,3384714	1,12622956	0,43359438	0,00469626	0,02862482	AT5G66700	AT5G66700 AT5G66710
Chr1-24732377.5	92,5487608	1,09719066	0,42384379	0,0048174	0,02931669	AT1G66330	AT1G66330 AT1G66340
Chr5-8161507.5	54,2959139	1,37618219	0,53235337	0,00486766	0,02956318	AT5G24130	AT5G24120 AT5G24130 AT5G24140
Chr3-22291650	105,088439	1,02173093	0,39538064	0,00488068	0,02956318	AT3G60310 AT3G60320	AT3G60310 AT3G60320
Chr2-7056389.5	70,8844419	1,23927628	0,47956875	0,004881	0,02956318		AT2G06605 AT2G16290
Chr4-15490177	520,233868	0,80973187	0,3135027	0,00489933	0,02961273	AT4G32020 AT4G32030	AT4G32020 AT4G32030
Chr2-13660440.5	106,149308	1,05466584	0,40839215	0,00490461	0,02961273	AT2G32150	AT2G32150 AT2G32160
Chr2-14150313.5	72,9007287	1,28453857	0,49775394	0,00493044	0,02972197	AT2G33385 AT2G33390	AT2G33385 AT2G33390 AT2G08575 AT2G33400
Chr4-10649812	140,696501	0,94769181	0,3673942	0,00494723	0,02973084		AT4G19520 AT4G19530
Chr5-872581	132,769491	1,10046654	0,4266227	0,0049474	0,02973084	AT5G03490 AT5G03495	AT5G03480 AT5G03490 AT5G03495
Chr4-18232047	68,2411799	1,22858433	0,47815941	0,00509369	0,03056215	AT4G39140	AT4G39140 AT4G39150
Chr5-6812416.5	111,572637	1,02855906	0,40054199	0,00511556	0,0306315	AT5G20180	AT5G20170 AT5G20180 AT5G20190
Chr1-25877612	70,1601774	1,22215455	0,47600284	0,0051212	0,0306315		AT1G68830 AT1G68840
Chr3-17442369	102,806437	1,36715822	0,532618	0,00513114	0,03064317	AT3G47340 AT3G47341	AT3G47340 AT3G47341 AT3G07715
Chr2-10165487	49,4918205	1,38034172	0,53781565	0,00513549	NA		
Chr5-5696272.5	69,4350116	1,22474235	0,47762493	0,00517018	0,03079542	AT5G17310	AT5G17310
Chr4-11425931	96,4316328	1,07736564	0,42017831	0,00517267	0,03079542	AT4G21445 AT4G21450	AT4G21445 AT4G21450 AT4G21460
Chr4-8373274	49,4559854	1,42735904	0,55725669	0,00521252	NA		AT4G06205 AT4G14590
Chr5-26002734	92,8450617	1,28162074	0,50136778	0,00529037	0,03138832	AT5G65080	AT5G65080 AT5G65090
Chr2-17734019	90,8341877	1,23969982	0,48498499	0,0052917	0,03138832	AT2G42590 AT2G42600	AT2G42580 AT2G42590 AT2G42600
Chr1-2225264	209,928841	0,91730749	0,3589082	0,00529678	0,03138832	AT1G07240 AT1G07250	AT1G07230 AT1G07240 AT1G07250 AT1G07260
Chr5-8501996.5	57,2583883	1,51412277	0,59343756	0,00536388	0,03173696	AT5G24770	AT5G24770
Chr3-21121135.5	77,4322776	1,13186533	0,4440213	0,0053997	0,03189974	AT3G57060 AT3G57062	AT3G57060 AT3G57062 AT3G08835 AT3G57070
Chr3-8640099.5	78,2977925	1,12898068	0,44320764	0,00542808	0,03201816	AT3G23910	AT3G23910 AT3G23920
Chr3-7177996	85,5078235	1,12226123	0,44087672	0,00545573	0,03213191	AT3G20550 AT3G20555	AT3G20550 AT3G20555 AT3G20557
Chr5-9799160	66,1525004	1,2224423	0,4803753	0,00546756	0,03215229	AT5G27680	AT5G27680
Chr3-5645950	116,721955	1,08070454	0,42481518	0,00548049	0,03217901	AT3G16570 AT3G03345	AT3G16570 AT3G03345 AT3G16580
Chr2-17793210	70,0266991	1,22519329	0,48189415	0,00550387	0,03226695	AT2G42740 AT2G42750	AT2G42730 AT2G42740 AT2G42750 AT2G42760
Chr5-22179154	40,4478074	1,50886676	0,59467923	0,0055859	NA	AT5G54590	AT5G54585 AT5G54590
Chr1-30190327	108,045619	1,02949987	0,40599238	0,00561016	0,03283993	AT1G80290	AT1G80290 AT1G80300
Chr1-21231093.5	88,4478017	1,20527312	0,47585628	0,00565695	0,03299159		AT1G56650
Chr3-22436179.5	216,472867	0,81495652	0,32175498	0,005657	0,03299159	AT3G60690	AT3G60690 AT3G60700
Chr4-10081944.5	63,880711	1,28408239	0,50703175	0,00566184	0,03299159	AT4G18230 AT4G18240	AT4G18215 AT4G18220 AT4G18230 AT4G18240
Chr2-12819745.5	186,761762	0,85876368	0,3393756	0,00569626	0,03307531	AT2G08360	AT2G08360 AT2G30040
Chr1-6946552.5	112,224849	1,01997432	0,40310932	0,00569878	0,03307531	AT1G20030	AT1G20020 AT1G20030 AT1G20040 AT1G20050
Chr1-27372155	87,2585853	1,11268159	0,43978353	0,00570205	0,03307531	AT1G72700 AT1G72710	AT1G72700 AT1G72710
Chr5-5211900	68,5918027	1,21550762	0,48063067	0,00571965	0,03312739	AT5G15970	AT5G15960 AT5G15970 AT5G15980
Chr1-22822768.5	90,0526646	1,12425501	0,44487505	0,00575002	0,03325314		AT1G61795 AT1G61800
Chr1-1713531.5	58,9062223	1,26910709	0,50282492	0,00580215	0,03350415	AT1G05700 AT1G04407	AT1G05700 AT1G04407 AT1G05710
Chr2-17130435.5	82,3079736	1,09256341	0,43348104	0,00586039	0,03375445	AT2G41060 AT2G41070 AT2G09215	AT2G41060 AT2G41070 AT2G09215 AT2G41080
Chr1-27759799.5	62,4621191	1,35578061	0,53794843	0,00586308	0,03375445	AT1G73830	AT1G73820 AT1G73830 AT1G09417
Chr5-3784841	253,124083	0,79074868	0,31399602	0,00589548	0,03389016	AT5G11730 AT5G00375	AT5G11730 AT5G11740 AT5G00375 AT5G01885 AT5G11750
Chr3-18000790	46,7775994	1,39667318	0,55550105	0,00596415	NA	AT3G48560	AT3G48560
Chr4-17281766	331,399862	0,72329387	0,28775484	0,00597569	0,03429992	AT4G36648	AT4G36640 AT4G36648 AT4G36650
Chr3-1257563.5	61,5070322	1,24320839	0,49490051	0,00600183	0,03439852	AT3G04620 AT3G04630	AT3G04610 AT3G04620 AT3G04630
Chr1-6627323	165,228249	0,89282681	0,35563469	0,00602773	0,03449552	AT1G19210 AT1G19220	AT1G19190 AT1G19200 AT1G19210 AT1G19220
Chr3-2564784	416,408468	0,78039947	0,31097971	0,00604534	0,03454478	AT3G08030	AT3G08020 AT3G08030 AT3G08040
Chr1-6754211.5	89,5615779	1,05268282	0,41986849	0,00608506	0,03472011	AT1G19490 AT1G19500	AT1G19485 AT1G19490 AT1G19500 AT1G19510
Chr1-6464636.5	312,106497	1,00642006	0,4016001	0,00610484	0,03477647	AT1G18740 AT1G18745	AT1G18730 AT1G18735 AT1G18740 AT1G18745 AT1G05417 AT1G05423 AT1G05427 A
Chr1-28285197.5	113,596601	1,00334498	0,40052069	0,00612081	0,03477647		AT1G75380
Chr4-14165847	80,3333655	1,15925784	0,46277264	0,00612211	0,03477647	AT4G28703	AT4G28700 AT4G28703 AT4G28706
Chr1-6515911	115,755924	1,06618134	0,42584265	0,00614515	0,03485578	AT1G18870	AT1G18870
Chr5-5205544.5	72,720962	1,16078486	0,46385318	0,00616627	0,03492401	AT5G15940 AT5G15950	AT5G15940 AT5G15950
Chr1-20010432	74,8530889	1,25225214	0,50083445	0,00620386	0,03508515	AT1G07917 AT1G53620	AT1G09615 AT1G07913 AT1G53610 AT1G07917 AT1G53620
Chr4-9440856.5	68,2454432	1,17637568	0,47087946	0,00624037	0,03523972		
Chr2-8324169.5	70,4089012	1,15287114	0,46231818	0,00632142	0,035645	AT2G19180	AT2G19180 AT2G19190
Chr5-23742364	58,9389532	1,30088656	0,52206301	0,00635454	0,03572691	AT5G58784 AT5G58787	AT5G58782 AT5G58784 AT5G58787 AT5G58790
Chr5-5007307.5	108,64707	0,98443499	0,39506693	0,00635455	0,03572691	AT5G15410 AT5G15420	AT5G15410 AT5G15420 AT5G15430
Chr3-536538	124,533227	0,94000887	0,37750643	0,0063863	0,03585294	AT3G02540 AT3G02550	AT3G02540 AT3G02550
Chr1-4540849.5	127,004558	1,08222358	0,43471252	0,00639587	0,0358542		AT1G13260
Chr5-4939023.5	82,8943761	1,16463806	0,46798364	0,00641182	0,03589124	AT5G15210	AT5G15200 AT5G15210 AT5G15220
Chr5-736658.5	60,4815808	1,28333021	0,51593707	0,00643444	0,03596543	AT5G03130 AT5G03140	AT5G03120 AT5G03130 AT5G03140
Chr2-12435674.5	67,5721064	1,20691103	0,48601048	0,00650852	0,03632665		AT2G28950 AT2G28960
Chr1-5979570	75,7340897	1,18165226	0,47629902	0,00655248	0,03651889	AT1G17420	AT1G17420 AT1G17430
Chr3-21828024.5	126,508094	1,05861716	0,42705288	0,00658959	0,03667253	AT3G59050 AT3G59060	AT3G59050 AT3G59060
Chr5-3444630	96,634819	1,15718075	0,46699117	0,00660698	0,03671609	AT5G10920 AT5G10930	AT5G10910 AT5G10920 AT5G10930
Chr1-25464346	66,1218203	1,21871252	0,49259024	0,0066788	0,03701027	AT1G67900	AT1G67890 AT1G67900
Chr4-16431393.5	89,3609747	1,10888332	0,44820228	0,0066792	0,03701027	AT4G34350 AT4G34360	AT4G34350 AT4G34360 AT4G34370
Chr4-10940305	102,176283	1,00109699	0,40485019	0,00670372	0,0370831	AT4G20250 AT4G20260	AT4G20250 AT4G20260
Chr5-7008414.5	70,9396743	1,15559465	0,46740994	0,00671166	0,0370831	AT5G20700	AT5G20700 AT5G20710
Chr3-23430335.5	145,427176	0,87817607	0,35540003	0,00673771	0,0371736	AT3G63450 AT3G63460	AT3G63450 AT3G63460
Chr3-8594204.5	134,848311	0,91402244	0,3700016	0,00674961	0,03718579		
Chr1-634999	94,6839844	1,18632699	0,48102277	0,00682662	0,03755618	AT1G02860	AT1G02850 AT1G02860 AT1G04147 AT1G02870 AT1G04153
Chr5-13672542	78,8683139	1,21257236	0,49210393	0,0068687	0,03773366	AT5G35450	AT5G35450 AT5G35460
Chr2-15193191	202,793799	0,82221768	0,33421791	0,00694444	0,03809522	AT2G36220 AT2G08780 AT2G36230	AT2G36220 AT2G08780 AT2G36230 AT2G36240
Chr1-23320522	71,8053793	1,17753018	0,47904858	0,00698449	0,03821717	AT1G62960	AT1G62950 AT1G62960 AT1G62970
Chr4-13920658.5	146,608716	0,91749778	0,37327721	0,00698658	0,03821717	AT4G27970 AT4G27980	AT4G27970 AT4G27980 AT4G27990
Chr3-22538431	79,38169	1,1796371	0,48033112	0,00702694	0,0383833	AT3G60960	AT3G60960 AT3G09515 AT3G60961
Chr1-22977631.5	77,2814941	1,13070864	0,46066109	0,00705335	0,03847283	AT1G62180	AT1G62170 AT1G62180 AT1G08477
Chr2-259072.5	48,8547742	1,33981188	0,5460694	0,00707257	NA	AT2G04015	AT2G01570 AT2G04015
Chr4-9376639	88,9525513	1,04910897	0,42787614	0,00710523	0,03870084	AT4G16650 AT4G16660	AT4G16650 AT4G16660
Chr1-11929073.5	244,278734	0,75258303	0,30766217	0,00721986	0,03926948	AT1G06627 AT1G06633 AT1G32920	AT1G32910 AT1G06627 AT1G06633 AT1G32920 AT1G32928 AT1G32930
Chr4-12536992.5	80,0005785	1,07974098	0,44226826	0,0073158	0,03973506	AT4G24150	AT4G24150 AT4G24160
Chr3-6538438.5	95,0710595	1,06558423	0,43662574	0,00733351	0,03977499	AT3G18950	AT3G18950 AT3G18952
Chr1-7992927.5	55,1948011	1,28439318	0,5265587	0,00735948	0,03985951		AT1G22620 AT1G22610
Chr5-19302097	69,3927909	1,13857098	0,4684053	0,00753403	0,04072661	AT5G47610 AT5G47620	AT5G47590 AT5G47600 AT5G47610 AT5G47620
Chr3-22303954	56,6339946	1,2299883	0,50608174	0,00754079	0,04072661	AT3G60330 AT3G60340	AT3G60330 AT3G60340 AT3G60350
Chr3-1121045	53,8834926	1,26582353	0,52211161	0,0076662	0,0413458	AT3G04240 AT3G04250	AT3G04240 AT3G04250 AT3G04260
Chr2-12359310	47,8595551	1,31862727	0,54411484	0,00768724	NA	AT2G28800	AT2G28800
Chr5-7358599	43,81425	1,38443622	0,57225453	0,00777592	NA	AT5G22210	AT5G22200 AT5G22210 AT5G22220
Chr4-17601191	65,1503746	1,15897316	0,47927796	0,0077995	0,04198974	AT4G37435 AT4G37440	AT4G37432 AT4G37430 AT4G37435 AT4G37440 AT4G37445

Postion	baseMean	log2(FC)	lfcSE	p-value	p-adj	gene 1 kb upstream to 1 kb downstream	gene 3 kb upstream to 3 kb downstream
Chr2-14546643.5	170,158716	0,90604459	0,37474026	0,00780747	0,04198974	AT2G34510	AT2G34510 AT2G34520 AT2G34530
Chr5-5939194	172,947249	0,81879015	0,33917039	0,00788714	0,04235888	AT5G17920 AT5G17930	AT5G17920 AT5G17930
Chr5-15378489.5	66,2196591	1,14567945	0,47511424	0,00794621	0,04261655	AT5G38410	AT5G38400 AT5G38410 AT5G05745 AT5G05725 AT5G38420
Chr5-24834069.5	54,2614314	1,23705609	0,51367286	0,00801445	0,04292259	AT5G61810 AT5G61820	AT5G61800 AT5G61810 AT5G61820 AT5G61830
Chr4-12687268	250,435686	0,96580587	0,401366	0,00805757	0,04309344	AT4G24570 AT4G24580	AT4G24560 AT4G24565 AT4G24570 AT4G24580
Chr5-23501249	126,371275	0,92987519	0,38705346	0,00814291	0,0434593	AT5G58060 AT5G58070 AT5G58080	AT5G58060 AT5G58070 AT5G58080
Chr1-7160719	69,5049322	1,12881644	0,46997016	0,00815531	0,0434593	AT1G20650	AT1G20640 AT1G20650
Chr3-19166506.5	83,8782165	1,03246422	0,42989351	0,00816012	0,0434593		AT3G51660 AT3G51670
Chr4-18558954.5	92,8472705	0,99229594	0,41325428	0,00817125	0,0434593	AT4G40040 AT4G40042 AT4G40045	AT4G40030 AT4G40040 AT4G40042 AT4G40045 AT4G40050
Chr5-8775060.5	373,270182	0,70722159	0,2950763	0,0082708	0,04392788	AT5G25280	AT5G25280 AT5G03955
Chr1-21036936.5	116,394304	0,91763565	0,38311867	0,00830625	0,04399984	AT1G56210	AT1G56210
Chr5-24543378.5	81,1837972	1,05947661	0,44234638	0,00830726	0,04399984	AT5G60980	AT5G08985 AT5G60980 AT5G60990
Chr1-25559191	68,937688	1,12159047	0,46857805	0,00834187	0,04407091	AT1G68185 AT1G68190	AT1G68185 AT1G68190 AT1G68200
Chr4-12612590.5	126,799731	0,9601516	0,40114514	0,00834363	0,04407091	AT4G24370 AT4G07260 AT4G24380 AT4G24390	AT4G24350 AT4G07255 AT4G24370 AT4G07260 AT4G24380 AT4G24390
Chr1-6034313	74,2814159	1,08628299	0,45420974	0,00838781	0,04424339	AT1G17545 AT1G17550	AT1G17540 AT1G17545 AT1G17550
Chr3-22086435	81,8448409	1,07220184	0,44856774	0,0084178	0,04434067	AT3G59770 AT3G59780	AT3G59770 AT3G59780
Chr1-11774314	63,5530452	1,14519901	0,479737	0,00849003	0,04461328	AT1G32550 AT1G32560	AT1G32550 AT1G32560 AT1G32570
Chr3-9375815.5	83,382413	1,05546775	0,44216967	0,00849279	0,04461328	AT3G25717	AT3G25716 AT3G25717 AT3G04935 AT3G04955
Chr1-25403374	97,4150966	1,15108138	0,48242036	0,00851511	0,04464858	AT1G67750	AT1G67750 AT1G67760
Chr3-1833694.5	193,352887	0,78242979	0,32796321	0,00852276	0,04464858	AT3G06080	AT3G06070 AT3G06080
Chr2-11059060	70,0398182	1,24318779	0,5213612	0,00855108	0,04473592	AT2G25930 AT2G08135	AT2G25920 AT2G25930 AT2G08135
Chr1-26699458.5	68,7759923	1,15275987	0,48467612	0,00869368	0,04537065	AT1G70790	AT1G09197 AT1G70790
Chr5-19365100	58,6177481	1,19205886	0,50122046	0,00869604	0,04537065		AT5G47820
Chr1-6939565.5	63,4765171	1,14148997	0,48144691	0,00887105	0,04622092	AT1G20010	AT1G19990 AT1G20000 AT1G20010 AT1G20015 AT1G05517
Chr1-4154901.5	84,8343999	1,20984135	0,511407	0,00899773	0,04681748	AT1G12240	AT1G12240 AT1G12244
Chr2-8542578	59,7813455	1,1942674	0,50551206	0,00907631	0,04711021		
Chr1-5265211.5	98,6919756	1,03872575	0,43969097	0,00907853	0,04711021	AT1G15290	AT1G15290
Chr1-11931540	124,724135	0,93895877	0,39806717	0,0091672	0,04750612	AT1G32928 AT1G32930	AT1G32920 AT1G32928 AT1G32930
Chr1-25890559	85,910023	1,01691245	0,43157845	0,00922991	0,04767841	AT1G68870 AT1G68872	AT1G68862 AT1G68870 AT1G68872 AT1G68875 AT1G68877 AT1G09017
Chr5-22369052.5	76,8012443	1,09093313	0,46299873	0,00923065	0,04767841	AT5G55110 AT5G55120	AT5G55110 AT5G55120 AT5G55125
Chr1-25657954	69,7175894	1,14396492	0,4855641	0,00923769	0,04767841	AT1G68440	AT1G68430 AT1G68440
Chr5-4445117.5	164,974551	0,93028258	0,39503009	0,00926219	0,04774069	AT5G13760 AT5G13770	AT5G13760 AT5G13770 AT5G13780
Chr5-20069600	80,7131144	1,0398004	0,44185497	0,00930476	0,04783819	AT5G49470 AT5G49480	AT5G49470 AT5G49480 AT5G00605
Chr5-25291096.5	206,455952	0,82487777	0,35053279	0,00930602	0,04783819	AT5G63040 AT5G09125 AT5G09130	AT5G63040 AT5G09125 AT5G09130 AT5G63050 AT5G09135
Chr5-19896392	144,688197	0,83901421	0,35672606	0,00933677	0,0479321	AT5G49100	AT5G49100
Chr3-18635457	142,521454	0,84053446	0,35751492	0,00936033	0,04798887	AT3G50260 AT3G50270	AT3G50260 AT3G50270 AT3G50280
Chr1-28876326.5	87,1049724	1,08219466	0,46067571	0,00940825	0,04817026	AT1G76890	AT1G76890 AT1G76892
Chr1-2283086.5	60,6884451	1,24811849	0,53170684	0,00945296	0,0483347	AT1G07430	AT1G07420 AT1G07430
Chr3-822743.5	56,8048356	1,25265173	0,53409247	0,00950376	0,04840199	AT3G03460	AT3G03450 AT3G03460 AT3G03470
Chr1-26079944.5	74,7837139	1,09172497	0,46547887	0,00950384	0,04840199	AT1G69370	AT1G69370 AT1G69380
Chr5-6170037	169,770844	0,90087681	0,38410751	0,00950393	0,04840199		AT5G18570
Chr4-10291783.5	115,117295	0,90351113	0,38543531	0,00953572	0,04849955	AT4G18700	AT4G18700
Chr3-5175768	72,0213309	1,16374121	0,49675714	0,00957299	0,04862472	AT3G15356 AT3G15351	AT3G15354 AT3G15359 AT3G15356 AT3G15351 AT3G15358
Chr2-17379315	92,3668326	0,97124623	0,4151073	0,00964839	0,04893482	AT2G41680	AT2G41680 AT2G41690
Chr1-22814161.5	95,1433581	1,10333611	0,47164892	0,00965953	0,04893482	AT1G61780 AT1G61790	AT1G61770 AT1G61780 AT1G61790
Chr3-1644435.5	110,163912	0,91717868	0,39248414	0,00972335	0,04919324	AT3G01665 AT3G05650 AT3G01675	AT3G05640 AT3G01665 AT3G05650 AT3G01675
Chr5-7179537.5	79,0686162	1,10388118	0,47257474	0,00974857	0,04925592		AT5G21105 AT5G21120
Chr4-6799936	69,3080429	1,10251747	0,4721261	0,00976601	0,04927922	AT4G11150	AT4G11150 AT4G11160
Chr3-18530105.5	65,731148	1,14860679	0,49222232	0,00981064	0,04933007	AT3G49970 AT3G49980	AT3G49970 AT3G49980 AT3G49990
Chr3-17778378	75,1167248	1,1990842	0,51386389	0,00981184	0,04933007	AT3G48140	AT3G48131 AT3G48140 AT3G48150
Chr4-14545889.5	67,057822	1,10729141	0,47467772	0,00983136	0,04933007	AT4G29700 AT4G08205 AT4G29710	AT4G08195 AT4G29700 AT4G08205 AT4G29710
Chr2-17504732	76,7618308	1,05169344	0,45085605	0,00983302	0,04933007	AT2G09320	AT2G41930 AT2G09320 AT2G41940
Chr2-17709961.5	78,2876254	1,11567039	0,47833962	0,00984032	0,04933007	AT2G42520 AT2G42530 AT2G42540	AT2G42520 AT2G42530 AT2G42540
Chr1-6622114	255,513124	0,71058288	0,30517283	0,00994383	0,04968552	AT1G19180	AT1G08925 AT1G05473 AT1G19180 AT1G19190 AT1G19200
Chr5-4193546.5	103,453256	0,98978957	0,42508726	0,00994441	0,04968552		AT5G00390 AT5G13180
Chr3-8213688.5	55,4603843	1,18923224	0,51078892	0,00995004	0,04968552	AT3G23090	AT3G23090

Table S2. Genes whose transcript levels were significantly changed in 3-day-old etiolated *bbx14-1* seedlings compared to Col-0.

target	adj.pval bbx14_dark-Col_dark	**log2FC bbx14_dark-Col_dark**	Gene Model Type	All Gene Symbols	Col_dark.brep1	Col_dark.brep2	Col_dark.brep3	bbx14_dark.brep1	bbx14_dark.brep2	bbx14_dark.brep3	glk1glk2_dark.brep1	glk1glk2_dark.brep2	glk1glk2_dark.brep3
AT5G35935	8,32E-05	**-3,28174727**	transposable_element_gene	0	21,67238	23,1827	18,34258	2,886879	2,158264	1,526182	1,992514	0,845762	1,235804
AT1G19050	0,0236877	**-2,41972181**	protein_coding	RESPONSE REGULATOR 7 (ARR7)	14,860644	21,100677	25,696069	3,792968	3,869425	3,561901	4,707734	5,921548	3,86554
AT4G08093	0,0236877	**5,74868025**	pseudogene	0	0,435084	0	0	7,300874	7,907234	7,878611	0,563972	0,699016	0,480411
AT5G26270	0,01112168	**-1,29586323**	protein_coding	0	61,659025	61,223475	84,543191	31,564524	28,985508	23,935153	24,918605	29,148114	32,673958
AT4G04223	0,00077126	**2,38742634**	other_rna	0	18,184059	21,605697	28,509125	119,230816	102,931929	139,177523	13,551214	8,725097	5,85488
AT5G43500	0,02018059	**-1,20121838**	protein_coding	ACTIN-RELATED PROTEIN 9 (ATARP9);ACTIN-RELATED PROTEIN 9 (ARP9)	30,70714	34,368455	25,619634	12,457122	13,574492	13,4853	8,868059	9,060376	10,151346
AT1G77870	0,0236877	**-1,14321792**	protein_coding	MEMBRANE-ANCHORED UBIQUITIN-FOLD PROTEIN 5 PRECURSOR (MUB5)	32,671947	38,035992	38,949317	15,772003	15,664028	18,869606	16,188171	20,544858	18,014208
AT3G30720	5,99E-05	**6,41170449**	protein_coding	QUA-QUINE STARCH (QQS)	2,410026	2,434022	3,947105	234,846939	230,127136	309,29721	0,24011	0,462585	0,705425
AT2G01422	0,03662701	**4,29779935**	other_rna	0	0	0,331422	0,325694	5,470839	4,112089	5,490648	0	0	0
AT2G01010	0,00383827	**1,59227802**	ribosomal_rna	0	226,494944	222,719814	201,449459	655,175181	776,031582	563,24936	783,524336	734,088637	790,902885
AT1G67105	0,0236877	**1,84864829**	other_rna	0	2,838764	5,255271	3,831474	15,342455	13,263554	14,670843	19,423588	21,34152	17,643313
AT3G29633	0,00329186	**7,43993473**	protein_coding	0	0	0	0,108841	17,903482	12,08179	13,748028	0	0	0

Table S3. Genes whose transcript levels were significantly changed in etiolated *bbx14-1* seedlings that were shifted to light for 1 day.

Locus Identifier	Base mean	log2(FC)	StdErr	p-value	p-adj	Locus Identifier	Gene Model Description	Primary Gene Symbol	Col_DL_1	Col_DL_2	Col_DL_3	*bbx14* _DL_1	*bbx14* _DL_2	*bbx14* _DL_3
AT5G46915	5,12976011	-3,67215745	0,90283106	4,75E-05	0,0045098	AT5G46915	transcriptional	.	5,04591946	10,0485621	8,06860315	0	0	0
AT2G42530	9,9554942	-3,63042362	0,63416089	1,04E-08	3,63E-06	AT2G42530	Encodes COR15	COLD REGULAT	29,4345302	16,3289134	42,3601666	1,59907859	2,14941828	2,00077889
AT4G36700	4,21734901	-3,46951518	0,99744487	0,00050441	0,02556878	AT4G36700	RmlC-like cupi	.	20,1836778	10,0485621	16,1372063	0	2,14941828	0
AT1G28870	2,10334231	-3,46160364	0,942711	0,00024069	0,01465429	AT1G28870	tRNA-Pro (anti	.	3,36394631	3,76821078	8,06860315	0	0	0
AT2G17040	7,12046594	-3,1850184	0,98419687	0,0012115	0,04781296	AT2G17040	Member of the	NAC DOMAIN C	15,1377584	2,51214052	4,03430158	0	0	0
AT1G07050	37,6474198	-3,15993484	0,39988054	2,74E-15	3,19E-12	AT1G07050	CCT motif fami	.	141,285745	102,997761	151,286309	11,1935501	19,3447646	12,0046734
AT4G01525	5,20040274	-3,01367043	0,78323836	0,00011923	0,00890232	AT4G01525	Member of Sad	SADHU NON-CO	8,40986577	12,5607026	6,05145237	1,59907859	0	0
AT3G05955	17,916159	-2,74648463	0,6208839	9,71E-06	0,00130076	.	.	.	19,3426913	17,5849837	30,2572618	5,59677506	2,14941828	0
AT5G42900	82,2739475	-2,67896269	0,44032668	1,17E-09	5,29E-07	AT5G42900	cold regulated	COLD REGULAT	338,91759	208,507663	279,375384	45,5737397	38,6895291	36,0140201
AT5G05200	944,014295	-2,6100464	0,17396767	7,01E-51	1,55E-46	AT5G05200	Protein kinase	.	2048,6433	1994,63957	2183,56573	369,387154	364,326399	274,106708
AT5G33395	11,8328027	-2,54921914	0,7560453	0,00074684	0,03438723	AT5G33395	CACTA-like trar	.	35,3214362	20,0971242	40,3430158	6,39631435	0	6,00233668
AT2G43620	35,2612809	-2,54765811	0,68371871	0,0001944	0,01259981	AT2G43620	Chitinase famil	.	206,882698	62,8035131	30,2572618	17,5898645	4,29883657	20,0077889
AT3G48280	15,9745755	-2,48949494	0,57851814	1,68E-05	0,00196837	AT3G48280	putative cytoc	CYTOCHROME	25,2295973	35,1699673	14,1200555	4,79723576	4,29883657	2,00077889
AT4G12480	55,7145763	-2,47170458	0,7044997	0,00045072	0,02349376	AT4G12480	Encodes a puta	EARLY ARABIDO	23,5476242	20,0971242	20,1715079	0	6,44825485	2,00077889
AT4G05130	10,422311	-2,441166	0,67432897	0,00029444	0,01721553	AT4G05130	equilibrative n	EQUILIBRATIVE	8,40986577	7,53642157	12,1029047	3,19815717	0	0
AT4G28520	40,997746	-2,35390633	0,72817857	0,00122671	0,04824129	AT4G28520	Encodes a 12S	CRUCIFERIN 3 (	275,843597	70,3399346	58,4973729	23,9861788	19,3447646	22,0085678
AT1G04587	4,53530161	-2,22407487	0,68474675	0,00116209	0,04644362	.	.	.	7,56887919	11,3046323	8,06860315	2,39861788	1,07470914	1,00038945
AT2G40130	26,1867128	-2,11375839	0,54433923	0,00010311	0,00791232	AT2G40130	Encodes a mem	SMAX1-LIKE 8 (	72,3248456	32,6578268	32,2744126	7,99539294	12,8965097	8,00311557
AT1G68050	299,097884	-2,07786154	0,15685222	4,68E-40	3,45E-36	AT1G68050	Encodes FKF1,	FLAVIN-BINDIN	1005,81995	921,955572	920,829335	227,868699	212,79241	230,089573
AT5G63530	26,2614689	-2,00377505	0,55098148	0,00027611	0,01640423	AT5G63530	Farnesylated p	FARNESYLATED	11,7738121	15,0728431	34,2915634	3,19815717	2,14941828	8,00311557
AT2G23110	5,01715786	-2,00059508	0,61818012	0,00121105	0,04781296	AT2G23110	Late embryoge	.	13,4557852	7,53642157	12,1029047	3,19815717	2,14941828	2,00077889
AT1G06693	18,4537881	-1,92693744	0,48727192	7,67E-05	0,0062763	.	.	.	27,752557	17,5849837	19,1629325	8,79493223	3,22412743	3,00116834
AT4G33980	94,83619	-1,91769971	0,26864743	9,45E-13	6,73E-10	AT4G33980	FUNCTIONS IN:	COLD-REGULAT	352,373376	273,823317	272,315356	67,1613007	91,3502771	77,0299874
AT2G33380	38,0037425	-1,81095023	0,45124565	5,99E-05	0,00531621	AT2G33380	Encodes a calci	RESPONSIVE TO	15,1377584	26,3774755	17,1457817	7,99539294	4,29883657	2,00077889
AT1G22490	56,5974994	-1,80523906	0,40855164	9,93E-06	0,00130778	AT1G22490	basic helix-loo	(BHLH094)	134,557852	178,361977	129,09765	40,776504	30,091856	50,0194723
AT5G46500	14,3124876	-1,78361757	0,54660595	0,00110209	0,04499758	AT5G46500	BEST Arabidop	.	10,0918389	17,5849837	17,1457817	1,59907859	4,29883657	6,00233668
AT1G57820	57,1153456	-1,77718574	0,43117264	3,76E-05	0,00370986	AT1G57820	Encodes a 645-	VARIANT IN ME	62,2330067	123,094886	50,4287697	27,184336	17,1953463	20,0077889
AT2G40080	8,43817723	-1,73369716	0,51769544	0,0008114	0,03667264	AT2G40080	Encodes a nove	EARLY FLOWER	18,5017047	27,6335457	32,2744126	6,39631435	6,44825485	10,0038945
AT5G66400	89,3801011	-1,68177762	0,302034	2,57E-08	8,37E-06	AT5G66400	Belongs to the	RESPONSIVE TO	134,557852	160,776993	119,011897	51,1705148	25,7930194	48,0186934
AT5G24470	1438,41844	-1,67972444	0,22116286	3,08E-14	2,84E-11	AT5G24470	Encodes a pseu	PSEUDO-RESPO	4459,75182	3622,50663	4376,20864	1090,5716	1464,82856	1289,502
AT4G12320	253,972631	-1,66953853	0,24822713	1,75E-11	1,10E-08	AT4G12320	member of CYP	CYTOCHROME	455,814725	297,688652	394,352979	102,34103	134,338643	120,046734
AT3G47380	19,5137695	-1,65347486	0,45023198	0,00024019	0,01465429	AT3G47380	Plant invertase	(ATPMEI11)	18,5017047	45,2185294	44,3773173	9,59447152	12,8965097	10,0038945
AT1G11210	109,543576	-1,61743708	0,39644788	4,51E-05	0,00434975	AT1G11210	Protein of unkr	.	222,020456	150,728431	157,337761	38,3778861	64,4825485	64,0249246
AT5G48250	172,612143	-1,59404894	0,18444571	5,51E-18	1,01E-14	AT5G48250	B-box type zinc	B-BOX DOMAIN	434,79006	405,710694	373,172896	105,539187	154,758116	141,054912
AT1G62260	21,5699681	-1,58593728	0,42096009	0,00016494	0,01118185	AT1G62260	Encodes MITOC	MITOCHONDRI	22,7066376	20,0971242	28,240111	7,99539294	4,29883657	10,0038945
AT5G43500	395,114121	-1,55024018	0,13909353	7,55E-29	3,34E-25	AT5G43500	encodes a prot	ACTIN-RELATED	635,785852	525,037369	599,093784	193,488509	228,913047	178,069321
AT3G28660	18,5669881	-1,49886443	0,43724818	0,00060816	0,02909295	AT3G28660	Tetratricopept	.	23,5476242	28,889616	18,1543571	7,99539294	9,67238228	6,00233668
AT3G26230	87,8419296	-1,40701918	0,25464316	3,29E-08	1,02E-05	AT3G26230	putative cytoc	CYTOCHROME	79,8937248	85,4127777	56,4802221	35,1797289	23,6436011	22,0085678
AT4G11900	85,7339836	-1,40620131	0,31986881	1,10E-05	0,00142392	AT4G11900	S-locus lectin p	.	112,692201	110,534183	114,977595	31,9815717	51,5860388	42,0163567
AT5G52310	506,502621	-1,40287936	0,20735307	1,33E-11	8,63E-09	AT5G52310	cold regulated	LOW-TEMPERA	1359,87529	1258,5824	1323,25092	393,373332	612,584211	474,184597
AT1G03790	105,662589	-1,38674727	0,40290536	0,00057771	0,02806152	AT1G03790	Encodes SOMN	SOMNUS (SOM	306,119114	231,116928	252,143849	103,140569	70,9308034	118,045955
AT4G21380	32,6894844	-1,33361576	0,40724783	0,00105773	0,04394155	AT4G21380	encodes a puta	RECEPTOR KINA	58,8690604	60,2913725	72,6174284	19,9884823	30,091856	24,0093467
AT5G35935	182,51907	-1,30157009	0,27918214	3,13E-06	0,00053629	AT5G35935	copia-like retro	.	220,338483	222,324436	201,715079	87,9493223	109,620332	60,0233668
AT4G15490	174,154122	-1,28654964	0,19963505	1,16E-10	5,96E-08	AT4G15490	Encodes a prot	(UGT84A3)	289,299382	346,675392	300,555467	119,930894	128,965097	132,051407
AT3G24420	357,271862	-1,27070596	0,29554843	1,71E-05	0,00199137	AT3G24420	alpha/beta-Hyc	(DLK2)	719,88451	1193,26675	1029,75548	473,327262	361,102272	365,142148
AT3G07650	169,981674	-1,27020693	0,19588043	8,90E-11	4,92E-08	AT3G07650	This gene belor	CONSTANS-LIK	397,786651	317,785776	423,601666	173,500027	152,608698	143,055691
AT1G01390	69,8828432	-1,2671267	0,38905597	0,00112626	0,04542223	AT1G01390	UDP-Glycosylt	.	75,6887919	110,534183	72,6174284	15,9907859	42,9883657	46,0179145
AT4G16146	77,8759818	-1,25187673	0,25567053	9,76E-07	0,00019787	AT4G16146	cAMP-regulate	.	124,466013	128,119167	133,131952	67,1613007	55,8848754	36,0140201
AT2G17730	176,560618	-1,24150182	0,12644058	9,34E-23	3,44E-19	AT2G17730	Intrinsic thylak	NEP-INTERACTI	364,988174	374,308938	380,232924	159,907859	156,907535	155,060364
AT4G12290	115,587423	-1,22538155	0,34792915	0,00042842	0,02257681	AT4G12290	Copper amine (	.	153,059557	97,9734804	125,063349	51,1705148	30,091856	76,0295979
AT4G34060	27,4636622	-1,18964665	0,30057045	7,56E-05	0,0062763	AT4G34060	Encodes a prot	DEMETER-LIKE	37,0034094	55,2670915	40,3430158	19,188943	19,3447646	18,00701
AT2G29090	144,40683	-1,18107576	0,1624666	3,60E-13	2,75E-10	AT2G29090	Encodes a prot	CYTOCHROME	226,225389	219,812296	201,715079	86,3502437	106,396205	93,0362185
AT5G46050	160,782645	-1,16514118	0,21504438	6,02E-08	1,73E-05	AT5G46050	Encodes a di- a	NRT1/ PTR FAM	380,966919	365,516446	349,975662	193,488509	171,953463	119,046344
AT2G16660	75,1570742	-1,14221504	0,32003987	0,00035838	0,01987603	AT2G16660	Major facilitate	.	132,875879	90,4370588	123,046198	41,5760433	51,5860388	62,0241457
AT5G61380	945,399515	-1,09554428	0,11590698	3,33E-21	8,29E-18	AT5G61380	Pseudo respon	TIMING OF CAE	2207,58976	2017,24884	2082,70819	992,228263	925,324571	1028,40035
AT5G15970	315,901048	-1,09489497	0,25066518	1,25E-05	0,00155717	AT5G15970	Encodes a gene	(KIN2)	366,670148	330,346479	538,579261	215,875609	176,252299	180,0701
AT4G04450	24,1975448	-1,08817338	0,32296912	0,00075365	0,03462303	AT4G04450	member of WR	(WRKY42)	50,4591946	65,3156536	42,3601666	22,3871002	25,7930194	25,0097362
AT1G17100	246,147834	-1,04750832	0,25284563	3,43E-05	0,00347324	AT1G17100	SOUL heme-bir	HAEM-BINDING	333,030684	363,004305	365,104293	132,723523	177,327008	199,0775
AT5G50450	227,067057	-1,03683166	0,28097306	0,00022413	0,01395321	AT5G50450	HCP-like super	.	433,108087	580,304461	465,961832	206,281138	232,137175	274,106708
AT2G16365	765,300447	-1,02137378	0,15694787	7,63E-11	4,44E-08	AT2G16365	PCH1 binds an	PHOTOPERIOD	1702,99782	1652,98846	1539,08605	839,516258	849,020222	714,278065
AT4G16690	211,590819	-1,01280248	0,30096342	0,00076488	0,03499912	AT4G16690	Encodes a prot	METHYL ESTERA	264,069785	439,624591	334,847031	126,327208	193,447646	188,073216
AT5G20630	2303,28654	-1,01244864	0,11908311	1,86E-17	2,74E-14	AT5G20630	Encodes a germ	GERMIN 3 (GER	4541,32751	4692,6785	5259,72068	2333,05566	2194,55607	2642,02853
AT1G27410	81,558683	-1,0018551	0,29918403	0,00081214	0,03667264	AT1G27410	DNA repair me	.	57,1870872	59,0353023	82,7031823	39,1774254	27,9424377	30,0116834
AT4G28230	68,7840565	1,00197773	0,29184046	0,00059627	0,02877317	AT4G28230	unknown prot	.	31,9574899	22,6092647	24,2058095	55,9677506	37,61482	68,0264823
AT4G09420	100,126002	1,00483417	0,27305934	0,00023332	0,01440362	AT4G09420	Disease resistar	.	79,0527382	62,8035131	70,6002776	175,898645	107,470914	148,057638
AT5G10800	55,2354781	1,00767583	0,26241789	0,00012305	0,00906519	AT5G10800	RNA recognitic	.	35,3214362	18,8410539	26,2229602	56,7672898	51,5860388	59,0229773
AT1G45201	333,494115	1,01476506	0,29011232	0,00046905	0,02422079	AT1G45201	Target of AtGRI	TRIACYLGLYCEI	179,971127	256,238333	227,938039	378,182086	598,612992	381,148379
AT5G53880	106,854514	1,01829652	0,27155942	0,00017697	0,01174525	AT5G53880	unknown prot	.	33,6394631	32,6578268	32,2744126	65,5622221	79,5284765	58,0225879
AT2G36050	368,182705	1,02292476	0,2348869	1,33E-05	0,00162371	AT2G36050	ovate family pr	OVATE FAMILY	203,518752	231,116928	203,73223	471,728183	315,964488	518,201733
AT1G08990	32,6559385	1,02440354	0,30891238	0,00091263	0,03939631	AT1G08990	plant glycogen	PLANT GLYCOG	40,3673557	35,1699673	48,4116189	102,34103	67,7066759	84,0327135
AT2G22810	69,5089299	1,03446679	0,31813312	0,00114725	0,04604037	AT2G22810	key regulatory	1-AMINOCYCLO	55,5051141	37,6821078	30,2572618	75,1566936	107,470914	77,0299874
AT4G22490	845,684299	1,03957079	0,22950485	5,91E-06	0,00090063	AT4G22490	Bifunctional in	.	23,5476242	52,754951	40,3430158	73,557615	77,3790582	86,0334924
AT4G37770	423,045777	1,0414726	0,24736248	2,55E-05	0,00274938	AT4G37770	Encodes an aux	1-AMINO-CYCL	132,875879	82,9006372	102,87469	236,663631	197,746482	232,090352
AT1G55200	54,5715467	1,0450845	0,31803648	0,00101602	0,04252858	AT1G55200	Protein kinase	.	33,6394631	33,913897	46,3944681	95,9447152	94,5744045	48,0186934
AT2G34620	700,709908	1,09083242	0,14044035	8,02E-15	8,06E-12	AT2G34620	Mitochondrial	.	558,415087	589,096952	595,059483	1204,10618	1257,4097	1260,4907
AT5G48490	528,84628	1,10040956	0,15064052	2,78E-13	2,19E-10	AT5G48490	Encodes a prot	DIR1-LIKE (DIR	502,909973	462,233856	547,656439	1167,32737	1104,801	984,383215
AT4G13500	319,737767	1,11088975	0,19597481	1,44E-08	4,90E-06	AT4G13500	unknown prot	.	228,748349	233,629069	294,504015	583,663684	569,595845	491,191218
AT3G23730	816,013734	1,11327058	0,1911162	5,71E-09	2,18E-06	AT3G23730	xyloglucan end	XYLOGLUCAN E	544,959302	698,375065	508,321999	1349,62233	1126,29518	1330,51796
AT3G55240	350,893219	1,11672797	0,31915363	0,00046695	0,02422079	AT3G55240	Overexpressior	.	40,3673557	30,1456863	56,4802221	86,3502437	117,143296	80,0311557
AT2G22330	207,980039	1,12772987	0,32287146	0,00047796	0,02462328	AT2G22330	Encodes a cyto	CYTOCHROME	88,3035906	85,4127777	48,4116189	153,511544	161,206371	180,0701
AT4G33610	108,216884	1,13030549	0,33815107	0,00082996	0,03705643	AT4G33610	glycine-rich pr	.	121,102067	168,313415	110,943293	259,050731	247,183103	382,148768
AT4G13575	512,693687	1,13435437	0,18878423	1,87E-09	7,80E-07	AT4G13575	unknown prot	.	79,0527382	80,3884967	111,951869	194,288048	210,642992	196,076331
AT1G01060	319,072792	1,13535874	0,26063142	1,32E-05	0,00162371	AT1G01060	LHY encodes a	LATE ELONGAT	74,0068188	108,022042	112,960444	161,506937	279,424377	214,083341
AT1G55990	31,0829095	1,13596375	0,31564572	0,00031962	0,01854043	AT1G55990	glycine-rich pr	.	37,0034094	40,1942484	37,3172896	95,1451759	62,3331302	95,0369974
AT1G26330	28,2637144	1,13677495	0,33001209	0,00057181	0,02783592	AT1G26330	DNA binding; F	.	16,8197315	12,5607026	20,1715079	31,9815717	42,9883657	38,014799
AT3G21330	835,760024	1,14837425	0,13480135	1,61E-17	2,54E-14	AT3G21330	basic helix-loo	.	287,617409	241,16549	280,38396	577,26737	580,342937	648,252361
AT4G39510	95,864351	1,14993422	0,26887467	1,90E-05	0,00218206	AT4G39510	member of CYP	CYTOCHROME	45,4132751	32,6578268	38,325865	74,3571543	98,8732411	92,035829
AT2G35290	42,8439927	1,15306323	0,344385	0,00081344	0,03667264	AT2G35290	unknown prot	SMALL AUXIN U	33,6394631	50,2428104	32,2744126	65,5622221	85,9767314	110,042839
AT1G60060	96,2945439	1,15587906	0,323211	0,00034858	0,01955299	AT1G60060	Serine/threoni	.	45,4132751	55,2670915	28,240111	108,737344	90,2755679	92,035829
AT3G29370	149,645791	1,17850014	0,22052233	9,09E-08	2,45E-05	AT3G29370	Encodes a atyp	P1R3 (P1R3)	37,0034094	30,1456863	32,2744126	68,7603792	66,6319668	95,0369974
AT1G66100	439,782649	1,1922733	0,1551949	1,56E-14	1,50E-11	AT1G66100	Predicted to er	.	119,420094	133,143448	147,252008	311,820324	315,964488	288,112161
AT1G21270	220,059188	1,19783729	0,33889998	0,00040857	0,0217062	AT1G21270	cytoplasmic se	WALL-ASSOCIA	40,3673557	45,2185294	26,2229602	63,9631435	103,172078	96,0373868

Locus Identifier	Base mean	log2(FC)	StdErr	p-value	p-adj	Locus Identifier	Gene Model Description	Primary Gene Symbol	Col_DL_1	Col_DL_2	Col_DL_3	*bbx14* _DL_1	*bbx14* _DL_2	*bbx14* _DL_3
AT2G20750	39,8214353	1,20545524	0,36961206	0,00110861	0,04499758	AT2G20750	member of BET	EXPANSIN B1 (I	16,8197315	22,6092647	20,1715079	51,9700541	58,0342937	30,0116834
AT1G63230	35,5113591	1,20947406	0,33931448	0,0003646	0,02009489	AT1G63230	Tetratricopept	.	9,25085235	20,0971242	12,1029047	28,7834146	38,6895291	28,0109045
AT5G13580	56,7994923	1,23709512	0,30610804	5,31E-05	0,00487326	AT5G13580	Belongs to a cl	ATP-BINDING C	63,9149798	57,779232	64,5488252	143,917073	155,832826	146,056859
AT3G53650	29,1560676	1,24821047	0,35086986	0,00037444	0,02053462	AT3G53650	Histone superf	.	25,2295973	15,0728431	10,0857539	39,9769647	47,2872022	38,014799
AT4G03210	738,644908	1,25705902	0,15969222	3,50E-15	3,86E-12	AT4G03210	encodes a mem	XYLOGLUCAN E	264,069785	246,189771	274,332507	665,216692	576,0441	644,250803
AT1G05310	40,7736013	1,27529052	0,36560699	0,00048638	0,02491483	AT1G05310	Pectin lyase-lik	.	20,1836778	32,6578268	22,1886587	60,7649863	45,137784	78,0303768
AT2G47440	1335,8291	1,29361134	0,15402398	4,51E-17	6,23E-14	AT2G47440	Tetratricopept	.	543,277329	507,452385	432,678844	1106,56238	1098,35274	1450,5647
AT3G14210	1029,36991	1,29550322	0,3023072	1,82E-05	0,00211084	AT3G14210	A semidomina	EPITHIOSPECIF	166,515342	95,4613398	108,926143	331,808807	292,320887	308,119949
AT1G13650	46,7843957	1,29632729	0,3919103	0,00094061	0,04028753	AT1G13650	BEST Arabidop	.	25,2295973	25,1214052	12,1029047	70,3594578	47,2872022	40,0155778
AT5G45650	67,5230441	1,3112565	0,28116441	3,11E-06	0,00053629	AT5G45650	subtilase famil	.	26,9115705	40,1942484	36,3087142	60,7649863	94,5744045	104,040502
AT4G04610	58,7389025	1,34720507	0,36420383	0,00021642	0,01358805	AT4G04610	Encodes a prot	APS REDUCTAS	23,5476242	15,0728431	24,2058095	44,7742004	66,6319668	56,021809
AT4G34770	105,514494	1,35232228	0,36855946	0,0002433	0,01477249	AT4G34770	SAUR-like auxi	SMALL AUXIN U	15,1377584	25,1214052	32,2744126	49,5714362	53,7354571	87,0338818
AT5G46690	180,176454	1,36741905	0,23127532	3,37E-09	1,35E-06	AT5G46690	beta HLH prote	BETA HLH PRO	61,3920201	42,7063889	66,565976	151,912466	139,712188	158,061532
AT1G62280	22,4524657	1,42216065	0,39175441	0,00028316	0,01677798	AT1G62280	Encodes a prot	SLAC1 HOMOL	20,1836778	20,0971242	30,2572618	55,9677506	75,2296399	62,0241457
AT2G21200	65,2579819	1,46349834	0,42022933	0,00049654	0,02528557	AT2G21200	SAUR-like auxi	SMALL AUXIN U	19,3426913	23,865335	25,2143849	76,7557722	64,4825485	55,0214195
AT1G66080	35,4202985	1,49860938	0,43164376	0,00051685	0,02607988	AT1G66080	unknown prot	.	11,7738121	15,0728431	12,1029047	49,5714362	38,6895291	26,0101256
AT3G17660	30,5740199	1,50847937	0,43871358	0,00058513	0,0282975	AT3G17660	A member of A	ARF-GAP DOM	10,0918389	10,0485621	8,06860315	17,5898645	27,9424377	40,0155778
AT5G24770	24,7160104	1,54347092	0,34790576	9,14E-06	0,00123995	AT5G24770	Has acid phosp	VEGETATIVE ST	16,8197315	17,5849837	16,1372063	43,1751219	60,1837119	48,0186934
AT5G43890	62,0664258	1,5545567	0,33668508	3,89E-06	0,00063663	AT5G43890	Encodes a YUC	YUCCA5 (YUC5	28,5935436	35,1699673	42,3601666	124,72813	79,5284765	114,044397
AT2G01008	3555,21896	1,56066853	0,2853549	4,52E-08	1,35E-05	AT2G01008	FUNCTIONS IN:	.	1528,07261	1958,21354	1087,24427	3693,87154	5258,55183	4795,86701
AT4G08950	1236,32076	1,58002655	0,19150329	1,58E-16	2,05E-13	AT4G08950	EXORDIUM (EX	EXORDIUM (EX	343,122523	472,282418	340,898483	1237,68683	1014,52543	1226,47746
AT1G64210	13,9850781	1,58490138	0,4523415	0,00045872	0,02385443	AT1G64210	Leucine-rich re	.	3,36394631	10,0485621	12,1029047	22,3871002	23,6436011	32,0124623
AT5G54190	67,2020752	1,64707391	0,30993484	1,07E-07	2,82E-05	AT5G54190	light-depender	PROTOCHLORO	11,7738121	17,5849837	14,1200555	41,5760433	40,8389474	56,021809
AT5G48740	16,0663895	1,66963441	0,49961988	0,00083234	0,03708788	AT5G48740	Leucine-rich re	.	6,72789261	5,02428104	2,01715079	19,188943	17,1953463	12,0046734
AT1G74440	22,7275501	1,67795522	0,46817975	0,00033837	0,01927428	AT1G74440	Protein of unk	.	11,7738121	2,51214052	10,0857539	30,3824932	33,3159834	23,0089573
AT3G21950	34,7331393	1,73045323	0,34089535	3,85E-07	9,05E-05	AT3G21950	S-adenosyl-L-m	.	16,8197315	10,0485621	10,0857539	37,5783468	42,9883657	50,0194723
AT3G29644	52,6202212	1,73306898	0,30426313	1,23E-08	4,24E-06	AT3G29644	Potential natu	SHORT OPEN R	21,865651	26,3774755	18,1543571	93,5460973	54,8101662	75,0292085
AT1G11070	37,5607011	1,80659044	0,43711787	3,58E-05	0,00356525	AT1G11070	BEST Arabidop	.	8,40986577	17,5849837	8,06860315	41,5760433	23,6436011	58,0225879
AT2G44910	162,046528	1,84559643	0,1952936	3,38E-21	8,29E-18	AT2G44910	Encodes a hom	HOMEOBOX-LE	57,1870872	46,4745997	54,4630713	171,101409	209,568283	200,077889
AT2G16586	425,606879	1,84615539	0,3907763	2,31E-06	0,00042879	AT2G16586	unknown prot	.	146,331664	218,556225	98,8403886	438,147533	790,985928	510,198618
AT1G01250	16,2847671	1,8785681	0,52466729	0,00034295	0,01943444	AT1G01250	encodes a mem	.	1,68197315	7,53642157	2,01715079	17,5898645	10,7470914	14,0054522
AT4G04223	116,182664	1,93558469	0,25697186	4,99E-14	4,41E-11	AT4G04223	Unknown gene	.	58,8690604	62,8035131	68,5831268	235,864092	277,274959	227,088404
AT1G67105	40,5900807	1,96016747	0,53298367	0,00023532	0,01448713	AT1G67105	other RNA	.	20,1836778	25,1214052	14,1200555	60,7649863	98,8732411	92,035829
AT5G35490	16,5182931	1,96478396	0,60413809	0,00114511	0,04604037	AT5G35490	Encodes MRU1	MTO 1 RESPON	3,36394631	6,28035131	2,01715079	9,59447152	22,568892	20,0077889
AT4G06120	64,9198059	2,23914403	0,65498503	0,0006294	0,03004393	.	.	.	0,84098658	10,0485621	1,00857539	23,9861788	31,1665651	13,0050628
AT1G45616	9,57129391	2,35856369	0,64407215	0,0002503	0,01511425	AT1G45616	receptor like p	RECEPTOR LIKE	1,68197315	7,53642157	0	14,3917073	16,1206371	22,0085678
AT2G07661	6,96750126	2,38074612	0,66364207	0,000334	0,01912357	.	.	.	1,68197315	1,25607026	1,00857539	7,19585364	12,8965097	8,00311557
AT3G16670	351,714073	2,41763332	0,72167762	0,00080806	0,03667141	AT3G16670	Pollen Ole e 1 a	.	1,68197315	2,51214052	0	7,99539294	4,29883657	30,0116834
AT1G73550	8,07249512	2,48974688	0,76187538	0,00108341	0,04452508	AT1G73550	Encodes a Prot	.	0	2,51214052	2,01715079	9,59447152	15,045928	10,0038945
AT5G16023	40,7455523	2,52306002	0,67439209	0,00018312	0,01204488	AT5G16023	Encodes a plan	ROTUNDIFOLIA	1,68197315	0	2,01715079	9,59447152	10,7470914	16,0062311
AT5G07105	8,10149323	2,67821236	0,69887397	0,00012701	0,00926749	.	.	.	0,84098658	2,51214052	0	10,3940108	10,7470914	8,00311557
AT5G07560	5,34608511	2,89821891	0,85707508	0,00072085	0,03326004	AT5G07560	Lipid-binding c	GLYCINE-RICH	1,68197315	0	0	3,19815717	9,67238228	16,0062311
AT5G25970	9,7594551	2,9249421	0,87370577	0,00081473	0,03667264	AT5G25970	Core-2/I-branc	.	0	0	0	7,99539294	4,29883657	2,00077889
AT5G53486	8,30795313	2,94099551	0,89015431	0,00095344	0,04052313	AT5G53486	unknown prot	.	0	0	0	4,79723576	4,29883657	6,00233668
AT3G14550	6,21792176	2,95475166	0,87133089	0,00069618	0,0323922	AT3G14550	Encodes a prot	GERANYLGERA	0	0	1,00857539	6,39631435	4,29883657	12,0046734
AT2G15800	20,3108903	2,99379813	0,6853486	1,25E-05	0,00155717	AT2G15800	transposable e	.	1,68197315	0	4,03430158	22,3871002	19,3447646	25,0097362
AT3G52160	6,37972422	3,17107596	0,89907164	0,00042021	0,02221774	AT3G52160	Encodes KCS15	3-KETOACYL-CO	0,84098658	0	0	3,19815717	8,59767314	17,0066206
AT5G35960	3,49221035	3,19239926	0,98259738	0,00115836	0,04637854	AT5G35960	Protein kinase	.	0	0	0	1,59907859	8,59767314	8,00311557
AT2G15810	27,8345191	3,25314958	0,59218396	3,94E-08	1,21E-05	AT2G15810	Mutator-like tr	.	1,68197315	10,0485621	0	33,5806503	42,9883657	52,0202512
AT3G06955	17,3411933	3,29152813	0,65694364	5,43E-07	0,00011888	.	.	.	3,36394631	0	0	13,592168	17,1953463	23,0089573
AT3G14630	10,9274018	3,37559007	0,90114576	0,00017976	0,01185917	AT3G14630	putative cytoc	CYTOCHROME	0	0	0	15,9907859	6,44825485	2,00077889
ATMG00240	3,86677515	3,78731811	0,93941451	5,54E-05	0,00497765	ATMG00240	Gag-Pol-relate	(ORF111A)	0	0	0	11,1935501	2,14941828	12,0046734
AT3G05170	18,5015043	5,98841071	0,83065587	5,63E-13	4,14E-10	AT3G05170	Phosphoglycer	.	0	0	0	32,781111	46,2124931	45,0175251
AT3G30720	290,545355	6,50390455	0,58222952	5,67E-29	3,13E-25	AT3G30720	QQS is an orph	QUA-QUINE ST	1,68197315	0	4,03430158	388,576097	272,976122	260,101256
AT3G29633	161,546171	6,77509237	0,47210189	1,05E-46	1,16E-42	AT3G29633	unknown prot	.	6,72789261	0	0	326,212032	386,895291	390,151884

Table S4. Primers used in this study.

Atg number	Description	Primer sequence (from 5' to 3')
Genotyping		
	SAIL-LB	GCATCTGAATTTCATAACCAATCTCGATACAC
AT1G68520	SAIL_1221_D02-LP	GTGTTGCCAAATTACTGCTGC
AT1G68520	SAIL_1221_D02-RP	TTTTTATCAATGGACCGCAAC
AT1G68520	AT1G68520_LP_check	GAATGAGATGAGTGGTGGGATT
AT1G68520	AT1G68520_RP_check	GAAACAAACCATGTCGAGGTCT
Overexpression of BBX14		
	BBX14-CDS-F	CACCATGATGAAAAGTTTGGCTAGTG
	BBX14-CDS-R	GCAACACCAATTGAAGATCTC
CRISPR/Cas		
	68520-CRISPR-F	ATTGGGGAGGCCAAGGGATCCCA
	68520-CRISPR-R	AAACTGGGATCCCTTGGCCTCCC
RT-qPCR		
AT4G36800	"Housekeeping" gene RCE1	CTGTTCACGGAACCCAATTC GGAAAAAGGTCTGACCGACA
AT1G29910	*LHCB1.2*	CCGTGAGCTAGAAGTTATCC GTTTCCCAAGTAATCGAGTCC
	LHCB2.1	CTCCGCAAGGTTGGTGTATC CGGTTAGGTAGGACGGTGTAT
AT3G27690	*LHCB2.4*	CACTTCAGCAATCCAACACTC GTACCAGATGCTCTGAGGAG
AT3G01500	*CA1*	GAGAAATACGAAACCAACCCT ACATAAGCCCTTTGATCCCA
AT1G67090	*RBCS1A*	ACAACGACATTACTTCCATCAC GTAGTCAACTTCCTTAGCCA
AT3G16140	*PSAH-1*	AATCCATCCGGGCTAATGGT CGCTGACATAAGTAAGCAAAGAG
AT2G28605	*PSBP*	TCCTACAGACAAGAAATCCATCAC ATCAAACCCTCCCTCAGAGG
AT3G21055	*PSBTn*	CTTAAACACATTCCCATCACCT CTACCTTAGCCAAAGAACAAACC
	BBX14	CATACCATGGGTGAAAGTGGA GAGATCTTCAATTGGTGTTGCT
	BBX15	TTTCCATGGTGGAGAATGGAG CGAATCTTCCTTTCATTCGTGG

8. Acknowledgement

My first thanks goes to my supervisor, PD Dr. Tatjana Kleine, for her constant guidance throughout my work and her excellent advice on thesis-related issues, as well as lab work.

I'd like to thank Prof. Dr. Dario Leister for giving me the opportunity to pursue PhD in his research group.

I'm also really thankful for the funding provided by the SFB TRR175 towards my PhD and for the successful collaboration with colleagues from HU Berlin.

I'd like to thank Dr. Duorong Xu for teaching me lab skills and methods. He's always been so helpful and approachable, as well as patient with me through all my failed experiments. He's also given me some really thoughtful feedback and improvement tips.

I'm really grateful to Ramona Kandler for her excellent technical assistance throughout my time in the lab. Thanks also to all the gardeners, especially Albert, who took such good care of my plants.

I'd also like to thank all the lovely people I've met at AG Leister for their expertise and help.

I'd also like to thank Prof. Dr. Thomas Nägele for his constant support and advice from the very beginning of my PhD to the very end.

I'd also like to thank my friends Nastya, Louis, and Sabrina for their positive contributions to my work, helpful tips, and for always being there for me, sharing drinks and food as well as for all the wonderful memories and experiences we shared both at work and outside.

And finally, I’d like to thank my family for their love, unwavering support, and for always encouraging me to keep going and never give up.

9. Permission for republishing

Permission for the Open Access article according to CC BY 4.0 for the article: Atanasov, V., Schumacher, J., Muiño, J. M., Larasati, C., Wang, L., Kaufmann, K., Leister, D., & Kleine, T. (2024). Arabidopsis BBX14 is involved in high light acclimation and seedling development. *The Plant journal : for cell and molecular biology*, *118*(1), 141–158.

Arabidopsis BBX14 is involved in high light acclimation and seedling development

Author: Jose M. Muiño, Catharina Larasati, Liangsheng Wang, et al

Publication: Plant Journal

Publisher: John Wiley and Sons

Date: Dec 21, 2023

Open Access Article

Order Date	15-May-2024	**Type of Use**	Republish in a thesis/dissertation
Order License ID	1484094-1		
ISSN	1365-313X	**Publisher**	BLACKWELL PUBLISHING
		Portion	Chapter/article

LICENSED CONTENT

Publication Title	The Plant journal	**Publication Type**	e-Journal
Article Title	Arabidopsis BBX14 is involved in high light acclimation and seedling development	**Start Page**	141
		End Page	158
		Issue	1
Author/Editor	Society for Experimental Biology (Great Britain)	**Volume**	118
		URL	http://onlinelibrary.wiley.com/journal/10.1111/(ISSN)1365-313X
Date	01/01/1991		
Language	English		
Country	United Kingdom of Great Britain and Northern Ireland		
Rightsholder	John Wiley & Sons - Books		

REQUEST DETAILS

Portion Type	Chapter/article	**Rights Requested**	Main product
Page Range(s)	1-18	**Distribution**	Worldwide
Total Number of Pages	18	**Translation**	Original language of publication
Format (select all that apply)	Print, Electronic	**Copies for the Disabled?**	No
Who Will Republish the Content?	Academic institution	**Minor Editing Privileges?**	Yes
		Incidental Promotional Use?	No
Duration of Use	Life of current edition		
Lifetime Unit Quantity	Up to 499	**Currency**	EUR

NEW WORK DETAILS

Title	Role of the Arabidopsis thaliana transcription factor BBX14 in retrograde and stress acclimation signaling pathways	**Institution Name**	LMU München
		Expected Presentation Date	2024-07-31

Instructor Name	Vasil Atanasov

ADDITIONAL DETAILS

The Requesting Person / Organization to Appear on the License	Vasil Atanasov

REQUESTED CONTENT DETAILS

Title, Description or Numeric Reference of the Portion(s)	BBX14 Permission	**Title of the Article / Chapter the Portion Is From**	Arabidopsis BBX14 is involved in high light acclimation and seedling development
Editor of Portion(s)	Atanasov, Vasil; Schumacher, Julia; Muiño, Jose M.; Larasati, Catharina; Wang, Liangsheng; Kaufmann, Kerstin; Leister, Dario; Kleine, Tatjana	**Author of Portion(s)**	Atanasov, Vasil; Schumacher, Julia; Muiño, Jose M.; Larasati, Catharina; Wang, Liangsheng; Kaufmann, Kerstin; Leister, Dario; Kleine, Tatjana
Volume / Edition	118		
Page or Page Range of Portion	141-158	**Publication Date of Portion**	2024-04-01